Switchable and chirally-amplified helices formed by hydrogen-bonded supramolecular polymers for asymmetric catalysis

Yan Li

Sorbonne Université

Ecole doctorale physique et chimie des matériaux (ED 397)

Institut Parisien de Chimie Moléculaire / Equipe de Chimie des Polymères (UMR 8232)

Switchable and chirally-amplified helices formed by hydrogen-bonded supramolecular polymers for asymmetric catalysis

Par Yan LI

Thèse de doctorat de Physique et Chimie des Matériaux

Dirigée par Matthieu RAYNAL

Présentée et soutenue publiquement le 03 Décembre 2019

Devant un jury composé de :

Mme. Anja Palmans	Professeur Eindhoven University of Technology	Rapporteur
M. Rafael Gramage-Doria	Chargé de Recherche Université Rennes I	Rapporteur
M. Paweł Dydio	Maître de Conférences Associé Université de Strasbourg	Examinateur
M. Perez-Luna Alejandro	Directeur de Recherche Sorbonne Université	Examinateur
M. Matthieu Raynal	Chargé de Recherche Sorbonne Université	Directeur de thèse
M. Laurent Bouteiller	Directeur de Recherche Sorbonne Université	Co-encadrant

In the Chinese language a large number of small forces adding up to a large force expresses the mutually intertwined ideas of cooperation and amplification, this finds parallel in the chiral properties of dynamic helices.

---Mark M. Green

Chinese character for cooperation-amplification.

Acknowledgements

First of all, I would like to thank Anja Palmans and Rafael Gramage-Doria for having agreed to be the reviewers of this thesis. I also want to express thanks to Paweł Dydio and Perez-Luna Alejandro for their agreements to be part of my thesis jury. Then my thanks also go to my supervisors: Matthieu Raynal, my thesis director and Laurent Bouteiller, my co-supervisor during all these years.

Thanks to the opportunity provided by Laurent and Matthieu, I have the chance to start my PhD in France, I really appreciate it. More than three years research work have allowed me to gain knowledge in the field of supramolecular polymer catalysis about monomer synthesis, coassemblies characterization and their catalytic function, which were almost new for me. I would like to thank Laurent more fully for all instructions about supramolecular polymer characterization. My deepest gratitude also goes to Matthieu. With the careful guidance of Matthieu, both my experiment and presentation skills have improved. I gradually learn how to design experiments and write papers to show my results. Thank you again not only for the research guidance but also for daily life. Then I want to express gratitude to the members of the analysis services: Claire (NMR), Aurélie (NMR), Gaelle (ITC), Omar (GC/HPLC), Geoffrey (XRD) and David (SEM).

Then I want to express thanks to my team members, firstly I thank Shuaiyuan, Weiei Fang who share one office with me. Thank you for your help in both research and daily life. Then my thanks go to Richard, Xavier, Ahmad, Gaetan, ludovic, Quentin, Laura, Danilo, thank you for your support. The rest of the team is not forgotten of course, thank Thomas, Léo, Benjamin and Sandrine. I would also like to thank all the members of the polymer group, especially Xiaolu, Tengteng, Xiao, Dizheng, Weiwei Du and Haixia. I am also grateful to my friends outside the lab and my family who supported me for 28 years and made it possible to get to my thesis. I therefore show gratitude to my parents, my grandparents and all other family members. Finally, I express thanks for Chinese Scholarship Council for supporting my PhD study.

Thank you for all the people who helped me during my PhD!

Merci à toutes les personnes qui m'ont aidé durant ma thèse !

谢谢博士期间所有帮助过我的人!

Table of contents

Abbreviations

e.e.: enantiomer excess

BTA: Benzene-1,3,5-tricarboxamide

alkyl BTA: *N*,*N*',*N*''-Trialkylbenzene-1,3,5-tricarboxamide

OPE: oligo(phenyleneethynylene)

TPA: triphenylamine

PQX: Poly(quinoxaline-2,3-diyl)

BUBA: *N*-substituted benzene-1-urea-3,5-biscarboxamide

DHN: decahydronaphthalene

DI: diisocyanideTrMA: triphenymethyl methacrylate

PPh_2: diphenylphosphine

CD: circular dichroism

NMR: nuclear magnetic resonance

SANS: small angle neutron scattering

HRP: helical reversal penalty

Ke: equilibrium constant for the elongation stage

Kn: equilibrium constant for the nucleation stage

S&S: sergeants-and-soldiers

MR: majority-rules

NPnone: 1-(4-nitrophenyl)ethanone

TPPCl: tetraphenylphosphonium chloride

FT-IR: Fourier-Transform Infrared

Tf=triflimide

DCM: dichloromethane

DP_n: degree of polymerization

Introduction

Parts II.3 and parts II.4 dealing with chirally-amplified helical catalysts and switchable helical catalysts, respectively, constitute the main topic of the thesis and, accordingly, have been covered comprehensively. They are the main parts of a mini-review published in ChemCatChem (Yan Li, Laurent Bouteiller, Matthieu Raynal, ChemCatChem, ***2019****, DOI: 10.1002/cctc.201901246)*

I Macromolecular helices: definition, classes and properties

I.1 Definition

As one basic property of nature, chirality plays a crucial role in living organisms. Among the hierarchical levels from subatomic to galactic scales, chirality at the molecular and supramolecular levels is vitally important for the field of chemistry and materials. Helicity, one special form of axial chirality, is defined as an entity that has an axis about which a set of substituents is held in a spatial arrangement that is not superimposable on its mirror image.[1] Macromolecular helices are a specific class of topological structures which are inherently chiral and adopt either a pure *P* or *M* helical configuration or an alternation of these two configurations within the same helix separated by helix reversals (Figure 1). Homochiral (single-handed) helices are key structural elements in nature, such as alpha helix and other types of helical secondary structures in proteins and the DNA double helix. It has been reported that non-covalent interactions play a crucial role in the construction and aggregation of helical biomacromolecules. For example, the formation of amyloid fibrils is driven by the aggregation of certain proteins into helical structures and lead to various pathologies. Another example is the hydrogen bonding and aromatic interactions between complementary bases that make DNA strands to assemble and form a stable helical structure. Inspired by nature, chemists have made huge efforts to design synthetic helices not only to mimic biological helices and properties but also for their potential applications in material science.[2]

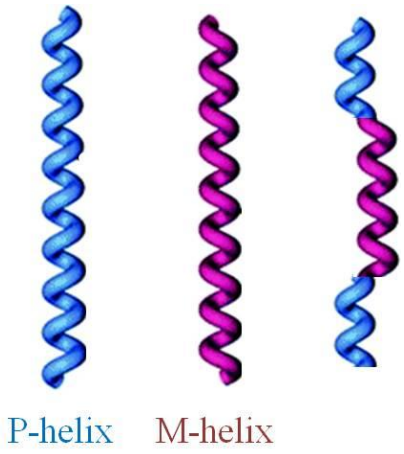

Figure 1 Schematic illustration of *P* and *M* homochiral helices and one (not optically pure) helix containing helix reversals[3]

I.2 Different classes of molecular helices

Inspired by nature, considerable efforts have been dedicated to construct helices from different kinds of building blocks. Herein helical scaffolds are divided into three classes: biomacromolecular helices, covalent helices and supramolecular helices, which will be described specifically in the following part. Shorter helices such as foldamers[2], helicenes[4] and helicates[5] have also been designed for numerous applications but will not be covered in this thesis.

I.2 a Biomacromecular helices

Natural DNA forms predictable, highly organized helical structures which can be easily functionalized for the construction of synthetic hybrids. A nice feature of DNA is the different structural features that it may adopt. For example, A-DNA and B-DNA are both right-handed double helices, but the helical structure of A-DNA is more compact, since the base pairs are not perpendicular to the helix-axis as in B-DNA. Z-DNA adopts a left-handed double helical structure, and thus expresses a different configuration at the supramolecular level although being constructed with the same base pairs than A-DNA and B-DNA. It is interesting to note that DNA strands can form additional supramolecular structures, such as G-quadruplexes.[6] In addition to DNA helices, polypeptides/proteins can also assemble into complex helical assemblies due to the interplay between van der Waals forces, hydrogen bonding, electrostatic, and aromatic interactions, such as for example the aggregation of G-actin into F-actin.[7] Structurally intricate helical peptides or proteins with the desired functions can now be constructed entirely from scratch ("de novo" design) or be designed by genetic or chemical modification of natural proteins.[8] (Figure 2)

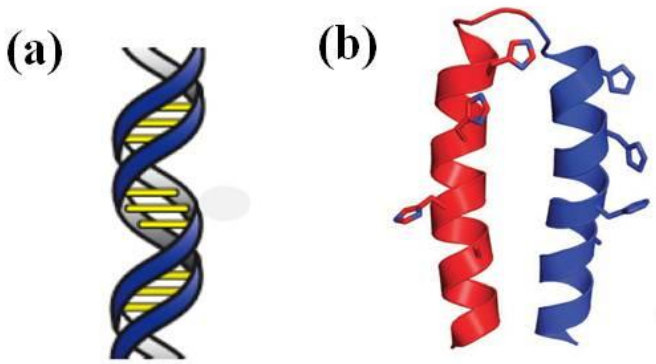

Figure 2 Schematic diagrams of (a) right-handed double-helix of DNA[6]; (b) Modelled structure of the hairpin helix-loop-helix motif formed by a synthetic 42-residues peptide (KO-42).[8] KO-42 dimerizes into an antiparallel four-helix bundle (not represented) and catalyses hydrolysis and transesterification reactions thanks to the highlighted histidines residues.[9]

I.2 b Covalent polymer helices

To mimic natural helical structures, huge effort has been devoted to the construction of artificial helices with synthetic macromolecules[10]. The first observation of a helical structure adopted by a covalent polymer referred to highly isotactic polypropylene (synthesized by a Ziegler-Natta catalyst) in the crystalline state. However the polypropylene could not maintain its helical conformation once dissolved into solvents.[11] A series of isotactic vinyl polymers, prepared by embedding chiral substituents in the polymer main chain, was found to be optically active but again the helical conformation was not satisfactorily stable in solvents.[11] One breakthrough happened with polymers adopting a stable helical conformation in solution, such as poly-triphenymethyl methacrylate (poly-TrMA) and polyisocyanates. For example, the anionic polymerization of TrMA with (−)-sparteine-*n*-Bu-Li(III) complex as chiral catalyst yields isotactic and optically active poly-(TrMA) as a consequence of the helical conformation adopted by the polymer backbone.[12-13] It is of high importance to increase the conformation stability and, in the case of poly-(TrMA) it has been achieved by incorporating bulky groups on the lateral chains of the polymers. However, subsequent studies on other families of monomers have demonstrated that introducing bulkiness in the monomer side chain is not a general requirement to get configurationally stable helical polymers.[11]

As can be seen in Figure 3, different polymer backbones exhibit varied helix inversion barriers. Helical polymers with high helix inversion barriers are named as “static helical polymers” since their handedness is set upon the formation of the polymer and cannot be reliably inversed thereafter .In contrast, dynamic helical polymers have low helix inversion barriers, leading to rapid interconversion between *P* and *M* conformations. Importantly, for a same family of monomers, the corresponding polymers can be classified either as static or dynamic which highlights the importance of the monomer side chain in tuning the inversion barrier. The different methods developed for preparing homochiral helical polymers will be shown in part I.3.

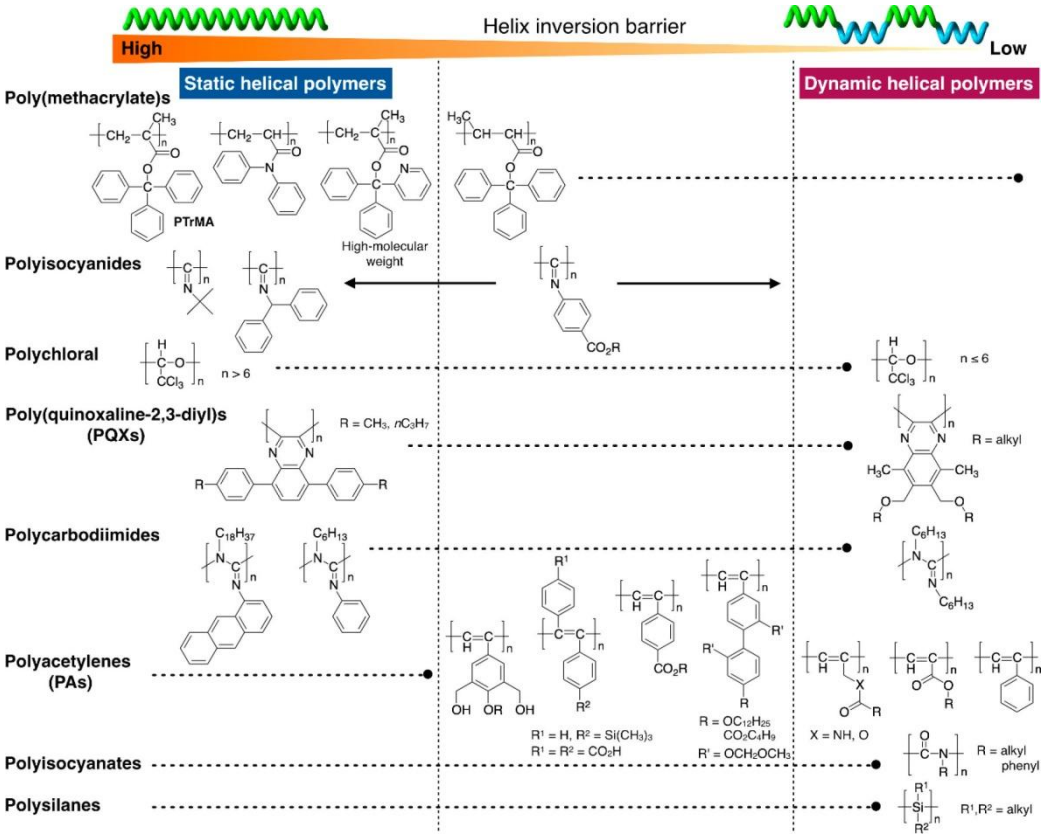

Figure 3 Examples of static and dynamic helical polymers with different helix inversion barriers.[2]

For helical polymers with accessible chromophores, the chiral optical activity can be directly quantified by circular dichroism (CD). The net helicity, *i.e.* the fraction between left-hand and right-handed fragments within the helical main chain, can be determined by measuring the CD intensity. Besides, it was reported that single-handed helical polymers show practical applications in different fields, such as enantiomer separation and asymmetric catalysis (see part II). For example, certain helical polymers afford significant chiral recognition ability and can be used as very efficient chiral stationary phases for high performance liquid chromatography (HPLC).[11] A nice example highlighting the dynamic properties of helical polymers is the switchable chiral HPLC stationary phase developed by Yashima and co-workers, which is constructed from polyacetylene bearing 2,2′-bisphenol-derived side chains. The handedness of the polymer can be selected in the solid state before use by interaction with a chiral alcohol, and the desired helicity is maintained after removal of this chiral additive (chiral memory). This feature enables the modulation of the elution order when this helical polymer is employed as a chiral HPLC stationary phase.[14]

I.2 c Supramolecular polymer helices

Definitions

Supramolecular polymers are defined *as "polymeric arrays of monomeric units that are brought together by reversible and highly directional secondary interactions, resulting in polymeric properties in dilute and concentrated solution as well as in the bulk. The directionality and strength of the supramolecular bonding are important features of systems that can be regarded as polymers and that behave according to well-established theories of polymer physics".*[15] Various kinds of non-covalent interactions have been utilized as the driving forces for the construction of supramolecular polymers, which include multiple hydrogen bonding, π-π stacking, metal coordination and host-guest interactions.

As one combination of polymer science and supramolecular chemistry, supramolecular polymers have attracted tremendous interests in various fields from adaptive materials to energy and medicine. The first truly supramolecular polymer was synthesized by Lehn group in 1990, which consists of two monomers bearing uracil and 2,6-diaminopyridine groups.[16] However, the binding constants of the repeating units are too low to form long assemblies. A benchmark class of supramolecular polymers is those constructed with the ureidopyrimidinone moiety, which could assemble through self-complementary 4-fold hydrogen bonding interactions, and form polymers with macroscopic properties that resemble those of covalent polymers. Moreover, the dynamic nature offers additional advantages, such as the low viscosity at higher temperature, facilitating polymer processing.[17-18]

Supramolecular polymers that adopt stable helical configurations usually form through a linear supramolecular polymerization mechanism which can be named as isodesmic or cooperative according to the following definitions (Figure 4). The isodesmic polymerization is similar to step growth polymerization for covalent polymers. The key feature is that the reactivity of end groups is constant during the whole process, leading to a high dispersity. For example, π-conjugated molecules with aromatic interactions as the main driving force often polymerize via an isodesmic mechanism. In contrast, in a cooperative mechanism the monomer binding constant changes during the assembly, the polymerization only starts above a critical concentration or below a critical temperature. Analogously to chain-growth polymerization, cooperative growth consists of at least two stages: nucleation and elongation. As a result of cooperative effect, the binding constant of elongation stage (K_e) is higher than that of nucleation stage (K_n).[15, 19] There are three origins of cooperativity: electronic effects, structural effects (allosteric conformational changes and helix

formation) and hydrophobic effects.[15] One example of cooperative growth is the polymerization of bisurea derivatives, which could form long tubular assemblies through hydrogen bonding interactions.[20] Temperature-dependent circular dichroism (CD) and UV-vis absorption analyses are classically utilized to distinguish between isodesmic and cooperative mechanisms. As could be seen in Figure 5, variable-temperature CD spectra of isodesmic and cooperative growth exhibit sigmoidal and non-sigmoidal shape, respectively.[21]

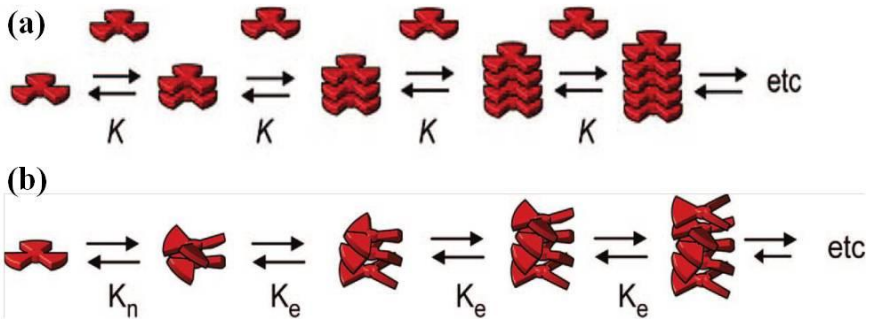

Figure 4 Scheme of (a) isodesmic supramolecular polymerization of disc-like monomers. The unchanged K indicates that binding constants are equal during the whole polymerization process. (b) cooperative supramolecular polymerization of discotic molecules [15]

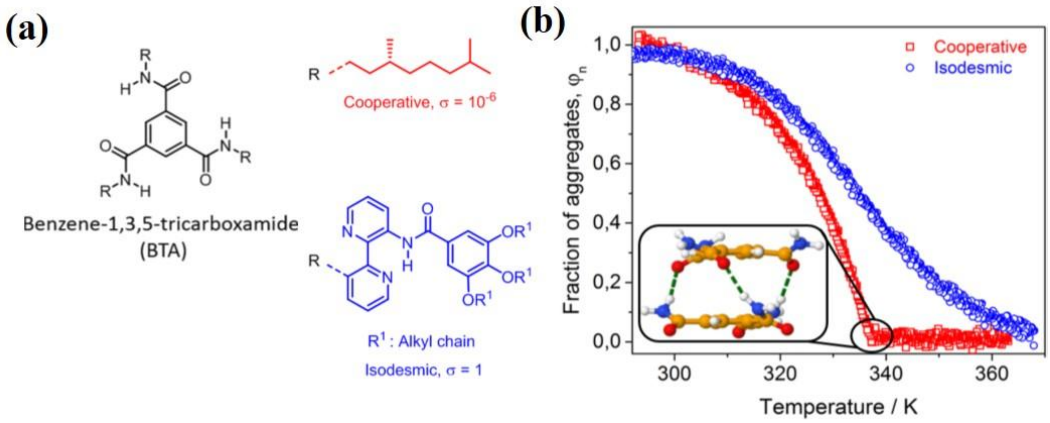

Figure 5 (a) Structure of two benzene-1,3,5-tricarboxamide (BTA) derivatives and (b) their temperature-dependent circular dichroism (CD) spectra indicative of cooperative and isodesmic polymerizations [21]

A variety of disk-shaped molecules has been employed for the bottom up construction of supramolecular polymer helices. They are mainly C_3-symmetrical monomers which consist of a central aromatic ring or conjugated rings decorated with hydrogen bonding moieties (Figure 6). The most simple and most studied class of monomers are benzene-1,3,5-tricarboxamide (BTA) which consist of three alkyl amide functions connected through their carbon atom to the central aromatic ring. This specific class of monomers has been investigated during this thesis and will be further

developed in a specific part below. Structurally-related to BTA-based monomers, Sánchez group reported a systematic study of oligo(phenyleneethynylene) (OPE)-based discotics decorated with three amide functions (OPE-TA).[22] Miyajima group synthesized propeller-shaped triphenylamine (TPA) molecules. High chirality amplification effect has notably been found for a TPA-based system with peripheral amide functions (TPA-TA). It was demonstrated that one TPA-TA enantiopure sergeant could control the handedness of almost 500 achiral TPA-TA soldiers. (This phenomenon called as the sergeants-and-soldiers effect will be described in detail in part I.3 b)[23] Theses molecules possess common features. From the structural point of view, all molecules share triangular shape, which comprise an aromatic core decorated with peripheral solubilizing groups. The main driving forces for the formation of the helices are π-π stacking and hydrogen-bonding interactions. In addition, all these molecules could be appropriately modified with functional groups to impart these supramolecular polymer helices with new properties.

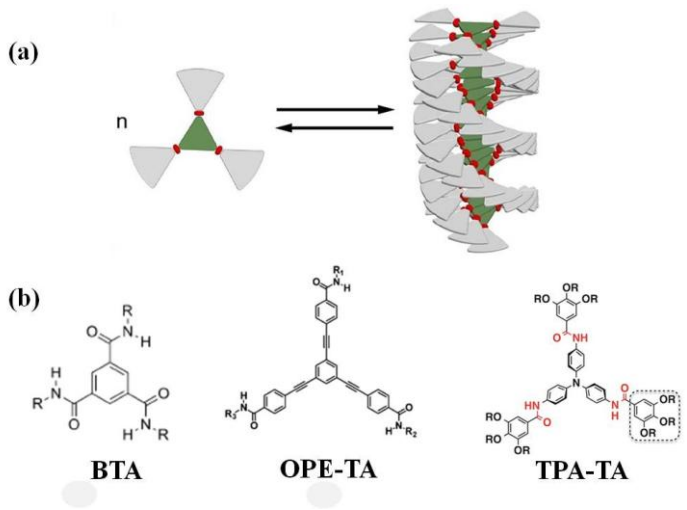

Figure 6 (a) Scheme of supramolecular polymerization of C_3-symmetrical monomers; (b) Molecular structures of different kinds of monomers[24]

Specific case of benzene-1,3,5-tricarboxamide (BTA) helical assemblies

As a ubiquitous monomer unit of supramolecular polymers, the BTA motif can be conveniently synthesized by a simple amide forming reaction between commercially available trimesic acid (or trimesoyl chloride) and the desired primary amines. BTA derivatives form helical stacks in apolar solvents through their three-fold hydrogen-bonding and π-π stacking interactions via a cooperative process. By incorporating chiral side chains, helices with a preferred handedness can be achieved conveniently.[25] As depicted in Figure 7, the presence of a negative Cotton effect centered at 225 nm in the CD spectrum of **1** in heptane indicates that the central BTA core adopts a chiral arrangement as the result of the stacking of BTA monomers into supramolecular helices. As

the maximal CD intensity is reached under these conditions, it means that an efficient transfer of chirality occurs between the stereogenic centre located in the side chains and the main chain helicity of the stacks. Further studies established that stacks of **1** are preferentially right handed[26] and that their structure in solution are similar to the one established in the crystalline state for a related BTA molecule.[27] Upon increasing the temperature to 90°C, the Cotton effect disappears and the intensity of the main absorption band of UV-Vis spectrum increases, which indicates the disaggregation of the supramolecular helices.[28] In **BTA 1**, the three amide functions are connected to alkyl groups (alkyl BTAs). Meijer, Palmans and coworkers reported how subtle modification in the nature of the alkyl side chain modifies the extent of cooperativity, the chiral nature and the stability of BTA polymers.[29-31]

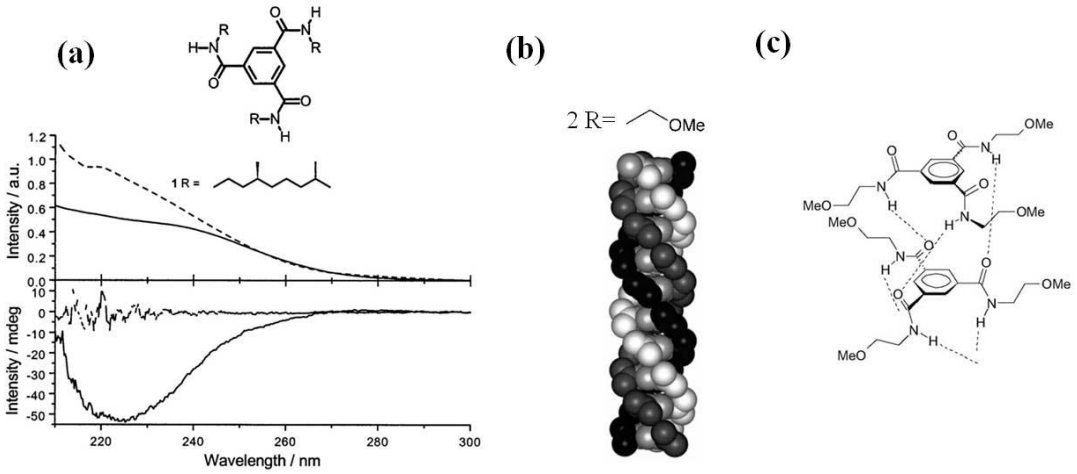

Figure 7 Chemical structure of (a) enantiopure **BTA 1** and its CD and UV spectra at 10 ℃ (solid line) and 90 ℃ (dashed line) in heptane ($6.5*10^{-5}$ M) (b) **BTA 2** and its triple-helical hydrogen bonding network. Each O, C, N(H)–O helical strand is a different shade of grey. Hydrogen atoms and methoxyalkyl side-arms omitted for clarity.(c) Helical packing of **BTA 2** in the stacks.[29]

In addition to alkyl BTAs, BTAs derived from α-amino esters (ester BTAs) is another kind of BTA molecules with good accessibility. Different kinds of chiral pendant groups can be incorporated in the α-position of the amide functions. Moreover, ester BTAs show unusual self-assembly properties in apolar solvents, since the nature of the pendant groups and the concentration determine the nature of predominant assemblies: stacks or ester-bonded dimers. The former structure is similar to the one formed by alkyl BTA *i.e.* the hydrogen bond network involves the amide moieties only (Figure 7). The latter species has been evidenced and characterized by several analytical techniques including a structural determination in the crystalline state by X-ray diffraction (case of **BTA (*S*)-Cha$^{i\text{-Pr}}$**, Figure 8a). In this D_3-symmetrical dimer, the N-H protons are bonded to the ester C=O, not to the amide C=O. Our group has precisely probed the competition between

dimers and stacks and determined the pseudo-phase diagrams of a set of ester BTAs in cyclohexane (Figure 8b).[32]

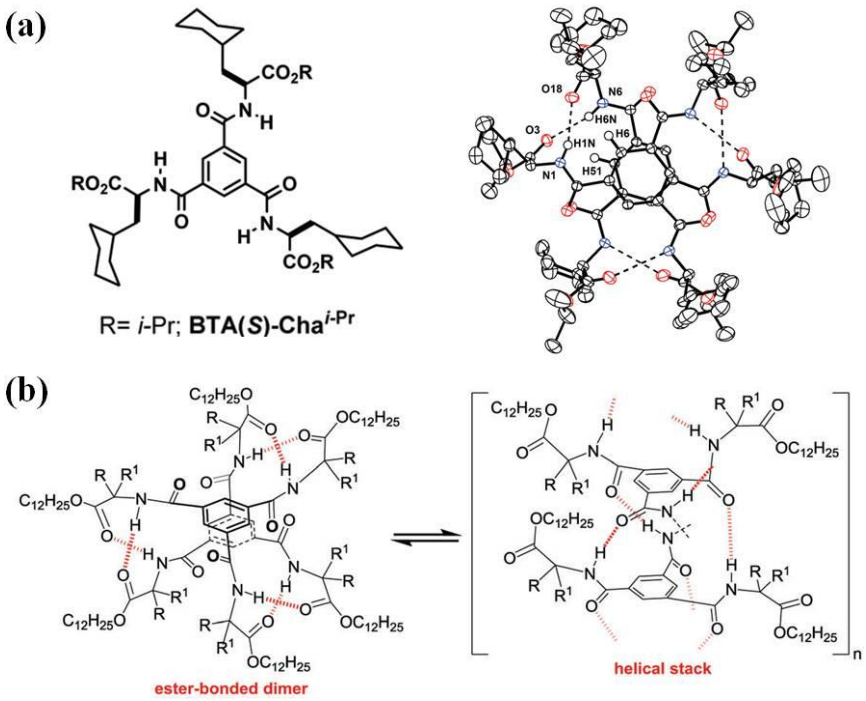

Figure 8 (a) Chemical structure of **BTA(*S*)-Cha$^{i\text{-Pr}}$** molecules and its X-ray crystal structure (BTA(*S*)-Cha$^{i\text{-Pr}}$•0.25CH_3CN•0.5H_2O). H atoms (except H1N, H6N, H6 and H51) and solvent molecules are omitted for clarity. Ellipsoids are represented at the 30% probability level[33]; (b) the equilibrium between helical stacks and ester-bonded dimers for ester BTA.[32]

One interesting feature of this class of monomers is that their assembly properties can be controlled by the stereochemistry. The heterochiral monomer of the BTA derived from valine (**BTA (*S*,*S*,*R*)-Val**, Figure 9a) as well as a racemic mixture of monomers derived from (*rac*)-Valine form long rods in cyclohexane, while the homochiral analogue **BTA (*S*)-Val** assembles only into dimers at the same concentration as demonstrated notably by FTIR analyses (Figure 9b)[33] This is related to the stronger destabilization of the dimeric structure, compared to the helical structure, upon incorporation of stereogenic centres of opposite configuration in the same monomer. Another important feature is the possibility to form co-assemblies by mixing ester BTAs and alkyl BTAs.[34-35] Notably, as a consequence of the different spectroscopic signature of their relative assemblies, it is possible to quantity the amount of ester BTAs incorporated into stacks of alkyl BTAs.

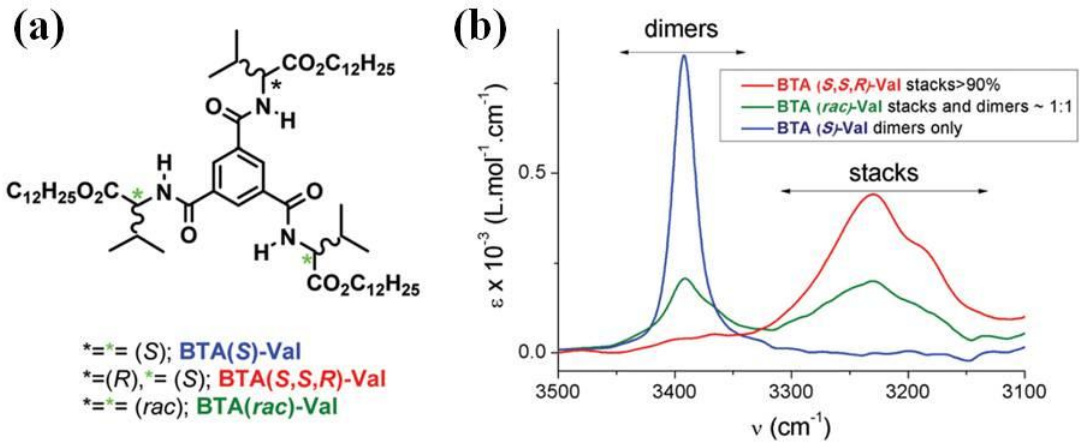

Figure 9 (a) Chemical structure of BTA-Val molecules and (b) their FT-IR spectra. **BTA(rac)-Val** was obtained by synthesis with racemic valine and consists of a mixture of **BTA(*S*,*S*,*R*)-Val** (37.5%), **BTA(*R*,*R*,*S*)-Val** (37.5%), **BTA(*S*)-Val** (12.5%) and **BTA(*R*)-Val** (12.5%).[33]

I.3 Preparation of homochiral helices

I.3.a. Different strategies

Different strategies have been utilized to construct homochiral helices, *i.e.* helices with a single handedness, and most of these strategies are common to covalent and supramolecular helices mentioned in the previous part. While chiral physical stimuli (CPL, vortices) or solvents have been sporadically used to induce a preferred handedness to molecular helices,[36] most examples rely on chemical agents. The simplest strategy is to build helices with chiral units only. Here, the chiral information, most often under of the form of stereogenic centres, is embedded either in the core or at the periphery of the monomer (method A, Figure 10). However, one specificity of molecular helices stems from the possibility of reducing the chirality input without lowering the optical purity of the helices thanks to chirality amplification phenomena. Chiral amplification refers to the control of the main chain helicity of the macro/supramolecule by means of cooperative (minute) conformational biases induced by the monomers.[37-39] These phenomena might arise when a new element of chirality is created upon the polymerization or assembly of monomers, as it happens when molecular helices forms. In the 80s-90s, Green and co-workers intensively investigated the occurrence of such effects for covalent poly(isocyanate)s,[37] *i.e.* polymers whose main chain adopts a stable but dynamic helical conformation in solution.[40-41] Since then, it was demonstrated that single-handed helices can be obtained not only from homopolymers of enantiopure monomers but also from copolymers consisting of a mixture of enantiopure ("sergeants") and achiral ("soldiers") monomers. The so-called "sergeants-and-soldiers" (S&S) effect [42] arises when a minor amount of sergeants is able to

control the local conformation of an excess of soldiers that cannot escape this influence except through rarely occurring helix reversals (method B, Figure 10). The same explanation is also valid for a non-racemic (*i.e.* scalemic) mixture of enantiomeric monomers in which the major enantiomer controls the main helicity of the polymer and accordingly such effect is named as "majority-rules" (MR) (method C, Figure 10).[43] Combining the sergeants-and-soldiers and majority-rules effects is possible in the case of terpolymers composed of achiral monomers and a scalemic mixture of monomers (diluted MR) ("diluted majority-rules", method D, Figure 10). The main chain helicity of polymers such poly(triphenymethyl methacrylate)s[12-13] and poly(quinoxaline-2,3-diyl)s[44] can also be controlled during the polymerization process. Indeed, asymmetric polymerization occurs when the local conformation of many achiral monomers can be imposed by a single chiral inducer or catalyst (method E, Figure 10). Finally, chiral additives, which are not units of the polymer chain, can be used to lock the handedness of the helix, which can also eventually be kinetically memorized after their removal (method F, Figure 10).[45] Whilst helix sense-selective reactions have been restricted to a few classes of covalent polymers,[46] chirality amplification through the S&S, MR and diluted MR effects have also been observed in self-assemblies, particularly in supramolecular polymers adopting a helical structure.[41, 47]

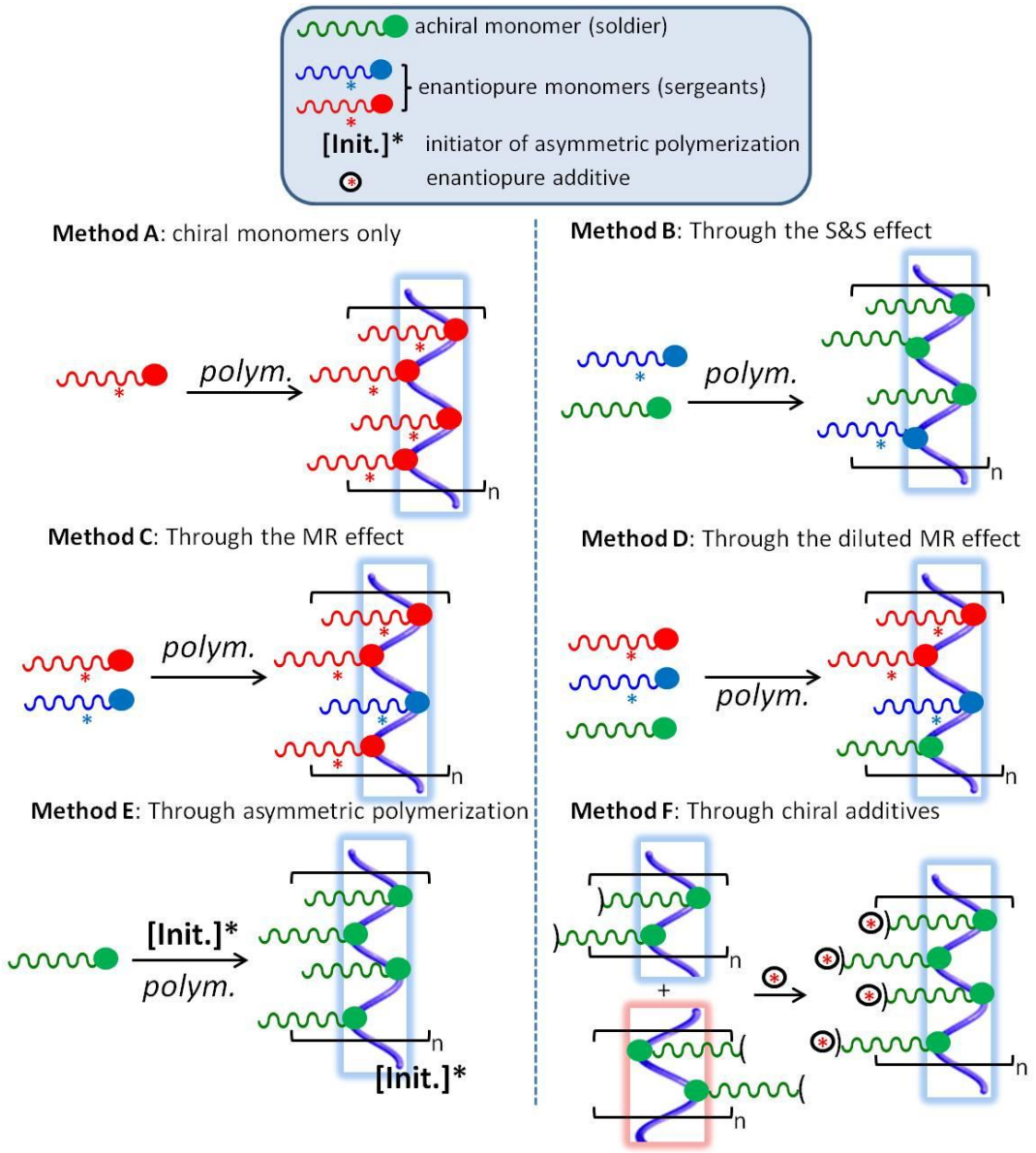

Figure 10 Different methods used to prepare single-handed helices. The purple helix represents a covalent or a non-covalent backbone.

b. Specific case of benzene-1,3,5-tricarboxamide (BTA) helical assemblies

It has been reported that homochiral helices can be constructed from BTA monomers by means of different strategies (methods A, B, C and D). By embedding stereogenic centres in the side chains of alkyl-[28] and ester-BTAs,[35] helical stacks with a preferred handedness are formed at room temperature in apolar solvents. Taking advantage of the remarkable chirality amplification properties of BTA system, S&S, MR and diluted MR effects have been utilized for the construction of homochiral BTA helices. In 1997, Meijer, Palmans and co-workers reported for the first time that the S&S principle is operative in dynamic helical stacks using **BiPy-BTAa** (sergeants) and achiral **BiPy-BTAb** (soldiers) (Figure 11).[48] 2.5% of **BiPy-BTAa** sergeants are enough to control the helicity of

the co-assembly. Then by modifying the side chains of **BiPy-BTA**, a mixture of chiral **BiPy-BTAc** and achiral **BiPy-BTAd** shows even higher chirality amplification effect in n-butanol, since maximum helicity was obtained with 1% of sergeant. By fitting the raw data by a model derived by Havinga, the authors found that one BiPy-BTAc is sufficient to control the chirality of 400 **BiPy-BTAd** monomers.[49] C_2-symmetrical BTA derivatives bearing only one chiral side chain also efficiently impose their helical bias to achiral rods.[50] The influence of the chemical structure of the monomers on the chirality amplification properties of a set of BTA has been precisely probed (Figure 12a). **BTA 3** and **5** with a stereogenic group at the α and γ positions of the amide functions exhibit a stronger S&S effect than **BTA 4** which bears a stereogenic centre at the β position (Figure 12b). An odd-even effect was also observed for the MR principle but this time **BTA 4** shows stronger chirality amplification properties than **BTA 3** and **BTA 5** (Figure 12c). This reflects the dichotomy between the SS and the MR effect which is also illustrated by their different response to temperature change: the SS effect is lowered and the MR is enhanced upon increasing the temperature. Chirality amplification properties on BTA and other supramolecular systems are quantified by different models.[50-53] In the van Gestel model,[41]54 the extent of chirality amplification is assessed by two energy penalties: the mismatch penalty (MMP) corresponds to the energetic cost of incorporation of the chiral monomer in columns with non-preferred helicity whilst the helix reversal penalty (HRP) corresponds to the penalty of introducing a helix inversion between columnar sections. The latter parameter strongly relies on the rigidity of the helical arrangement and will thus be rather constant for the same type of helical assemblies. The former parameter will strongly depend on the chemical structure of the monomers (nature and number of stereogenic centres) and the experimental conditions (concentration, temperature). The above experiments infer that the MMP value for achieving optimal chirality amplification properties is not identical for the SS and MR effects.

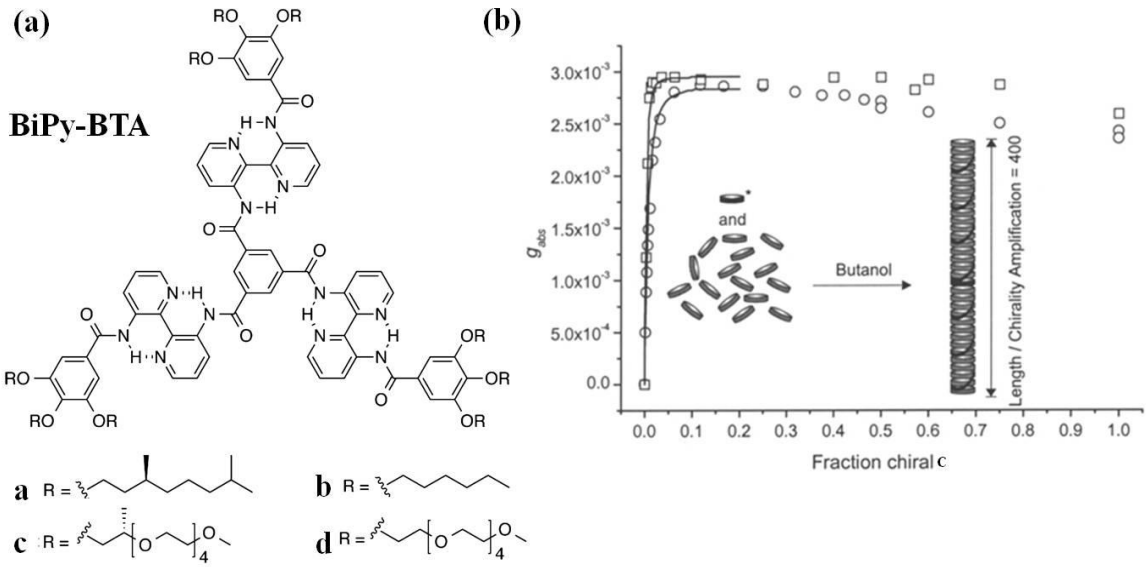

Figure 11 (a) Chemical structures of **BiPy-BTA** molecules and (b) sergeants and soldiers experiments for **BiPy-BTAc** and **d**:plots of the anisotropy factor g as a function of the sergeant fraction (**BiPy-BTAc**) in n-butanol at 5 ^{o}C at two different concentrations (circles: 10^{-5} M, squares: 10^{-4} M). [49]

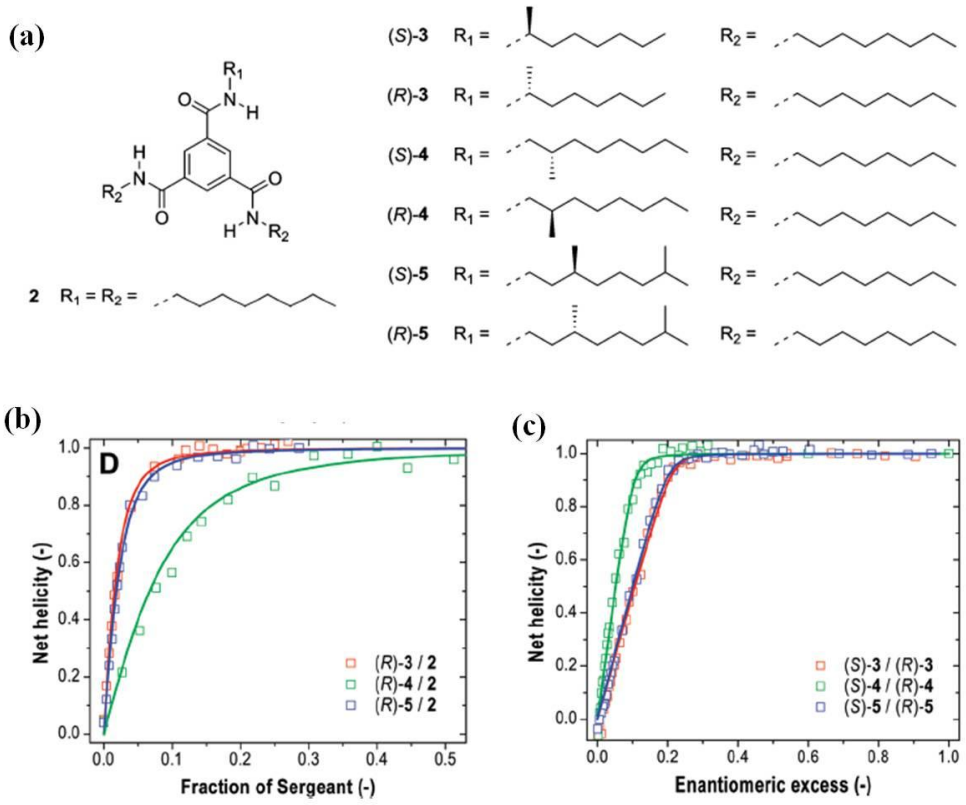

Figure 12 (a) Chemical structures of BTA molecules investigated for enhancing the chirality amplification properties of BTA helices; (b) net helicity vs sergeant fraction for different mixtures; (c) net helicity vs sergeant enantiomeric excess for different mixtures. [50]

II Asymmetric catalysis with helical scaffolds

Asymmetric homogenous catalysis is the ubiquitous method for the preparation of optically active compounds. This is because in this process a catalytic amount of a well-designed chiral non-racemic species is able to assemble prochiral/achiral reagents and generate multiple copies of a chiral molecule, preferentially in the form of a single enantiomer. Since major breakthroughs achieved in the early 1970s, great effort has been devoted to the development first of enantiopure ligands and organometallic catalysts[55-59] and later of chiral organocatalysts for a plethora of reactions and compounds[60-62], many of them being of industrial interest.

II.1 Advantages of the helical scaffold

As one kind of chiral structures, helices with preferred handedness show potential in a variety of chirality-based applications such as chiral sensing, chiral electronic, chiral separation and more recently asymmetric catalysis.[10] As can be seen in Figure 13, helices possessing catalytic properties can be divided into three classes: (i) helices bearing intrinsically chiral catalytic groups (class A), (ii) helices bearing intrinsically achiral catalytic groups but composed of chiral monomers only (class B); and (iii) helices bearing achiral catalytically active monomers and integrating catalytically inactive monomers as chiral inducers/amplifiers (class C). The last class encompasses helical catalysts for which the handedness is controlled by an asymmetric polymerization reaction (C1), the S&S effect (C2), the diluted MR effect (C3) or chiral additives (C4).

Compared to other catalytic scaffolds, helices have several features. Firstly, the helical architectures can be fabricated precisely from small building blocks, which enables fine modulation of the catalytic performance by modifying the structure and, potentially, the position of the monomers. Secondly, the chiral microenvironment provided by the helical scaffold[10] offers an additional possibility for selectivity control.[63] Thirdly, chirality amplification phenomena have been observed in different helical structures, and it is quite appealing to apply this property for the construction of a new class of asymmetric catalysts. Indeed, lower amount or optical purity of chiral units can be used which could decrease the cost of the catalytic process.[64] Fourthly, the dynamic property of a certain kind of helices may render the respective catalyst stimulus-responsive which can also be useful to design switchable catalytic systems.[65] Catalytic helices built on supramolecular polymers exhibit additional advantages: (1) The construction of supramolecular polymer helices is more convenient than covalent ones, since they can be prepared by simply mixing desired monomers in solution, thus avoiding tedious synthesis procedures and facilitating catalyst optimization. Moreover it is possible to manipulate some structural properties of the helices such as composition,

length and helicity by modifying the structure of the monomers. (2) The non-covalent backbone of supramolecular polymer enables the fast dynamics of helices which can make the respective catalyst highly sensitive to environment (temperature, solvent, co-monomer, etc.), which is beneficial for the design of a new class of switchable catalysts.

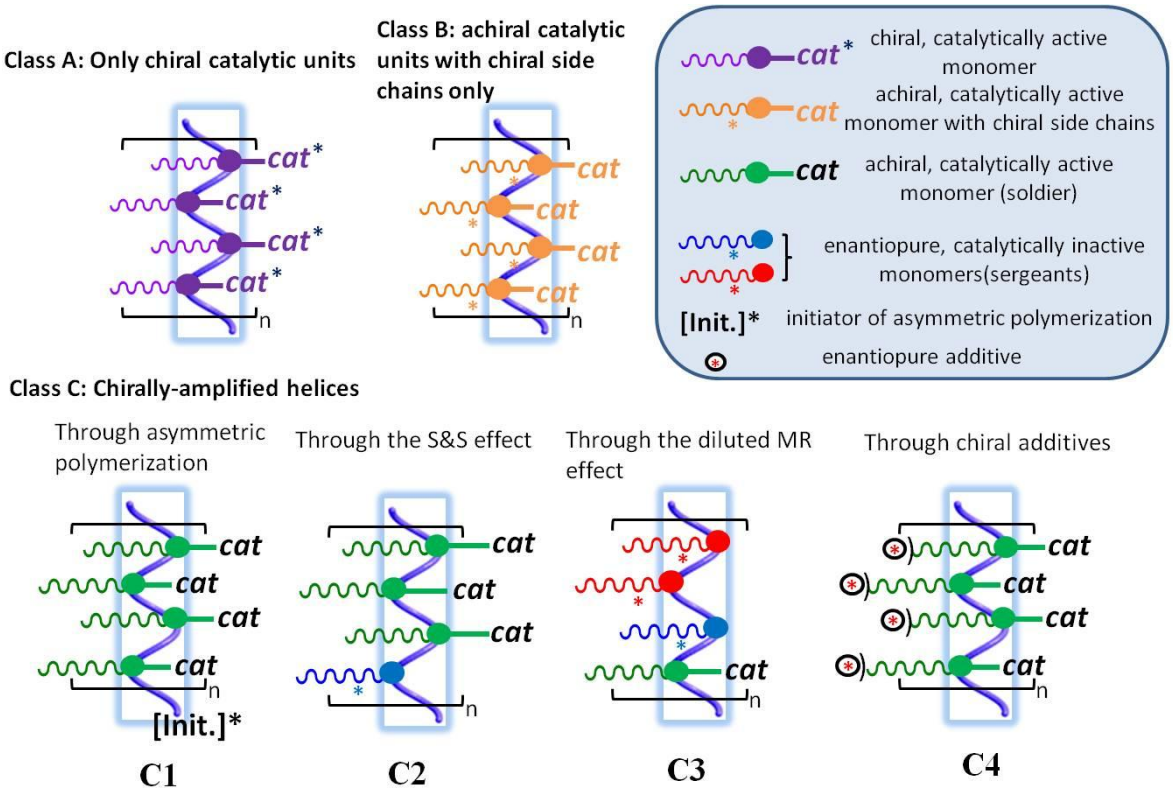

Figure 13 Different classes of catalytic helices.

II.2 Examples of helical catalysts composed of chiral units only (classes A and B)

II.2.a DNA-based hybrids as helical catalysts (class B)

By mimicking enzyme catalysis, biomolecular hybrids have been developed aiming to combine the catalytic ability of transition metals with inherent chirality of biopolymers. One key feature of bio-hybrid catalysis is that the metal center and the biomolecular scaffold could be finely tuned by chemical and genetic methods independently.[66] In parallel to the flourishing field of metalloenzymes, helical structures formed by double-helical DNA have attracted huge interest in the field of asymmetric catalysis. In 2005, Feringa and Roelfes first reported the utilization of a DNA-based hybrid catalyst in a copper-catalysed Diels-Alder reaction.[67]

As show in Figure 14, there are two strategies, supramolecular and covalent, for anchoring of transition metal complexes to the DNA scaffold. For non-covalent anchoring methods, aromatic

ligands intercalate within the base pairs by means of hydrophobic, π-π stacking, electrostatic and/or hydrogen bonding interactions. In contrast, covalent connection is achieved by nucleotide synthesis or post-functionalization of a DNA strand. Both approaches have their advantages and limitations. For the former one, the anchoring could form in an easy and convenient way, however, the intercalation can occur at different sites and thus different catalytic sites might be present along the DNA scaffold. For the latter one, a better control of the catalyst structure could be achieved but at the cost of tedious synthetic procedures. Some examples of both strategies are shown in Figure 15. It should be mentioned here that as flexible linkers are used between the metal centre and the chiral units of the DNA, the overall catalytic sites can be considered as intrinsically achiral. The chirality is transferred upon incorporation of these sites within the scaffold of the macromolecule (composed of chiral nucleobases only) and so the respective systems belong to the class B of our classification of helical catalysts.

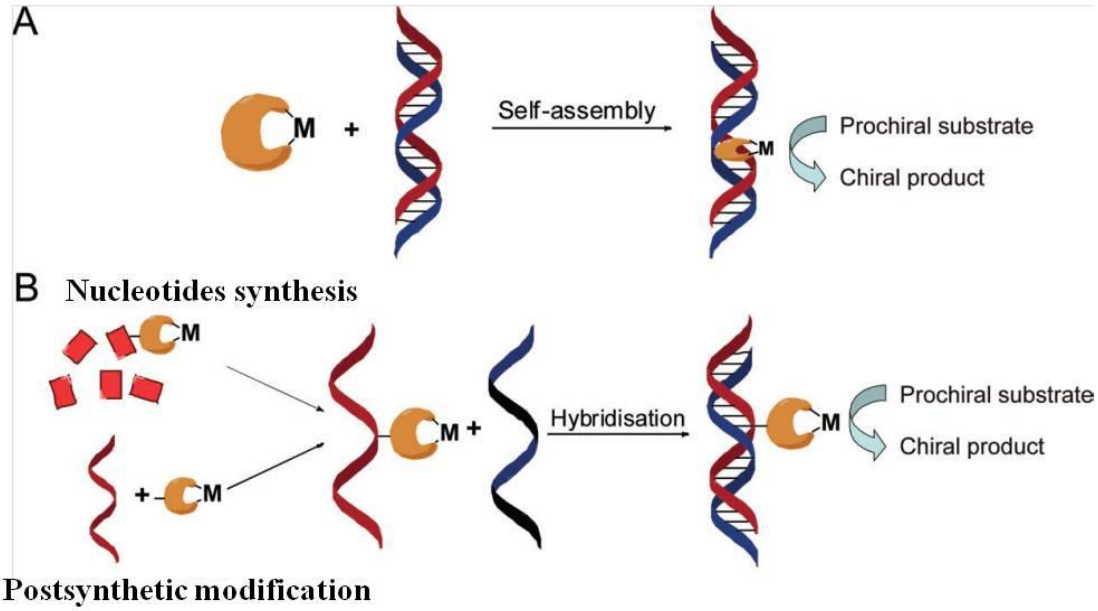

Figure 14 Supramolecular (A) and covalent (B) anchoring strategies for construction of DNA-based asymmetric catalysts.[66]

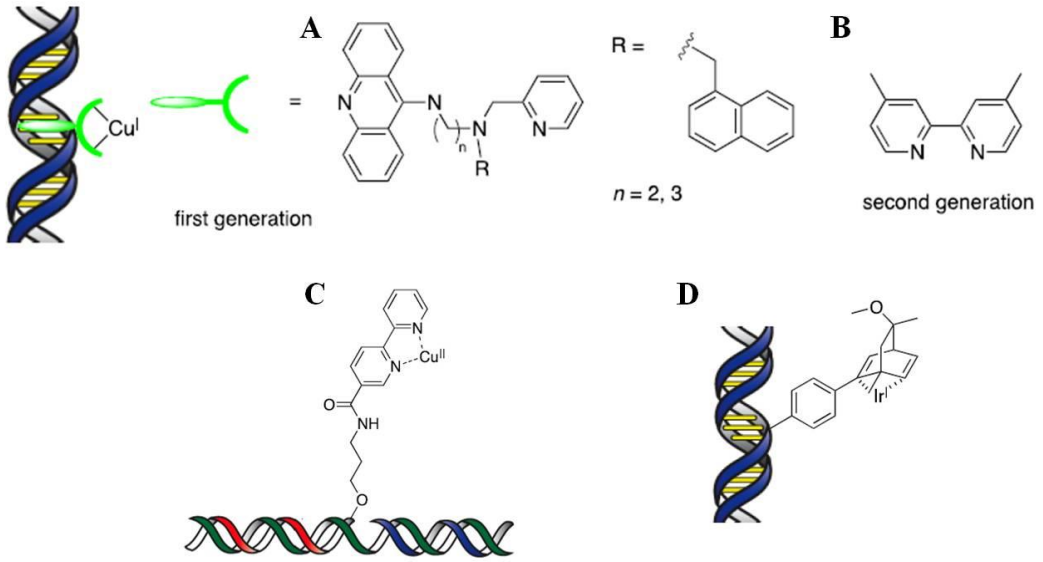

Figure 15 Examples of supramolecular (A, B) and covalent (C,D) DNA-based hybrid catalysts[6]

Even though different metals have been tested, including Pd and Ir, the DNA-Cu hybrids have been the most intensively investigated, providing good reactivity and selectivity in a range of catalytic reactions. These different reactions could be divided into carbon-carbon and carbon-heteroatom bond forming reactions. As can be seen in Figure 16, the power of DNA hybrid catalysis has been demonstrated in different C-C bond formation reactions, such as Dies-Alder reaction, Michael addition and Friedel-Crafts alkylation (> 80% *e.e.*). In all cases, the catalyst loading can be hugely decreased, for example, only 0.3 mol% catalysts is needed for Friedel-Crafts alkylations. The creation of carbon-heteroatom bond by DNA hybrids has also been developed. For example, Toru and co-workers have successfully performed the electrophilic-fluorination of aromatic compounds with good selectivity (74% *e.e.*) (Figure 17).[68] Feringa group has reported the enantioselective *syn* hydration of enones in aqueous environment using DNA-based catalyst. 82% *e.e.* was obtained for the chiral $_{\beta}$-hydroxy ketone product.[69] All precedent examples benefit from the Lewis acid properties of Cu^{II} for the activation of the substrates. Organometallic catalysis will considerably extend the scope of reactions and products supplied by DNA hybrids. Towards that direction, the Jäschke group has successfully exploited DNA-conjugated iridium (Ir) complex for the allylic amination of racemic allylic acetate in aqueous medium. The DNA-based ligand is a diene which forms a highly active and stable catalyst with Ir, as demonstrated by the high turnover number (4600), but provides only modest enantioselectivity (28% *e.e.*).

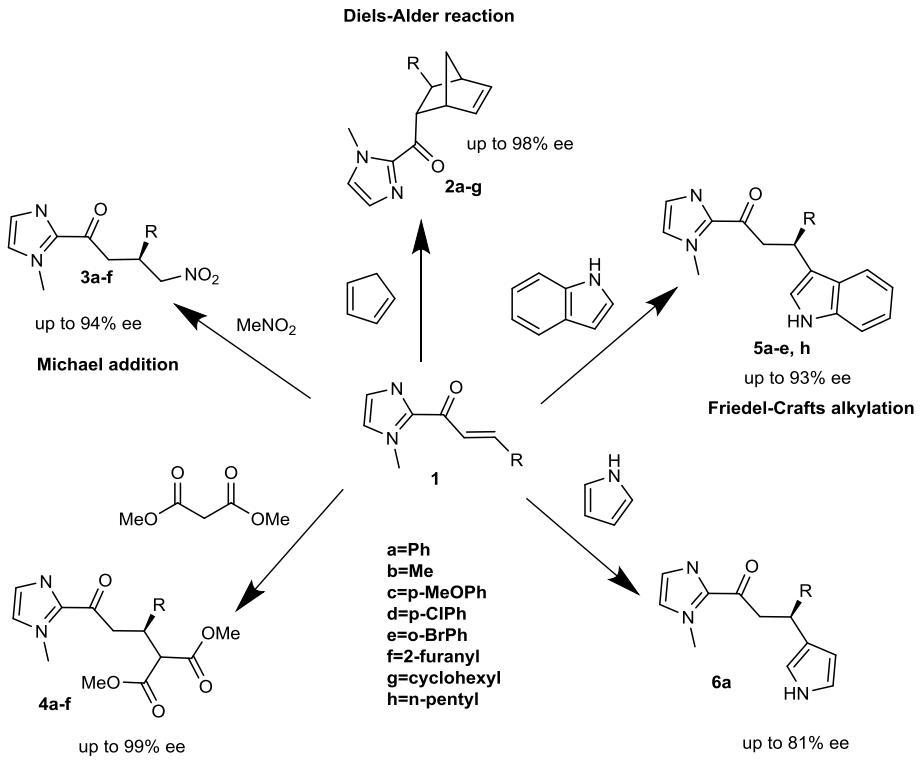

Figure 16 Examples of carbon-carbon bond forming reactions catalysed by supramolecular DNA-hybrids[66]

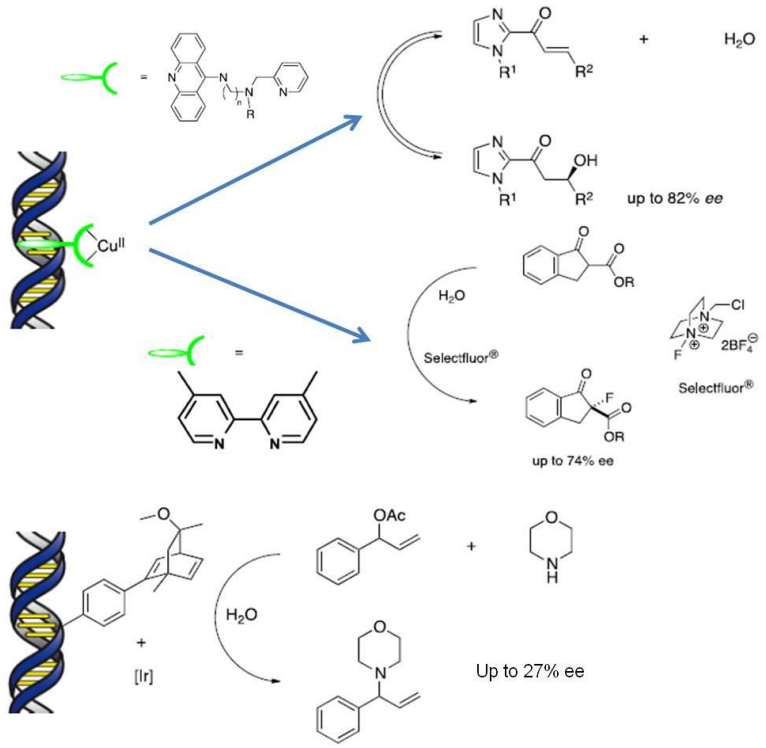

Figure 17 Examples of carbon-heteroatom bond forming reactions catalysed by DNA-hybrids[6]

DNA plays different roles in the catalytic reactions. As already mentioned, DNA helices provide the chiral environment required for the chiral enantioinduction. Chirality information is transferred to the micro-environment of catalytic centers through different DNA-binding modes (*e.g.*, groove binding and intercalation between base pairs). dNTP, *i.e.* a mixture of the four deoxyribonucleotides, and short single strand DNA provided low selectivity. Longer non-complementary single strand DNA (10 bases) gave higher selectivity but still lower than the one observed for DNA:DNA duplexes.[70] Moreover it was reported that the reaction selectivity of DNA duplexes decreases when their length is reduced from a dodecamer to an octamer.[71] Moreover, it has been found that DNA sequence is a crucial parameter in the catalytic system. The oligonucleotides with sequences $d(TCAGGGCCCTGA)_2$ afford highest enantioselectivity for the intermolecular Friedel-Crafts reactions. One another interesting question is whether the presence of DNA influences the activity. Kinetic studies of different systems have been undertaken to gain insight into impact of DNA on the reaction kinetics. Both deceleration and acceleration of the catalytic rate has been observed upon binding of the metal catalyst by the DNA scaffold.[66] Surprisingly, Roelfes group reported 700- to 900-fold rate acceleration of Friedel-Crafts alkylation/enantioselective protonation reaction caused by DNA scaffold.[72] One possible explanation is the stabilization of the transition state by means of non-covalent interactions between the metal complex and the environing nucleotides in the duplex.

II.2.b Helical catalysts built on covalent polymers (class A)

Different kinds of helical polymers could serve as scaffold for asymmetric catalysis and in this section we will mention specifically the ones embedding intrinsically chiral catalytic groups.[73] The chiral catalyst is located at the periphery of the helical macromolecule or incorporated into the main chain of the polymer backbone. For example, helical polyacetylenes bearing chiral primary amines or oligo-alanine pendant groups were used as organocatalysts for asymmetric aldol reactions[74] and epoxidation reactions,[75] respectively. Yashima and co-workers synthesized poly(phenylacetylene)s bearing optically pure amino-functionalized cinchona alkaloid pendant groups connected to the phenyl rings through an amide linkage (poly-AQn, Figure 18). High enantioselectivity (94% *e.e.*) was achieved for the Henry reaction between various benzaldehydes and nitromethane by means of this polymeric organocatalyst. Moreover it is important to note that the selectivity provided by the helical catalyst was remarkably higher than that of the nonhelical one (18% *e.e.*), the latter being obtained upon grinding the polymer before use. Moreover, the chiral monomeric counterpart (M-AQn, Figure 18) also provided a lower selectivity (28% *e.e.*). This

demonstrates a synergistic effect between the chiral catalytic sites (the cinchona alkaloid moiety) and the chiral environment provided by the helical backbone. [63]

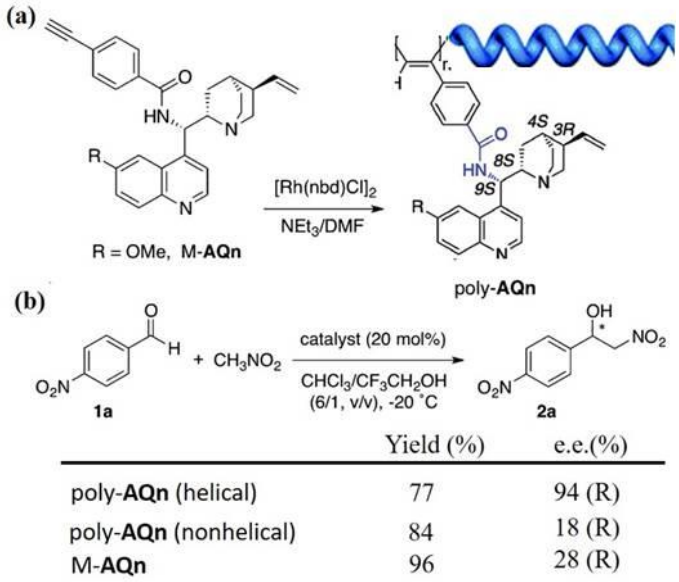

	Yield (%)	e.e.(%)
poly-**AQn** (helical)	77	94 (R)
poly-**AQn** (nonhelical)	84	18 (R)
M-**AQn**	96	28 (R)

Figure 18 (a) Synthetic scheme for the preparation of helical poly-AQn; (b) Catalytic results obtained in the Henry reaction between 4-nitrobenzaldehyde and nitromethane.[63]

As an example of polymers with main chain chiral catalytic centers, Pu and coworkers have synthesized poly-(binaphthol), in which binaphthol units are enantiomerically pure, and which upon coordination of metal centres provided efficient catalysts for a range of reactions.[76-77] It was demonstrated that poly-(binaphthol) adopted a stable helical configuration but despite the chirality of the binaphthol units, the respective complexes exhibited no enantioselectivity. A great achievement was made by incorporating achiral spacers at the 6,6'-position or 3,3'-position of the polybinaphthol since not only great activity but also great level of enantioselectivity were obtained with these helical catalysts (see one example in Figure 19). In comparison with monomeric models, a better selectivity was obtained with the helical catalyst which again suggests a synergistic effect between the helical backbone and the chiral catalytic sites.[78-79]

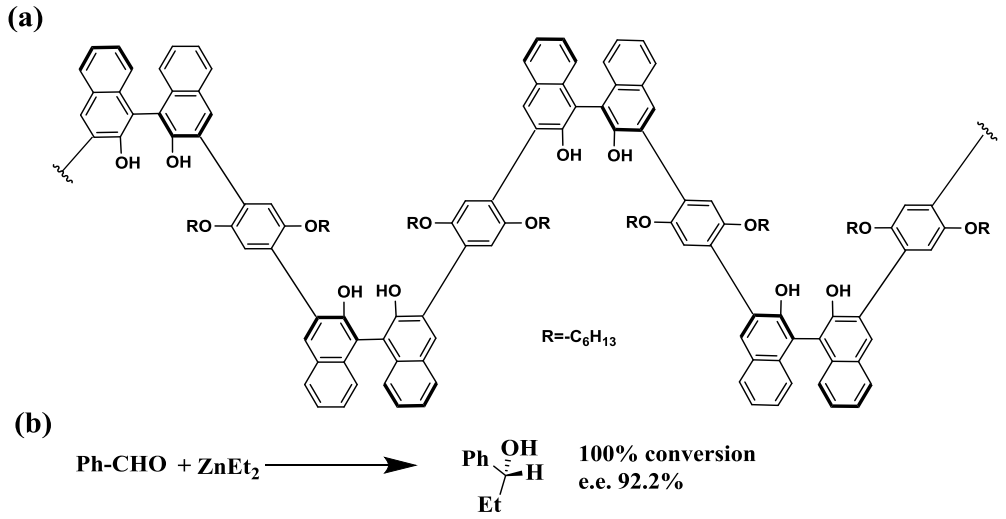

Figure 19 (a) Helical catalyst consisting of enantiomerically pure (binaphthol)s linked by an aromatic ring bearing long alkyl groups. ; (b) asymmetric addition of diethylzinc to aldehydes with the poly-(binaphthol) catalyst shown in (a) [79]

II.2.c Helical catalysts built on supramolecular polymers (classes A and B)

Supramolecular polymer helices could also catalyze some asymmetric reactions when functionalized with catalytic centers. Meijer, Palmans and co-workers synthesized a series of BTA monomers decorated with an enantiopure (*R*) or (*S*)-proline moiety and various alkyl amide side chains and evaluated the resulting assemblies in the aldol reaction between *p*-nitrobenzaldehyde and cyclohexanone in water (Figure 20).[80] After a temperature treatment, the helical catalyst formed upon self-assembly of the BTA monomers bearing one (*S*) proline unit and two (*S*)-stereogenic centres in the side chain, **(*S*)-BTA-$_{L}$-Pro** (Figure 20), provided the best catalytic performance (99% conversion, TOF> 11.4 $\times 10^{-4}$ s^{-1}, de_{anti} = 90%, ee_{anti} = 99%). As expected, its enantiomer, **(*R*)-BTA-$_{D}$-Pro**, provided the aldol product with opposite configuration and similar enantioselectivity. **(*R*)-BTA-$_{L}$-Pro**, with a mismatched configuration between the amide side chains and the proline units, and **(*S*)-MeBTA-$_{L}$-Pro**, with methylated amide functions, displayed significant enantioselectivity for the same reaction but significantly lower activity and diastereoselectivity. It infers that the best catalytic system is achieved by a synergistic effect between the ponctual chirality of the proline catalytic sites and the supramolecular chirality of the helices. **(*S*)-BTA-$_{L}$-Pro** indeed forms very stiff, long fibres after thermal treatment of its aqueous solution as demonstrated by cryo-TEM measurements. Subsequently, a more soluble BTA monomer was designed in which the alkyl amide side chains have been replaced by amphiphilic side chains composed of a terminal tetra(ethylene oxide) group. Catalytic assemblies are formed directly upon dissolution of this monomer in pure water and no thermal treatment is needed to achieve catalytic performance similar to that obtained

with **(*S*)-BTA-$_L$-Pro**. Moreover, the addition of a proline-free BTA monomer allows to decrease the catalytic loading up to 1 mol% without eroding the selectivity.[81]

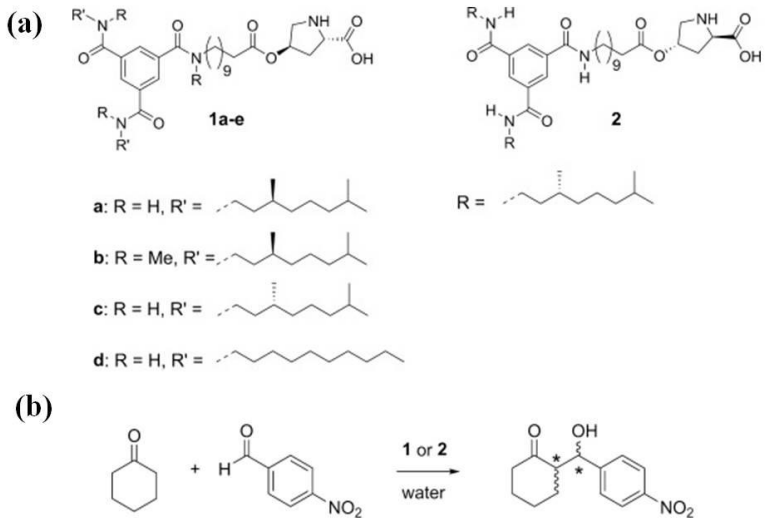

Catalyst	Conversion (%)	TOF [x10^{-4} s^{-1}]	*d.e.*$_{anti}$ (%)	*e.e.*$_{anti}$ (%)
1a	>99	>11.4	90	99
2	82	9.5	94	-97
1b	45	5.2	85	97
1c	45	5.2	77	92
1d	42	4.9	82	94

Figure 20(a) Chemical structures of BTA monomers functionalized with proline as catalytically active sites and (b) their catalytic results in the aldol reaction between 4-nitrobenzaldehyde and cyclohexanone.[80]

Our group has developed chiral BTA ligands with diphenylphosphino catalytic group and remote enantiopure 1-methylheptyl side chains (Figure 21). Good enantioselectivity (82% *e.e.*) was achieved with the BTA ligand, **^{H}BTA^{PPh2}(*S*),(*S*)**, in the rhodium-catalyzed asymmetric hydrogenation of dimethyl itaconate when the reaction was performed in hexane. By inverting the configuration of side chains, *i.e.* with **^{H}BTA^{PPh2}(*R*),(*R*)**, the product with similar optical purity but opposite configuration was obtained. The fact that the rhodium atom and the chiral center(s) are separated by more than 12 covalent bonds discards a direct influence of the stereogenic centres on the selectivity outcome. Indeed, several control experiments and spectroscopic analyses demonstrated that the enantioselectivity arises from the formation of chiral helical polymers by self-association of the BTA monomers through noncovalent interactions. Performing the reaction with **^{Me}BTA^{PPh2}(*S*),(*S*)**, which has the same enantiopure side chains than **^{H}BTA^{PPh2}(*S*),(*S*)**, yields no

selectivity since this ligand is unable to form assemblies as the result of the alkylation of two over three of its amide functions. Mixing **^{H}BTA^{PPh2}(*S*),(*S*)** with a phosphine-free chiral BTA (**^{H}BTA(S)**) enhances the selectivity from 82% *e.e.* to 88% *e.e.* and a control experiment confirms that it is related to the formation of a co-assembly between these two monomers (Figure 21).[82] This result illustrates the possibility of tuning the selectivity of the reaction by simply mixing different types of complementary monomers. Further exploitation of the same platform for the design of sergeants-and-soldiers and majority-rules type catalysts is presented in II.3b.

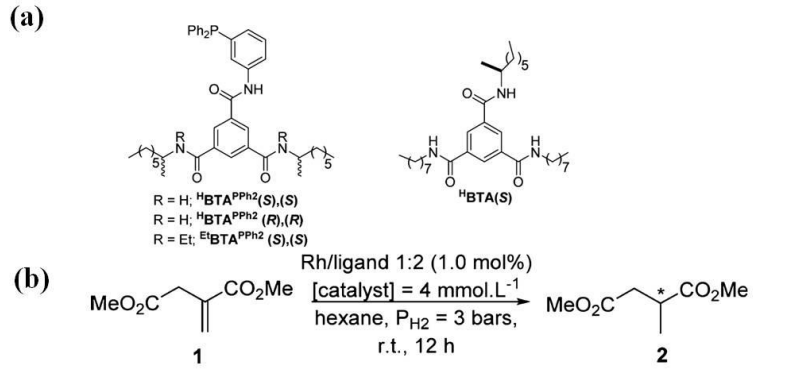

ligand	additive	e.e. (%)
^{H}BTA^{pph2}(*S*),(*S*)	no	82
^{H}BTA^{pph2}(*R*),(*R*)	no	-81
^{Et}BTA^{pph2}(*S*),(*S*)	no	0
^{H}BTA^{pph2}(*S*),(*S*)	^{H}BTA(*S*)	88

Figure 21 (a) Chemical structures of chiral BTA ligands and (b) their catalytic results in the rhodium-catalyzed asymmetric hydrogenation of dimethyl itaconate.[82]

The group of M. Liu group has developed a series of metal-coordinated nanotubes (M-HN) by coordinating metal centres to tubular self-assemblies formed by an L-glutamic acid terminated bolaamphiphile in water. The metal on the surface serves as a catalytic site, and thanks to the synergetic effect of the aligned multicatalytic sites, high reactivities and enantioselectivities were realized for different catalytic reactions. Like the BTA example mentioned above, the selectivity of the reaction and the configuration of the product are related to the optical purity and handedness of the M-HN, respectively. **Bi(III)-HN** proved to be very efficient for the asymmetric Mukaiyama aldol reaction (up to 97% *e.e.*) while up to 91% *e.e.* within 60 min was achieved in the asymmetric Diels−Alder reaction performed with **Cu(II)-HN** (Figure 22).[83-84]

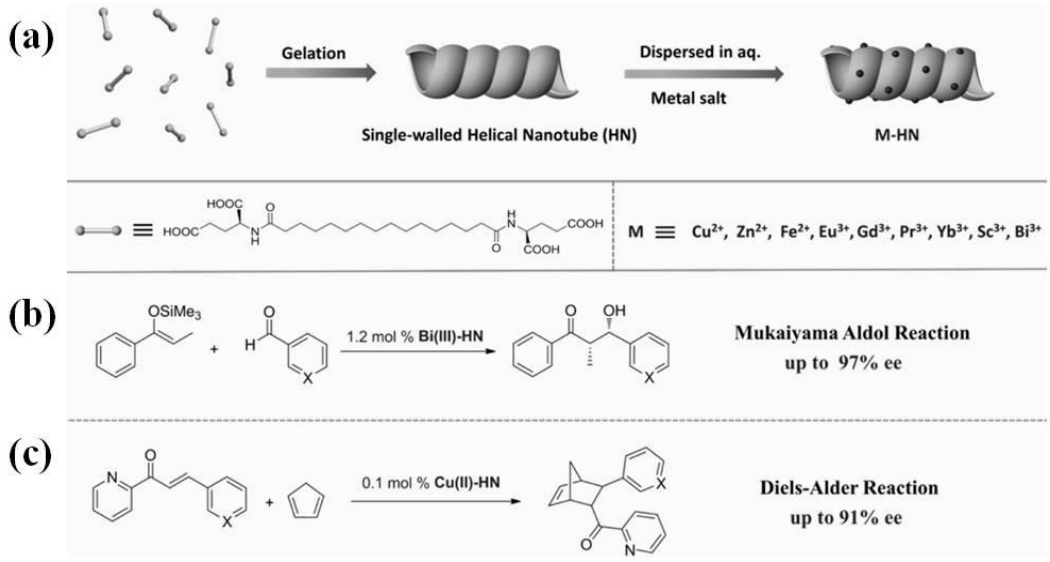

Figure 22 (a) Schematic representation of nanotube formation procedure: the bolaamphiphile terminated with L-glutamic acids was self-assembled through gelation first, which provided a larger amount of single-walled nanotubes. Subsequently, such nanotubes were dispersed into aqueous solutions containing various metal ions, yielding metal-functionalized helical nanotubes; (b) asymmetric Mukaiyama aldol reaction catalyzed by **Bi(III)-HN**; (c) asymmetric Diels−Alder reaction catalyzed by **Cu(II)-HN**.

II.3 Chirally-amplified helical catalysts (class C)

Alongside with optimizing reaction parameters (*e.g.* catalytic loading and selectivity), minimizing the cost of a catalytic process is desirable for practical applications. Along this line, harnessing asymmetric processes that get rid of or minimize the need of an enantiopure chemical species is currently under exploration by means of a variety of physical and chemical approaches.[85-86]

In the context of catalytic science, the term asymmetric amplification[87] almost exclusively refers to reactions whose enantioselectivity is higher than the one calculated by considering only the optical purity of the catalyst.[88-90] In other words, the apparent optical purity of the ligand or organocatalyst[91] is enhanced during the enantiodiscriminating step. Strong positive non-linear effects (NLE) are observed when a mixture of enantiopure ligands that is only slightly biased from the racemic mixture yields an enantioenriched product. The study of NLE emerged as a powerful mechanistic tool to probe the nature of the active species, mainly in the context of asymmetric organometallic reactions.[92] Alternatively, chiral non-racemic additives are commonly employed to perform asymmetric reaction with otherwise racemic catalysts.[93-94] As an extreme case of

asymmetric amplification, the Soai reaction produces a highly enantioenriched pyrimidyl alkanol from addition of diisopropylzinc to the respective aldehyde in presence of a nearly racemic seed or of various chiral environments.[95-96] The formation of tetramer or higher oligomer structures might explain the incredibly high level of amplification observed in this reaction[97] and in related autocatalytic (or autoinductive) asymmetric processes.[98-99]

In the conclusion of his seminal review on chirality amplification in macromolecules in 1999,[37] M. Green questioned whether it can be envisaged to "design a catalytic helical polymer directed to asymmetric synthesis in which the enantiomeric excess of the products were independent, over a wide range, of the enantiomeric excess of the units making up the polymer?". Herein, we will show that indeed, a range of helical covalent and supramolecular catalytic polymers[100] have been developed which deliver optically-active products with a selectivity that is, in a certain range, neither related to optical purity of the monomers nor to the number of chiral units constituting the helix. The necessary condition for such an achievement is that *intrinsically achiral catalytically-active* monomers, instead of *chiral non-racemic catalysts* in the case of NLE, are embedded in a helical macromolecule. The following section will thus comprehensively cover helical catalysts built on a chirally-amplified scaffold, *i.e.* those classified as C in Figure 13. Examples illustrating these criteria will be sorted firstly according to the covalent or non-covalent nature of their scaffolds, secondly by the method (C1-C4) implemented to control the handedness of the helix and finally by the chemical nature of the macromolecule (see the used nomenclature in Figure 23).

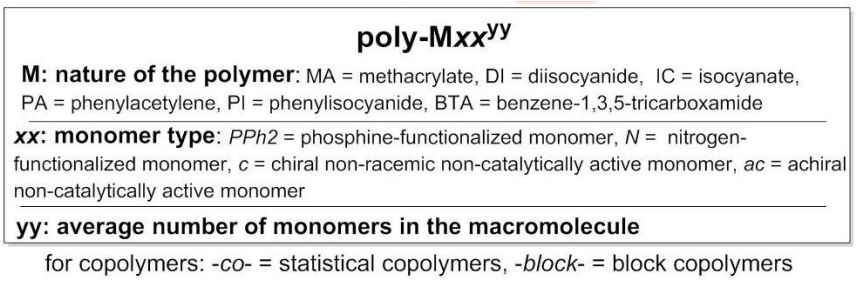

Figure 23 Nomenclature used in this section for the different types of chirally-amplified helical catalysts

II.3.a Chirally-amplified covalent polymer catalysts

Through asymmetric polymerization (C1)

Reggelin and co-workers investigated in 2002 the possibility of using polymethacrylates (poly-(MA)s) as scaffolds for asymmetric reactions. MA monomers with pyridine rings were

polymerized with a mixture of **DPEDA/(+)-PMP/*n*-BuLi** yielding poly-(MA)s which were optically active even though they were initiated by the achiral DPEDA moiety (Figure 24).[101-103] Upon mixing with a Pd precursor, these helical polymers catalyzed an allylic substitution reaction with good activity but modest enantioselectivity.[101] The most efficient catalyst of this series was obtained by copolymerization of MA*N* and TrMA. The 1:1 copolymer**, poly-(MA*N*^{35}-*co*-TrMA^{30})**, yielded the product of the substitution reaction with 60% *e.e.*.[102] These seminal studies demonstrated that, in the ideal case, multiple homochiral catalytic sites might be generated from one chiral inducer thus amplifying the number of chiral catalytic units. However, the limited conformational stability and the difficult functionalization of the poly-(MA) backbone seriously limited the scope and efficiency of this class of polymer catalysts.[102-103]

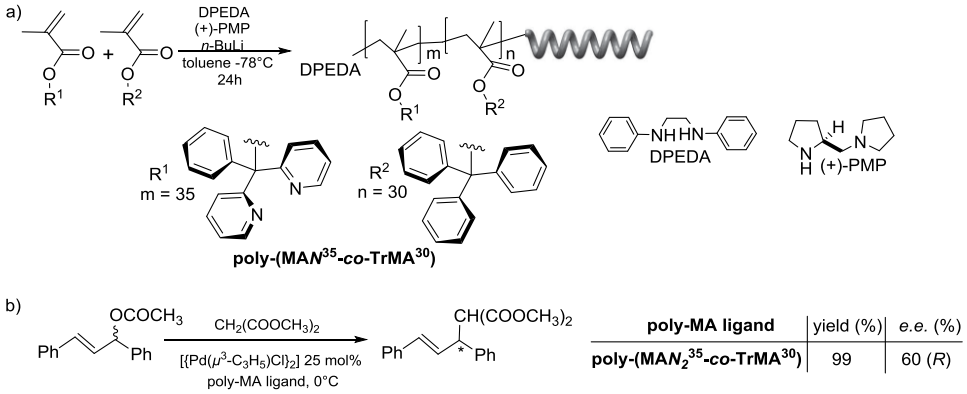

Figure 24 Asymmetric Pd-catalyzed allylic substitution reaction with a catalytic helical poly-(MA).[102] a) Synthetic scheme for the preparation of a catalytic poly-(MA) by asymmetric polymerization and its formula. b) Result obtained in the allylic substitution reaction. The handedness of the helical catalyst has not been determined.

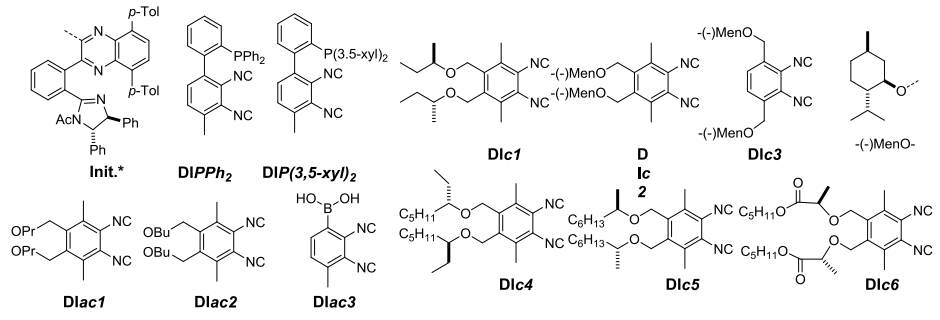

Figure 25 Chemical structures of the chiral initiator and the DI monomers used to prepare the PQX ligands mentioned throughout part II.3.a.

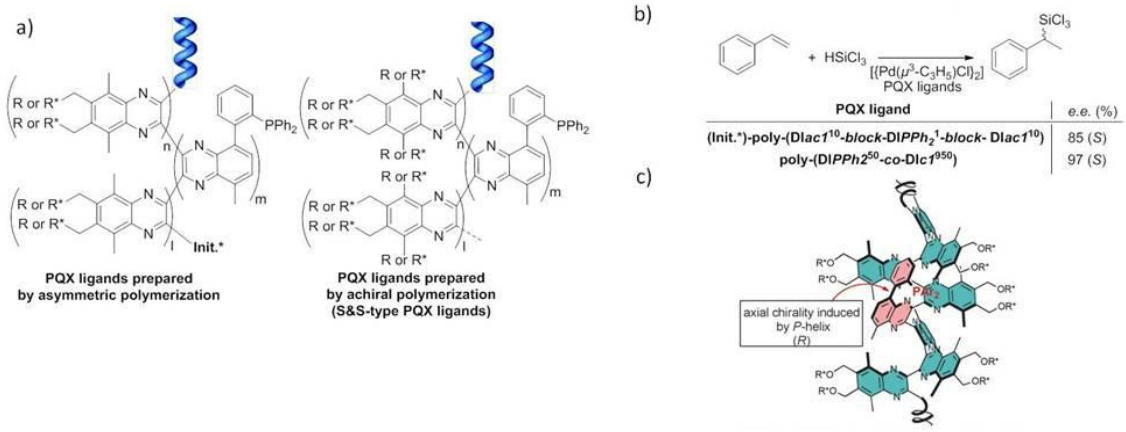

Figure 26 Asymmetric palladium-catalysed hydrosilylation of styrene with PQX ligands.[104-105] a) General formula of the PQX ligands (see the chemical structures of all monomers in Fig.19). b) Result obtained in the hydrosilylation reaction. c) Proposed stereochemical model for the transfer of chirality (central to helical to axial) in PQX ligands.

In 2009, building on well-established procedures for the helix-sense selective and living polymerization of diisocyanide (DI) monomers, Suginome and co-workers[44, 106] reported on the co-polymerization of the phosphine-functionalized monomer DI*PPh*$_2$ and non-functionalized monomer DI*ac1* in the presence of a chiral organopalladium initiator, Init.*Pd(PPhMe$_2$)I (Figures 25a and 26a).[104] Poly(quinoxaline-2,3-diyl) (PQX) block copolymers of the type (Init.*)-poly-(DI*ac1-block*-DI*PPh*$_2$*-block*-DI*ac1*) were prepared which differed by the number of units of the different blocks. In spite of the presence of a single chiral unit located at the extremity of the polymer chain, the resulting copolymers exhibited a stable helical conformation (at r.t.) and a preferred handedness as quantified by a screw-sense excess[107] superior to 90%. Copolymers with a single phosphine unit surrounded by two DI*ac1* blocks provided the best result in the presence of a palladium precursor for the hydrosilylation of styrene (Figure 26b) and styrene derivatives (up to 98% yield and 87% *e.e.*). The stereochemical direction of the catalytic reaction is fully controlled by the handedness of the polymers as demonstrated by similar selectivity but opposite configuration of the products obtained by (*P*)- and (*M*)-PQXs. These results were remarkable both in terms of the level of enantioinduction achieved in an asymmetric reaction with helical polymers and the extent of chirality amplification since a single chiral group was enough to control the chiral conformation of 21 achiral units including one that was catalytically active. The high enantiodiscrimination ability of this family of PQX ligands had been attributed to efficient chirality transfer between the helical polymer main chain and the axis of chirality supporting the PPh$_2$ group (Figure 26c).[105, 108]

Polymers with high molecular weights are required not only for facilitating their recycling and reusability but also for exalting their chiral amplification properties. However, chiral initiators usually fail to control the handedness of long polymer chains and even for the relatively short ones, the helical induction might not be optimal. For instance, a 1000 mer-based random copolymer of DI*PPh*$_2$ and DI*ac1*, (Init.*)-poly-(DI*PPh*$_2^{50}$-*co*-DI*ac1*^{950}), which only had the chiral terminal group as a source of screw-sense induction was a poorly selective ligand.[105] A more suitable strategy to generate high-molecular-weight and single-handed PQX ligands relies on mixing achiral and chiral monomers, through the sergeants-and-soldiers approach.

Through the S&S and dilute MR effects (C2 and C3)

Living polymerization reactions between achiral catalytically active monomers (the soldiers) and chiral non-racemic catalytically inactive monomers (the sergeants) constitute a facile and easily tunable method for the preparation of dynamic helical catalysts. One important challenge in this strategy is to maintain a good level of enantioinduction because any achiral catalysts that will not be located in the chiral environment provided by the helical polymer scaffold will significantly decrease the selectivity of the reaction. Seminal studies on the induction of a stable and single helical configuration by means of a few percent of sergeants traced back to 1989.[42] However, it is only recently that efficient sergeants-and-soldiers (S&S) type helical polymers for asymmetric catalysis had been disclosed in the literature.

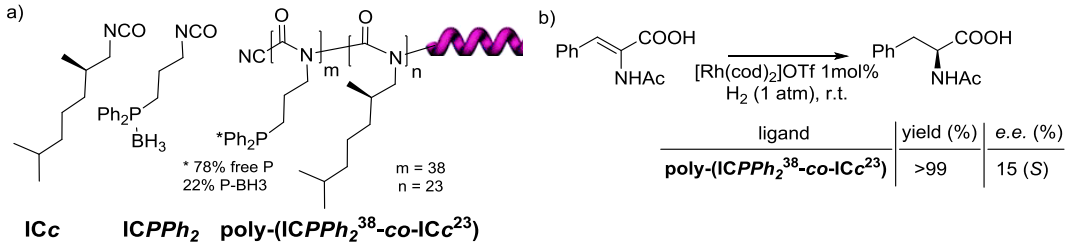

Figure 27 Asymmetric rhodium-catalysed hydrogenation catalyzed by a S&S-type helical poly-(IC)s.[102] a) Chemical structure of the IC monomers and of the polyisocyanate ligand. b) Result obtained in the hydrogenation reaction.

Green and co-workers demonstrated that 15% of a chiral non-racemic isocyanate monomer (IC*c*, sergeant) was enough to get single handed polyisocyanate when co-polymerized with an achiral isocyanate monomer (soldier).[42] In 2004, Reggelin and co-workers attempted to design a catalytic version of these S&S-type polymers by mixing IC*c* with a phosphine-functionalized monomer (IC*PPh*$_2$, Figure 27). When coordinated to rhodium, polymer poly-(IC*PPh2*^{38}-*co*-IC*c*^{23})

proved to catalyze the hydrogenation of *N*-acetamidocinnamic acid efficiently (conversion>99%) but with low enantioselectivity (15% *e.e.*).[102]

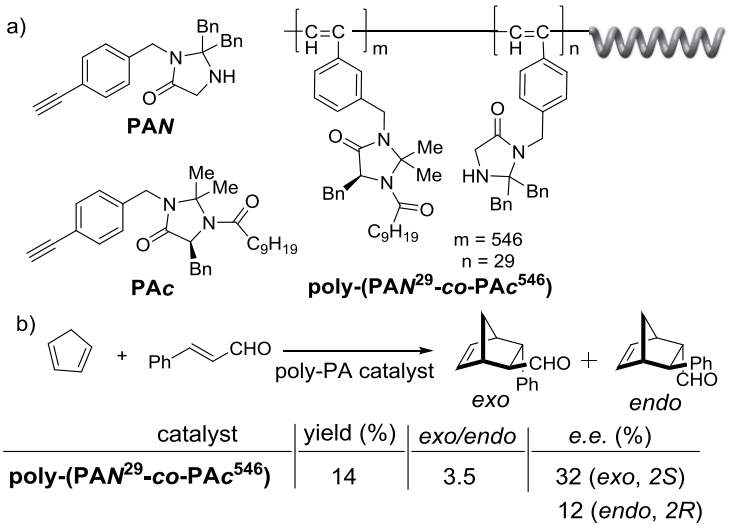

catalyst	yield (%)	*exo*/*endo*	*e.e.* (%)
poly-(PA*N*^{29}-*co*-PA*c*^{546})	14	3.5	32 (*exo*, *2S*) 12 (*endo*, *2R*)

Figure 28 Asymmetric Diels-Alder reaction catalysed by S&S-type helical poly-(PA)s.[109] a) Chemical structure of the PA monomers and of the polyacetylene catalyst. b) Result obtained in the Diels-Alder reaction. The handedness of the helical catalyst has not been determined.

More recently, Yashima and co-workers prepared a range of helical poly(phenylacetylene)s, poly-(PA)s, composed of chiral and achiral PA monomers endowed with different imidazolinone side chains.[109] The achiral monomer contained a basic secondary amine which is known to activate carbonyl compounds while the chiral monomer embedded a cyclic tertiary amide moiety and was thus catalytically inactive. After screening the influence of the structure of a range of monomers on the rate and selectivity of a Diels-Alder reaction of reference, they established that the random copolymers incorporating achiral PA*N* and chiral non-racemic PA*c* monomers provided the best enantioselectivity (Figure 28). Poly-(PA*N*^{29}-*co*-PA*c*^{546}) with 95% of PA*c* furnished the Diels-Alder adduct with unusual *exo* selectivity (*exo*/*endo*=3.5) and modest enantioselectivities (32% *e.e.* and 12% *e.e.* for *exo* and *endo* products, respectively). The non-helical version of this copolymer, obtained upon isomerization of the PA backbone upon grinding, was almost non-selective which demonstrated that the macromolecular helicity (not the chiral side chains) dictated the selectivity outcome of the reaction. Lowering the fraction of chiral monomers in the copolymer resulted in a non-linear decrease of the enantioselectivity, yet the highest enantioselectivity was obtained for the copolymer containing 95% of chiral monomers.

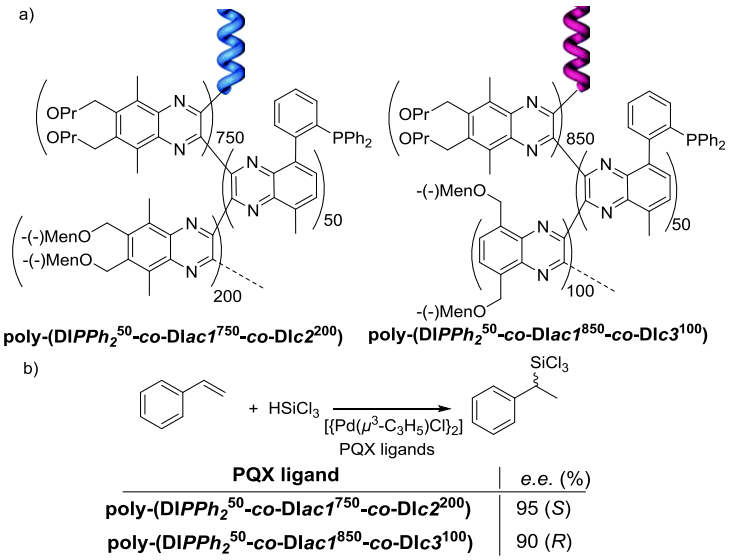

Figure 29 Asymmetric palladium-catalysed hydrosilylation of styrene with PQX ligands derived from (−)-menthol.[110] a) Structure of the PQX ligands. b) Result obtained in the hydrosilylation reaction.

Far higher degree of enantioselection has been reported with sergeants-and-soldiers type PQXs ligands. A 1000 mer-based PQX ligand obtained by polymerization of DI*PPh2* (5%) and DI*c1* (95%) with an achiral organonickel initiator furnished the hydrosilylation product with 97% *e.e.* (Figure 26b).[105] A related PQX ligand with only 5% of DI*c1* was still significantly selective (70% *e.e.*). This demonstrated a good control of the handedness of the helix by a small fraction of sergeants in these S&S-type PQX ligands. Co-polymers of the type poly-(DI*PPh2*^{50}-*co*-DI*c1*^{950}), *i.e.* with 95% of chiral units and 5% of phosphine-functionalized units, were investigated in different catalytic reactions. In addition to the above-mentioned hydrosilylation reaction,[105, 111] they proved to be remarkably selective as ligands for palladium-catalyzed asymmetric Suzuki-Miyaura reactions[108, 112-113] (up to 98% *e.e.*) and arylative ring-opening of 1,4-epoxy-1,4-dihydronaphthalene (up to 94% *e.e.*).[114] In the silaborative cleavage of *meso*-methylenecyclopropanes[115] (up to 97% *e.e.*), these PQXs ligands provided comparable or higher selectivities than known discrete chiral ligands. Changing the nature of the catalytically active monomer to a nitrogen-containing unit extended the scope of these PQX catalysts towards other asymmetric metal-catalyzed reactions[116] or organocatalytic reactions.[117]

The influence of the chemical nature of sergeants on the optical purity of the resulting PQXs has been precisely probed with the aim of intensifying the extent of chirality amplification and the dynamic nature of PQX ligands.[118] Notably, improved levels of chirality amplification were reported for DI sergeants having a (−)-menthol moiety located at the 6- and 7-positions (DI*c2*) or at

the 5- and 8-positions (DI*c3*) of the quinoxaline ring (Figure 29).[110] CD spectroscopy analyses revealed that polymers incorporating DI*c2 or* DI*c3* adopt opposite handedness even though these sergeants possess the same chiral moiety. The PQX ligand, poly-(DI*PPh2*^{50}-*co*-DI*ac1*^{750}-co-DI*c2*^{200}), with only 20% of sergeants units, adopted a pure (*P*)-helical conformation and provided the (*S*) hydrosilylation product with 95% *e.e.* Consistently with the CD data, the (*R*)-hydrosilylation product was the main enantiomer when the reaction was conducted with the PQX ligands containing DI*c3* sergeants. Likewise, the enantioselectivity of the hydrosilylation reaction was precisely probed as a function of the fraction of DI*c3* in these PQX ligands. Despite the fact that the helical backbone required 15% of DI*c3* to adopt an absolute (*M*)-helical configuration, the selectivity was found to be maximal (90% *e.e.*) for 10% of DI*c3* and then decreased for PQX ligands having higher ratios of DI*c3*. This intriguing effect was attributed to disorder of the helical structure induced by the sergeant and more precisely by the bulkiness of the chiral groups at the 5- and 8-positions.

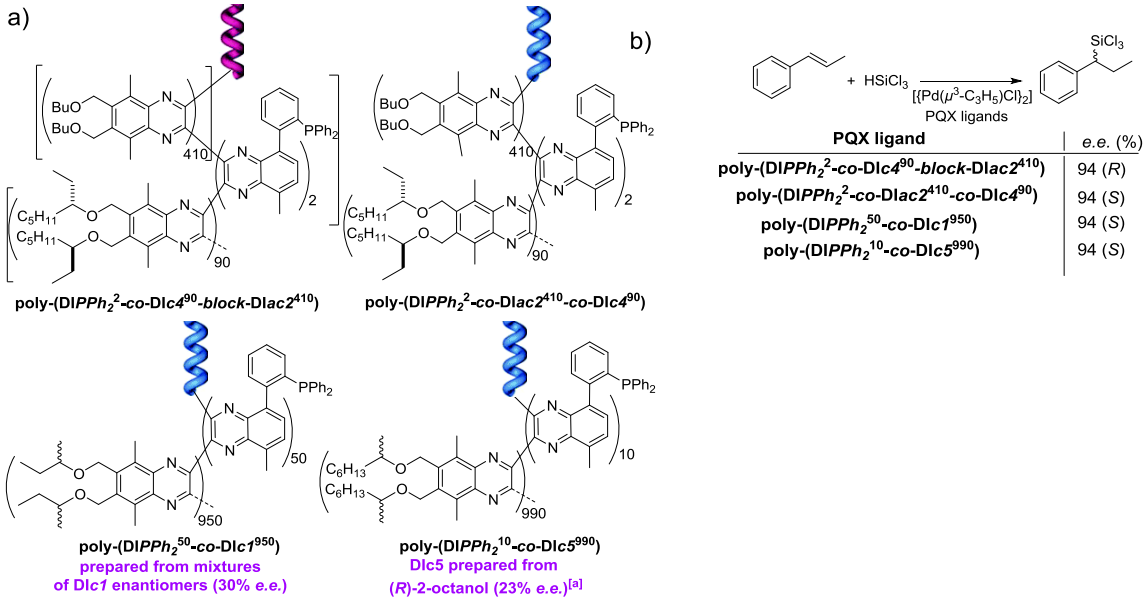

Figure 30 Asymmetric palladium-catalysed hydrosilylation of □-methylstyrene with S&S- (a) and MR-type (b) PQX ligands.[119-120] [a] DI*c5* is a mixture of the *d*, *l*, and *meso* isomers in a ratio of 38.8 : 15.8 : 45.4, respectively.

Further work revealed that, for the same sergeant, the handedness of PQX helix can be controlled by its fraction and position in the co-polymer. 100 mer-based random copolymers of DI*c4* and DI*ac2* exhibited a single handed (*P*)-helix with 16%-20% of DI*c4* and a pure (*M*)-helix with more than 60% of DI*c4*.[119] Such an abnormal S&S effect[121] occurs when the preference of screw-sense induction of the sergeant depends on the nature of monomer units (sergeants or soldiers) in its immediate vicinity. This phenomenon was thus exploited to control the handedness of the PQX ligand by changing solely the sequence of the sergeants and soldiers. Two PQX ligands were

prepared which both contained 18% of sergeants but distributed differently along the PQX main chain (Figure 30). The palladium complexes of the random PQX ligand, poly-(DI*PPh*$_2$^{2}-*co*-DI*a*$_2$^{410}-*co*-DI*c4*^{90}), and of the block PQX ligand, poly-(DI*PPh*$_2$^{2}-*co*-DI*c4*^{90}-*block*-DI*a2*^{410}), furnished the (*S*) and (*R*) hydrosilylation product of methylstyrene, respectively, with the same selectivity (94% *e.e.*, Figure 30).

Chirality-amplification in PQX ligands was also achieved by means of non-racemic mixtures of enantiopure sergeants (diluted MR effect). A 1000 mer-based PQX ligand was found to adopt an almost absolute (*P*)-helical configuration even though the optical purity of DI*c1* was as low as 30% *e.e.* (biased in favor of the (*R*,*R*)-enantiomer, Figure 30).[120] As a result of the chirally-amplified nature of its scaffold, this PQX ligand promoted the palladium-catalysed hydrosilylation of β-methylstyrene with excellent enantioselectivity (94% *e.e.*). In addition, a monomer with 2-octyloxymethyl side chains, DI*c5*, was prepared from 23% *e.e.* (*R*)-2-octanol, a readily available enantio-enriched mixture of alcohols, and used as a non-optically pure chiral inducer. The resulting PQX ligand, poly-(DI*PPh*$_2$^{10}-*co*-DI*c5*^{990}) exhibited excellent enantioselectivities in both the palladium-catalysed hydrosilylation of □-methylstryrene (94% *e.e.*, Figure 29) and the Suzuki-Miyaura coupling between dimethoxyphosphinyl-substituted 1-naphthyl bromide and 1-naphthaleneboronic acid (93% *e.e.*). These results highlighted the possibility of using a single chiral source with low *e.e.* value to generate highly selective helical catalysts.

By addition of chiral additives (C4)

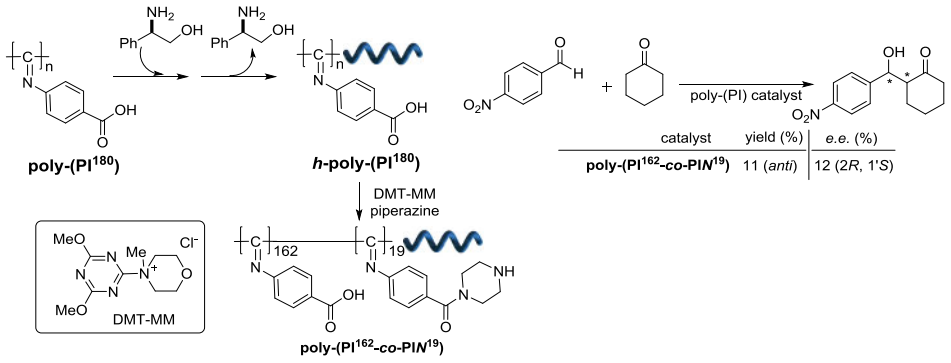

Figure 31. Asymmetric aldol reaction promoted by poly-(phenyl isocyanide)s with memorized helicity.

Chiral additives, that are not part of the polymer main chain, can also be employed to impose a preferred handedness to covalent macromolecules. Removal of these additives may not be accompanied by racemization of the main chain at the condition that the helicity is kinetically locked (chiral memory effect). Yashima and co-workers demonstrated that such phenomena are operative

for poly(4-carboxyphenyl isocyanide), poly-(PI), a racemic helical polymer that folds into a single-handed helix upon induction by an optically-active amine in water.[45] After removal of the chiral inducer, *h*-poly-(PI^{180}) (*h* stands for memorized chiral *h*elix) retains its helicity during a timescale that allows for its derivatization (Figure 31). The acidic groups of poly-(PI^{180}) served to introduce various amounts of piperazine (PI*N*) functions at the periphery of the polymer.[122] Importantly, no significant racemization of the helix occurred during the functionalization process. Poly-(PI^{162}-*co*-PI*N*^{19}), which contained ≈ 10% of piperazine units for activation of ketones, promoted the aldol reaction between cyclohexanone and 4-nitrobenzaldehyde with modest enantioselectivity (12% *e.e.*, *anti* isomer). Yet, this example exploits the unique ability of some macromolecular helices to amplify and retain their inherent chirality in order to support catalytic centres that can be employed to produce optically-enriched compounds.

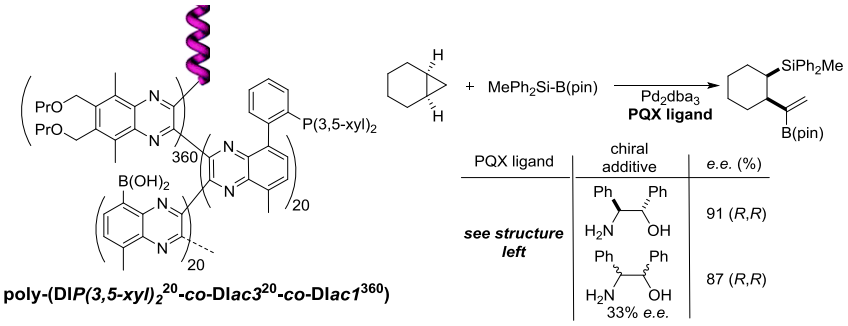

Figure 32 Asymmetric palladium-catalysed silaborative C−C bond cleavage of *meso*-methylenecyclopropane with a combination of a PQX ligand and a chiral additive.[123]

Condensation of chiral additives, such as diols, diamines and amino alcohols, to the boronic acid side chains of PQX polymers successfully induced a preferred handedness to the polymer main chain.[123] A polymer endowed with both boronyl (5%, DI*ac3*) and 2-[bis(3,5-dimethylphenyl)phosphino]phenyl pendants (5%, DI*P(3,5-Xyl)$_2$*) was designed as a PQX ligand with a dynamic helical backbone (Figure 32). This PQX ligand and (*S*,*S*)-2-amino-1,2-diphenylethanol, the chiral inducer, proved to be the combination of choice for the palladium-catalysed silaborative C−C bond cleavage of *meso*-methylenecyclopropane (91% *e.e.*). Since this result was achieved with only 1 equivalent of chiral inducer per 19 achiral units (including 1 boronyl pendant), it means that chirality amplification was strongly operative in this PQX ligand. A similar experiment was performed with the same ligand but by adding a non-optically pure mixture of 2-amino-1,2-diphenylethanol enantiomers as chiral additives (33% *e.e.*, 10 equiv. per boronic pendants). The reaction also proceeded selectively albeit the *e.e.* was slightly lower (87% *e.e.*). In these examples, the chiral additives constitute an alternative to enantiopure monomers for controlling and amplifying the main chain chirality of the helical catalyst.

II.3.b Chirally-amplified supramolecular polymer catalysts

As mentioned in part I, impressive efforts have been made in the control of the chirality of supramolecular polymers, notably by means of the S&S and MR effects.[41, 47, 124] However, asymmetric catalytic reactions whose enantioselectivity is solely controlled by the helicity of the supramolecular polymers have only been reported by the groups of Liu[125-128] and Raynal[34, 129-131] and only the latter has investigated chirally-amplified assemblies in that context.

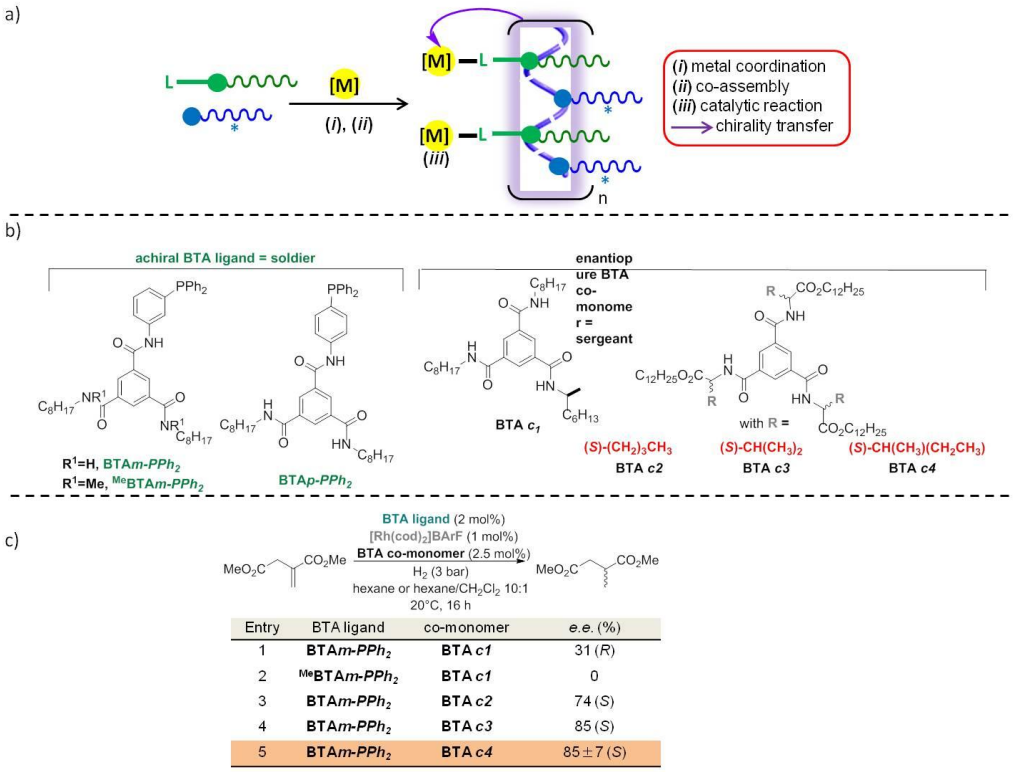

Entry	BTA ligand	co-monomer	*e.e.* (%)
1	BTA*m-PPh*$_2$	BTA *c1*	31 (*R*)
2	^{Me}BTA*m-PPh*$_2$	BTA *c1*	0
3	BTA*m-PPh*$_2$	BTA *c2*	74 (*S*)
4	BTA*m-PPh*$_2$	BTA *c3*	85 (*S*)
5	BTA*m-PPh*$_2$	BTA *c4*	85±7 (*S*)

Figure 33. Asymmetric metal-catalysed reactions with supramolecular helical catalysts. a) Schematic representation of the preparation and mode of action of S&S type non-covalent helical catalysts. b) Chemical structures of the BTA monomers. c) Result in the asymmetric rhodium-catalysed hydrogenation of dimethyl itaconate.[34, 129]

The ability of benzene-1,3,5-tricarboxamide (BTA) molecules[132] to predictably assemble into robust threefold hydrogen-bonded helical assemblies in apolar solvents was exploited to control the handedness of supramolecular helical BTA catalysts (Figure 33a). The combination of the achiral monomer **BTA**$^{m\text{-}PPh2}$ (Figure 33b) and the enantiopure but phosphorus-free BTA monomer, **BTA*c1***, in a 1:1.25 ratio, proved to be slightly selective for the rhodium-catalysed hydrogenation of dimethyl itaconate (31% *e.e.*, Figure 33c).[129] Similarly to the control experiments performed with the chiral ligand (part II.2.c) the reaction performed with an analogue of **BTA**$^{m\text{-}PPh2}$that is unable to self-

assemble (**^{Me}BTA$^{m\text{-}PPh2}$**), showed no selectivity under the same conditions which demonstrates that the observed enantioselectivity, albeit modest, stems from the helical nature of the co-assembly formed between **BTA$^{m\text{-}PPh2}$** and **BTA*c1***. The role of BTA*c1* in these co-assemblies is thought to be similar to the role of a sergeant in the S&S-type covalent helical catalysts mentioned above.

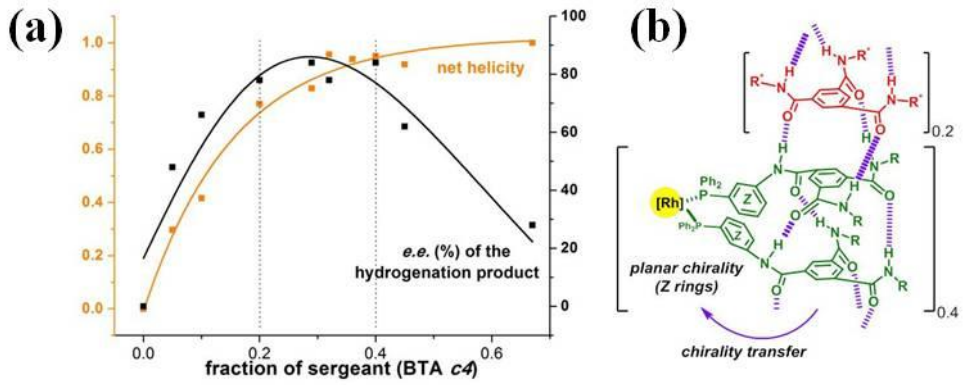

Figure 34. S&S type supramolecular helical BTA catalysts. (a) Plot of the selectivity and net helicity as a function of the amount of **BTA*c4*** in the catalytic mixture. and (b) Schematic representation of the selective S&S type helical catalyst. [34]

BTA derived from α-amino esters[35, 133-137] were found to be far more efficient sergeants than BTA*c1*. The selectivity was remarkably increased for the same catalytic reaction when BTA*m-PPh$_2$* was mixed with 1.25 equivalent of the BTAs derived from norleucine (**BTA*c2***, 74% *e.e.*), valine (**BTA*c3***, 85% *e.e.*) or isoleucine (**BTA*c4***, 85% *e.e.*).[34] Likewise, the amount of **BTA*c4*** in the catalytic mixture was varied (Figure 34). For mixtures with a minority of sergeants, the selectivity of the reaction increased non linearly and reached a plateau corresponding to the optimal selectivity for the mixture with *ca.* 20% of **BTA*c4***. It means that one molecule of sergeant is sufficient to induce a chiral environment to four achiral ligands (or two rhodium catalytic centres). A series of spectroscopic and scattering analyses confirmed the formation of a chirally-amplified co-assembly with a single BTA molecule in the cross-section for this mixture. The major enantiomer and the selectivity of the catalytic reaction are thus related to the handedness and the net helicity of the co-assemblies, respectively. It is worth mentioning here that the chirally-amplified PQX asymmetric catalysts mentioned in the preceding section (Figure 29) require the use of an achiral monomer acting as a spacer between the catalytic sites and thus the amount of sergeant in these systems is actually *larger* than the catalytic loading. The supramolecular asymmetric catalyst built on the BTA scaffold thus constituted the first example in which a *substoichiometric* amount of a chiral inducer relative to the achiral ligand can be used without eroding the stereoselectivity of the catalytic reaction. Conversely, the selectivity noticeably decreased for mixtures containing a higher content of

enantiopure co-monomer (≥ 60%). However, CD analyses showed that the helices were still single-handed which discarded the occurrence of an abnormal S&S effect as mentioned above for PQX ligands. We postulated that this erosion of selectivity was rather due to a change in the coordination mode of the supramolecular ligand: from a selective chelating ligand in low-content **BTA*c4*** mixtures (see a representation in Figure 34) to poorly selective bridging ligand in high-content sergeant mixtures. This change in the coordination mode of the ligand is a consequence of the dynamic nature of this class of hydrogen-bonded catalysts. However, further exploitation of the dynamic properties of this class of supramolecular catalysts, *e.g.* for the design of a switchable asymmetric catalyst, has not been demonstrated at this stage.

II.4 Switchable asymmetric catalysts built on a helical scaffold

With the development of modern organic chemistry and the demanding synthesis of complex molecules, the field of artificial switchable catalysis has attracted huge interests for chemists, not only for mimicking the high performance of enzymes, but also for the design of smart materials. Upon exposure to certain stimuli (such as light, pH, redox potential and chemical additives), switchable catalysts could undergo reversible conformational change, offering the possibility to control activity and chemo-/regio-/stereo-selectivity.[138-139] Among different stimuli-responsive catalysts reported to date, few examples of predictable switchable enantioselective catalysts have been reported. Dual control of enantioselectivity with a single catalyst is important for asymmetric reactions, since it avoids the synthesis of catalyst with opposite handedness and facilitates the preparation of molecules containing more than two stereocentres.[65]

Their dynamic properties make helices good candidates for the design of switchable asymmetric catalyst, since in some cases their helical twist (*P* and *M*) can be tuned or switched. For example, Feng's group synthesised phenylalanine-based helices, whose handedness can be controlled by pH (*M* for pH≥7, *P* for pH<7).[140] Feringa and co-workers constructed double-stranded helicates based on molecular motors functionalized with oligobipyridyl ligands. Upon exposure to light, the helical structure could be switched between oligomers and double-stranded helicates with opposite handedness.[141] However, few examples of switchable catalysts with a helical scaffold have been reported. The following part will show that PQX helical catalysts constitute a unique class of predictable and efficient switchable asymmetric catalysts.

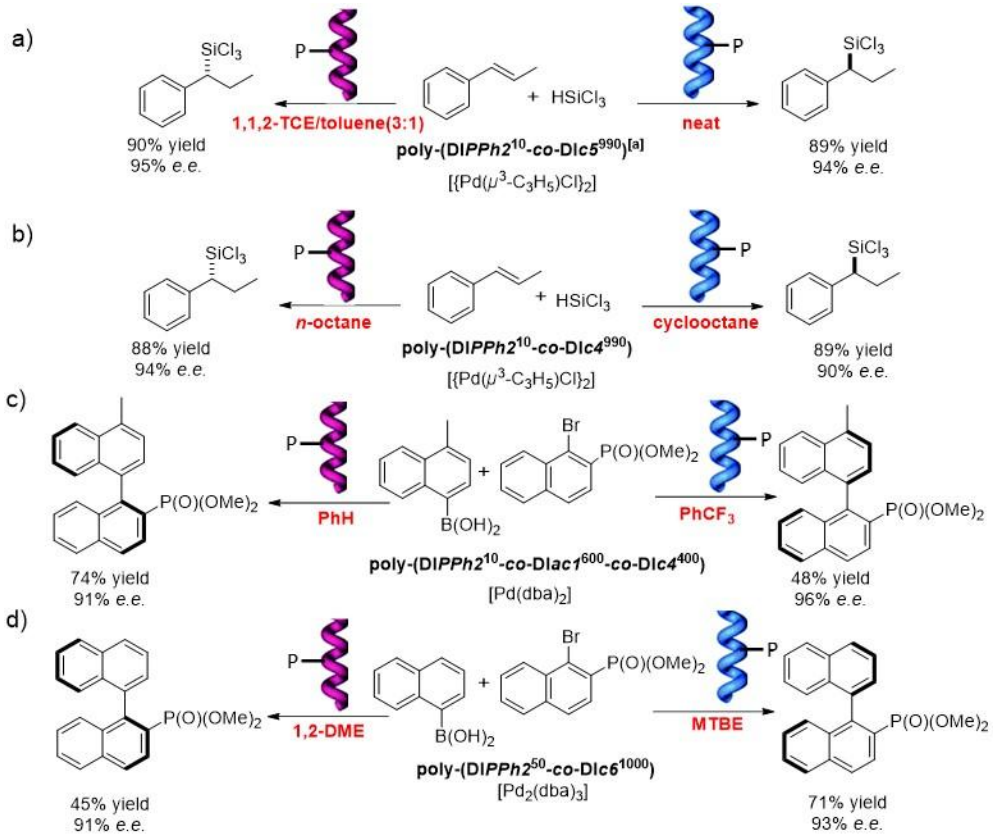

Figure 35 Selectivity-switchable PQX ligands triggered by the solvent. a)[105]; b)[142]; c)[143]; d)[144] [a] DI*c5* is a mixture of the *d*, *l*, and *meso* isomers in a ratio of 38.8 : 15.8 : 45.4, respectively.

As a consequence of the conformational flexibility of their main chain, a range of helical macromolecules undergo a reversible switch of their handedness upon activation by various chemical or photophysical stimuli.[40-41] The helical backbone of PQXs is particularly prone to stereochemical inversion since bidirectional induction had been achieved by changing the position of the chiral moiety on the quinaxoline ring (Figure 29)[110] by modifying the structure of the soldier[119] or the sergeant,[118] by controlling the sequence of the monomers (Figure 30a),[119] or by the solvent.[105, 108, 110-113, 115-118, 145-147] The use of the solvent effect[148] to switch the main helical sense of PQX-based catalysts offers the possibility to predictably produce both enantiomers of a reaction starting from the same chiral catalyst.

Based on the initial finding that PQXs bearing chiral (*R*)-2-butoxymethyl side chains adopt pure but opposite screw senses in $CHCl_3$ and 1,1,2-trichloroethane (TCE),[146] switchable PQX ligands were prepared by co-polymerization of DI*PPh*$_2$ and DI*c1*. Helical inversion to (*M*)-helix occurred upon heating a solution of the as synthesized (*P*)-helical ligands in TCE/THF or TCE/toluene. Full inversion of the handedness of the PQX ligand resulted in the highly enantioselective production of both enantiomers in a range of catalytic reactions.[105, 108, 113, 115-117]

Interestingly, the MR-type PQX ligand mentioned in Figure 29a with a highly chirally-amplified helical backbone also exhibited inversion of the selectivity in these solvent mixtures (Figure 35a).[120]

The need of halogenated solvents somewhat impedes the general applicability of the PQX ligand, notably for metal-catalyzed cross-coupling reactions, and thus PQXs which can invert their handedness in other solvents have been developed. An important element of design is the nature of the chiral monomer. Poly-(DI*c1*^{100}) showed no inversion of its helicity in alkanes while poly-(DI*c4*^{100}) adopted a (*P*)- or (*M*)-helix in cyclooctane and *n*-octane, respectively.[111] Consequently, the PQX ligand incorporating 99% of DI*c4* and 1% of DI*PPh*$_2$ yielded both enantiomers in the hydrosilylation of styrene depending on the nature of the alkane solvent selected to conduct the reaction (Figure 35b). When considering S&S-type PQXs, the selection of the soldier was also found to be crucial for the observation of the solvent-induced reversal of selectivity. Poly-(DI*c4*^{5}-*co*-DI*ac2*^{100}) adopted exclusively a (*P*)-helical conformation in various aromatic solvents. Conversely, poly-(DI*c4*^{5}-*co*-DI*ac1*^{100}), which contains the same sergeants but a different soldier, exhibited opposite handedness in benzene ((*M*)-helix) and $PhCF_3$ ((*P*)-helix).[145] This result was exploited to design a PQX ligand mainly composed of DI*c4*^{5} and DI*ac1*^{100} and with only 1% of DI*PPh*$_2$ in order to maintain the solvent effect. This S&S-type PQX ligand, poly-(DI*PPh2*^{10}-*co*-DI*ac1*^{600}-*co*-DI*c4*^{400}), promoted the palladium-catalyzed Suzuki-Miyaura reaction shown in Figure 35c with high and opposite enantioselectivities in benzene (91% *e.e.*, (*R*)-product) and $PhCF_3$ (96% *e.e.*, (*S*)-product).

Such a stereochemical inversion of the catalytic outcome by the solvent is particularly valuable when the chiral catalyst is derived from a naturally occurring chiral compound. The PQX homopolymer derived from $_L$-lactic acid, poly-(DI*c6*^{40}), was found to be right-handed in MTBE and left-handed in a range of other ether solvents.[112] The PQX ligand incorporating 95% of DI*c6*, poly-(DI*PPh2*^{50}-*co*-DI*c6*^{1000}), adopted almost absolute (*M*)- and (*P*)-helical structures in 1,2-DME and MTBE, respectively, and thus furnished both enantiomers in the Suzuki-Miyaura coupling shown in Figure 35d when the reaction was performed in these solvents.

III Objectives of the project

As mentioned above, chirality induction, chirality amplification, and reversibility are key features of dynamic helices, and the implementation of these properties in the field of asymmetric catalysis have attracted much interest. High level of enantioselectivity has notably been obtained for catalysts located at the periphery of the helical scaffold of PQX covalent polymers and of BTA supramolecular polymers. The fact that the extent of enantioinduction and the configuration of the product of the catalytic reaction are related to the net helicity and handedness, respectively, of these

helical catalysts paves the way towards various unique potential applications for this class of catalysts. In particular, our group is interested in developing the switchability and chirality amplification properties of BTA helical catalysts.

A solvent effect has been reported for PQX ligands which allowed switching the handedness of the ligand, *prior to catalysis*, in order to obtain both configuration of the product of the reaction from the same catalytic system. However, this class of PQX catalyst loses their dynamic properties when coordinated to a metal centre [149] and thus, switching their handedness during the course of the catalytic reaction cannot be envisaged. In fact, controlling the enantiomeric state of a single catalyst *in situ* is a current challenge in particular for metal-catalyzed reactions since the presence of the metal center may impede the efficiency and the dynamics of the chiroptical switch. Inverting the enantioselectivity of a single catalyst during a reaction presents promising perspectives of using such a catalyst to select the desired diastereoisomer in one pot stereoselective cascade reactions[150-151] or to control the tacticity of stereoblock copolymers.[152-153] Based on our previous design of catalysts supported on BTA supramolecular helices, the **first objective** of this thesis is to implement a strategy which allows to tune and control *in real time* the enantioselectivity of a catalytic reaction. Two strategies have been utilized to control the selectivity displayed by helices formed by mixing achiral BTA ligands and enantiopure comonomers. The first strategy relies on the possibility of switching the handedness, and thus the selectivity, of the chirally-amplified BTA helical ligand by changing the nature of the major enantiopure comonomer in the co-assemblies thanks to the diluted MR effect (Chapter 2, Figure 36a). For the second strategy, it was anticipated that the selectivity provided by the helical BTA co-assemblies can be tuned to a certain extent by changing the average length of the supramolecular helices. Accordingly, suitable salts were added to the catalytic mixtures in order to disrupt and restore the co-assemblies and thus switch the catalytic outcome between non-selective and selective states, respectively (Chapter 3, Figure 36b).

The sergeants-and-soldiers and majority-rule effects can be utilized to control the handedness of dynamic helices with a low amount of enantiopure monomers or a non-optically pure mixture of enantiopure monomers, respectively. Extremely high chirally amplified effects which allow optically pure helices to be obtained with less than 1% of sergeant or with 10% *e.e.* scalemic mixture exist but are scarce.[23, 35, 154] Moreover, helical catalysts reported to date displayed selectivity superior to 80% *e.e.* only when their content in sergeants was superior to 10% or when the optically purity of the enantiomer was superior or equal to 20% *e.e.* Enhancing the chirality amplification properties of these helical catalysts is particularly desired for decreasing the amount of chiral inducer in the catalytic mixture (*i.e.* significantly below the catalytic loading) and for allowing their

stereochemical switch to be achieved with a lower amount of enantiopure comonomers. Our **second objective** is therefore to improve the chirality amplification properties of our catalytic BTA helices. Firstly, our investigation reveals that the S&S and diluted MR effects dictating the helicity of precatalytic BTA co-assemblies are exalted upon the addition of *an achiral BTA monomer*. This improvement of the chirality amplification properties by addition of this achiral additive also holds for catalytic BTA mixtures which thus allows optimal selectivity to be obtained with as low as 0.25% of sergeants and a 10% *e.e.* scalemic mixture of BTA enantiomers (Chapter 4, Figure 36c). Finally, we investigate the self-assembly properties of a new platform: *N*-substituted benzene-1-urea-3,5-biscarboxamide (BUBA) monomers, C_2-symmetric analogues of BTA monomers in which one amide function has been replaced by a urea function. We are particularly interested in probing the influence of the substitution of a single group on the chirality amplification properties of the resulting assemblies (Chapter 6, Figure 36d).

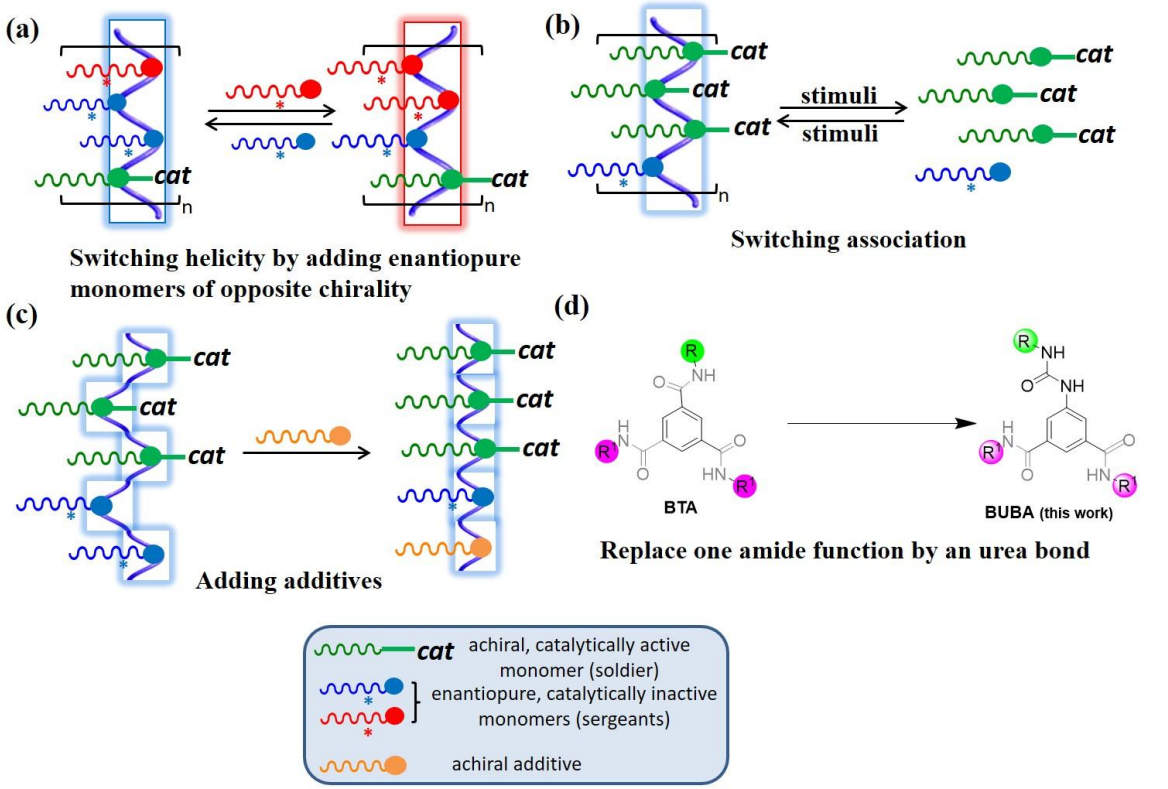

Figure 36 Schematic representation of the different concepts developed in the chapters of this manuscript. (a) selectivity-switchable catalyst (chapter 2); (b) selectivity-tunable catalyst (chapter 3); (c) extremely chirally-amplified helical catalyst (chapter 4); (d) structure-property relationships of the assemblies formed by a new class of C_2-symmetrical monomers (chapter 5).

IV References

1. Liu, M.; Zhang, L.; Wang, T., Supramolecular Chirality in Self-Assembled Systems. *Chem. Rev.* **2015,** *115* (15), 7304-7397.

2. Yashima, E.; Ousaka, N.; Taura, D.; Shimomura, K.; Ikai, T.; Maeda, K., Supramolecular Helical Systems: Helical Assemblies of Small Molecules, Foldamers, and Polymers with Chiral Amplification and Their Functions. *Chem. Rev.* **2016,** *116* (22), 13752-13990.

3. Ishidate, R.; Markvoort, A. J.; Maeda, K.; Yashima, E., Unexpectedly Strong Chiral Amplification of Chiral/Achiral and Chiral/Chiral Copolymers of Biphenylylacetylenes and Further Enhancement/Inversion and Memory of the Macromolecular Helicity. *J. Am. Chem. Soc.* **2019,** *141* (18), 7605-7614.

4. Schaack, C.; Arrico, L.; Sidler, E.; Górecki, M.; Di Bari, L.; Diederich, F., Helicene Monomers and Dimers: Chiral Chromophores Featuring Strong Circularly Polarized Luminescence. *Chem. Eur. J.* **2019,** *25* (34), 8003-8007.

5. Miyake, H.; Tsukube, H., Coordination chemistry strategies for dynamic helicates: time-programmable chirality switching with labile and inert metal helicates. *Chem. Soc. Rev.* **2012,** *41* (21), 6977-6991.

6. Park, S.; Sugiyama, H., DNA as a Chiral Scaffold for Asymmetric Synthesis. *Molecules* **2012,** *17* (11).

7. Dominguez, R.; Holmes, K. C., Actin structure and function. *Annu. Rev. Biophys.* **2011,** *40*, 169-186.

8. Zozulia, O.; Dolan, M. A.; Korendovych, I. V., Catalytic peptide assemblies. *Chem. Soc. Rev.* **2018,** *47* (10), 3621-3639.

9. Broo, K. S.; Brive, L.; Ahlberg, P.; Baltzer, L., Catalysis of Hydrolysis and Transesterification Reactions of p-Nitrophenyl Esters by a Designed Helix−Loop−Helix Dimer. *J. Am. Chem. Soc.* **1997,** *119* (47), 11362-11372.

10. Zhang, L.; Wang, T.; Shen, Z.; Liu, M., Chiral Nanoarchitectonics: Towards the Design, Self-Assembly, and Function of Nanoscale Chiral Twists and Helices. *Adv. Mater.* **2016,** *28* (6), 1044-1059.

11. Yashima, E.; Maeda, K.; Iida, H.; Furusho, Y.; Nagai, K., Helical Polymers: Synthesis, Structures, and Functions. *Chem. Rev.* **2009,** *109* (11), 6102-6211.

12. Okamoto, Y.; Suzuki, K.; Ohta, K.; Hatada, K.; Yuki, H., Optically-Active Poly(Triphenylmethyl Methacrylate) with One-Handed Helical Conformation. *J. Am. Chem. Soc.* **1979,** *101* (16), 4763-4765.

13. Nakano, T.; Okamoto, Y., Synthetic helical polymers: Conformation and function. *Chem. Rev.* **2001,** *101* (12), 4013-4038.

14. Shimomura, K.; Ikai, T.; Kanoh, S.; Yashima, E.; Maeda, K., Switchable enantioseparation based on macromolecular memory of a helical polyacetylene in the solid state. *Nat. Chem.* **2014,** *6*, 429.

15. De Greef, T. F. A.; Smulders, M. M. J.; Wolffs, M.; Schenning, A. P. H. J.; Sijbesma, R. P.; Meijer, E. W., Supramolecular Polymerization. *Chem. Rev.* **2009,** *109* (11), 5687-5754.

16. Armstrong, G.; Buggy, M., Hydrogen-bonded supramolecular polymers: A literature review. *J. Mater. Sci.* **2005,** *40* (3), 547-559.

17. Goor, O. J. G. M.; Hendrikse, S. I. S.; Dankers, P. Y. W.; Meijer, E. W., From supramolecular polymers to multi-component biomaterials. *Chem. Soc. Rev.* **2017,** *46* (21), 6621-6637.

18. Sijbesma, R. P.; Beijer, F. H.; Brunsveld, L.; Folmer, B. J. B.; Hirschberg, J. H. K. K.; Lange, R. F. M.; Lowe, J. K. L.; Meijer, E. W., Reversible Polymers Formed from Self-Complementary Monomers Using Quadruple Hydrogen Bonding. *Science* **1997,** *278* (5343), 1601-1604.

19. Yang, L.; Tan, X.; Wang, Z.; Zhang, X., Supramolecular Polymers: Historical Development, Preparation, Characterization, and Functions. *Chem. Rev.* **2015,** *115* (15), 7196-7239.

20. Simic, V.; Bouteiller, L.; Jalabert, M., Highly Cooperative Formation of Bis-Urea Based Supramolecular Polymers. *J. Am. Chem. Soc.* **2003,** *125* (43), 13148-13154.

21. Kulkarni, C.; Meijer, E. W.; Palmans, A. R. A., Cooperativity Scale: A Structure–Mechanism Correlation in the Self-Assembly of Benzene-1,3,5-tricarboxamides. *Acc.Chem. Res.* **2017,** *50* (8), 1928-1936.

22. García, F.; Sánchez, L., Structural Rules for the Chiral Supramolecular Organization of OPE-based Discotics: Induction of Helicity and Amplification of Chirality. *J. Am. Chem. Soc.* **2012,** *134* (1), 734-742.

23. Kim, T.; Mori, T.; Aida, T.; Miyajima, D., Dynamic propeller conformation for the unprecedentedly high degree of chiral amplification of supramolecular helices. *Chem. Sci.* **2016,** *7* (11), 6689-6694.

24. Dorca, Y.; Matern, J.; Fernández, G.; Sánchez, L., C3-symmetrical π-Scaffolds: Useful Building Blocks to Construct Helical Supramolecular Polymers. *Isr. J. Chem.* **2019,** *0* (0).

25. Cantekin, S.; de Greef, T. F. A.; Palmans, A. R. A., Benzene-1,3,5-tricarboxamide: a versatile ordering moiety for supramolecular chemistry. *Chem. Soc. Rev.* **2012,** *41* (18), 6125-6137.

26. Smulders, M. M. J.; Buffeteau, T.; Cavagnat, D.; Wolffs, M.; Schenning, A. P. H. J.; Meijer, E. W., C3-symmetrical self-assembled structures investigated by vibrational circular dichroism. *Chirality* **2008,** *20* (9), 1016-1022.

27. P. Lightfoot, M.; S. Mair, F.; G. Pritchard, R.; E. Warren, J., New supramolecular packing motifs: π-stacked rods encased in triply-helical hydrogen bonded amide strands. *Chem. Commun.* **1999,** (19), 1945-1946.

28. L., B.; A.P.H.J., S.; M.A.C., B.; H.M., J.; J.A.J.M., V.; E.W., M., Chiral Amplification in Columns of Self-Assembled N,N′,N″-Tris((S)-3,7-dimethyloctyl)benzene-1,3,5-tricarboxamide in Dilute Solution. *Chem. Lett.* **2000,** *29* (3), 292-293.

29. Stals, P. J. M.; Smulders, M. M. J.; Martín-Rapún, R.; Palmans, A. R. A.; Meijer, E. W., Asymmetrically Substituted Benzene-1,3,5-tricarboxamides: Self-Assembly and Odd–Even Effects in the Solid State and in Dilute Solution. *Chem. Eur. J.* **2009,** *15* (9), 2071-2080.

30. Cantekin, S.; Balkenende, D. W. R.; Smulders, M. M. J.; Palmans, A. R. A.; Meijer, E. W., The effect of isotopic substitution on the chirality of a self-assembled helix. *Nat. Chem.* **2010,** *3*, 42.

31. Veld, M. A. J.; Haveman, D.; Palmans, A. R. A.; Meijer*, E. W., Sterically demanding benzene-1,3,5-tricarboxamides: tuning the mechanisms of supramolecular polymerization and chiral amplification. *Soft Matter* **2011,** *7* (2), 524-531.

32. Desmarchelier, A.; Alvarenga, B. G.; Caumes, X.; Dubreucq, L.; Troufflard, C.; Tessier, M.; Vanthuyne, N.; Idé, J.; Maistriaux, T.; Beljonne, D.; Brocorens, P.; Lazzaroni, R.; Raynal, M.; Bouteiller, L., Tuning the nature and stability of self-assemblies formed by ester benzene 1,3,5-tricarboxamides: the crucial role played by the substituents. *Soft Matter* **2016,** *12* (37), 7824-7838.

33. Caumes, X.; Baldi, A.; Gontard, G.; Brocorens, P.; Lazzaroni, R.; Vanthuyne, N.; Troufflard, C.; Raynal, M.; Bouteiller, L., Tuning the structure of 1,3,5-benzene tricarboxamide self-assemblies through stereochemistry. *Chem. Commun.* **2016,** *52* (91), 13369-13372.

34. Desmarchelier, A.; Caumes, X.; Raynal, M.; Vidal-Ferran, A.; van Leeuwen, P. W. N. M.; Bouteiller, L., Correlation between the Selectivity and the Structure of an Asymmetric Catalyst Built on a Chirally Amplified Supramolecular Helical Scaffold. *J. Am. Chem. Soc.* **2016,** *138* (14), 4908-4916.

35. Desmarchelier, A.; Raynal, M.; Brocorens, P.; Vanthuyne, N.; Bouteiller, L., Revisiting the assembly of amino ester-based benzene-1,3,5-tricarboxamides: chiral rods in solution. *Chem. Commun.***2015,** *51* (34), 7397-7400.

36. Kim, J.; Lee, J.; Kim, W. Y.; Kim, H.; Lee, S.; Lee, H. C.; Lee, Y. S.; Seo, M.; Kim, S. Y., Induction and control of supramolecular chirality by light in self-assembled helical nanostructures. *Nat. Commun.* **2015,** *6*, 6959.

37. Green, M. M.; Park, J. W.; Sato, T.; Teramoto, A.; Lifson, S.; Selinger, R. L. B.; Selinger, J. V., The macromolecular route to chiral amplification. *Angew. Chem. Int. Ed.* **1999,** *38* (21), 3139-3154.

38. Pino, P.; Ciardelli, F.; Montagno., G.; Pieroni, O., On Relationship between Monomer Optical Purity and Polymer Rotatory Power in Some Linear Poly-Alpha-Olefines. *J. Polym. Sci. Polym. Lett.* **1967,** *5* (4pb), 307-311.

39. Carlini, C.; Ciardelli, F.; Pino, P., Optical Activity and Conformation in Solution of Stereoregular Copolymers of (S)-4-Methyl-1-Hexene with 4-Methyl-1-Pentene. *Makromol. Chem.* **1968,** *119* (Dec), 244-248.

40. Yashima, E.; Maeda, K.; Iida, H.; Furusho, Y.; Nagai, K., Helical Polymers: Synthesis, Structures, and Functions. *Chem. Rev.* **2009,** *109* (11), 6102-6211.

41. Yashima, E.; Ousaka, N.; Taura, D.; Shimomura, K.; Ikai, T.; Maeda, K., Supramolecular Helical Systems: Helical Assemblies of Small Molecules, Foldamers, and Polymers with Chiral Amplification and Their Functions. *Chem. Rev.* **2016,** *116* (22), 13752-13990.

42. Green, M. M.; Reidy, M. P.; Johnson, R. J.; Darling, G.; Oleary, D. J.; Willson, G., Macromolecular Stereochemistry - the out-of-Proportion Influence of Optically-Active Co-Monomers on the Conformational Characteristics of Polyisocyanates - the Sergeants and Soldiers Experiment. *J. Am. Chem. Soc.* **1989,** *111* (16), 6452-6454.

43. Green, M. M.; Garetz, B. A.; Munoz, B.; Chang, H. P.; Hoke, S.; Cooks, R. G., Majority Rules in the Copolymerization of Mirror-Image Isomers. *J. Am. Chem. Soc.* **1995,** *117* (14), 4181-4182.

44. Suginome, M.; Yamamoto, T.; Nagata, Y., Poly(quinoxaline― 2,3― diyl)s: A Fascinating Helical Macromolecular Scaffold for New Chiral Functions. *J. Synth. Org. Chem. Jpn.* **2015,** *73*, 1141-1155.

45. Ishikawa, M.; Maeda, K.; Mitsutsuji, Y.; Yashima, E., An unprecedented memory of macromolecular helicity induced in an achiral polyisocyanide in water. *J. Am. Chem. Soc.* **2004,** *126* (3), 732-733.

46. Zhang, W.; Jin, W. S.; Fukushima, T.; Mori, T.; Aida, T., Helix Sense-Selective Supramolecular Polymerization Seeded by a One-Handed Helical Polymeric Assembly. *J. Am. Chem. Soc.* **2015,** *137* (43), 13792-13795.

47. Palmans, A. R. A.; Meijer, E. W., Amplification of chirality in dynamic supramolecular aggregates. *Angew. Chem. Int. Ed.* **2007,** *46* (47), 8948-8968.

48. Palmans, A. R. A.; Vekemans, J. A. J. M.; Havinga, E. E.; Meijer, E. W., Sergeants-and-Soldiers Principle in Chiral Columnar Stacks of Disc-Shaped Molecules with C3 Symmetry. *Angew. Chem. Int. Ed.* **1997,** *36* (23), 2648-2651.

49. Brunsfeld, L.; Lohmeijer, B. G. G.; Vekemans, J. A. J. M.; Meijer, E. W., Amplification of Chirality in Helical Supramolecular Columns. *J.Incl. Ph. Macr. Chem.* **2001,** *41* (1), 61-64.

50. Smulders, M. M. J.; Stals, P. J. M.; Mes, T.; Paffen, T. F. E.; Schenning, A. P. H. J.; Palmans, A. R. A.; Meijer, E. W., Probing the Limits of the Majority-Rules Principle in a Dynamic Supramolecular Polymer. *J. Am. Chem. Soc.* **2010,** *132* (2), 620-626.

51. van Gestel, J., Amplification of Chirality of the Majority-Rules Type in Helical Supramolecular Polymers: The Impact of the Presence of Achiral Monomers. *J. Phys. Chem. B* **2006,** *110* (9), 4365-4370.

52. Markvoort, A. J.; ten Eikelder, H. M. M.; Hilbers, P. A. J.; de Greef, T. F. A.; Meijer, E. W., Theoretical models of nonlinear effects in two-component cooperative supramolecular copolymerizations. *Nat. Commun.* **2011,** *2*, 509.

53. ten Eikelder, H. M. M.; Markvoort, A. J.; de Greef, T. F. A.; Hilbers, P. A. J., An Equilibrium Model for Chiral Amplification in Supramolecular Polymers. *J. Phys. Chem. B* **2012,** *116* (17), 5291-5301.

54. van Gestel, J., Amplification of Chirality in Helical Supramolecular Polymers: The Majority-Rules Principle. *Macromolecules* **2004,** *37* (10), 3894-3898.

55. Kagan, H. B.; Dang, T. P., Asymmetric Catalytic Reduction with Transition-Metal Complexes .1. Catalytic System of Rhodium(I) with (-)-2,3-O-Isopropylidene-2,3-Dihydroxy-1,4-Bis(Diphenylphosphino)Butane - New Chiral Diphosphine. *J. Am. Chem. Soc.* **1972,** *94* (18), 6429-6433.

56. Miyashita, A.; Yasuda, A.; Takaya, H.; Toriumi, K.; Ito, T.; Souchi, T.; Noyori, R., Synthesis of 2,2'-Bis(Diphenylphosphino)-1,1'-Binaphthyl (Binap), an Atropisomeric Chiral Bis(Triaryl)Phosphine, and Its Use in the Rhodium(I)-Catalyzed Asymmetric Hydrogenation of Alpha-(Acylamino)Acrylic Acids. *J. Am. Chem. Soc.* **1980,** *102* (27), 7932-7934.

57. Kolb, H. C.; Vannieuwenhze, M. S.; Sharpless, K. B., Catalytic Asymmetric Dihydroxylation. *Chem. Rev.* **1994,** *94* (8), 2483-2547.

58. Noyori, R., Asymmetric catalysis: Science and opportunities (Nobel lecture). *Angew. Chem. Int. Ed.* **2002,** *41* (12), 2008-2022.

59. Trost, B. M., Asymmetric catalysis: An enabling science. *Proc. Natl. Acad. Sci. U. S. A.* **2004,** *101* (15), 5348-5355.

60. List, B.; Lerner, R. A.; Barbas III, C. F., Proline-Catalyzed Direct Asymmetric Aldol Reactions. *J. Am. Chem. Soc.* **2000,** *122*, 2395-2396.

61. Ahrendt, K. A.; Borths, C. J.; MacMillan, D. W. C., New Strategies for Organic Catalysis: The First Highly Enantioselective Organocatalytic Diels-Alder Reaction. *J. Am. Chem. Soc.* **2000,** *122*, 4243-4244.

62. Dondoni, A.; Massi, A., Asymmetric Organocatalysis: From Infancy to Adolescence. *Angew. Chem. Int. Ed.* **2008,** *47*, 4638-4660.

63. Tang, Z.; Iida, H.; Hu, H.-Y.; Yashima, E., Remarkable Enhancement of the Enantioselectivity of an Organocatalyzed Asymmetric Henry Reaction Assisted by Helical Poly(phenylacetylene)s Bearing Cinchona Alkaloid Pendants via an Amide Linkage. *ACS Macro Letters* **2012,** *1* (2), 261-265.

64. Palmans, A. R. A.; Meijer, E. W., Amplification of Chirality in Dynamic Supramolecular Aggregates. *Angew. Chem. Int. Ed.* **2007,** *46* (47), 8948-8968.

65. Romanazzi, G.; Degennaro, L.; Mastrorilli, P.; Luisi, R., Chiral Switchable Catalysts for Dynamic Control of Enantioselectivity. *ACS Catalysis* **2017,** *7* (6), 4100-4114.

66. Boersma, A. J.; Megens, R. P.; Feringa, B. L.; Roelfes, G., DNA-based asymmetric catalysis. *Chem. Soc. Rev.* **2010,** *39* (6), 2083-2092.

67. Roelfes, G.; Feringa, B. L., DNA-Based Asymmetric Catalysis. *Angew. Chem. Int. Ed.* **2005,** *44* (21), 3230-3232.

68. Shibata, N.; Yasui, H.; Nakamura, S.; Toru, T., DNA-Mediated Enantioselective Carbon-Fluorine Bond Formation. *Synlett* **2007,** *2007* (07), 1153-1157.

69. Boersma, A. J.; Coquière, D.; Geerdink, D.; Rosati, F.; Feringa, B. L.; Roelfes, G., Catalytic enantioselective syn hydration of enones in water using a DNA-based catalyst. *Nat. Chem.* **2010,** *2* (11), 991-995.

70. Boersma, A. J.; Klijn, J. E.; Feringa, B. L.; Roelfes, G., DNA-Based Asymmetric Catalysis: Sequence-Dependent Rate Acceleration and Enantioselectivity. *J. Am. Chem. Soc.* **2008,** *130* (35), 11783-11790.

71. Park, S.; Ikehata, K.; Watabe, R.; Hidaka, Y.; Rajendran, A.; Sugiyama, H., Deciphering DNA-based asymmetric catalysis through intramolecular Friedel–Crafts alkylations. *Chem. Commun.***2012,** *48* (84), 10398-10400.

72. García-Fernández, A.; Megens, R. P.; Villarino, L.; Roelfes, G., DNA-Accelerated Copper Catalysis of Friedel–Crafts Conjugate Addition/Enantioselective Protonation Reactions in Water. *J. Am. Chem. Soc.* **2016,** *138* (50), 16308-16314.

73. Megens, R. P.; Roelfes, G., Asymmetric Catalysis with Helical Polymers. *Chem. Eur. J.* **2011,** *17* (31), 8514-8523.

74. Deng, J.; Zhao, B.; Deng, J., Optically Active Helical Polyacetylene Bearing Ferrocenyl Amino-Acid Derivative in Pendants. Preparation and Application as Chiral Organocatalyst for Asymmetric Aldol Reaction. *Ind. Eng. Chem. Res.* **2016,** *55* (27), 7328-7337.

75. Maeda, K.; Tanaka, K.; Morino, K.; Yashima, E., Synthesis of Optically Active Helical Poly(phenylacetylene)s Bearing Oligopeptide Pendants and Their Use as Polymeric Organocatalysts for Asymmetric Epoxidation. *Macromolecules* **2007,** *40* (19), 6783-6785.

76. Hu, Q.-S.; Zheng, X.-F.; Pu, L., The First Optically Active and Sterically Regular Poly(1,1'-bi-2-naphthol)s: Precursors to a New Generation of Polymeric Catalysts. *J. Org. Chem.* **1996,** *61* (16), 5200-5201.

77. Hu, Q.-S.; Vitharana, D.; Zheng, X.-F.; Wu, C.; Kwan, C. M. S.; Pu, L., Poly(1,1'-bi-2-naphthol)s: Synthesis, Characterization, and Application in Lewis Acid Catalysis. *J. Org. Chem.* **1996,** *61* (24), 8370-8377.

78. Huang, W.-S.; Hu, Q.-S.; Zheng, X.-F.; Anderson, J.; Pu, L., Development of Highly Enantioselective Polymeric Catalysts Using Rigid and Sterically Regular Chiral Polybinaphthols. *J. Am. Chem. Soc.* **1997,** *119* (18), 4313-4314.

79. Hu, Q.-S.; Huang, W.-S.; Vitharana, D.; Zheng, X.-F.; Pu, L., Functionalized Major-Groove and Minor-Groove Chiral Polybinaphthyls: Application in the Asymmetric Reaction of Aldehydes with Diethylzinc. *J. Am. Chem. Soc.* **1997,** *119* (51), 12454-12464.

80. Huerta , E.; van Genabeek , B.; Lamers, B. A. G.; Koenigs, M. M. E.; Meijer, E. W.; Palmans, A. R. A., Triggering Activity of Catalytic Rod-Like Supramolecular Polymers. *Chem. Eur. J.* **2015,** *21* (9), 3682-3690.

81. Neumann, L. N.; Baker, M. B.; Leenders, C. M. A.; Voets, I. K.; Lafleur, R. P. M.; Palmans, A. R. A.; Meijer, E. W., Supramolecular polymers for organocatalysis in water. *Org. Biomolec. Chem.* **2015,** *13* (28), 7711-7719.

82. Raynal, M.; Portier, F.; van Leeuwen, P.; Bouteiller, L., Tunable Asymmetric Catalysis through Ligand Stacking in Chiral Rigid Rods. *J. Am. Chem. Soc.* **2013,** *135* (47), 17687-17690.

83. Jiang, J.; Meng, Y.; Zhang, L.; Liu, M., Self-Assembled Single-Walled Metal-Helical Nanotube (M-HN): Creation of Efficient Supramolecular Catalysts for Asymmetric Reaction. *J. Am. Chem. Soc.* **2016,** *138* (48), 15629-15635.

84. Jin, Q.; Zhang, L.; Cao, H.; Wang, T.; Zhu, X.; Jiang, J.; Liu, M., Self-Assembly of Copper(II) Ion-Mediated Nanotube and Its Supramolecular Chiral Catalytic Behavior. *Langmuir* **2011,** *27* (22), 13847-13853.

85. Avalos, M.; Babiano, R.; Cintas, P.; Jimenez, J. L.; Palacios, J. C.; Barron, L. D., Absolute asymmetric synthesis under physical fields: Facts and fictions. *Chem. Rev.* **1998,** *98* (7), 2391-2404.

86. Feringa, B. L.; van Delden, R. A., Absolute asymmetric synthesis: The origin, control, and amplification of chirality. *Angew. Chem. Int. Ed.* **1999,** *38* (23), 3419-3438.

87. Merad, J.; Borkar, P.; Caijo, F.; Pons, J. M.; Parrain, J. L.; Chuzel, O.; Bressy, C., Double Catalytic Kinetic Resolution (DoCKR) of Acyclic anti-1,3-Diols: The Additive Horeau Amplification. *Angew. Chem. Int. Ed.* **2017,** *56* (50), 16052-16056.

88. Noyori, R.; Kitamura, M., Enantioselective Addition of Organometallic Reagents to Carbonyl-Compounds - Chirality Transfer, Multiplication, and Amplification. *Angew. Chem. Int. Ed. Engl.* **1991,** *30* (1), 49-69.

89. Guillaneux, D.; Zhao, S. H.; Samuel, O.; Rainford, D.; Kagan, H. B., Nonlinear Effects in Asymmetric Catalysis. *J. Am. Chem. Soc.* **1994,** *116* (21), 9430-9439.

90. Satyanarayana, T.; Abraham, S.; Kagan, H. B., Nonlinear Effects In Asymmetric Catalysis. *Angew. Chem. Int. Ed.* **2009,** *48* (3), 456-494.

91. Klussmann, M.; Iwamura, H.; Mathew, S. P.; Wells, D. H.; Pandya, U.; Armstrong, A.; Blackmond, D. G., Thermodynamic control of asymmetric amplification in amino acid catalysis. *Nature* **2006,** *441* (7093), 621-623.

92. Kagan, H. B., Practical consequences of non-linear effects in asymmetric synthesis. *Adv. Synth. Catal.* **2001,** *343* (3), 227-233.

93. Faller, J. W.; Lavoie, A. R.; Parr, J., Chiral poisoning and asymmetric activation. *Chem. Rev.* **2003,** *103* (8), 3345-3367.

94. Mikami, K.; Yamanaka, M., Symmetry breaking in asymmetric catalysis: Racemic catalysis to autocatalysis. *Chem. Rev.* **2003,** *103* (8), 3369-3400.

95. Soai, K.; Shibata, T.; Morioka, H.; Choji, K., Asymmetric Autocatalysis and Amplification of Enantiomeric Excess of a Chiral Molecule. *Nature* **1995,** *378* (6559), 767-768.

96. Soai, K.; Kawasaki, T.; Matsumoto, A., Asymmetric Autocatalysis of Pyrimidyl Alkanol and Its Application to the Study on the Origin of Homochirality. *Acc. Chem. Res.* **2014,** *47* (12), 3643-3654.

97. Matsumoto, A.; Abe, T.; Hara, A.; Tobita, T.; Sasagawa, T.; Kawasaki, T.; Soai, K., Crystal Structure of the Isopropylzinc Alkoxide of Pyrimidyl Alkanol: Mechanistic Insights for Asymmetric Autocatalysis with Amplification of Enantiomeric Excess. *Angew. Chem. Int. Ed.* **2015**, 15218-15221.

98. Weissbuch, I.; Lahav, M., Crystalline Architectures as Templates of Relevance to the Origins of Homochirality. *Chem. Rev.* **2011,** *111* (5), 3236-3267.

99. Ribó, J. M.; Blanco, C.; Crusats, J.; El-Hachemi, Z.; Hochberg, D.; Moyano, A., Absolute Asymmetric Synthesis in Enantioselective Autocatalytic Reaction Networks: Theoretical Games, Speculations on Chemical Evolution and Perhaps a Synthetic Option. *Chem. Eur. J.* **2014,** *20* (52), 17250-17271.

100. Megens, R. P.; Roelfes, G., Asymmetric Catalysis with Helical Polymers. *Chem. Eur. J.* **2011,** *17* (31), 8514-8523.

101. Reggelin, M.; Schultz, M.; Holbach, M., Helical chiral polymers without additional stereogenic units: A new class of ligands in asymmetric catalysis. *Angew. Chem. Int. Ed.* **2002,** *41* (9), 1614-1617.

102. Reggelin, M.; Doerr, S.; Klussmann, M.; Schultz, M.; Holbach, M., Helically chiral polymers: A class of ligands for asymmetric catalysis. *Proc. Natl. Acad. Sci. U.S.A* **2004,** *101* (15), 5461-5466.

103. Muller, C. A.; Hoffart, T.; Holbach, M.; Reggelin, M., Pyridyl N-oxide substituted helically chiral poly(methacrylate)s in asymmetric organocatalysis. *Macromolecules* **2005,** *38* (13), 5375-5380.

104. Yamamoto, T.; Suginome, M., Helical Poly(quinoxaline-2,3-diyl)s Bearing Metal-Binding Sites as Polymer-Based Chiral Ligands for Asymmetric Catalysis. *Angew. Chem. Int. Ed.* **2009,** *48* (3), 539-542.

105. Yamamoto, T.; Yamada, T.; Nagata, Y.; Suginome, M., High-Molecular-Weight Polyquinoxaline-Based Helically Chiral Phosphine (PQXphos) as Chirality-Switchable, Reusable, and Highly

Enantioselective Monodentate Ligand in Catalytic Asymmetric Hydrosilylation of Styrenes. *J. Am. Chem. Soc.* **2010,** *132* (23), 7899-7901.

106. Suginome, M.; Yamamoto, T.; Nagata, Y.; Yamada, T.; Akai, Y., Catalytic asymmetric synthesis using chirality-switchable helical polymer as a chiral ligand. *Pure Appl. Chem.* **2012,** *84* (8), 1759-1769.

107. , The screw-sense excess adopted by helical covalent polymers quantitatively refers to the ratio of left-handed and right-handed fragments in a polymer chain. It is calculated by dividing the ellipticity value of a given polymer to the ellipticity value for the same polymer in a single-handed configuration (CD spectroscopy). The term „net helicity“ employed in the context of supramolecular helices is equivalent. .

108. Yamamoto, T.; Akai, Y.; Nagata, Y.; Suginome, M., Highly Enantioselective Synthesis of Axially Chiral Biarylphosphonates: Asymmetric Suzuki-Miyaura Coupling Using High-Molecular-Weight, Helically Chiral Polyquinoxaline-Based Phosphines. *Angew. Chem. Int. Ed.* **2011,** *50* (38), 8844-8847.

109. Takata, L. M. S.; Iida, H.; Shimomura, K.; Hayashi, K.; dos Santos, A. A.; Yashima, E., Helical Poly(phenylacetylene) Bearing Chiral and Achiral Imidazolidinone-Based Pendants that Catalyze Asymmetric Reactions due to Catalytically Active Achiral Pendants Assisted by Macromolecular Helicity *Macromol. Rapid. Commun.* **2015,** *36*, 2047-2054.

110. Yamamoto, T.; Adachi, T.; Suginome, M., Complementary Induction of Right- and Left-Handed Helical Structures by the Positioning of Chiral Groups on the Monomer Units: Introduction of (-)-Menthol as Side Chains of Poly(quinoxaline-2,3-diyl)s. *ACS Macro Lett.* **2013,** *2* (9), 790−793.

111. Nagata, Y.; Nishikawa, T.; Suginome, M., Poly(quinoxaline-2,3-diyl)s Bearing (S)-3-Octyloxymethyl Side Chains as an Efficient Amplifier of Alkane Solvent Effect Leading to Switch of Main-Chain Helical Chirality. *J. Am. Chem. Soc.* **2014,** *136* (45), 15901-15904.

112. Nagata, Y.; Kuroda, T.; Takagi, K.; Suginome, M., Ether solvent-induced chirality inversion of helical poly(quinoxaline-2,3-diyl)s containing L-lactic acid derived side chains. *Chem. Sci.* **2014,** *5* (12), 4953-4956.

113. Akai, Y.; Konnert, L.; Yamamoto, T.; Suginome, M., Asymmetric Suzuki-Miyaura cross-coupling of 1-bromo-2-naphthoates using the helically chiral polymer ligand PQXphos. *Chem. Commun.* **2015,** *51* (33), 7211-7214.

114. Yamamoto, T.; Akai, Y.; Suginome, M., Chiral Palladacycle Catalysts Generated on a Single-Handed Helical Polymer Skeleton for Asymmetric Arylative Ring Opening of 1,4-Epoxy-1,4-dihydronaphthalene. *Angew. Chem. Int. Ed.* **2014,** *53* (47), 12785-12788.

115. Akai, Y.; Yamamoto, T.; Nagata, Y.; Ohmura, T.; Suginome, M., Enhanced Catalyst Activity and Enantioselectivity with Chirality-Switchable Polymer Ligand PQXphos in Pd-Catalyzed Asymmetric Silaborative Cleavage of meso-Methylenecyclopropanes. *J. Am. Chem. Soc.* **2012,** *134* (27), 11092-11095.

116. Yoshinaga, Y.; Yamamoto, T.; Suginome, M., Chirality-Switchable 2,2 '-Bipyridine Ligands Attached to Helical Poly(quinoxaline-2,3-diyl)s for Copper-Catalyzed Asymmetric Cyclopropanation of Alkenes. *ACS Macro Lett.* **2017,** *6* (7), 705-710.

117. Yamamoto, T.; Murakami, R.; Suginome, M., Single-Handed Helical Poly(quinoxaline-2,3-diyl)s Bearing Achiral 4-Aminopyrid-3-yl Pendants as Highly Enantioselective, Reusable Chiral Nucleophilic Organocatalysts in the Steglich Reaction. *J. Am. Chem. Soc.* **2017,** *139* (7), 2557-2560.

118. Nagata, Y.; Yamada, T.; Adachi, T.; Akai, Y.; Yamamoto, T.; Suginome, M., Solvent-Dependent Switch of Helical Main-Chain Chirality in Sergeants-and-Soldiers-Type Poly(quinoxaline-2,3-

diyl)s: Effect of the Position and Structures of the "Sergeant" Chiral Units on the Screw-Sense Induction. *J. Am. Chem. Soc.* **2013,** *135*, 10104-10113.

119. Nagata, Y.; Nishikawa, T.; Suginome, M., Exerting Control over the Helical Chirality in the Main Chain of Sergeants-and-Soldiers-Type Poly(quinoxaline-2,3-diyl)s by Changing from Random to Block Copolymerization Protocols. *J. Am. Chem. Soc.* **2015,** *137* (12), 4070−4073.

120. Ke, Y.-Z.; Nagata, Y.; Yamada, T.; Suginome, M., Majority-Rules-Type Helical Poly(quinoxaline-2,3-diyl)s as Highly Efficient Chirality-Amplification Systems for Asymmetric Catalysis. *Angew. Chem. Int. Ed.* **2015,** *54*, 9333−9337.

121. Sato, T.; Terao, K.; Teramoto, A.; Fujiki, M., On the Composition-Driven Helical Screw-Sense Inversion of Chiral-Achiral Random Copolymers. *Macromolecules* **2002,** *35*, 5355-5357.

122. Miyabe, T.; Hase, Y.; Iida, H.; Maeda, K.; Yashima, E., Synthesis of Functional Poly(phenyl isocyanide)s with Macromolecular Helicity Memory and Their Use as Asymmetric Organocatalysts. *Chirality* **2009,** *21* (1), 44-50.

123. Yamamoto, T.; Murakami, R.; Komatsu, S.; Suginome, M., Chirality-Amplifying, Dynamic Induction of Single-Handed Helix by Chiral Guests to Macromolecular Chiral Catalysts Bearing Boronyl Pendants as Receptor Sites. *J. Am. Chem. Soc.* **2018,** *140*, 3867.

124. Liu, M. H.; Zhang, L.; Wang, T. Y., Supramolecular Chirality in Self-Assembled Systems. *Chem. Rev.* **2015,** *115* (15), 7304-7397.

125. Jin, Q. X.; Zhang, L.; Cao, H.; Wang, T. Y.; Zhu, X. F.; Jiang, J.; Liu, M. H., Self-Assembly of Copper(II) Ion-Mediated Nanotube and Its Supramolecular Chiral Catalytic Behavior. *Langmuir* **2011,** *27* (22), 13847-13853.

126. Jiang, J.; Meng, Y.; Zhang, L.; Liu, M. H., Self-Assembled Single-Walled Metal-Helical Nanotube (M-HN): Creation of Efficient Supramolecular Catalysts for Asymmetric Reaction. *J. Am. Chem. Soc.* **2016,** *138* (48), 15629-15635.

127. Yuan, C. H.; Jiang, J.; Sun, H.; Wang, D. C.; Hu, Y. H.; Liu, M. H., Opposite Enantioselectivity by Nanotubes and Nanospheres Self-Assembled from Dirhodium(II) and an L-Glutamic Acid Terminated Bolaamphiphile. *ChemCatChem* **2018,** *10* (10), 2190-2194.

128. Sun, H.; Jiang, J.; Sun, Y. M.; Zhang, Q. W.; Liu, M. H., Self-assembled organic nanotube promoted allylation of ketones in aqueous phase. *Chem. Commun.* **2019,** *55* (22), 3254-3257.

129. Raynal, M.; Portier, F.; van Leeuwen, P. W. N. M.; Bouteiller, L., Tunable Asymmetric Catalysis through Ligand Stacking in Chiral Rigid Rods. *J. Am. Chem. Soc.* **2013,** *135* (47), 17687-17690.

130. Zimbron, J. M.; Caumes, X.; Li, Y.; Thomas, C. M.; Raynal, M.; Bouteiller, L., Real-Time Control of the Enantioselectivity of a Supramolecular Catalyst Allows Selecting the Configuration of Consecutively Formed Stereogenic Centers. *Angew. Chem. Int. Ed.* **2017,** *56* (45), 14016-14019.

131. Li, Y.; Caumes, X.; Raynal, M.; Bouteiller, L., Modulation of catalyst enantioselectivity through reversible assembly of supramolecular helices. *Chem. Commun.* **2019,** *55* (15), 2162-2165.

132. Cantekin, S.; de Greef, T. F. A.; Palmans, A. R. A., Benzene-1,3,5-tricarboxamide: a versatile ordering moiety for supramolecular chemistry. *Chem. Soc. Rev.* **2012,** *41* (18), 6125-6137.

133. de Loos, M.; van Esch, J. H.; Kellogg, R. M.; Feringa, B. L., C-3-symmetric, amino acid based organogelators and thickeners: a systematic study of structure-property relations. *Tetrahedron* **2007,** *63* (31), 7285-7301.

134. Veld, M. A. J.; Haveman, D.; Palmans, A. R. A.; Meijer, E. W., Sterically demanding benzene-1,3,5-tricarboxamides: tuning the mechanisms of supramolecular polymerization and chiral amplification. *Soft Matter* **2011,** *7* (2), 524-531.

135. Desmarchelier, A.; Alvarenga, B. G.; Caumes, X.; Dubreucq, L.; Troufflard, C.; Tessier, M.; Vanthuyne, N.; Ide, J.; Maistriaux, T.; Beljonne, D.; Brocorens, P.; Lazzaroni, R.; Raynal, M.; Bouteiller, L., Tuning the nature and stability of self-assemblies formed by ester benzene 1,3,5-tricarboxamides: the crucial role played by the substituents. *Soft Matter* **2016,** *12* (37), 7824-7838.

136. Caumes, X.; Baldi, A.; Gontard, G.; Brocorens, P.; Lazzaroni, R.; Vanthuyne, N.; Troufflard, C.; Raynal, M.; Bouteiller, L., Tuning the structure of 1,3,5-benzene tricarboxamide self-assemblies through stereochemistry. *Chem. Commun.* **2016,** *52* (91), 13369-13372.

137. Basuyaux, G.; Desmarchelier, A.; Gontard, G.; Vanthuyne, N.; Moussa, J.; Amouri, H.; Raynal, M.; Bouteiller, L., Extra hydrogen bonding interactions by peripheral indole groups stabilize benzene-1,3,5-tricarboxamide helical assemblies. *Chem. Commun.* **2019**, DOI: 10.1039/c9cc03906f.

138. Choudhury, J., Recent developments on artificial switchable catalysis. *Tetrah. Lett.* **2018,** *59* (6), 487-495.

139. Vlatković, M.; Collins, B. S. L.; Feringa, B. L., Dynamic Responsive Systems for Catalytic Function. *Chem. Eur. J.* **2016,** *22* (48), 17080-17111.

140. Kousar, A.; Liu, J.; Mehwish, N.; Wang, F.; Dang-i, A. Y.; Feng, C., pH-Regulated supramolecular chirality of phenylalanine-based hydrogels. *Mater. Tod. Chem.* **2019,** *11*, 217-224.

141. Zhao, D.; van Leeuwen, T.; Cheng, J.; Feringa, B. L., Dynamic control of chirality and self-assembly of double-stranded helicates with light. *Nat. Chem.* **2017,** *9* (3), 250-256.

142. Nagata, Y.; Nishikawa, T.; Suginome, M., Poly(quinoxaline-2,3-diyl)s Bearing (S)-3-Octyloxymethyl Side Chains as an Efficient Amplifier of Alkane Solvent Effect Leading to Switch of Main-Chain Helical Chirality. *J. Am. Chem. Soc.* **2014,** *136* (45), 15901-15904.

143. Nagata, Y.; Nishikawa, T.; Suginome, M., Solvent Effect on the Sergeants-and-Soldiers Effect Leading to Bidirectional Induction of Single-Handed Helical Sense of Poly(quinoxaline-2,3-diyl)s Copolymers in Aromatic Solvents. *ACS Macro Lett.* **2016,** *5* (4), 519-522.

144. Nagata, Y.; Kuroda, T.; Takagi, K.; Suginome, M., Ether solvent-induced chirality inversion of helical poly(quinoxaline-2,3-diyl)s containing l-lactic acid derived side chains. *Chem. Sci* **2014,** *5* (12), 4953-4956.

145. Nagata, Y.; Nishikawa, T.; Suginome, M., Solvent Effect on the Sergeants-and-Soldiers Effect Leading to Bidirectional Induction of Single-Handed Helical Sense of Poly(quinoxaline-2,3-diyl)s Copolymers in Aromatic Solvents. *ACS Macro Lett.* **2016,** *5* (4), 519-522.

146. Yamada, T.; Nagata, Y.; Suginome, M., Non-hydrogen-bonding-based, solvent-dependent helix inversion between pure P-helix and pure M-helix in poly(quinoxaline-2,3-diyl)s bearing chiral side chains. *Chem. Commun.* **2010,** *46*, 4914-4916.

147. Nagata, Y.; Nishikawa, T.; Suginome, M., Abnormal sergeants-and-soldiers effects of poly(quinoxaline-2,3-diyl)s enabling discrimination of one-carbon homologous n-alkanes through a highly sensitive solvent-dependent helix inversion *Chem. Commun.* **2018,** *54*, 6867-6870.

148. Nagata, Y.; Nishikawa, T.; Suginom, M.; Sato, S.; Sugiyama, M.; Porcar, L.; Martel, A.; Inoue, R.; Sato, N., Elucidating the Solvent Effect on the Switch of the Helicity of Poly(quinoxaline-2,3-diyl)s: A Conformational Analysis by Small-Angle Neutron Scattering. *J. Am. Chem. Soc.* **2018,** *140*, 2722-2726.

149. Private communication with Michinori Suginime

150. Lin, L.; Feng, X., Catalytic Strategies for Diastereodivergent Synthesis. *Chem. Eur. J.* **2017**.

151. Krautwald, S.; Carreira, E. M., Stereodivergence in Asymmetric Catalysis. *J. Am. Chem. Soc.* **2017,** *139* (16), 5627-5639.

152. Coates, G. W.; Waymouth, R. M., Oscillating Stereocontrol: A Strategy for the Synthesis of Thermoplastic Elastomeric Polypropylene. *Science* **1995,** *267* (5195), 217-219.

153. Thomas, C. M., Stereocontrolled ring-opening polymerization of cyclic esters: synthesis of new polyester microstructures. *Chem. Soc. Rev.* **2010,** *39* (1), 165-173.

154. Smulders, M. M. J.; Filot, I. A. W.; Leenders, J. M. A.; van der Schoot, P.; Palmans, A. R. A.; Schenning, A. P. H. J.; Meijer, E. W., Tuning the Extent of Chiral Amplification by Temperature in a Dynamic Supramolecular Polymer. *J. Am. Chem. Soc.* **2010,** *132* (2), 611-619.

Chapter 2 Real-time control of the enantioselectivity of a supramolecular catalyst allows selecting the configuration of consecutively formed stereogenic centres

Abstract：The enantiomeric state of a supramolecular copper catalyst can be switched *in situ* in *ca.* five seconds. The dynamic property of the catalyst is provided by the non-covalent nature of the helical assemblies supporting the copper centres. These assemblies are formed by mixing an achiral benzene-1,3,5-tricarboxamide (BTA) phosphine ligand (for copper coordination) and both enantiomers of a chiral phosphine-free BTA co-monomer (for chirality amplification). The enantioselectivity of the hydrosilylation reaction is fixed by the BTA enantiomer in excess, which can be altered by simple BTA addition. As a result of the complete and fast stereochemical switch, any combination of the enantiomers was obtained during the conversion of a mixture of two substrates. This work was published as *Angew. Chem. Int. Ed.* **2017**, *56*, 14016-14019 （*Jeremy M. Zimbron, Xavier Caumes, Yan Li, Christophe M. Thomas, Matthieu Raynal and Laurent Bouteiller*）, and was reported here as published with formatting to match with the rest of the thesis. My participation for this publication mainly involves (i) finding the optimal conditions for controlling the configuration of the enantiomers formed during the transformation of a mixture of two substrates (Figure 1 and Table S5), (ii) determining the time necessary to a get a full stereochemical switch (Table S4) and (iii) performing the stereochemical switch during the conversion of a single substrate (Scheme S1).

I Introduction

Dynamic and stimuli-responsive catalysts potentially allow tuning their performance during a chemical process.[1-5] These catalysts can be switched between different states by means of a suitable input (*i.e.* light, redox, thermal or chemical) with a significant impact on reaction rate,[1-5] substrate selectivity[6] or diastereoselectivity.[7-8] Conversely, inverting the enantioselectivity of a single catalyst during a reaction remains an elusive goal despite the promising perspectives of using such a catalyst to select the desired diastereoisomer in one pot stereoselective cascade reactions[9-10] or to control the tacticity of stereoblock copolymers.[11-12]

In fact, both enantiomers of a product can be obtained from the same catalyst[13-14] in a predictable manner by connecting a catalytic unit to a chiroptical switch.[15-21] However, the switch is commonly performed *before* the catalytic experiment.[8] Controlling the enantiomeric state of a single catalyst *in situ*[22-23] faces additional challenges: i) the catalytic system should be dynamic in the conditions of the catalytic reaction, ii) the stereochemical switch should be fast and lead to opposite chiral environments and, iii) the input should preserve the integrity of the catalyst. These issues are particularly significant in the case of metal-catalysed reactions since the presence of the metal centre may impede the efficiency and the dynamics of the chiroptical switch.[24] Previous attempts to switch the enantioselectivity *in situ* were also hampered by the poor stability of the metal catalysts or reactants when exposed to an oxidizing agent[22] or to ultraviolet light.[21] Based on our previous design of catalysts supported on supramolecular helices,[25-26] we now describe a strategy which allows to control in real time the enantioselectivity displayed by intrinsically achiral phosphine-copper complexes located at the periphery of a chirally-amplified[12] supramolecular polymer platform. This approach relies on the complete and fast stereochemical switch of the handedness of the dynamic helices producing enantiomeric catalytic centres.

II Results and discussion

Benzene 1,3,5-tricarboxamide (BTA) monomers have been selected given their chirality amplification properties and their fast dynamics.[27-29] As shown in Scheme 1, we used supramolecular BTA polymers composed of three types of monomers, two enantiopure co-monomers of opposite configuration and one phosphine-functionalized achiral monomer (for copper coordination). Thanks to chirality amplification effects, homochiral helices are expected to be formed even though the polymers are composed of a scalemic mixture of enantiomers and of achiral monomers. Thus, dual stereocontrol

of the asymmetric reaction should be possible by *in situ* addition of one of the enantiopure co-monomers to invert the handedness of the supramolecular helices (Scheme 1).

We chose the copper-catalysed hydrosilylation of prochiral aromatic ketones using 1-(4-nitrophenyl)ethanone (NPnone) as model substrate, because of the wide scope of reactions catalyzed by phosphine copper hydride species,[30] that include stereoselective cascade transformations.[31] We first mixed **BTA^{PPh2}** (6.0 mol%), an enantiopure BTA co-monomer (6.6 mol%) and $Cu(OAc)_2 \cdot H_2O$ (3.0 mol%) at 20°C using $PhSiH_3$ as the silane source (Table 1). We found that significant enantiomeric excesses (47%<*e.e.*<54%) were obtained with BTA co-monomers having a branched alkyl chain attached to the stereogenic centre. Notably, **BTA (*S*)-Cha** and **BTA (*R*)-Cha** provided the hydrosilylation product with opposite optical purities in a fully reproducible way (54 ±1% *e.e.*, Table S.1).

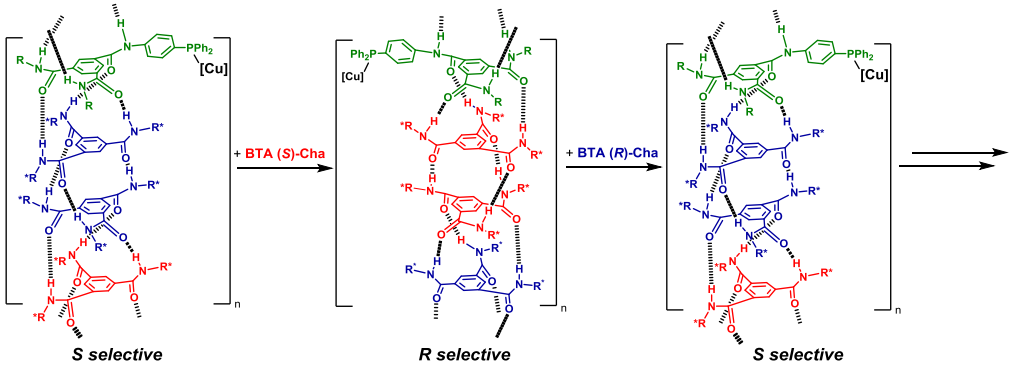

Scheme 1. Real-time control of the enantioselectivity of a supramolecular metal catalyst. The outcome of the catalytic reaction and the structure of the BTA assemblies were correlated according to various spectroscopic and scattering analyses. For the chemical structure of BTA Cha see Chart 1.

Chart 1. Chemical structures of BTA monomers screened in this study.

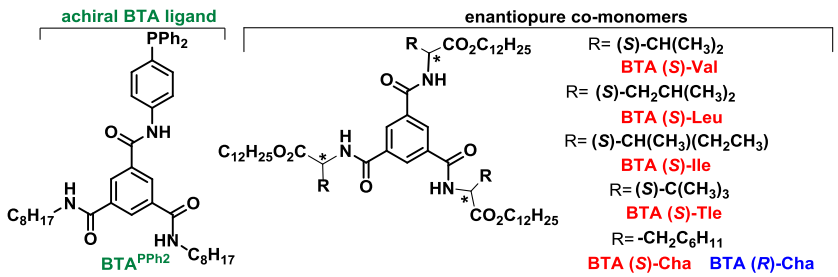

Table 1: Catalytic screening of BTA monomers for the copper-catalysed hydrosilylation of NPnone.[a]

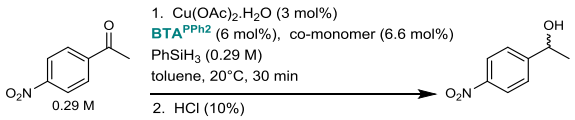

1. Entry	2. co-monomer	3. *e.e.* (%)
1. 1	2. **BTA (*S*)-Tle**	3. +47 (*R*)
4. 2	5. **BTA (*S*)-Val**	6. +48 (*R*)
7. 3	8. **BTA (*S*)-Leu**	9. +53 (*R*)
10. 4	11. **BTA (*S*)-Ile**	12. +53 (*R*)
13. 5	14. **BTA (*S*)-Cha**	15. +54 (*R*)
16. 6	17. **BTA (*R*)-Cha**	18. -54±1 (*S*)[b]

[a] Conversion>99%. [b] Based on repeatability tests (Table S.1).

In order to implement our concept, a scalemic mixture of enantiopure co-monomers has to promote the asymmetric reaction with a level of selectivity similar to that of the enantiopure monomer. We thus probed the selectivity obtained by mixing **BTA^{PPh2}** and a scalemic mixture of **BTA Cha** (25% *e.e.* in favour of **BTA (*R*)-Cha**) for the hydrosilylation of NPnone. Whatever the conditions probed (temperature, molar ratio of **BTA Cha** over **BTA^{PPh2}**), the enantioselectivity of the reaction remains higher than expected when considering only the optical purity of the engaged scalemic mixture (Table S.2). These chirality amplification effects are particularly strong at 20°C since a 25% *e.e.* scalemic mixture provides the product with 85% of the optimal selectivity. We further assessed the selectivity obtained for various scalemic mixtures of **BTA Cha** at 0°C (Figure 1a, blue curve). The plot displays a sigmoidal shape with a plateau, corresponding to the optimal selectivity, reached at a value of *ca.* 50% *e.e.* of **BTA Cha**. The chirality amplification is slightly decreased at this temperature since 33% *e.e.* scalemic mixtures are required to get 88% of the optimal selectivity. This reduction of the chirality amplification effect at lower temperatures has been observed previously in majority-rule experiments conducted with alkyl BTAs (see further detail in Table S.2).[32] The curve is symmetrical (inversion point at x=0): it demonstrates that the enantiomeric state of the catalyst can be inverted by simply changing the nature of the major enantiomer in the co-assemblies (*vide infra*). To further ascertain the origin of this chirality amplification effect, we precisely investigated the nature of the assemblies. When studied individually, **BTA^{PPh2}** (Figure S.1) and **BTA (*S*)-Cha** (Figure S.2) assemble into stacks[25-26] and dimers[33-35] respectively at mM concentration in toluene, in agreement with our previous results. The formation of co-assemblies between **BTA^{PPh2}** and **BTA (*S*)-Cha** ([**BTA(*S*)-Cha**]/[**BTA^{PPh2}**]=1.1) in toluene is confirmed by FT-IR (Figures S.3 and S.4) and Small Angle Neutron Scattering analyses (SANS, Figure S.5). According to a quantitative analysis of such data,[26] the amount of **BTA (*S*)-Cha**

incorporated into the stacks is ~50% meaning that *ca.* 35% of the BTA monomers present in the co-assemblies are enantiopure. The chiroptical properties of the co-assemblies were then assessed by Circular Dichroism (CD, Figure S.6).[36] All mixtures of **BTA Cha** and **BTA^{PPh2}** show a Cotton effect centred at λ=310 nm, the sign of which depends on the nature of the major enantiomer present in the co-assemblies (Figure S.7). As only **BTA^{PPh2}** absorbs in this region, the presence of this induced CD signal[37] confirms that the phosphine groups of the ligand are located in the chiral environment provided by the co-assemblies and that the direction of the induced chirality is controlled by the co-monomer. As expected, the plot of the net helicity as a function of the *e.e.* of **BTA Cha** for various scalemic mixtures shows that chirality amplification effects govern the formation of single-handed helices (Figure 1a, black curve). Indeed, 33% *e.e.* scalemic mixtures form homochiral assemblies.[38] This demonstrates that the chirality amplification effect observed in the catalytic experiments mentioned above stems from the chirally-amplified nature of the helical scaffold of the catalyst. Based on the sign of the CD signal in the 200-270 nm region (Figure S.8),[29] the outcome of the catalytic reaction can be correlated to the structure of the co-assemblies: scalemic mixtures biased in favour of **BTA (*R*)-Cha** form left-handed helices supporting Cu catalytic centres which in turn provide the (*S*) enantiomer of the hydrosilylation product (see a schematic representation in Scheme 1).

a)

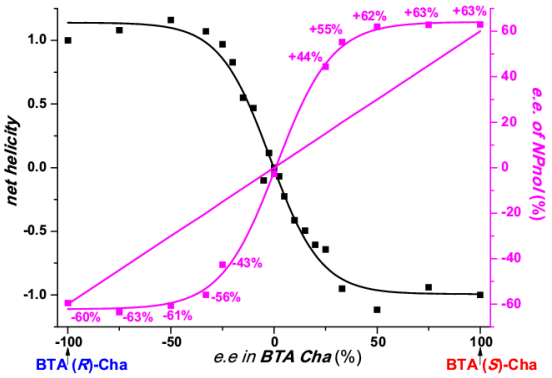

b)

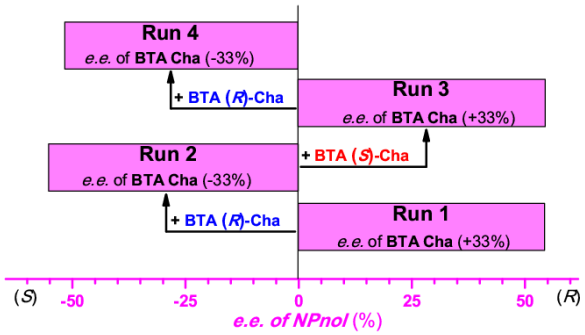

c)

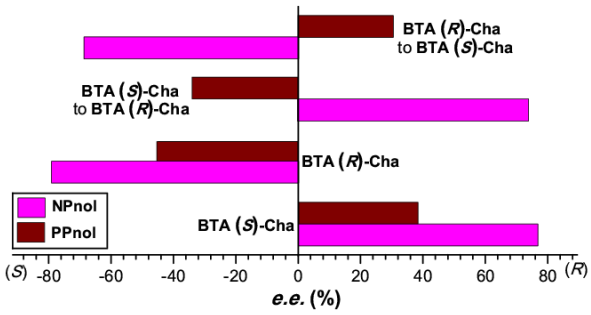

Figure 1. a) Enantiomeric excess of 1-(4-nitrophenyl)ethanol (NPnol) and net helicity versus BTA Cha enantiomeric excess. See Table S.2 for reaction conditions. The blue line represents the selectivity that would be obtained in absence of chirality amplification. The net helicity for the various co-assemblies was measured by CD spectroscopy by dividing the ellipticity (□=305 nm) of each mixture by the ellipticity of the mixture containing enantiopure BTA Cha (Figure S.7). The curves are guides to the eye. b) Copper-catalysed hydrosilylation of NPnone with sequential additions of substrate and $PhSiH_3$. Amount of BTA Cha added during the reaction: **BTA (*R*)-Cha** (13.0 mol%, run 2), **BTA (*S*)-Cha** (26.0 mol%, run 3), **BTA (*R*)-Cha** (52.0 mol%, run 4). See Table S.3 for more experimental details. c) Copper-catalysed hydrosilylation of a 1:1 mixture of NPnone and PPnone. For the selectivity-inverting experiments, 20.0 mol% of BTA Cha was added during the reaction. See Table S.5 for more experimental details.

To demonstrate the dynamic nature of the catalytic system, we first envisaged to switch its selectivity *in situ* in a procedure involving sequential additions of NPnone and $PhSiH_3$ (Table S.3). The reaction was started with a scalemic mixture biased in favour of **BTA (*S*)-Cha** (+33% *e.e.*, run 1). After 15 minutes, complete conversion of the substrate was achieved leading to (*R*)-1-(4-nitro)phenylethanol with 53% *e.e*. Then **BTA (*R*)-Cha** was added in order to invert the enantiomer bias in the mixture (-33% *e.e.* of **BTA Cha**, run 2) and thus the handedness of the co-assemblies. The same protocol was reproduced in order to get 4 successive runs corresponding to three switches of the selectivity. The enantioselectivity for each run was deduced from the cumulative selectivity measured by chiral Gas Chromatography (GC). The full inversion of the selectivity observed for each consecutive run (Figure 1b) confirms that the enantiomeric state of the catalyst can be completely switched *in situ*. In addition, thanks to the chirally-amplified helical scaffold (*vide supra*), the selectivity of the run (54% *e.e.* on average) is close to the optimal selectivity (63% *e.e.*) achievable under these experimental conditions. In comparison, 21% *e.e.* would have been obtained in absence of chirality amplification (Figure S.10).

We then measured the time required for the stereochemical switch by adding the BTA co-monomer (switch trigger) and $PhSiH_3$ (reaction trigger) at different time intervals. According to the result presented in Table S.4, full enantioinversion is achieved in *ca.* 5 seconds. The reaction time of NPnone is of the same order and thus the chirality switch cannot be fully accomplished during the conversion of this substrate. In contrast, the reaction rate of 1-(4-biphenylyl)ethanone (PPnone) is lower which allows the enantioinversion process to be performed during its transformation with no negative impact on the obtained selectivity (Scheme S.1).

The previous experiments prompted us to probe the possibility of inverting the selectivity of the catalyst during the hydrosilylation of a 1:1 mixture of NPnone and PPnone. We performed two experiments with enantiopure co-monomers (**BTA (*S*)-Cha** and **BTA (*R*)-Cha**) and two selectivity-inverting experiments starting with a scalemic mixture of enantiopure co-monomers (+60% *e.e.*→-60% *e.e.* and -60% *e.e.*→+60% *e.e.,* Table S.5). As expected, 1-(4-nitrophenyl)ethanol (NPnol) and 1-(4-biphenylyl)ethanol (PPnol) were obtained with the same preferred configuration, *i.e.* predominantly (*R*) or (*S*), when the reaction was conducted with a single enantiomer of the BTA co-monomer (Figure 1c). More precisely, the experiment performed in the presence of **BTA (*S*)-Cha** (respectively **BTA (*R*)-Cha**) provided the alcohols with optimal selectivities: +77%/+38% *e.e.* (respectively -79%/-45% *e.e.*) for NPnol and PPnol. In contrast, the alcohols were obtained with an opposite preferred configuration, *e.g.* one is predominantly (*R*) whilst the other is predominantly (*S*), when the enantiomer in excess in the co-assemblies was changed during the course of the catalytic reaction. The selectivities obtained for

these experiments +74%/-34% *e.e.* or -69%/+30% *e.e.* (NPnol/PPnol) compared well with those obtained with a single co-monomer (Figure 1c). Any combination of the enantiomers is thus obtained in a one-pot procedure without significant dwindling of the catalyst selectivity.[21-23]

III Conclusion

We have exploited the chirality amplification properties of supramolecular polymer helices to control *in situ* the enantioselectivity displayed by phosphine copper catalytic centres located at their periphery. Switching the enantiomeric state of a catalyst in between sequential transformations could provide access to any diastereomer in cascade stereoselective reactions without purification of the reaction intermediate.[31] Also, a fast stereochemical switch is key for a precise stereocontrol of polymerization reactions.[11-12] The selectivity of the present catalytic system can be inverted both in between different reactions and in real time during the reaction. Improving the catalytic efficiency should be possible by combining the present concept with the recent advances achieved in tuning the composition, the structure, the stability and the stimuli-responsiveness of supramolecular polymers and assemblies.[39-42]

IV Supporting Information

Supplementary Tables. Catalytic experiments: chirality induction and amplification [Tables S.1 and S.2]

Table S.1 Repeatability of the catalytic experiments for the hydrosilylation of 1-(4-nitrophenyl)ethanone.[a]

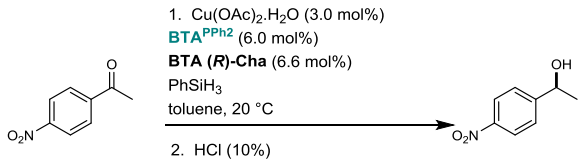

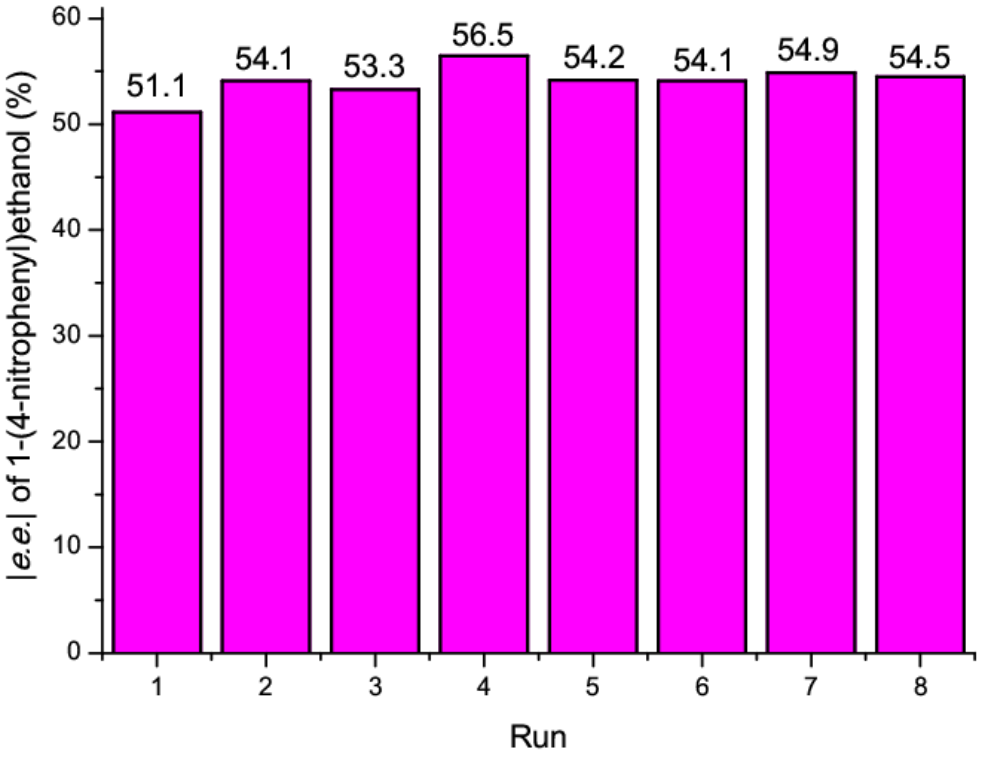

[a] The above table summarizes 8 batches of reactions that have been repeated in the same conditions namely: 1-(4-nitrophenyl)ethanone (0.29 M), $Cu(OAc)_2 \cdot H_2O$ (3.0 mol%), **BTA^{PPh2}** (6.0 mol%, 16.9 mM), **BTA (*R*)-Cha** (6.6 mol%, 18.6 mM), $PhSiH_3$ (0.29 M), toluene, 20°C, 30 min. Conversion >99% was obtained for all runs as determined by GC and ^{1}H NMR analyses. Based on this repeatability assessment, a mean *e.e.* value of 54.1% is determined over the 8 runs. The standard deviation is s=1.4 and the variance is s^2=2.0. Accordingly, an error bar of ± ½ variance (±1% *e.e.*) was set to the *e.e.* values obtained with mixtures of **BTA^{PPh2}** and **BTA (*R*)-Cha** (Table 1).

Table S.2 Hydrosilylation of 1-(4-nitrophenyl)ethanone with a scalemic mixture of enantiopure **BTA Cha** co-monomers (25% *e.e.*).[a]

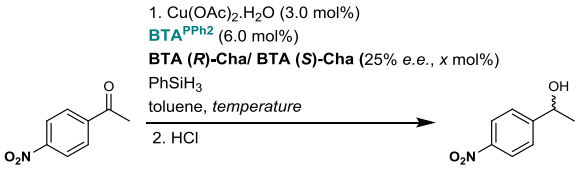

Entry	T (°C)	**BTA (*R*)-Cha** (mol%)	**BTA (*S*)-Cha** (mol%)	expected unamplified *e.e.* (%)[b]	obtained *e.e.* (%)	R_{ampl}[c]
1	**20**	6.6	0	-	-54	-
2	**20**	4.1	2.5	-13.5	-39	2.86
3	**20**	13.2	0	-	-54	-
4	**20**	8.2	5.0	-13.5	-45	3.33
5	**0**	6.6	0	-	-63	-
6	**0**	4.1	2.5	-15.8	-27	1.72
7	**0**	13.2	0	-	-63	-
8	**0**	8.2	5.0	-15.8	-45	2.87
9	**-25**	6.6	0	-	-78	-
10	**-25**	4.1	2.5	-19.5	-29	1.47
11	**-25**	13.2	0	-	-78	-
12	**-25**	8.2	5.0	-19.5	-34	1.72

[a] Reaction conditions: 1-(4-nitrophenyl)ethanone (0.29 M), $Cu(OAc)_2 \cdot H_2O$ (3.0 mol%), **BTA^{PPh2}** (6.0 mol%, 16.9 mM), 25% *e.e.* scalemic mixture biased in favour of **BTA (*R*)-Cha** (x mol%), $PhSiH_3$ (0.29 M), toluene. Conversion >99% was obtained for all entries as determined by GC and ^{1}H NMR analyses. [b] Expected *e.e.* in the absence of any chirality amplification effect, considering the optical purity of the engaged scalemic mixture of enantiopure **BTA Cha**. [c] Majority-rule factor defined as R_{ampl}= (obtained *e.e.*)/(expected *e.e.* in absence of chirality amplification). R_{ampl}=1.0 means no chirality amplification and the higher R_{ampl} the higher the chirality amplification effect. Conditions highlighted in orange have been selected for probing the chirality amplification effect displayed by the catalytic assemblies (Fig. 1a). Reaction conditions: 1-(4-nitrophenyl)ethanone (0.29 M), $Cu(OAc)_2 \cdot H_2O$ (3.0 mol%), **BTA^{PPh2}** (6.0 mol%, 16.9 mM), **BTA (R)-Cha**/**BTA (S)-Cha** (x % e.e., 13.2 mol%), $PhSiH_3$ (0.29 M), toluene, 0°C. Conversion >99% was obtained in all cases as determined by GC and ^{1}H NMR analyses.

Supplementary Tables and Figures: Characterization of the Cu supramolecular catalyst by means of various spectroscopic and scattering analyses [Figures S.1 to S.9]

Postulated active copper hydride species (made by reacting **BTA^{PPh2}**, $Cu(OAc)_2 \cdot H_2O$ and $PhSiH_3$) are poorly stable under our experimental conditions in the absence of substrate or product. Accordingly, in the following, we will focus on the characterization of the co-assemblies formed by mixing: i) **BTA^{PPh2}** and **BTA (*R*)-Cha**, and ii) **BTA^{PPh2}** coordinated to Cu (**BTA^{PPh2}**/$Cu(OAc)_2 \cdot H_2O$= 2.0) and **BTA (*R*)-Cha**.

a)

b)

c)

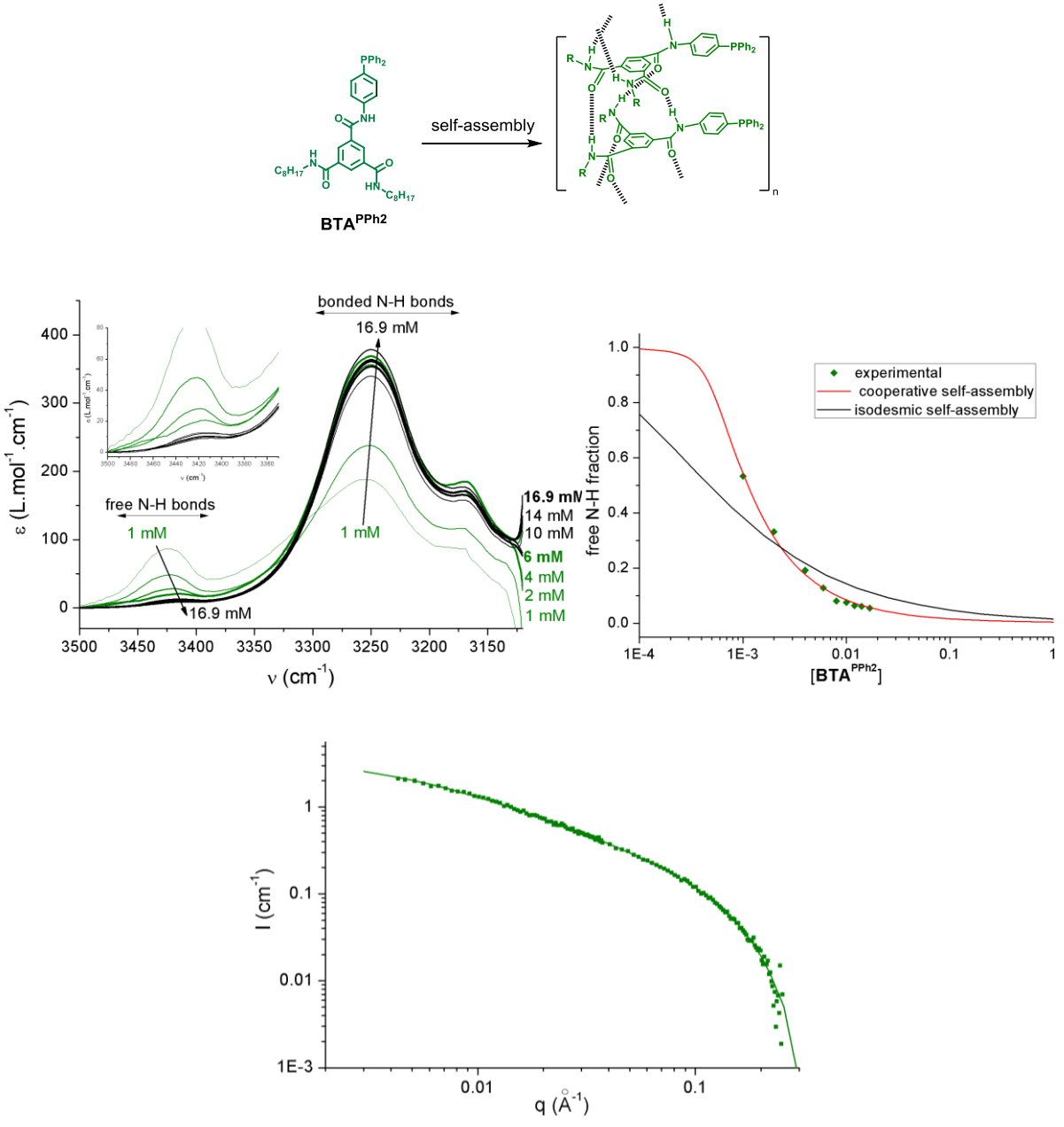

Figure S.1 Characterization of the homo-assemblies formed by **BTA^{PPh2}**. (a) FT-IR analyses of **BTA^{PPh2}** at various concentrations in toluene (20 °C). Zoom on the N-H region. (b) Plot of the free N-H fraction as a function of the concentration in **BTA^{PPh2}**. (c) SANS analysis of **BTA^{PPh2}** (11.7 $g.dm^{-3}$, 16.9 mM) in toluene-d_8 (20°C).

The absorption band at ν=3235 cm^{-1} (a) is diagnostic of the bonded N-H present in stacks whilst the absorption band at ν=3430 cm^{-1} is diagnostic of free N-H (belonging either to monomers or to BTA molecules located at the chain-ends of the assemblies). The fraction of free N-H can be deduced from these FT-IR data by a linear regression of the plot of ([**BTA**$^{\mathbf{PPh2}}$]×l)/A_b^{N-H} versus A_f^{N-H}/A_b^{N-H} with [**BTA**$^{\mathbf{PPh2}}$] = total concentration in **BTA**$^{\mathbf{PPh2}}$, l = cell pathlength, A_b^{N-H} = maximum of the absorption band for bonded N-H, A_f^{N-H} = maximum of the absorption band for free N-H. It provides the following value for the molar extinction coefficients: ε_b^{N-H}=390 $L.mol^{-1}.cm^{-1}$ and ε_f^{N-H}=158 $L.mol^{-1}.cm^{-1.}$ The data in (b) can be perfectly fitted by a cooperative model for self-assembly[43] (K_2/K model) but not by an isodesmic model.[44] The fit gives the following values: K_2=35 M^{-1}, K=1794 M^{-1}, K/K_2=51 (DPn=18 and DPw=75 for [BTA^{PPh2}]=16.9 mM). SANS analysis of **BTA**$^{\mathbf{PPh2}}$ (c) is fitted with the form factor for long and rigid rods with a circular cross-section and a uniform scattering length density (with the DANSE software SasView). The fit yields a radius of 11.5 Å and a length of 204 Å for the stacks formed by **BTA**$^{\mathbf{PPh2}}$.

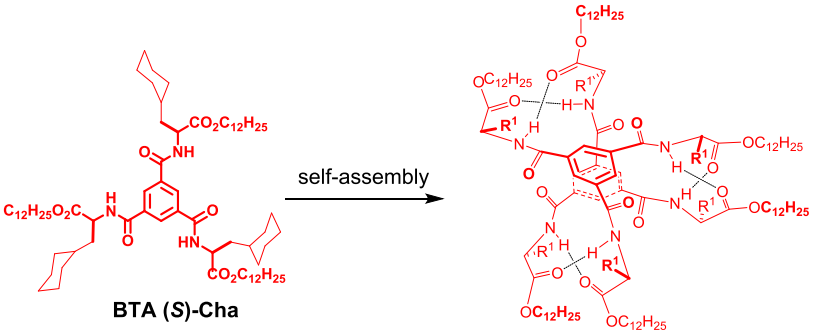

a)

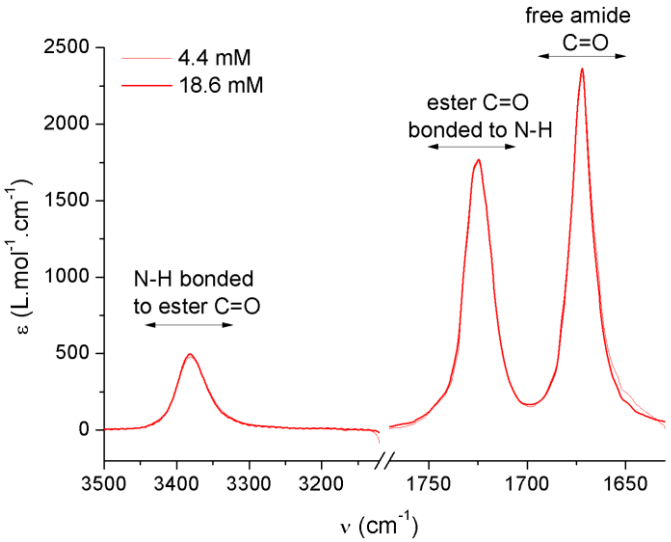

b)

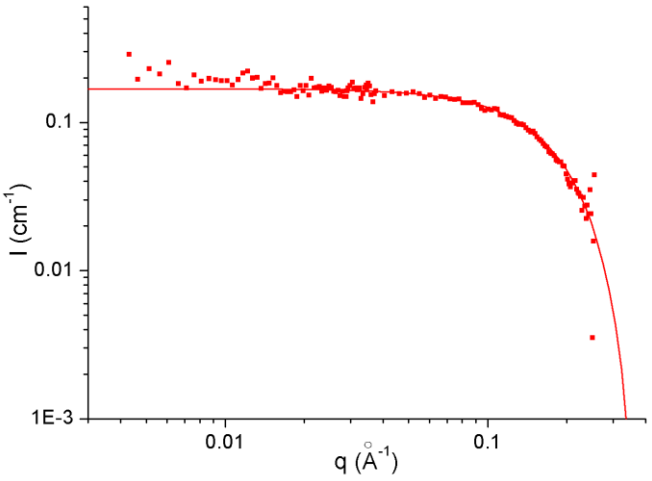

Figure S.2 Characterization of the homo-assemblies formed by **BTA (*S*)-Cha**. (a) FT-IR analyses of **BTA Cha** at 4.4 mM and 18.6 mM in toluene (20 °C). Zoom on the N-H and C=O region. (b) SANS analysis of **BTA (*S*)-Cha** (21.9 g.dm^{-3}, 18.6 mM) in toluene-d_8 (20°C).

The absorption band at ν=3381 cm^{-1} (a) corresponds to N-H bonded to carbonyl ester functions and is diagnostic of the hydrogen-bonded network present in the ester-bonded dimers formed by ester

BTAs. SANS analysis of **BTA (*S*)-Cha** (b) confirms the formation of small assemblies since the scattering curve can be fitted according to a form factor for spherical objects having 1.5 times the molar mass of the monomer (result of the fit: r = 12.0 Å and M = 1750 g.mol^{-1}). More details on the structure and stability of the ester-bonded dimers formed by ester BTAs can be found in the literature.[33-35]

Characterization of the co-assemblies formed by BTA^{PPh2}, coordinated or not to copper, and BTA (*S*)-Cha.

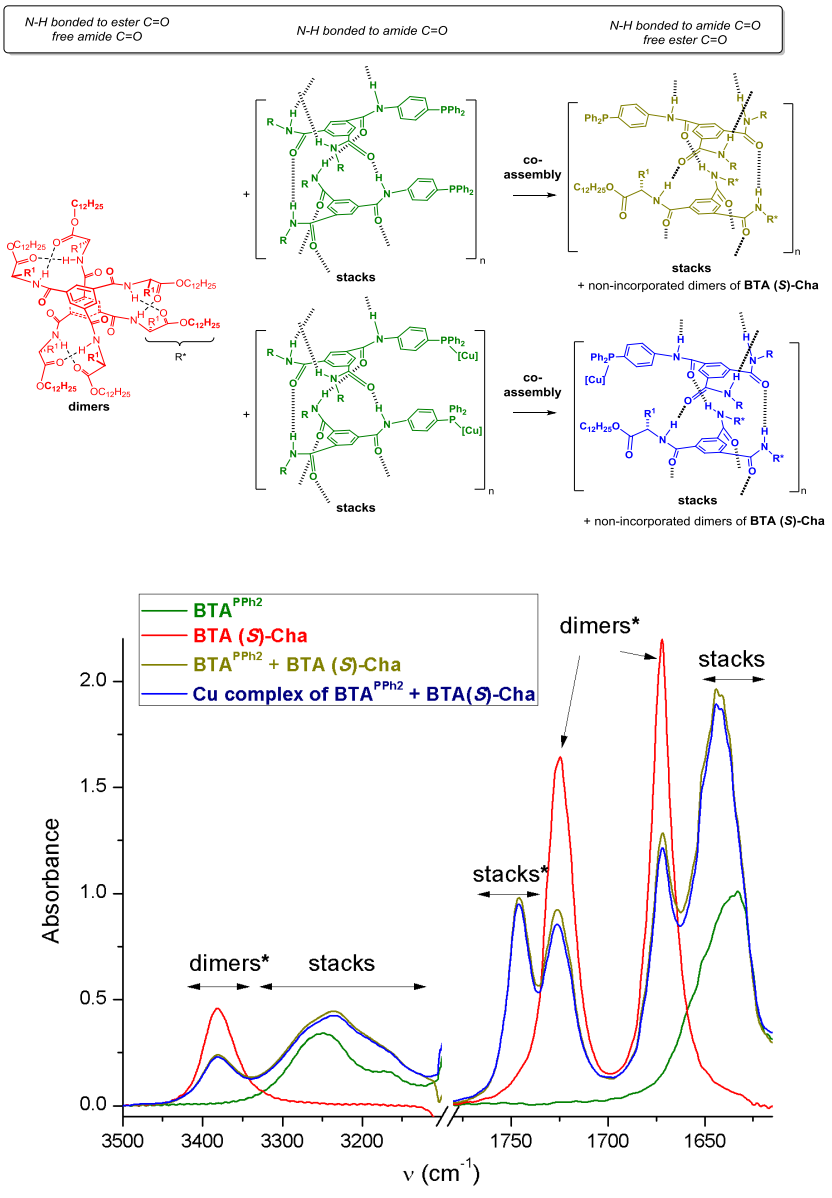

Figure S.3 FT-IR analyses of **BTA^{PPh2}** (16.9 mM), of **BTA (*S*)-Cha** (18.6 mM) and of the mixtures of **BTA^{PPh2}** (16.9 mM) and **BTA (*S*)-Cha** (18.6 mM) with and without Cu coordinated to **BTA^{PPh2}** in toluene at 20 °C. ***** These absorption bands belong exclusively to **BTA (*S*)-Cha** either in dimers or in stacks (co-assembly).

Upon co-assembly, a fraction of **BTA (*S*)-Cha** molecules is incorporated into the stacks formed by **BTA^{PPh2}** as indicated by: i) the decreased intensity of the absorption bands belonging to **BTA (*S*)-Cha** (ν_{N-H}=3380 cm^{-1}, $\nu_{esterC=O}$=1725 cm^{-1} and $\nu_{amideC=O}$=1672 cm^{-1}), ii) the increased intensity of the absorption bands corresponding to stacks (ν_{N-H}=3235 cm^{-1} and $\nu_{amideC=O}$=1645 cm^{-1}) and iii) the emergence of a new absorption band at ν=1745 cm^{-1} which corresponds to free ester C=O functions and thus belongs exclusively to **BTA (*S*)-Cha** molecules incorporated into stacks. The FT-IR spectra of the mixtures with and without Cu coordinated to **BTA^{PPh2}** are virtually identical indicating that the presence of the Cu has little influence on the composition of the co-assemblies. For the determination of the amount of **BTA (*S*)-Cha** incorporated into stacks, see below.

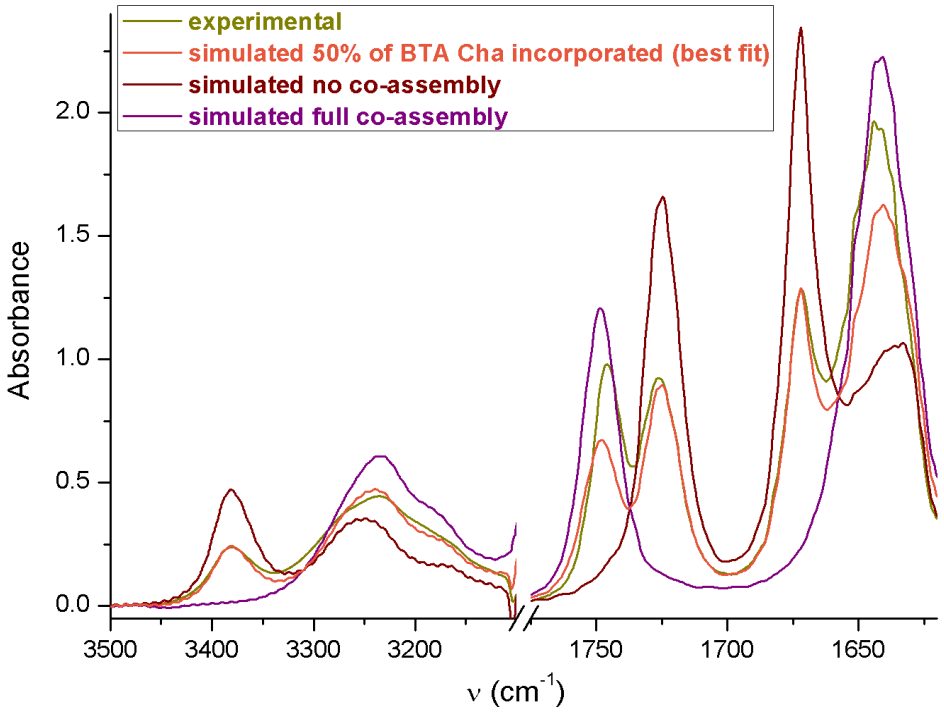

Figure S.4 Quantification of the amount of **BTA (*S*)-Cha** present in the co-assemblies.[26] FT-IR analysis of the mixture of **BTA^{PPh2}** (16.9 mM) and **BTA (*S*)-Cha** (18.6 mM) in toluene at 20°C. Simulated spectra for the extreme cases for which all or no **BTA (*S*)-Cha** is present in the co-assemblies. The fraction of **BTA (*S*)-Cha** incorporated into stacks (relatively to the amount of **BTA (*S*)-Cha** introduced initially, *i.e.* 18.6 mM) is 50% as deduced from the best fit with the simulated FT-IR spectra (estimated error 10%). It means that ~35% of the BTA co-monomers present in the co-assemblies are **BTA Cha**.

* The simulated spectrum of the stacks for the co-assemblies is the weighted average of the contribution of each monomer (**BTA^{PPh2}** and **BTA (*S*)-Cha**) present in the stacks. The spectroscopic signature of

BTA (*S*)-Met,[33, 35] an ester BTA which forms stacks in solution contrarily to **BTA (*S*)-Cha**, was selected for the spectrum representing **BTA (*S*)-Cha** in the co-assemblies. The quality of the fit validates the hypothesis that the conformation of **BTA (*S*)-Cha** molecules in the co-assembly is similar to that of **BTA (*S*)-Met** molecules in the stacks.

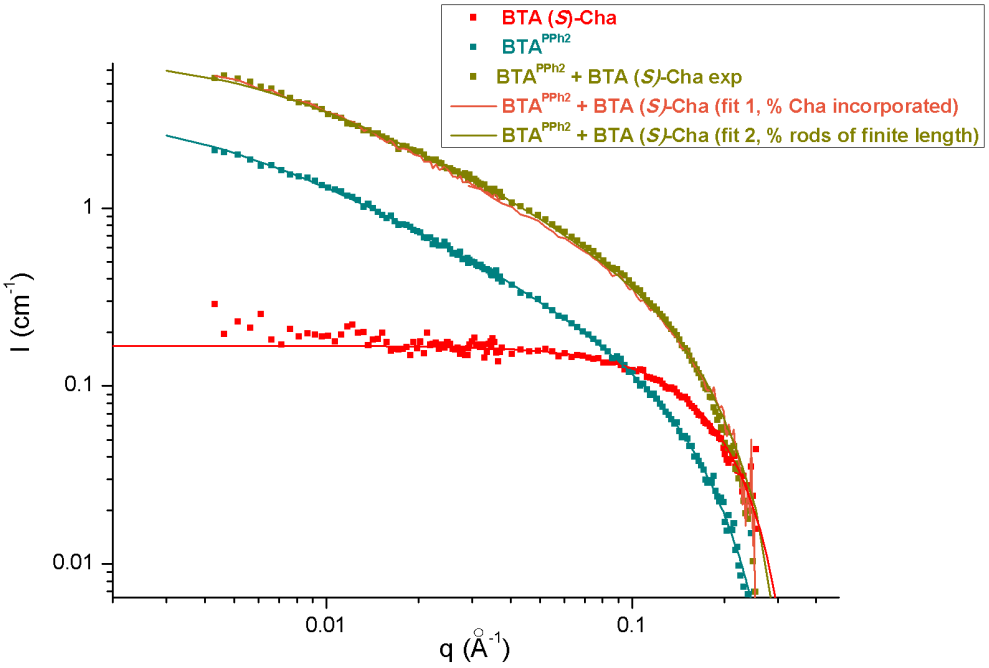

Figure S.5 Characterization by SANS analyses of the composition of the co-assemblies formed between **BTA^{PPh2}** (11.7 g.dm^{-3}, 16.9 mM) and **BTA (*S*)-Cha** (21.9 g.dm^{-3}, 18.6 mM) in toluene-d_8 (20°C).

Fit 1: the experimental curve for the mixture of **BTA^{PPh2}** and **BTA (*R*)-Cha** is fitted according to the hypothesis that **BTA (*R*)-Cha** in part co-assembles with **BTA^{PPh2}** and that the remaining **BTA (*R*)-Cha** exists as dimers. The hypothesis is confirmed by the quality of the fit and by FT-IR analyses presented above (Figure S.4). The fit gives the following results: 67% of **BTA (*R*)-Cha** is incorporated into stacks. This value is in agreement with that deduced from FT-IR analysis (50 %, see Figure S.4).

Fit 2: the length of the co-assemblies formed by **BTA^{PPh2}** and **BTA (*R*)-Cha** is determined by fitting the SANS analysis with a form factor for rigid rods of finite length with a circular cross-section and a uniform scattering length density. It gives a length of 145 Å for the co-assemblies which are hence shorter than the stacks formed by **BTA^{PPh2}** (204 Å). For the results of the fits corresponding to SANS analyses of BTAPPh2 and BTA (R)-Cha, see Figures S.1 and S.2 respectively.

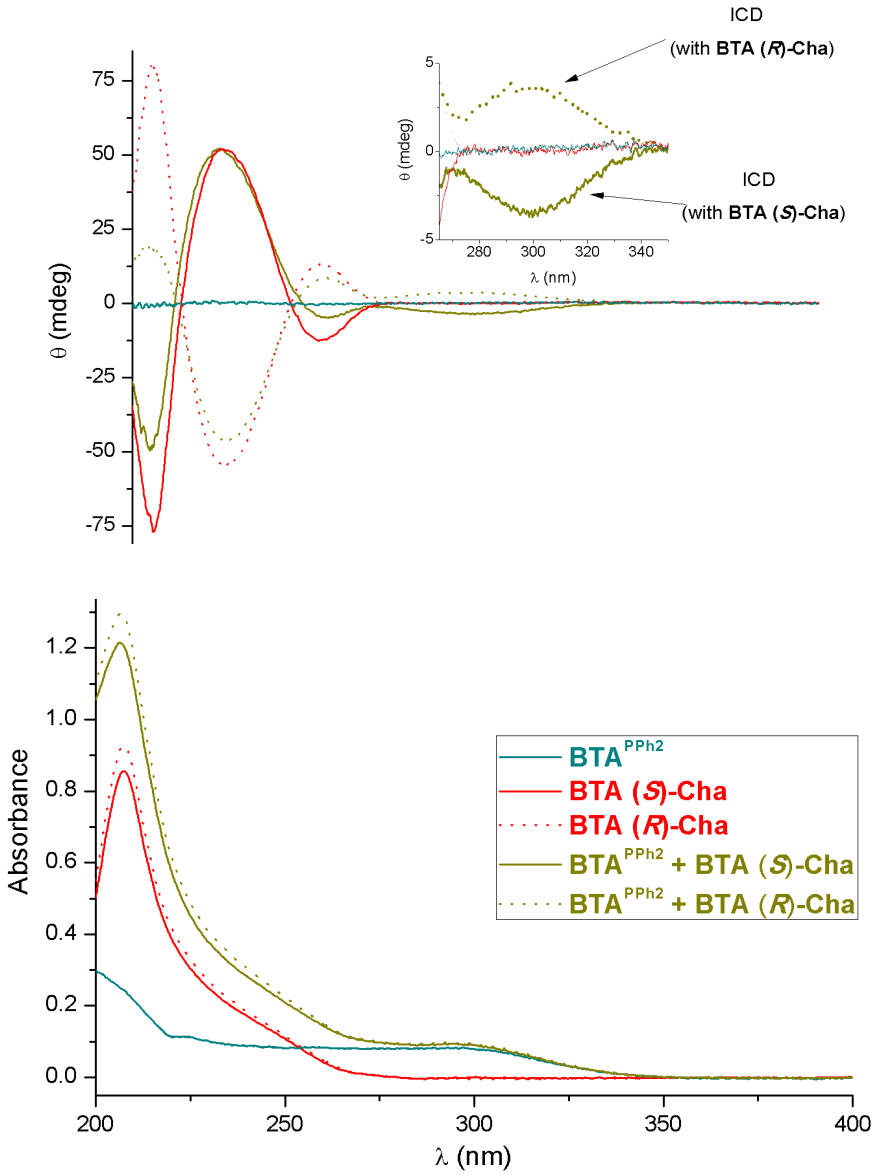

Figure S.6 CD (top) and UV (bottom) analyses of **BTA^{PPh2}** (0.625 mM), of **BTA (*S*)-Cha** (1.375 mM), of **BTA (*R*)-Cha** (1.375 mM) and of the mixtures of **BTA^{PPh2}** (0.625 mM) and **BTA (*S*)-Cha** (1.375 mM) and of **BTA^{PPh2}** (0.625 mM) and **BTA (*R*)-Cha** (1.375 mM) in methylcyclohexane at 20 °C.

CD analyses of **BTA (*S*)-Cha** and **BTA (*R*)-Cha** with three maxima in the region of 200-270 nm are diagnostic of the ester-bonded dimers.[33-35] Mixtures of **BTA^{PPh2}** and **BTA Cha** show, in addition to CD signals in the 200-270 nm region, a Cotton effect centered at □=310 nm, of same intensity but opposite sign depending on the enantiomer of **BTA Cha** present in the mixture. As only **BTA^{PPh2}** absorbs in this region, this signal is called an induced CD signal (ICD)[37] and thus indicates that the achiral ligand is located in the chiral environment formed by the helical BTA co-assemblies. Also, enantiomers of **BTA Cha** are able to fully switch the chirality induced to **BTA^{PPh2}**.

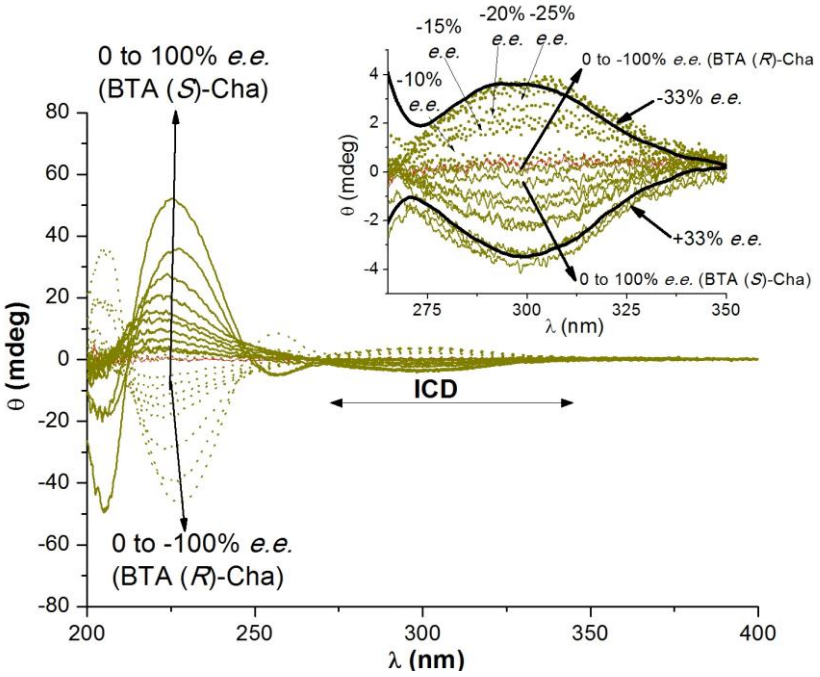

Figure S.7 CD analyses of mixtures of **BTA^{PPh2}** (0.625 mM) and **BTA Cha** of various enantiomeric excesses (1.375 mM) in methylcyclohexane at 20°C. Inset: zoom on the ICD signals.

The mixtures with +33% *e.e.* and -33% *e.e.* have been thickened since a maximum intensity of the ICD signal is reached for these mixtures. CD analyses were recorded for the following $|e.e.|$ in **BTA Cha**: 0%, 2.5%, 5%, 10%, 15%, 20%, 25%, 33%, 50%, 75% and 100%.

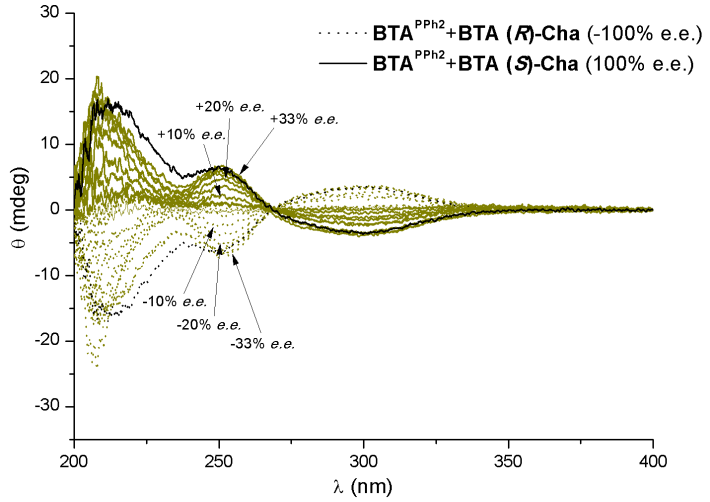

Figure S.8 "Diluted majority rule experiments" of Fig. S.7 processed in order to remove the contribution of **BTA Cha** dimers to the overall CD signal. The amount of **BTA Cha** that remains as dimers in the mixtures (conditions indicated in Fig. S.7) has been quantified to 80% by means of FT-IR analyses (data not shown).

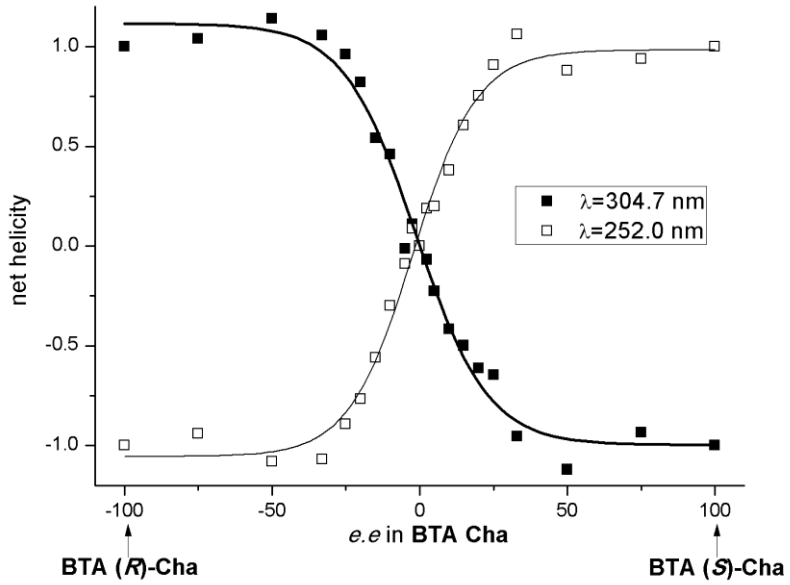

Figure S.9 "Diluted majority rule experiments": Net helicity as a function of the enantiomeric excess of **BTA Cha** determined according to CD analyses shown in Figures S.8. The net helicities were obtained by dividing the ellipticities at λ=305 nm and λ=252 nm for each mixture by the ellipticities measured for the mixture containing enantiopure **BTA Cha**. The lines are drawn as a guide to the eye.

Supplementary Tables, Schemes and Figures: selectivity-switching experiments [Tables S.3 to S.5, Scheme S.1, Figure S.10]

Table S.3 Copper-catalysed hydrosilylation of 1-(4-nitrophenyl)ethanone with successive additions of substrate and $PhSiH_3$.[a],[b],[c]

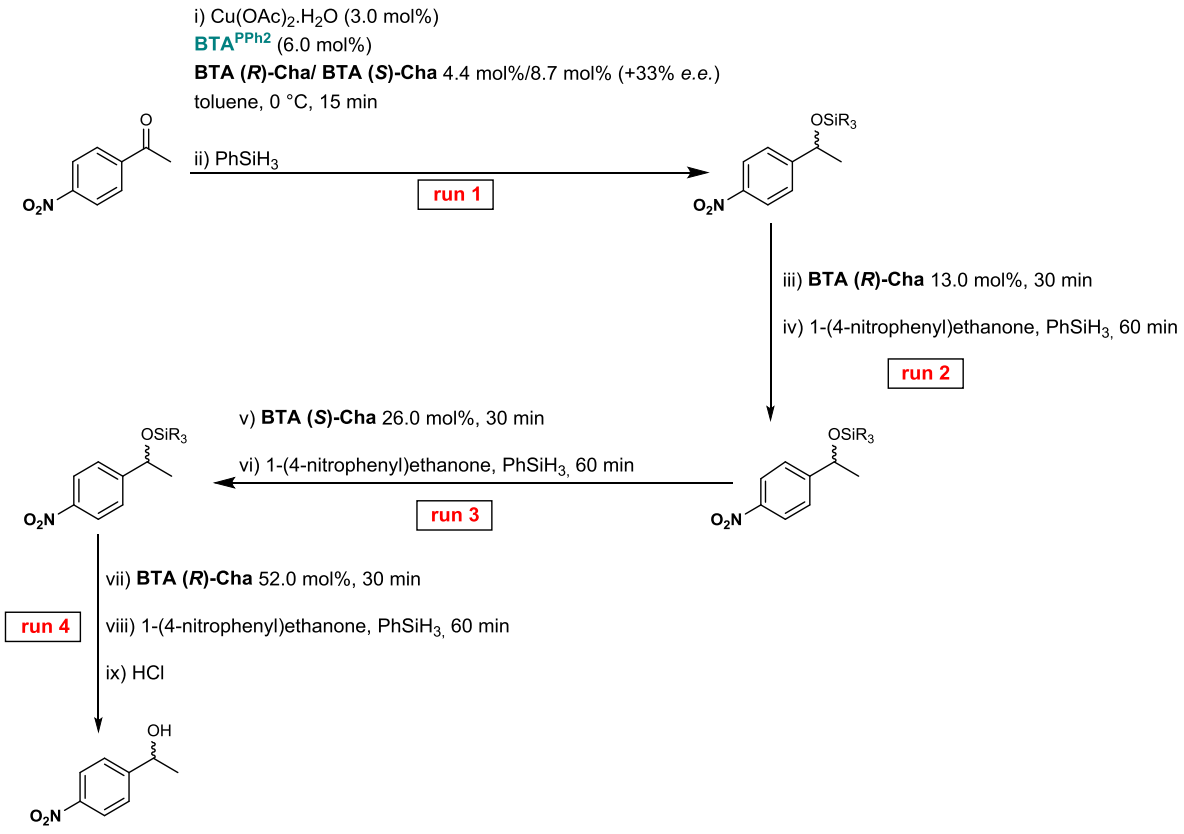

Run	**BTA (*R*)-Cha** (mol%)	**BTA (*S*)-Cha** (mol%)	obtained *e.e.* (%)	*e.e.* for the run *(%)*
1	4.4	8.7	+53 (*R*)	+53 (*R*)
2	17.4	8.7	-2 (*S*)	-56 (*S*)
3	17.4	34.7	+17 (*R*)	+53 (*R*)
4	69.4	34.7	0	-52 (*S*)

[a] Reaction conditions: 1-(4-nitrophenyl)ethanone (4×100 mol% = 400 mol% in total), $Cu(OAc)_2 \cdot H_2O$ (3.0 mol%), **BTA^{PPh2}** (6.0 mol%), **BTA (*R*)-Cha/BTA (*S*)-Cha** ($|e.e.| = 33\ \%$), $PhSiH_3$ (200 mol% for run 1and then 100 mol% for run 2, run 3 and run 4 = 500 mol% in total), toluene, 0 °C. For the exact amount of BTA Cha present in each run, see the table. Conversion >99% was obtained for all runs as determined by GC and ^1H NMR analyses. For the GC analyses corresponding to each run see pages S.23 and S.24.

[b] The optimal selectivity for the supramolecular Cu catalyst under these conditions as determined in Fig. 1a is 63% *e.e.* This is the selectivity expected for a catalyst with a fully chirally-amplified helical backbone. In contrast, 21% *e.e.* (0.33 × 63) would be obtained in absence of chirality amplification. [c] The reaction times for the conversion of the substrate and for the stereochemical switch were not optimized (see Table S.4).

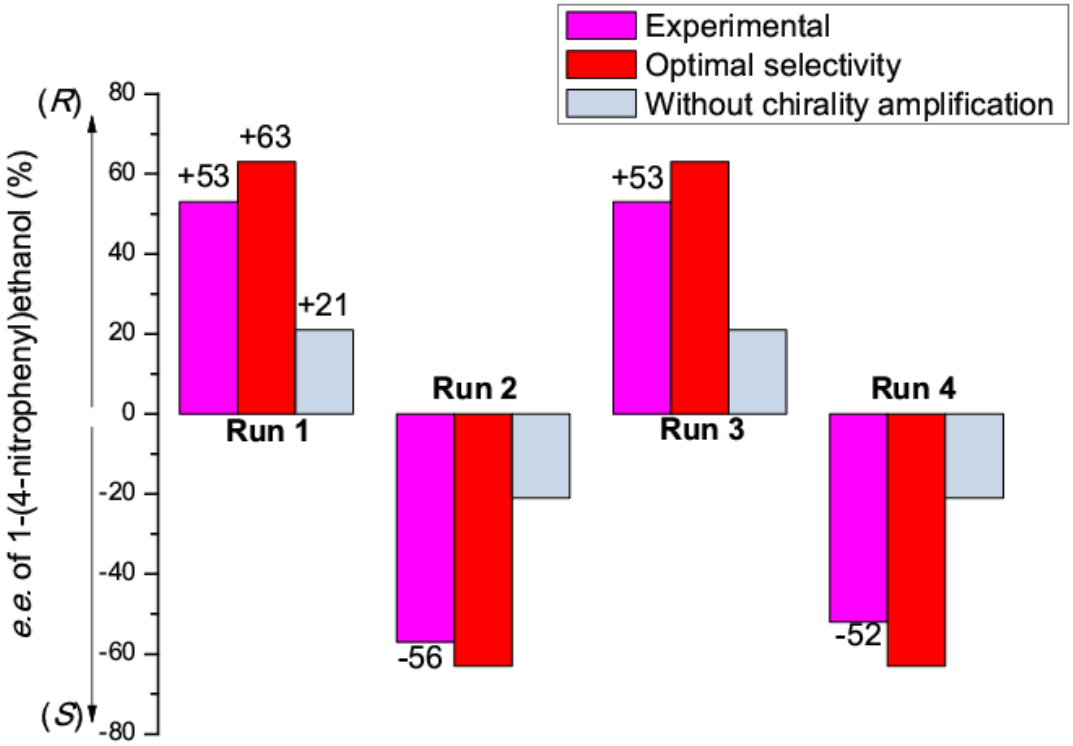

Figure S.10 Copper-catalysed hydrosilylation of 1-(4-nitrophenyl)ethanone with successive additions of substrate and $PhSiH_3$. Comparison of the enantioselectivity of the runs, the optimal selectivity and the selectivity in absence of chirality amplification. For the conditions and results of the sequential reaction and the definitions of the optimal selectivity and of the selectivity in absence of chirality amplification see the Table S.3.

Table S.4 Determination of the time required for switching the selectivity for the copper-catalysed hydrosilylation of 1-(4-nitrophenyl)ethanone.[a]

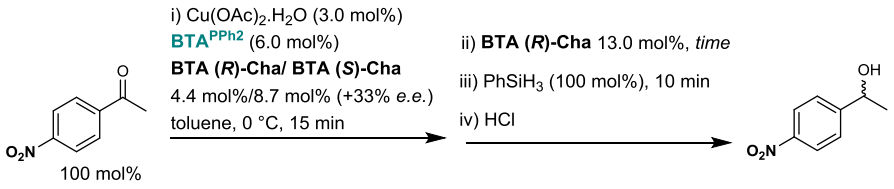

Entry	Time (s)	*e.e. (%)*
0	no **BTA (*R*)-Cha** addition	+60 (*R*)
1	0	+17 (*R*)[b]
2	5	-56 (*S*)
3	20	-60 (*S*)
4	60	-62 (*S*)

[a] Reaction conditions: 1-(4-nitrophenyl)ethanone (100 mol%), $Cu(OAc)_2 \cdot H_2O$ (3.0 mol%), **BTA^{PPh2}** (6.0 mol%), **BTA (*R*)-Cha**/**BTA (*S*)-Cha** (4.4 mol%/8.7 mol%, +33% *e.e.*), toluene, 0 °C. **BTA (*R*)-Cha** (13.0 mol%) was added and then $PhSiH_3$ (100 mol%) after a given time. Conversion >99% was obtained for all entries as determined by GC and ^1H NMR analyses. For the GC analyses corresponding to a time of 5 seconds (entry 2) see page S.35. [b] **BTA (*R*)-Cha** and $PhSiH_3$ were mixed together and added together to the precatalytic mixture. In these conditions, the selectivity switch was not complete. It means that the conversion of 1-(4-nitrophenyl)ethanone and the stereochemical switch occur at the same timescale.

Scheme S.1 Stereochemical switch during the conversion of 1-(4-biphenylyl)ethanone.[a]

a)

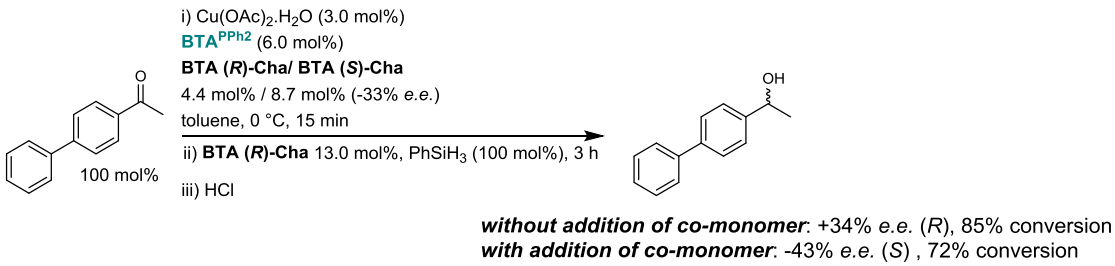

Reaction conditions: 1-(4-biphenylyl)ethanone (100 mol%), $Cu(OAc)_2 \cdot H_2O$ (3.0 mol%), **BTA^{PPh2}** (6.0 mol%), **BTA (*R*)-Cha/BTA (*S*)-Cha** (4.4 mol%/8.7 mol%, +33% *e.e.*), toluene, 0 °C. **BTA (*R*)-Cha** (13.0 mol%) and $PhSiH_3$ (100 mol%) were mixed and added at the same time. The conversion was determined by GC and ^{1}H NMR analyses. For the chiral HPLC analyses with and without switch, see pages S.26 and S.27.

b)

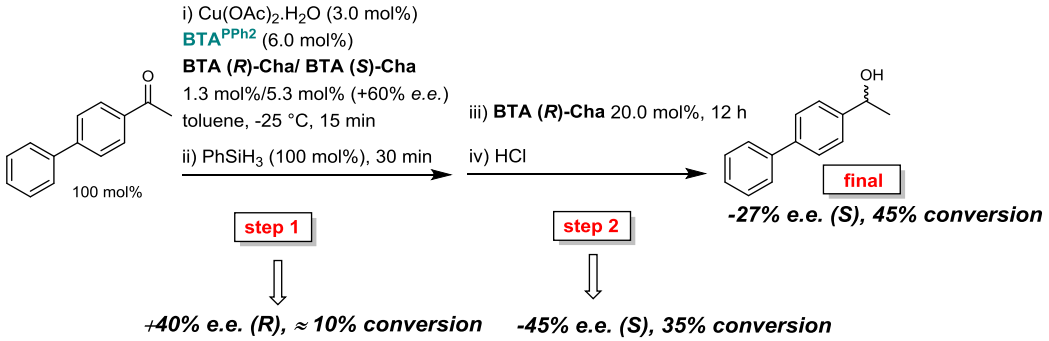

Reaction conditions: 1-(4-biphenylyl)ethanone (100 mol%), $Cu(OAc)_2 \cdot H_2O$ (3.0 mol%), **BTA^{PPh2}** (6.0 mol%), **BTA (*R*)-Cha/BTA (*S*)-Cha** (1.3 mol%/5.3 mol%, +60% *e.e.*), $PhSiH_3$ (100 mol%), toluene, -25 °C. **BTA (*R*)-Cha** (20.0 mol%) was added after 30 minutes**.** The conversion was determined by GC and ^{1}H NMR analyses. For the chiral HPLC analyses of step 1 (aliquot) and at the end of the reaction, see page S.28.

[a] The selectivity for step 2 was calculated according to the selectivities and conversions obtained in step 1 and at the end of the reaction. The selectivity of step 2 is optimal and inversed compared to step 1 confirming that full stereochemical switch occurs during the hydrosilylation of 1-(4-biphenylyl)ethanone.

Table S.5 Copper-catalysed hydrosilylation of 1:1 mixture of 1-(4-nitrophenyl)ethanone and 1-(4-biphenylyl)ethanone.[a]

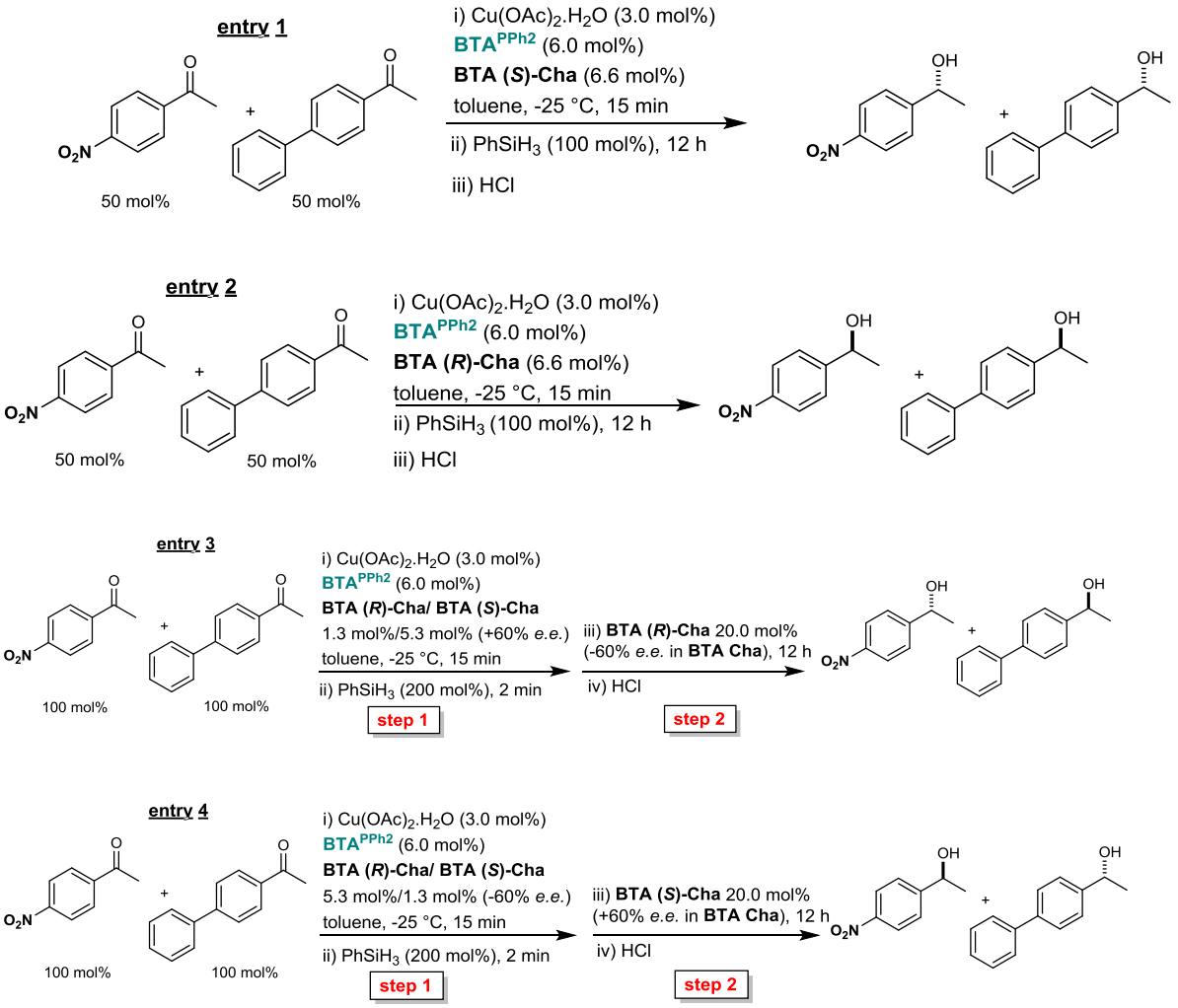

	1st step		2nd step		e.e. (%)	
Entry	BTA (*R*)-Cha (mol%)	BTA (*S*)-Cha (mol%)	BTA (*R*)-Cha (mol%)	BTA (*S*)-Cha (mol%)	4-NO_2	4-Ph
1	**BTA (*S*)-Cha** (6.6)				+77 (*R*)	+38 (*R*)
2	**BTA (*R*)-Cha** (6.6)				-79 (*S*)	-45 (*S*)
3	1.3	5.3	21.3	5.3	+74 (*R*)	-34 (*S*)
4	5.3	1.3	5.3	21.3	-69 (*S*)	+30 (*R*)

[a] Reaction conditions: 1-(4-nitrophenyl)ethanone (50 mol%, entries 1 and 2, 100 mol% entries 3 and 4), 1-(4-biphenylyl)ethanone (50 mol% entries 1 and 2, 100 mol% entries 3 and 4), $Cu(OAc)_2 \cdot H_2O$ (3.0 mol%), **BTA^{PPh2}** (6.0 mol%), enantiopure BTA Cha (entries 1 and 2) or **BTA (*R*)-Cha**/**BTA (*S*)-Cha** (e.e. value= 60%, entries 3 and 4) , $PhSiH_3$ (100 mol% entries 1-2, 200 mol% entries 3-4), toluene, -25 °C. For the exact amount of BTA Cha present in each step, see the table. The conversion was determined by GC and ^1H NMR analyses. Conversion of 1-(4-nitrophenyl)ethanone was

superior to 99% for all entries. Conversion of 1-(4-biphenylyl)ethanone was of 84% and 60% for entries 3 and 4 respectively. The optical purity of 1-(4-nitrophenyl)ethanol and 1-(4-biphenylyl)ethanol was determined by chiral GC and chiral HPLC analyses, respectively. For chiral GC analyses of entries 1-4, see pages S.30 and S.31.

General Procedures.

Preparation of new compounds**:** The synthetic procedure for the preparation of **BTA^{PPh2}** is detailed below. N,N-dimethylaminopyridine (DMAP), N-(3-dimethylaminopropyl)-N′-ethylcarbodiimide hydrochloride (EDC·HCl), phenylsilane, $Cu(OAc)_2 \cdot H_2O$, 1-(4-nitrophenyl)ethanone and 1-(4-biphenylyl)ethanone were acquired from commercial suppliers and used directly. 3,5-bisoctylaminocarbonyl-benzoic acid,[45] 4-diphenylphosphinoaniline,[46] **BTA (*S*)-Val**,[26] **BTA (*S*)-Tle**,[26] **BTA (*S*)-Leu**,[26] **BTA (*S*)-Ile**,[26] **BTA (*S*)-Cha**[35] and **BTA (*R*)-Cha**[35] were prepared following published procedures. Racemic phenyl alcohols were prepared by reduction of the corresponding aromatic ketones with $NaBH_4$ in methanol. Solvents for catalytic experiments were obtained from an SPS solvent purification system (IT-Inc). Chromatography-grade solvents were used for samples analysed by FT-IR and CD spectroscopy. NMR spectra were recorded on a Bruker Avance 300 spectrometer and calibrated to the residual solvent peak: DMSO-d_6 (^{1}H: 2.50 ppm; ^{13}C: 39.52 ppm). Peaks are reported with their corresponding multiplicity (s: singlet; d: doublet, t: triplet; m: multiplet) and integration, and respective *J* coupling constants are given in Hertz. Exact mass measurements (HRMS) were obtained on TQ R30-10 HRMS spectrometer by ESI+ ionization and are reported in m/z for the major signal.

Chiral GC and HPLC analyses: **1-(4-nitrophenyl)ethanol**. The optical purity was determined by GC analysis: Chiral Cyclosil-B column, 30 m × 250 µm x 0.25 µm, inlet pressure = 12.6 psi. Injection temperature = 220°C; detector temperature = 300°C; column temperature = 165°C. Retention time: 8.6 min (1-(4-nitrophenyl)ethanone), 18.9 min ((*R*)-enantiomer), 19.3 min ((*S*)-enantiomer).[47] **1-(4-biphenylyl)ethanol**. The optical purity was determined by HPLC analysis: Chiralpak AD-H column, heptane/isopropanol 97/3, flow=1 mL.min^{-1}, detection at 254 nm. Retention time: 17.8 min ((*S*)-enantiomer) and 20.2 min ((*R*)-enantiomer).[48] **Mixture of 1-(4-nitrophenyl)ethanol and 1-(4-biphenylyl)ethanol**. GC analysis: Chiral Cyclosil-B column, 30 m × 250 µm x 0.25 µm, inlet pressure = 12.6 psi. Injection temperature = 220°C; detector temperature = 300°C; column temperature = 165°C for 25 min, then 180°C for 20 min. Retention time: 18.9 min (1-(4-nitrophenyl)ethanol, (*R*)-

enantiomer), 19.3 min (1-(4-nitrophenyl)ethanol, (*S*)-enantiomer), 29.6 min (1-(4-biphenylyl)ethanol, (*R*)-enantiomer), 29.9 min (1-(4-biphenylyl)ethanol, (*S*)-enantiomer).

Preparation of BTA solutions for analyses: the desired BTA was weighed into a ø11.6 mm HPLC vial or a ø20 mm glass vial, the volume of solvent was adjusted to the desired end concentration with an adequate glass microsyringe, and verified by weighing the sample. Vials were sealed with PTFE-coated caps to avoid contamination from leaching plasticizer.

Fourier-Transform Infrared (FT-IR) analyses: FT-IR measurements were performed on a Nicolet iS10 spectrometer. Solution spectra were measured in CaF_2 cells by adjusting the pathlength (0.1 cm or 0.05 cm) to the concentration and were corrected for air, solvent and cell absorption.

Circular dichroism (CD) analyses: CD measurements were performed on a Jasco J-1500 spectrometer equipped with a Peltier thermostated cell holder and Xe laser. Data were recorded at 20°C with the following parameters: 20 $nm.min^{-1}$ sweep rate, 0.1 nm data pitch, 2.0 nm bandwidth, and between 400 and 200 nm. Spectra were corrected for solvent and cell contribution. A 0.1 mm dismountable quartz cell (2×10^{-3} M) was used. For all samples, LD contribution was negligible ($\Delta LD < 0.005$ dOD) and the shape of the CD signal was independent of the orientation of the quartz slide.

UV-Vis analyses: UV-Vis absorption spectra were extracted from CD on each of the above samples and obtained after correction of the absorption of air, solvent, and cell at the same temperature.

Small-angle neutron scattering (SANS) analyses: SANS measurements were made at the LLB (Saclay, France) on the PA20 instrument, at two distance-wavelength combinations to cover the 4.2×10^{-3} to $0.25 Å^{-1}$ q-range, where the scattering vector q is defined as usual, assuming elastic scattering, as $q=(4\pi/\lambda)\sin(\theta/2)$, where θ is the angle between incident and scattered beam. Data were corrected for the empty cell signal and the solute and solvent incoherent background. A light water standard was used to normalize the scattered intensities to cm^{-1} units.

Synthetic procedures.

Synthesis of **BTA^{PPh2}**: 3,5-bisoctylaminocarbonyl-benzoic acid[45] (1.50 g, 3.5 mmol) and dry THF (100 mL) were mixed in an oven-dried Schlenk flask under argon and then N,N-dimethylaminopyridine (0.72 g, 5.9 mmol), N-(3-Dimethylaminopropyl)-N′-ethylcarbodiimide hydrochloride (1.13 g, 5.9 mmol) and 4-diphenylphosphinoaniline[46] (1.44 g, 5.2 mmol) were added as solids. The reaction mixture was refluxed for 2 days. After cooling to room temperature, the mixture

was evaporated under vacuum and the crude product was purified by column chromatography on silica gel eluting with DCM/AcOEt (95/5 to 7/1) to yield **BTA^{PPh2}** (1.90 g, 79%) as a colourless solid. **^{1}H NMR** (300 MHz, DMSO-d_6) δ 10.62 (s, 1H), 8.68 (t, *J* = 5.6 Hz, 2H), 8.45 (dd, *J* = 7.7, 1.6 Hz, 3H), 7.84 (d, *J* = 8.1 Hz, 2H), 7.46-7.37 (m, 6H), 7.31-7.21 (m, 6H), 3.29-3.22 (m, 4H), 1.61-1.47 (m, 4H), 1.36-1.11 (m, 20H), 0.90-0.79 (m, 6H). **^{31}P{^{1}H} NMR** (122 MHz, DMSO-d_6) δ -7.7. **^{13}C{^{1}H} NMR** (75 MHz, DMSO-d_6) δ 165.2, 165.0, 139.9, 137.0 (d, *J* = 11.4 Hz), 135.2, 135.1, 134.1 (d, *J* = 20.6 Hz), 133.1 (d, *J* = 19.4 Hz), 129.0, 128.9, 128.8, 128.7 (d, *J* = 6.8 Hz), 120.4 (d, *J* = 7.4 Hz), 39.6 (below the solvent peak), 31.3, 29.0, 28.8, 28.7, 26.5, 22.1, 13.9. **HRMS**: Calculated for $C_{43}H_{55}N_3O_3P$ $[M+H]^+$: 692.3976, found: 692.3973.

Catalytic experiments.

Catalytic screening (Tables 1 and S.1): An oven-dried test tube was loaded with $Cu(OAc)_2 \cdot H_2O$ (1.0 mg, 3.0 mol%) and **BTA^{PPh2}** (6.9 mg, 6.0 mol%) in dry THF (500 µL) and the mixture was stirred for 30 minutes. The solvent was removed under vacuum and the test tube was further put under vacuum (1.10^{-3} mbar) for 1 hour. 1-(4-nitrophenyl)ethanone (28.0 mg, 0.17 mmol) was added before flushing the tube with argon for 10 seconds. The BTA co-monomer (6.6 mol% in 200 µL of dry toluene) was added to the test tube as well as dry toluene in order to get a total volume of 590 µL. The mixture was stirred for 15 min at room temperature. $PhSiH_3$ (21.0 µL, 0.17 mmol) was added to the test tube and the mixture was stirred for 17 hours. Typical work-up: Aqueous solution of HCl (10 wt%, 400 µL) was added and the mixture was stirred for 30 min (until the solution became transparent). Then, the products were extracted with Et_2O (3x1 mL) and AcOEt (1x1 mL) and the solvents were evaporated under vacuum. The residue was taken up in DCM and passed through a silica plug eluting with DCM. The solvents were evaporated and the conversion and enantioselectivity were determined by ^{1}H NMR and chiral GC respectively.

Screening for chirality amplification (Table S.2): An oven-dried test tube was loaded with $Cu(OAc)_2 \cdot H_2O$ (1.0 mg, 3.0 mol%) and **BTA^{PPh2}** (6.9 mg, 6.0 mol%) in dry THF (500 µL) and the mixture was stirred for 30 minutes. The solvent was removed under vacuum and the test tube was further put under vacuum (1.10^{-3} mbar) for 1 hour. 1-(4-nitrophenyl)ethanone (28.0 mg, 0.17 mmol) was added before flushing the tube with argon for 10 seconds. A 25% *e.e.* scalemic mixture biased in favour of **BTA (*R*)-Cha** (x mol%) in 200 µL of toluene was added to the test tube as well as dry toluene in order to get a total volume of 590 µL. The mixture was stirred for 15 min at room temperature. The mixture was cooled to the desired temperature and further stirred for 15 min. $PhSiH_3$ (21.0 µL, 0.17

mmol) was added to the test tube and the mixture was stirred until completion of the reaction. The typical work-up procedure was followed.

Chirality amplification effect under optimized conditions (Figure 1a): An oven-dried test tube was loaded with $Cu(OAc)_2 \cdot H_2O$ (1.0 mg, 3.0 mol%) and **BTA^{PPh2}** (6.9 mg, 6.0 mol%) in dry THF (500 µL) and the mixture was stirred for 30 minutes. The solvent was removed under vacuum and the test tube was further put under vacuum (1.10^{-3} mbar) for 1 hour. 1-(4-nitrophenyl)ethanone (28.0 mg, 0.17 mmol) was added before flushing the tube with argon for 10 seconds. A scalemic mixture of **BTA Cha** (25.8 mg, 13.2 mol%, x% *e.e.*) in 200 µL of toluene was added to the test tube as well as dry toluene in order to get a total volume of 590 µL. The mixture was stirred for 15 min at room temperature. The mixture was cooled to 0 °C and further stirred for 15 min. $PhSiH_3$ (21.0 µL, 0.17 mmol) was added to the test tube and the mixture was stirred until completion of the reaction. The typical work-up procedure was followed.

Hydrosilylation of 1-(4-nitrophenyl)ethanone with sequential additions of substrate and $PhSiH_3$ (Table S.3, Figures 1b and S.10): A Schlenk tube tube was loaded with $Cu(OAc)_2 \cdot H_2O$ (1.0 mg, 3.0 mol%) and **BTA^{PPh2}** (6.9 mg, 6.0 mol%) in dry THF (500 µL) and the mixture was stirred for 30 minutes. The solvent was removed under vacuum and the Schlenk tube was further put under vacuum (1.10^{-3} mbar) for 1 hour. Then 1-(4-nitrophenyl)ethanone (28.0 mg, 0.17 mmol) was added before flushing the tube with argon for 10 seconds. **BTA (*R*)-Cha** (8.6 mg, 4.4 mol%) and **BTA (*S*)-Cha** (17.2 mg, 8.7 mol%) in 80 µL of dry toluene was added to the Schlenk tube as well as dry toluene in order to get a total volume of 590 µL. The mixture was stirred for 15 min at room temperature. The mixture was cooled to 0 °C and further stirred for 15 min. $PhSiH_3$ (42.0 µL, 0.34 mmol) was added and the mixture was stirred for 15 minutes. An aliquot was taken up, hydrolyzed with aqueous HCl and analyzed by chiral GC (*run 1*). Then, **BTA (*R*)-Cha** (25.4 mg, 13.0 mol%) in 200 µL of toluene was added and the mixture was stirred for 30 min before addition of 1-(4-nitrophenyl)ethanone (28.0 mg, 0.17 mmol) and $PhSiH_3$ (21.0 µL, 0.17 mmol). The mixture was stirred for 60 minutes and an aliquot was taken up, hydrolyzed with aqueous HCl and analyzed by chiral GC (*run 2*). Then, **BTA (*S*)-Cha** (50.7 mg, 26.0 mol%) in 100 µL of toluene was added and the mixture was stirred for 30 min before addition of 1-(4-nitrophenyl)ethanone (28.0 mg, 0.17 mmol) and $PhSiH_3$ (21.0 µL, 0.17 mmol). The mixture was stirred for 60 minutes and an aliquot was taken up, hydrolyzed with aqueous HCl and analyzed by chiral GC (*run 3*). Then, **BTA (*R*)-Cha** (100.0 mg, 52.0 mol%) in 200 µL of toluene was added and the mixture was stirred for 30 min before addition of 1-(4-nitrophenyl)ethanone (28.0 mg, 0.17 mmol) and $PhSiH_3$

(21.0 µL, 0.17 mmol). The mixture was stirred for 60 minutes and the typical work-up procedure was followed (*run 4*).

Table S.6 Determination of the enantiomeric excess in 1-(4-nitrophenyl)ethanol for each run of for the sequential copper-catalysed hydrosilylation of 1-(4-nitrophenyl)ethanone.

run	*e.e.*from the aliquots[a]	eq. of (*R*)/(*S*) product[b]	*e.r.* for the run	*e.e.* for the run
1	53%	0.765/0.235	76.5/23.5	53%
2	-2%	0.984/1.016	22.0/78.0	-56%
3	17%	1.75/1.25	76.5/23.5	53%
4	-1%	1.99/2.01	24.0/76.0	-52%

[a] "Cumulated" *e.e.* in 1-(4-nitrophenyl)ethanol (determined from the aliquots) for the different run, full conversion for each run. [b] "Cumulated" equivalents in (*R*) and (*S*) 1-(4-nitrophenyl)ethanol for the different run (100 mol% of 1-(4-nitrophenyl)ethanone is converted by run).

GC analyses From the aliquots of the different run**.**

Tables S.3, run 1:

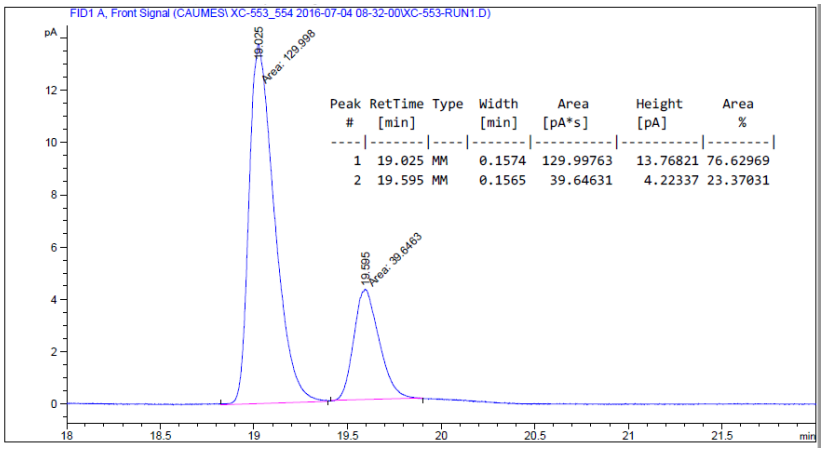

Tables S.3, run 2:

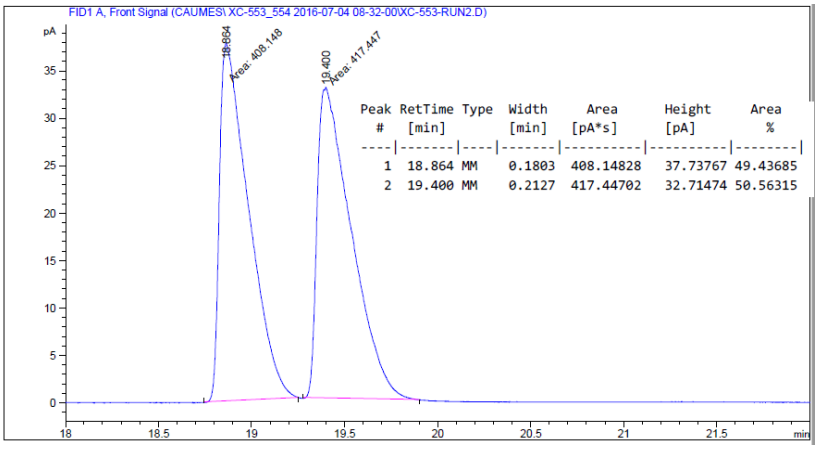

Tables S.3, run 3:

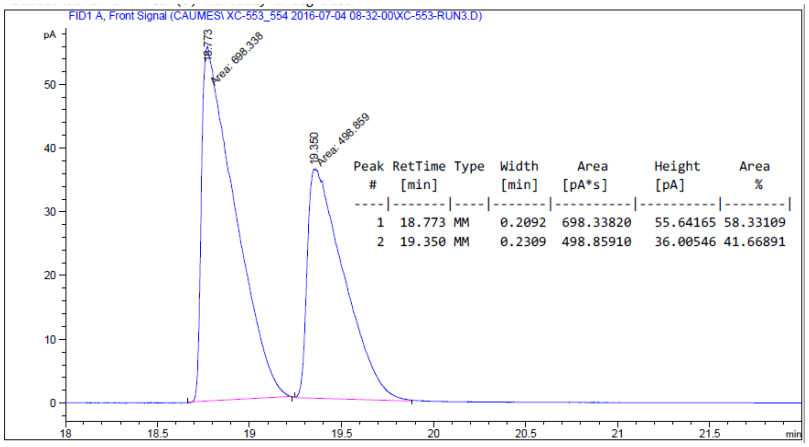

Tables S.3, run 4:

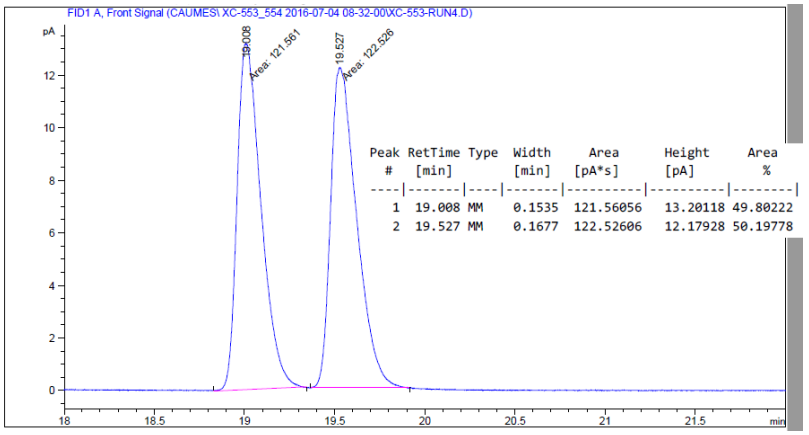

Determination of the time required for the stereochemical switch (Table S.4): A test tube was loaded with $Cu(OAc)_2 \cdot H_2O$ (1.0 mg, 3.0 mol%) and **BTA**$^{\mathbf{PPh2}}$ (6.9 mg, 6.0 mol%) in dry THF (500 µL)

and the mixture was stirred for 30 minutes. The solvent was removed under vacuum and the test tube was further put under vacuum (1.10^{-3} mbar) for 1 hour. Then 1-(4-nitrophenyl)ethanone (28.0 mg, 0.17 mmol) was added before flushing the tube with argon for 10 seconds. **BTA (*R*)-Cha** (8.6 mg, 4.4 mol%) and **BTA (*S*)-Cha** (17.2 mg, 8.7 mol%) in 80 µL of dry toluene was added to the test tube as well as dry toluene in order to get a total volume of 590 µL. The mixture was stirred for 15 min at room temperature. The mixture was cooled to 0 °C and further stirred for 15 min. **BTA (*R*)-Cha** (25.4 mg, 13.0 mol%) in 200 µL of toluene was added as well as $PhSiH_3$ (21.0 µL, 0.17 mmol) after a measured time. The mixture was stirred for 10 minutes and the typical work-up procedure was followed.

GC analyses

Tables S.4, no switch: + 60% *e.e.(R)*

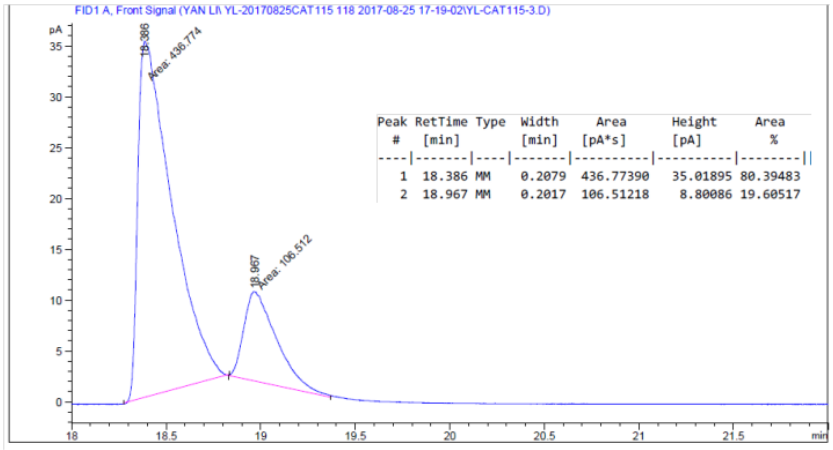

Tables S.4, entry 2 (5 seconds): -56% *e.e.(S)*

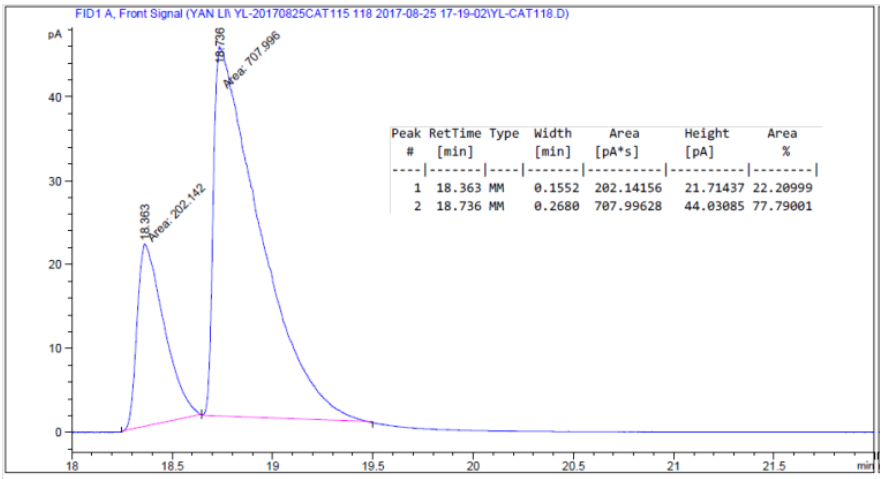

Stereochemical switch during the conversion of 1-(4-biphenylyl)ethanone (Scheme S.1a): A test tube was loaded with $Cu(OAc)_2 \cdot H_2O$ (1.0 mg, 3.0 mol%) and **BTA^{PPh2}** (6.9 mg, 6.0 mol%) in dry THF (500 µL) and the mixture was stirred for 30 minutes. The solvent was removed under vacuum and the test tube was further put under vacuum (1.10^{-3} mbar) for 1 hour. Then 1-(4-biphenylyl)ethanone (34.0 mg, 0.17 mmol) was added before flushing the tube with argon for 10 seconds. **BTA (*R*)-Cha** (8.6 mg, 4.4 mol%) and **BTA (*S*)-Cha** (17.2 mg, 8.7 mol%) in 80 µL of dry toluene was added to the test tube as well as dry toluene in order to get a total volume of 590 µL. The mixture was stirred for 15 min at room temperature. The mixture was cooled to 0 °C and further stirred for 15 min. Then, a solution of toluene (200 µL) containing **BTA (*R*)-Cha** (25.4 mg, 13.0 mol%) and $PhSiH_3$ (21.0 µL, 0.17 mmol) was added. The mixture was stirred for 3h and the typical work-up procedure was followed.

HPLC analyses

Scheme S.1a, no switch: + 34% *e.e.(R)*

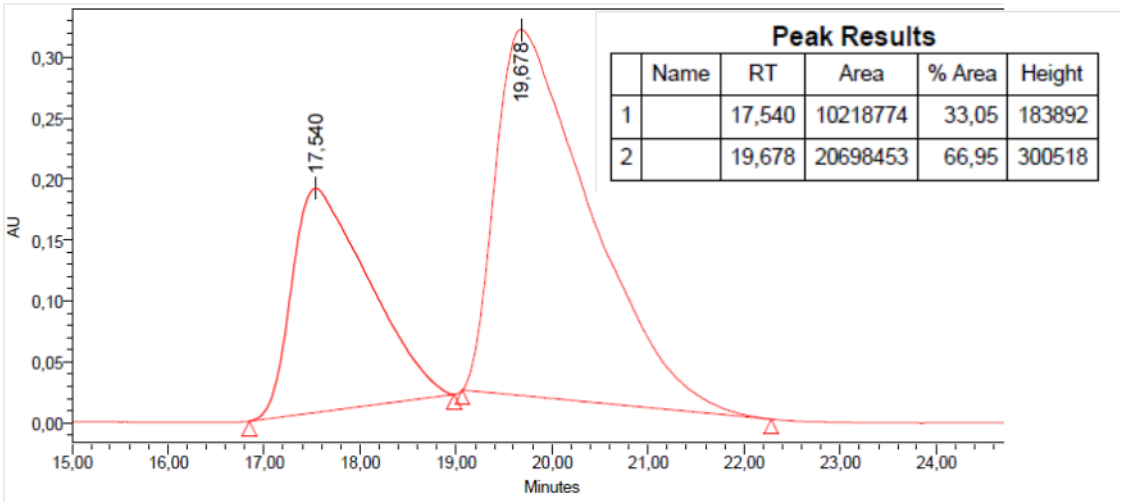

Scheme S.1a, switch: - 43% *e.e.(S)*

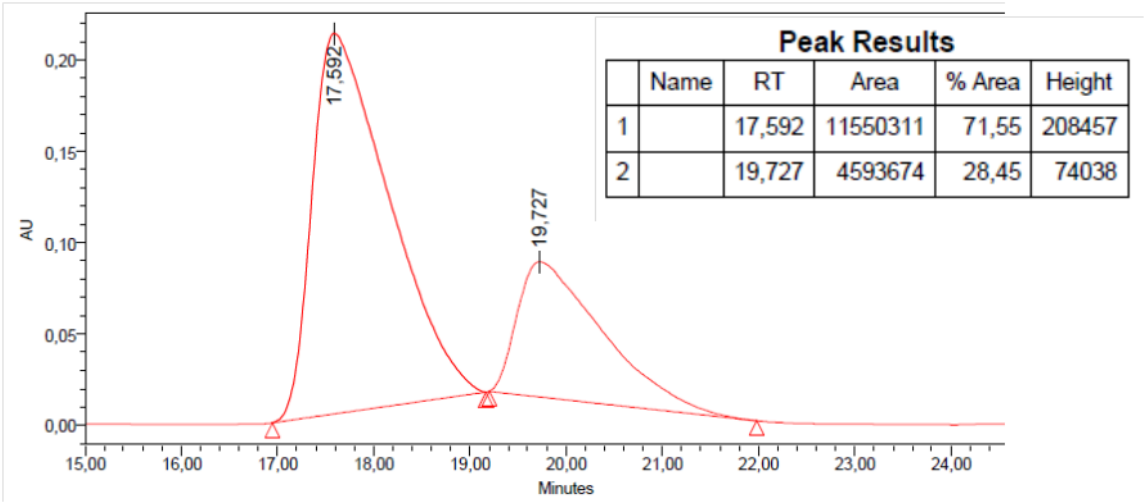

Stereochemical switch during the conversion of 1-(4-biphenylyl)ethanone (Scheme S.1b): A test tube was loaded with $Cu(OAc)_2 \cdot H_2O$ (1.0 mg, 3.0 mol%) and **BTA^{PPh2}** (6.9 mg, 6.0 mol%) in dry THF (500 µL) and the mixture was stirred for 30 minutes. The solvent was removed under vacuum and the test tube was further put under vacuum (1.10^{-3} mbar) for 1 hour. Then 1-(4-biphenylyl)ethanone (34.0 mg, 0.17 mmol) was added before flushing the tube with argon for 10 seconds. **BTA (*R*)-Cha** (2.6 mg, 1.3 mol%) and **BTA (*S*)-Cha** (10.3 mg, 5.3 mol%) in 80 µL of dry toluene was added to the test tube as well as dry toluene in order to get a total volume of 590 µL. The mixture was stirred for 15 min at room temperature. The mixture was cooled to -25 °C and further stirred for 15 min and then $PhSiH_3$ (21.0 µL,

0.17 mmol) was added. The mixture was stirred for 30 minutes, an aliquot was taken up and hydrolyzed (*step 1*) and **BTA (*R*)-Cha** (38.9 mg, 20.0 mol%) in 200 µL of toluene was added. The reaction mixture was stirred overnight and the typical work-up procedure was followed (*step 2*).

HPLC analyses

Scheme S.1b, aliquot (step 1): +40% *e.e. (R)*

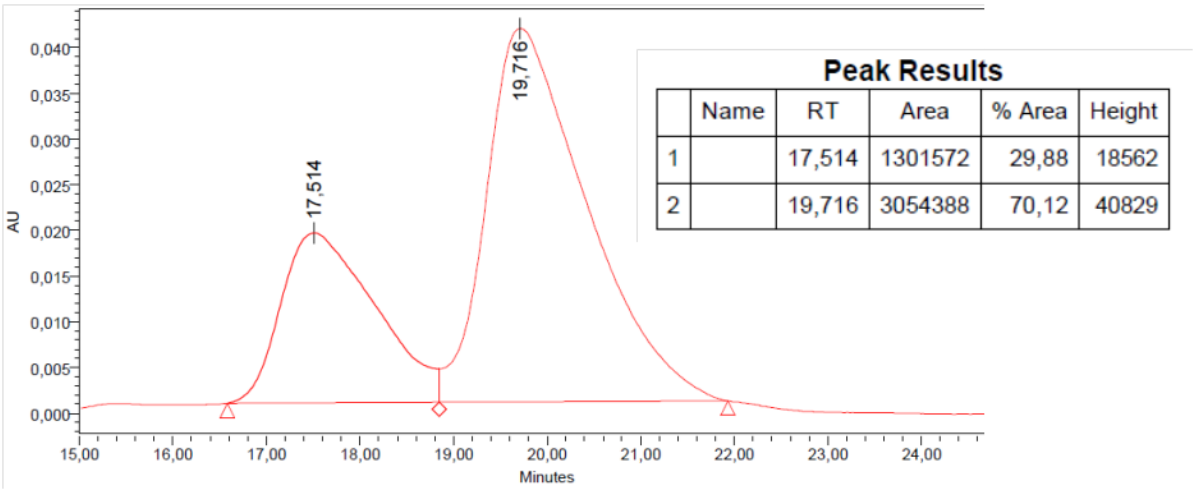

Peak Results

	Name	RT	Area	% Area	Height
1		17,514	1301572	29,88	18562
2		19,716	3054388	70,12	40829

Scheme S.1b, final: -27% *e.e (S)*

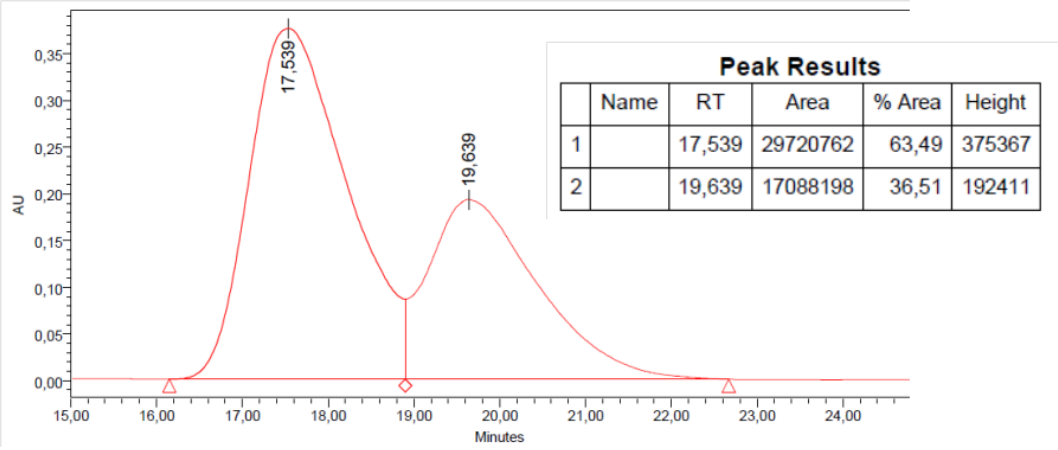

Peak Results

	Name	RT	Area	% Area	Height
1		17,539	29720762	63,49	375367
2		19,639	17088198	36,51	192411

Copper-catalysed hydrosilylation of 1:1 mixture of 1-(4-nitrophenyl)ethanone and 1-(4-biphenylyl)ethanone (Table S.5, Figure 1c): A Schlenk tube was loaded with $Cu(OAc)_2 \cdot H_2O$ (1.0 mg, 3.0 mol%) and **BTA^{PPh2}** (6.9 mg, 6.0 mol%) in dry THF (500 µL) and the mixture was stirred for 30 minutes. The solvent was removed under vacuum and the Schlenk tube was further put under vacuum (1.10^{-3} mbar) for 1 hour. 1-(4-nitrophenyl)ethanone (28.0 mg, 0.17 mmol) and 1-(4-biphenylyl)ethanone (34.0 mg, 0.17 mmol) were added before flushing the Schlenk tube with argon for 10 seconds. **BTA**

(*R*)-Cha (2.6 mg, 1.3 mol%) and **BTA (*S*)-Cha** (10.3 mg, 5.3 mol%) in 200 µL of dry toluene was added to the Schlenk tube as well as dry toluene in order to get a total volume of 590 µL. The mixture was stirred for 15 min at room temperature. The mixture was cooled to -25 °C and further stirred for 15 min and then $PhSiH_3$ (42.0 µL, 0.34 mmol) was added. The mixture was stirred for 2 minutes (*step 1*) and then **BTA (*R*)-Cha** (38.9 mg, 20.0 mol%) in 200 µL of toluene was added. The reaction mixture was stirred for 12 h (*step 2*) and the typical work-up procedure was followed.

GC analyses. GC analyses below have been performed under conditions for which the enantiomers of 1-(4-nitrophenyl)ethanol and 1-(4-biphenylyl)ethanol are not perfectly separated, yet it indicated the configuration of the major enantiomer obtained and was thus a good demonstration of the success of the selectivity switch. The enantiomeric excesses (indicated above peaks) were precisely measured using adequate separation conditions for 1-(4-nitrophenyl)ethanol and 1-(4-biphenylyl)ethanol (page S.18). The peak at 26.8 min corresponds to 1-(4-biphenylyl)ethanone.

Table S.5, entry 1:

Peak #	RetTime [min]	Type	Width [min]	Area [pA*s]	Height [pA]	Area %
1	18.242	MF	0.2300	460.95221	33.40541	26.70793
2	18.841	FM	0.2372	75.29533	5.29038	4.36267
3	29.493	MF	0.1721	729.81598	70.69049	42.28611
4	29.759	FM	0.2324	459.83664	32.97412	26.64329

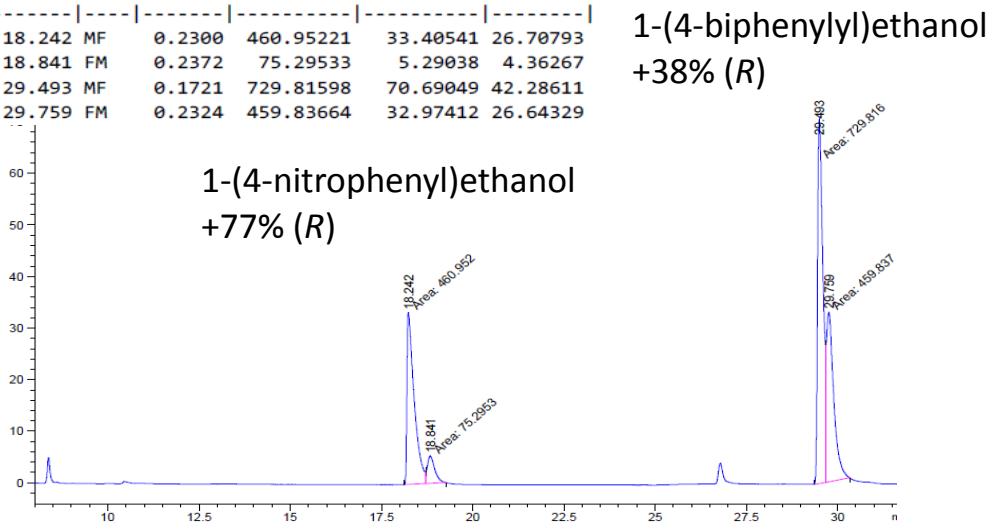

Table S.5, entry 2:

Peak #	RetTime [min]	Type	Width [min]	Area [pA*s]	Height [pA]	Area %
1	18.347	MM	0.1500	48.17480	5.35189	3.05227
2	18.716	MM	0.2320	415.54865	29.85732	26.32844
3	29.535	MF	0.1216	242.67874	33.25002	15.37570
4	29.728	FM	0.2286	871.92413	63.56655	55.24359

1-(4-biphenylyl)ethanol
-45% (*S*)

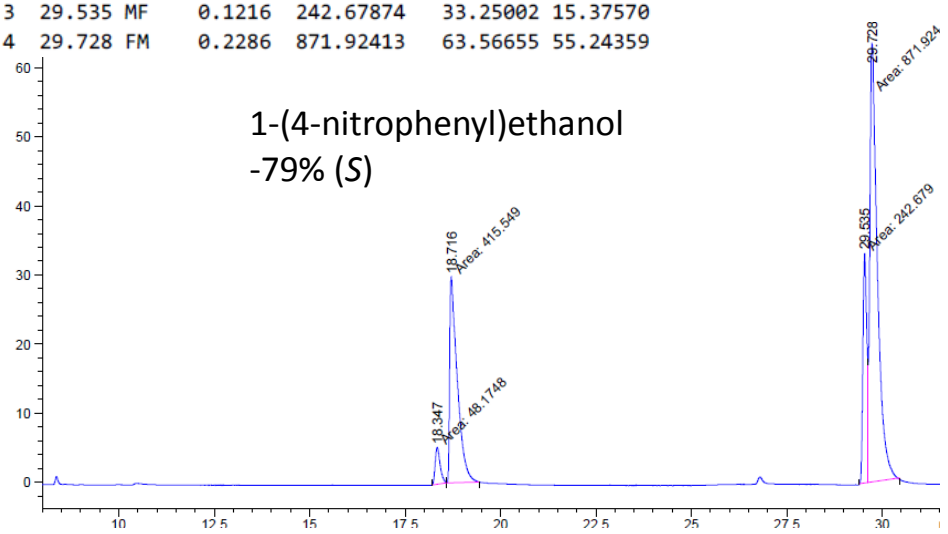

Table S.5, entry 3:

Peak #	RetTime [min]	Type	Width [min]	Area [pA*s]	Height [pA]	Area %
1	18.421	MM	0.1918	272.00754	23.63305	23.28780
2	18.986	MM	0.1799	41.17962	3.81563	3.52557
3	29.649	MF	0.1261	236.66132	31.28087	20.26165
4	29.853	FM	0.2130	618.17761	48.36099	52.92498

1-(4-biphenylyl)ethanol
-34% (*S*)

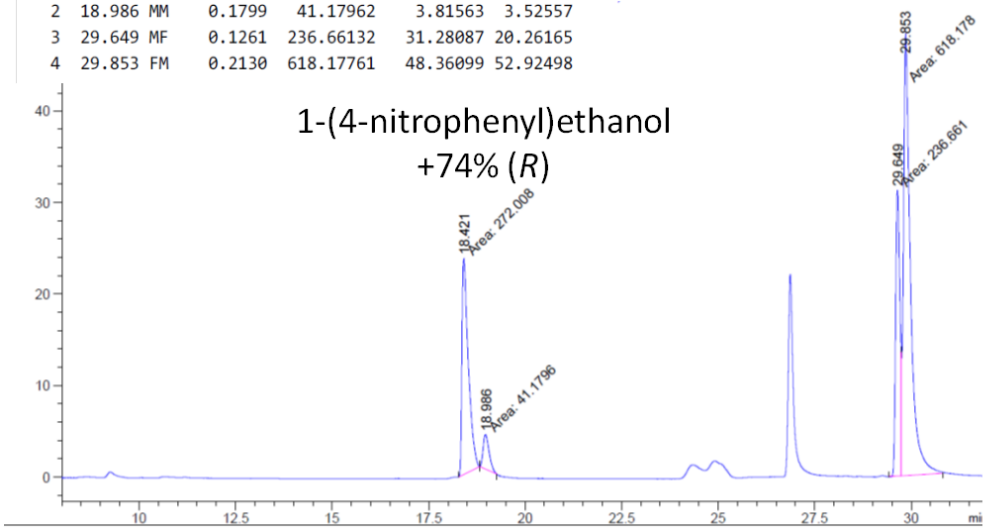

Table S.5, entry 4:

Peak #	RetTime [min]	Type	Width [min]	Area [pA*s]	Height [pA]	Area %
1	18.542	MM	0.1616	34.87117	3.59671	4.43060
2	18.979	MM	0.2011	187.59395	15.54638	23.83501
3	26.877	MM	0.1482	249.10402	28.01308	31.65025
4	29.694	MM	0.2670	315.48309	19.69057	40.08414

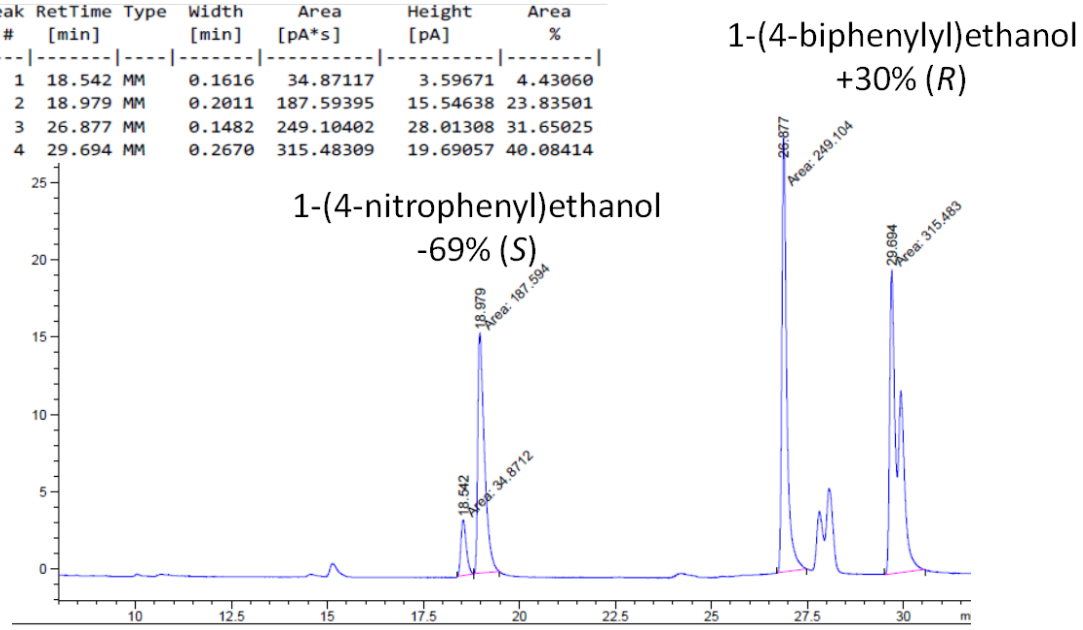

BTA^{PPh2}

^{1}H (DMSO-d$_6$):

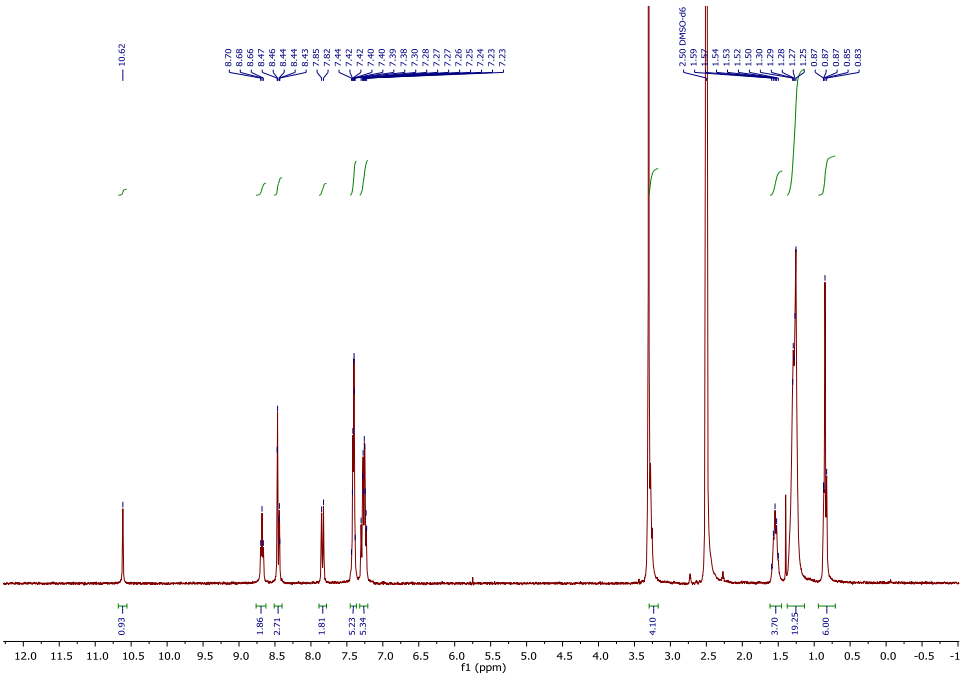

$^{31}P\{^{1}H\}$ (DMSO-d_6):

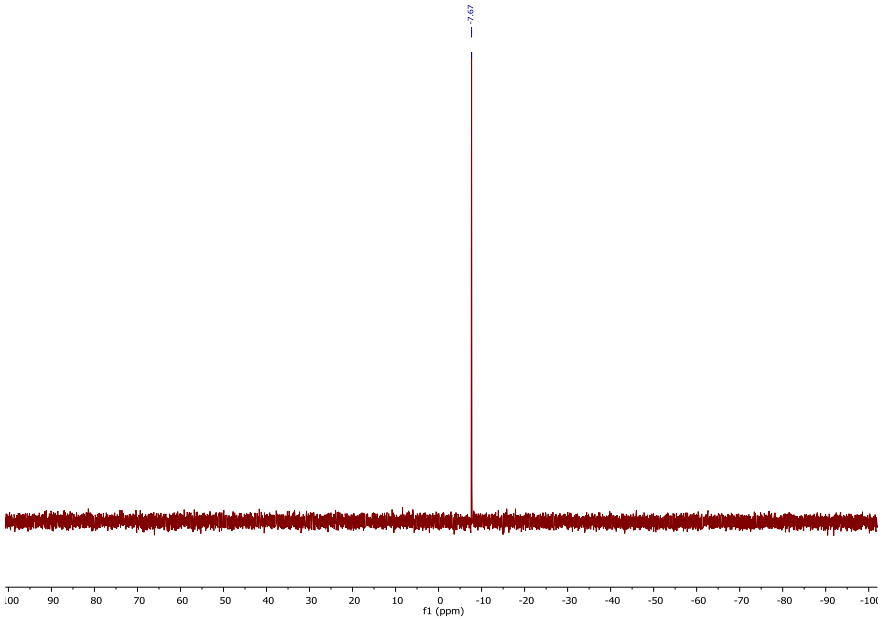

$^{13}C\{^{1}H\}$ (DMSO-d_6):

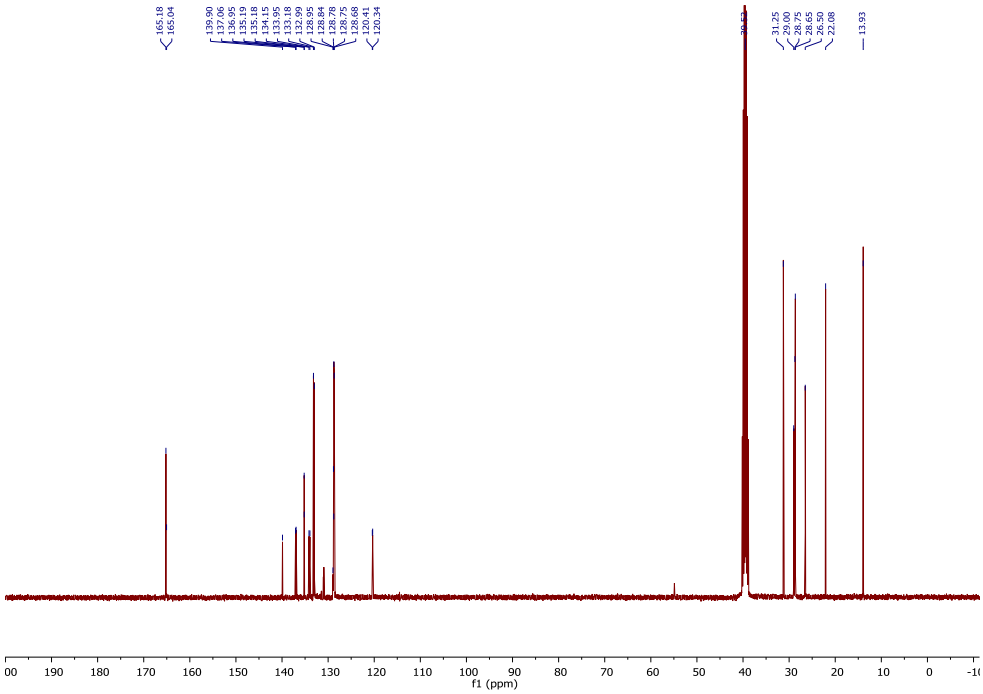

V References

1. Sohtome, Y.; Nagasawa, K., Dynamic asymmetric organocatalysis: cooperative effects of weak interactions and conformational flexibility in asymmetric organocatalysts. *Chem. Commun.* **2012,** *48* (63), 7777-7789.

2. Neilson, B. M.; Bielawski, C. W., Illuminating Photoswitchable Catalysis. *ACS Catal.* **2013,** *3* (8), 1874-1885.

3. Kumagai, N.; Shibasaki, M., Catalytic chemical transformations with conformationally dynamic catalytic systems. *Catal. Sci. Technol.* **2013,** *3* (1), 41-57.

4. Blanco, V.; Leigh, D. A.; Marcos, V., Artificial switchable catalysts. *Chem. Soc. Rev.* **2015,** *44* (15), 5341-5370.

5. Vlatković, M.; Collins, B. S. L.; Feringa, B. L., Dynamic Responsive Systems for Catalytic Function. *Chem. Eur. J.* **2016,** *22*, 17080-17111.

6. Wang, X. K.; Thevenon, A.; Brosmer, J. L.; Yu, I. S.; Khan, S. I.; Mehrkhodavandi, P.; Diaconescu, P. L., Redox Control of Group 4 Metal Ring-Opening Polymerization Activity toward L-Lactide and epsilon-Caprolactone. *J. Am. Chem. Soc.* **2014,** *136* (32), 11264-11267.

7. Nojiri, A.; Kumagai, N.; Shibasaki, M., Linking Structural Dynamics and Functional Diversity in Asymmetric Catalysis. *J. Am. Chem. Soc.* **2009,** *131* (10), 3779-3784.

8. Tian, X.; Cassani, C.; Liu, Y. K.; Moran, A.; Urakawa, A.; Galzerano, P.; Arceo, E.; Melchiorre, P., Diastereodivergent Asymmetric Sulfa-Michael Additions of alpha-Branched Enones using a Single Chiral Organic Catalyst. *J. Am. Chem. Soc.* **2011,** *133* (44), 17934-17941.

9. Lin, L. L.; Feng, X. M., Catalytic Strategies for Diastereodivergent Synthesis. *Chem. Eur. J.* **2017,** *23* (27), 6464-6482.

10. Krautwald, S.; Carreira, E. M., Stereodivergence in Asymmetric Catalysis. *J. Am. Chem. Soc.* **2017,** *139*, 5627-5639.

11. Dijkstra, P. J.; Du, H.; Feijen, J., Single site catalysts for stereoselective ring-opening polymerization of lactides. *Polym. Chem.* **2011,** *2*, 520-527.

12. Thomas, C. M., Stereocontrolled ring-opening polymerization of cyclic esters: synthesis of new polyester microstructures. *Chem. Soc. Rev.* **2010,** *39*, 165-173.

13. Escorihuela, J.; Burguete, M. I.; Luis, S. V., New advances in dual stereocontrol for asymmetric reactions. *Chem. Soc. Rev.* **2013,** *42* (12), 5595-5617.

14. Romanazzi, G.; Degennaro, L.; Mastrorilli, P.; Luisi, R., Chiral Switchable Catalysts for Dynamic Control of Enantioselectivity. *ACS Catal.* **2017,** *7*, 4100-4114.

15. Wang, J. B.; Feringa, B. L., Dynamic Control of Chiral Space in a Catalytic Asymmetric Reaction Using a Molecular Motor. *Science* **2011,** *331* (6023), 1429-1432.

16. Vlatković, M.; Bernardi, L.; Otten, E.; Feringa, B. L., Dual stereocontrol over the Henry reaction using a light- and heat-triggered organocatalyst. *Chem. Commun.* **2014,** *50* (58), 7773-7775.

17. Chen, C.-T.; Tsai, C.-C.; Tsou, P.-K.; Huang, G.-T.; Yu, C.-H., Enantiodivergent Steglich rearrangement of Ocarboxylazlactones catalyzed by a chirality switchable helicene containing a 4-aminopyridine unit. *Chem. Sci.* **2016,** *8*, 524-529.

18. Mortezaei, S.; Catarineu, N. R.; Canary, J. W., A Redox-Reconfigurable, Ambidextrous Asymmetric Catalyst. *J. Am. Chem. Soc.* **2012,** *134* (19), 8054-8057.

19. Mortezaei, S.; Catarineu, N. R.; Duan, X. Y.; Hu, C. H.; Canary, J. W., Redox-configurable ambidextrous catalysis: structural and mechanistic insight. *Chem. Sci.* **2015,** *6* (10), 5904-5912.

20. Le Bailly, B. A. F.; Byrne, L.; Clayden, J., Refoldable Foldamers: Global Conformational Switching by Deletion or Insertion of a Single Hydrogen Bond. *Angew. Chem. Int. Ed.* **2016,** *55* (6), 2132-2136.

21. Zhao, D. P.; Neubauer, T. M.; Feringa, B. L., Dynamic control of chirality in phosphine ligands for enantioselective catalysis. *Nat. Commun.* **2015,** *6*.

22. Mortezaei, S.; Catarineu, N. R.; Canary, J. W., Dial-in selection of any of four stereochemical outcomes among two substrates by in situ stereo-reconfiguration of a single ambidextrous catalyst. *Tetrahedron Lett.* **2016,** *57* (4), 459-462.

23. Sohtome, Y.; Yamaguchi, T.; Tanaka, S.; Nagasawa, K., Sequential enantiodivergent organocatalysis: reversibility in enantioswitching controlled by a conformationally flexible guanidine/bisthiourea organocatalyst. *Org. Biomol. Chem.* **2013,** *11* (17), 2780-2786.

24. Sud, D.; Norsten, T. B.; Branda, N. R., Photoswitching of stereoselectivity in catalysis using a copper dithienylethene complex. *Angew. Chem. Int. Ed.* **2005,** *44* (13), 2019-2021.

25. Raynal, M.; Portier, F.; van Leeuwen, P. W. N. M.; Bouteiller, L., Tunable Asymmetric Catalysis through Ligand Stacking in Chiral Rigid Rods. *J. Am. Chem. Soc.* **2013,** *135* (47), 17687-17690.

26. Desmarchelier, A.; Caumes, X.; Raynal, M.; Vidal-Ferran, A.; van Leeuwen, P. W. N. M.; Bouteiller, L., Correlation between the Selectivity and the Structure of an Asymmetric Catalyst Built on a Chirally Amplified Supramolecular Helical Scaffold. *J. Am. Chem. Soc.* **2016,** *138*, 4908-4916.

27. Cantekin, S.; de Greef, T. F. A.; Palmans, A. R. A., Benzene-1,3,5-tricarboxamide: a versatile ordering moiety for supramolecular chemistry. *Chem. Soc. Rev.* **2012,** *41* (18), 6125-6137.

28. Stals, P. J. M.; Smulders, M. M. J.; Martín-Rapún, R.; Palmans, A. R. A.; Meijer, E. W., Asymmetrically Substituted Benzene-1,3,5-tricarboxamides: Self-Assembly and Odd-Even Effects in the Solid State and in Dilute Solution. *Chem. Eur. J.* **2009,** *15* (9), 2071-2080.

29. According to the assignment made by Meijer and co-workers: Nakano, Y.; Hirose, T.; Stals, P. J. M.; Meijer, E. W.; Palmans, A. R. A., Conformational analysis of supramolecular polymerization processes of disc-like molecules. *Chem. Sci.* **2012,** *3*, 148-151.

30. Jordan, A. J.; Lalic, G.; Sadighi, J. P., Coinage Metal Hydrides: Synthesis, Characterization, and Reactivity. *Chem. Rev.* **2016,** *116*, 8318-8372.

31. Shi, S.-L.; Wong, Z. L.; Buchwald, S. L., Copper-catalysed enantioselective stereodivergent synthesis of amino alcohols. *Nature* **2016,** *532*, 353-356.

32. Smulders, M. M. J.; Filot, I. A. W.; Leenders, J. M. A.; Van der Schoot, P.; Palmans, A. R. A.; Schenning, A. P. H. J.; Meijer, E. W., Tuning the Extent of Chiral Amplification by Temperature in a Dynamic Supramolecular Polymer. *J. Am. Chem. Soc.* **2010,** *132*, 611-619.

33. Desmarchelier, A.; Raynal, M.; Brocorens, P.; Vanthuyne, N.; Bouteiller, L., Revisiting the assembly of amino ester-based benzene-1,3,5-tricarboxamides: chiral rods in solution. *Chem. Commun.* **2015,** *51* (34), 7397-7400.

34. Caumes, X.; Baldi, A.; Gontard, G.; Brocorens, P.; Lazzaroni, R.; Vanthuyne, N.; Troufflard, C.; Raynal, M.; Bouteiller, L., Tuning the structure of 1,3,5-benzene tricarboxamide self-assemblies through stereochemistry. *Chem. Commun.* **2016,** *52* (91), 13369-13372.

35. Desmarchelier, A.; Giordano Alvarenga, B.; Caumes, X.; Dubreucq, L.; Troufflard, C.; Tessier, M.; Vanthuyne, N.; Idé, J.; Maistriaux, T.; Beljonne, D.; Brocorens, P.; Lazzaroni, R.; Raynal, M.; Bouteiller, L., Tuning the nature and stability of self-assemblies formed by ester benzene 1,3,5-tricarboxamides: the crucial role played by the substituents. *Soft Matter* **2016,** *12*, 7824-7838.

36. Sang, Y.; Yang, D.; Duan, P.; Liu, M., Towards homochiral supramolecular entities from achiral molecules by vortex mixing-accompanied self-assembly. *Chem. Sci.* **2019**.

37. Allenmark, S., Induced Circular Dichroism by Chiral Molecular Interaction. *Chirality* **2003,** *15*, 409-422.

38. Wang, Z.; Lorandi, F.; Fantin, M.; Wang, Z.; Yan, J.; Wang, Z.; Xia, H.; Matyjaszewski, K., Atom Transfer Radical Polymerization Enabled by Sonochemically Labile Cu-carbonate Species. *ACS Macro Lett.* **2019,** *8* (2), 161-165.

39. Kang, J.; Miyajima, D.; Mori, T.; Inoue, Y.; Itoh, Y.; Aida, T., A rational strategy for the realization of chain-growth supramolecular polymerization. *Science* **2015,** *347* (6222), 646-651.

40. Besenius, P., Controlling supramolecular polymerization through multicomponent self-assembly. *J. Polym. Sci. Pol. Chem.* **2017,** *55* (1), 34-78.

41. Nitschke, J. R., SYSTEMS CHEMISTRY Molecular networks come of age. *Nature* **2009,** *462* (7274), 736-738.

42. Hunt, R. A. R.; Otto, S., Dynamic combinatorial libraries: new opportunities in systems chemistry. *Chem. Commun.* **2011,** *47* (3), 847-858.

43. Simic, V.; Bouteiller, L.; Jalabert, M., Highly cooperative formation of bis-urea based supramolecular polymers. *J. Am. Chem. Soc.* **2003,** *125* (43), 13148-13154.

44. De Greef, T. F. A.; Smulders, M. M. J.; Wolffs, M.; Schenning, A. P. H. J.; Sijbesma, R. P.; Meijer, E. W., Supramolecular Polymerization. *Chem. Rev.* **2009,** *109* (11), 5687-5754.

45. Roosma, J.; Mes, T.; Leclère, P.; Palmans, A. R. A.; Meijer, E. W., Supramolecular Materials from Benzene-1,3,5-tricarboxamide-Based Nanorods. *J. Am. Chem. Soc.* **2008,** *130*, 1120-1121.

46. Gelman, D.; Jiang, L.; Buchwald, S. L., Copper-Catalyzed C-P Bond Construction via Direct Coupling of Secondary Phosphines and Phosphites with Aryl and Vinyl Halides. *Org. Lett.* **2003,** *5* (13), 2315-2318.

47. Uray, G.; Stampfer, W.; Fabian, W. M. F., Comparison of Chirasil-DEX CB as gas chromatographic and ULMO as liquid chromatographic chiral stationary phase for enantioseparation of aryl- and heteroarylcarbinols. *J. Chromatogr. A* **2003,** *992* (1-2), 151-157.

48. Junge, K.; Wendt, B.; Addis, D.; Zhou, S. L.; Das, S.; Beller, M., Copper-Catalyzed Enantioselective Hydrosilylation of Ketones by Using Monodentate Binaphthophosphepine Ligands. *Chem. Eur. J.* **2010,** *16* (1), 68-73.

Chapter 3 Modulation of catalyst enantioselectivity through reversible assembly of supramolecular helices

Abstract: A multi-configurable catalyst, for which the degree of enantioinduction in successive reactions is varied between 6% *e.e.* and 52% *e.e.*, is achieved by supporting copper centres at the periphery of supramolecular helices. Precise characterization of the co-assemblies corroborates the relation between helices length and catalyst selectivity. This work was published as *Chem. Commun.* **2019**, *55*, 2162-2165（*Yan Li, Xavier Caumes, Matthieu Raynal and Laurent Bouteiller*）, and was reported here as published with formatting to match with the rest of the thesis.

I Introduction

External triggers such as light, redox potential, chemical species or mechanical energy emerged as a new strategy to control chemical processes.[1-4] Temporal control of chemical reactions has been achieved by toggling a catalyst back and forth between its active and inactive states. This switchable capacity of the catalyst is exploited in the realm of sequential reactions, *e.g.* allowing to finely control polymerization processes[5-7] or tandem reactions.[8-9] Much less effort has been devoted to the design of stimuli-responsive asymmetric catalysts.[10] Predictable control of the stereochemical direction for a single catalyst is achieved by supporting intrinsically achiral centres on a chirally-switchable platform such as overcrowded alkenes,[11-15] stereodynamic ligands,[16] redox-configurable copper complexes,[17-19] foldamers[20] or polymers.[21-30] Alternatively, chemical additives,[31-32] light[33] and redox potential[34] were employed to improve the degree of enantioinduction,[35] including a recent example of a rationally-designed asymmetric auto-inductive process.[36] However, implementation of these elaborated catalytic systems in consecutive reactions or polymerization reactions will require a better control of their dynamic properties. Molecular catalysts for the preparation of atactic isotactic multi stereoblock copolymers are sparse[37] and, in that regard, establishing the design elements for a dynamic and multi-configurable catalytic system will constitute an important advance.

In parallel, the reversible and dynamic properties of supramolecular chiral assemblies[38-39] have been exploited in asymmetric catalysis.[40] We previously demonstrated that a significant degree of enantiocontrol can be achieved by supporting metal catalytic centres at the periphery of the helical assemblies formed by benzene-1,3,5-tricarboxamide monomers (BTA).[29, 41-42] Co-assembly between an achiral BTA ligand and an enantiopure BTA co-monomer into homochiral helices allows real-time control of the enantioselectivity. The stereochemical direction and the degree of asymmetric induction of the catalytic reaction are related to the handedness and the optical purity, respectively, of the helical BTA assemblies. For further development of this new class of catalysts, it is of utmost importance to probe how the enantioselectivity is affected by the average length of the helices. Herein, we show that reversible assembly of BTA monomers into helices of different length constitutes a simple method to vary the degree of enantioinduction of a catalytic reaction (Chart 1).

II Results and discussion

The preparation of BTA helices of controlled sizes is hampered by the dynamic character of the assemblies. Moreover, hydrogen-bonded supramolecular polymers form one-dimensional assemblies

whose stability are particularly sensitive to the environment.[43] Anions have notably been used to reduce the chain length of urea-based supramolecular polymers without affecting their structure.[44] Therefore, we envisioned that the length of BTA assemblies could be modulated *in a reversible manner* by first adding an anion and then removing it, *e.g.* through a salt metathesis reaction leading to its co-precipitation with a cation (Chart 1).[45-47]

To implement our concept, we chose as a reference the catalytic mixture composed of an achiral BTA ligand **BTA^{PPh2}** (6 mol%) an enantiopure co-monomer **BTA (*R*)-Cha** (6.6 mol%), $[Cu(OAc)_2 \cdot H_2O]$ (3 mol%) and $PhSiH_3$ since it furnished the hydrosilylation product of 1-(4-nitrophenyl)ethanone (NPnone) with significant enantioselectivity (54±1% *e.e.* at 293 K in toluene).[29] A combination of spectroscopic analyses and catalytic experiments indicated that the chirality of the co-monomer controls the handedness of the helices and thus the stereochemical direction of the hydrosilylation reaction. Two preliminary experiments now confirm that the size of the BTA assemblies also affects the level of asymmetric induction (Table S1, ESI†): (i) in THF, BTAs are molecularly dissolved and no selectivity is observed, and (ii) when the reaction is conducted with a concentration in **BTA^{PPh2}** close to its critical concentration in toluene, the selectivity is significantly decreased (19% *e.e.*). In the latter case, it is likely that at this concentration the assemblies are too short to arrange all the copper centers in a suitable chiral environment.

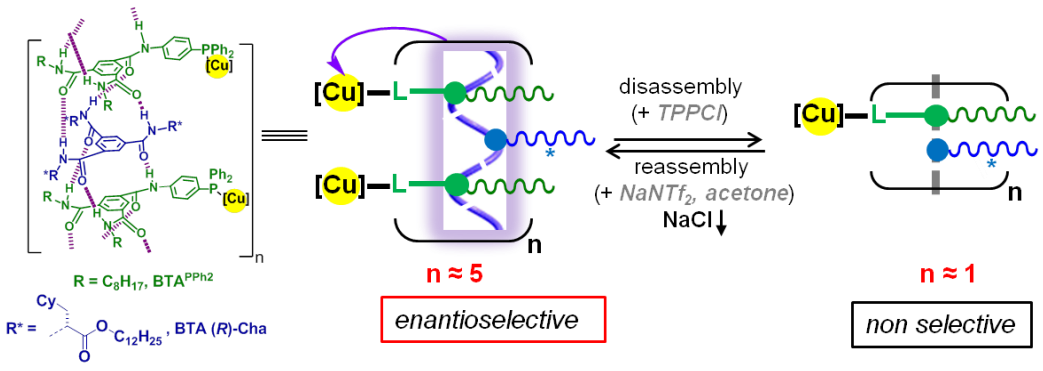

Chart 1 Schematic representation of the present concept. Supramolecular helices, formed by co-assembly between an achiral BTA ligand (**BTA^{PPh2}**) coordinated to Cu and an enantiopure BTA co-monomer (**BTA (*R*)-Cha**), are shortened and lengthened reversibly by means of an appropriate combination of salts. This schematic representation of the co-assemblies is supported by analytical data but the coordination mode of Cu and the fraction of coordinated PPh_2 groups in the co-assemblies are not known.

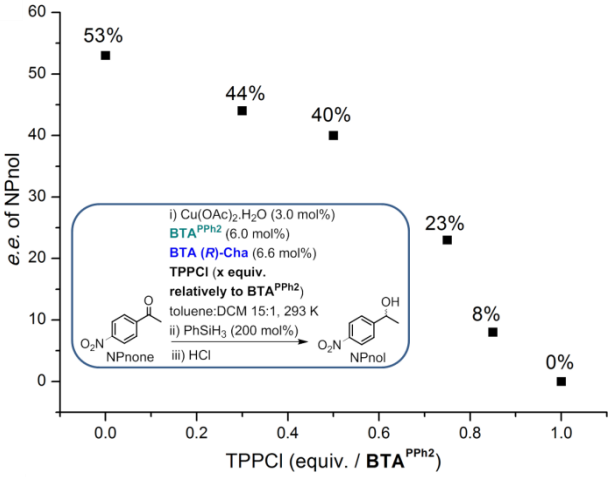

Fig. 1 Enantioselectivity as a function of the amount of TPPCl. See the precise conditions in Table S.1. Conversions (after 1h): >99% (0 and 0.3 equiv. of TPPCl), 97% (0.5 equiv.), 91% (0.75 equiv.), 75% (0.85 equiv.) and 63% (1.0 equiv.).

We next investigated the influence of TPPCl (tetraphenylphosphonium chloride) on the performance of the catalytic system of reference (Fig. 1).[45-47] The first (unanticipated) effect is the slowdown of the reaction rate: the higher the amount of TPPCl, the lower the rate (Table S1). Whilst the origin of this negative effect of chloride anions on the reaction rate has not been established for the present case, inhibition of metal-catalysed reactions by soluble halogen anions has some precedent in the literature.[48-49] The decreased rate for the non-selective state of the supramolecular catalyst is not detrimental since good conversions can be achieved by increasing the amount of silane and the reaction time (vide infra). The second (anticipated) effect is a gradual decrease of the enantioselectivity as a function of the amount of chloride anions in the catalytic mixture: from 44% *e.e.* (0.3 equiv. relative to BTAPPh2) to 0% *e.e.* (1.0 equiv.).‡ The fact that a high content of TPPCl relatively to BTAPPh2 is required to completely erase the selectivity suggests that the length of the assemblies should be shortened down to very short aggregates to be non-selective (*vide infra*). It is interesting to note that TPPCl does not act as dual on-off selectivity switch but rather allows programmable modulation of the degree of enantioinduction (signal output) in between fully racemic, and optimal enantiomeric preference (53% *e.e.*) by simply changing the concentration of TPPCl (signal input).

The nature of the co-assemblies formed between **BTA^{PPh2}** and **BTA (*R*)-Cha** in toluene and their reversible assembly have been precisely characterized by means of Fourier-Transform Infrared (FT-IR), Nuclear Magnetic Resonance (NMR), Small Angle Neutron Scattering (SANS) and Circular Dichroism (CD) analyses. The "pristine" co-assemblies, *i.e.* in absence of any additives, are very long

($DP_n \approx 250$), stack with a single molecule in the cross-section and contain approximately two **BTA^{PPh2}** molecules for one **BTA (*R*)-Cha** (Figs. S1-S2). They form homochiral left-handed helices as deduced from CD analysis (Fig. 2b).[29] The coordination of **BTA^{PPh2}** to copper does not significantly change the structure of the helical co-assemblies (Fig. S4). However, both SANS (Fig. S5) and FT-IR (Figs. 2a) analyses confirm that the length of the co-assemblies is drastically decreased in presence of 1.0 equiv. of TPPCl. Notably, in FT-IR, the bonded amide band is reduced whereas the free amide band is increased in presence of TPPCl (green arrows in Fig. 2a). Deconvolution of the ester C=O and amide C=O bands yields an estimation of $DP_n \approx 2$ for the average length of the co-assemblies in presence of 1.0 equiv. of TPPCl (Fig. S7). The absence of an Induced CD (ICD) signal[50] for this mixture (Fig. 2b) corroborates the fact that these objects are likely too small to adopt a helical configuration and explains the absence of selectivity for the catalytic reaction (*vide supra*).

$NaNTf_2$ (Tf=triflimide) was selected to trigger the metathesis reaction because of the weak coordination ability and the known chemical stability of the NTf_2 anion.[51] $NaNTf_2$ is introduced in solution in acetone as we observe a good solubility of this salt in the three-solvent mixture (toluene:DCM:acetone 15:1:1). In these conditions, reassembly is evidenced by the increased intensity of the bonded amide band and the decreased intensity of the free amide band (wine arrows in Fig. 2a). Also, this sample exhibits a significant ICD signal (Fig. 2b) which infers that the ligand has recovered a chiral environment.

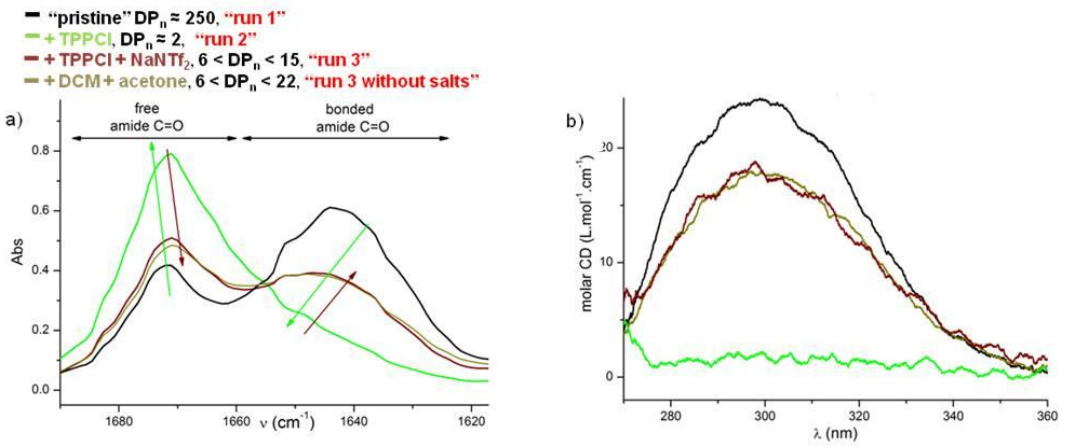

Fig. 2 Characterization of the reversible assembly of supramolecular helices. FT-IR (a) and CD (b) analyses of the co-assemblies in absence and presence of salts (293 K). The concentrations in ligand and co-monomer are close to those of catalytic experiments indicated in red. The DP_n values have been estimated by means of SANS and FT-IR analyses (Figs. S1 and S7). In the FT-IR spectra, both dimers of **BTA (*R*)-Cha**[52-54] and stack ends contribute to the free amide C=O band. The observed CD signal

belongs to **BTA^{PPh2}** only and is thus an ICD signal[50] which reflects the chiral environment of the ligand.[29] For the "pristine" co-assemblies, this signal is of comparable intensity ($\Delta\varepsilon$=24 L.mol^{-1}.cm^{-1}) to that previously observed in methylcyclohexane ($\Delta\varepsilon$=17 L.mol^{-1}.cm^{-1})[29,130] inferring the presence of homochiral left-handed helices.[29]

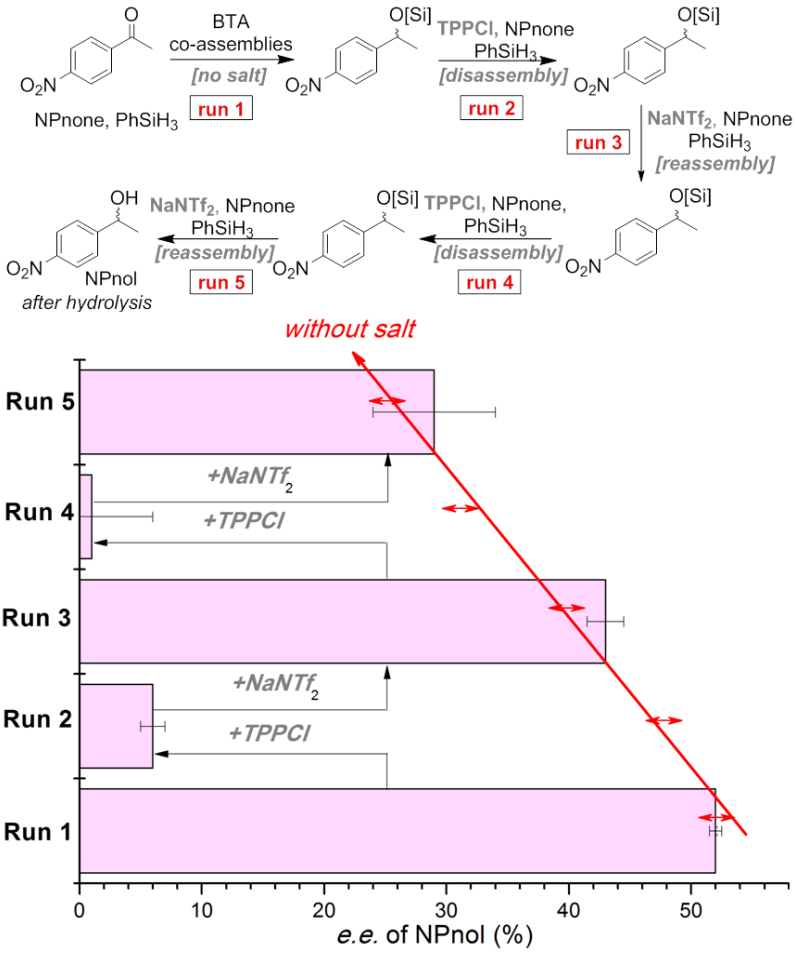

Fig.3 Modulation of the enantioselectivity of the supramolecular catalyst involved in the hydrosilylation of several equivalents of NPnone added sequentially in the reaction mixture. **Top**: description of the run. TPPCl and $NaNTf_2$ are added as solutions in DCM and acetone, respectively so that the solvent nature is: toluene (run 1), toluene:DCM 15:1 (run 2), toluene:DCM:acetone 15:1:1 (run 3), toluene:DCM:acetone 15:2:1 (run 4) and toluene:DCM:acetone 15:2:2 (run 5). B**ottom**: enantioselectivity obtained for each run. Conversions: 99% (run 1), 86% (run 2), 89% (run 3), 53% (run 4) and 84% (run 5). Double arrows represent the selectivity obtained in the same solvent but in absence of salts. For the determination of the *e.es.* and the conversions, see Table S3.

The above experiments have established the use of TPPCl (1.0 equiv., added as a solution in DCM) and $NaNTf_2$ (1.0 equiv., added as a solution in acetone) as a suitable combination of salts for the

reversible assembly of the supramolecular helices. We thus investigated whether this strategy can be used to switch the enantioselectivity of our catalytic system of reference. Sequential additions of NPnone, silane and salts (Fig. 3 top) have been performed in the following order: no salt (run 1), TPPCl (run 2), $NaNTf_2$ (run 3), TPPCl (run 4) and $NaNTf_2$ (run 5). An excess of silane has been engaged and the reaction times have been adapted so that a conversion superior or equal to 84% was achieved for each run (except for run 4, conversion=53%). The enantiomeric excess for each run was calculated from the cumulated *e.e.* obtained by chiral GC analyses of the aliquots as detailed in Table S3. As shown in Fig. 3, the state of the supramolecular copper catalyst is alternatively selective (29-52% *e.e.*) and poorly selective (0-6% *e.e.*). More precisely, a significant decrease of the enantioselectivity is found for the run 2 (6±1% *e.e.*) and run 4 (0±5% *e.e.*), as a result of the disassembly of the supramolecular helices supporting the catalytic centres in presence of TPPCl. The selectivities of run 3 (43±1.5% *e.e.*) and run 5 (29±5% *e.e.*) are significantly higher than those of run 2 and run 4, which corroborates the reversible assembly of the BTA helices and validates our concept. We were intrigued by the decreased selectivity for run 3 and 5 compared to run 1 and therefore investigated its origin. After reassembly (in presence of TPPCl and $NaNTf_2$, run 3), the co-assemblies have DP_n in between 6 and 15 much lower than that of "pristine" co-assemblies (run 1, $DP_n \approx 250$) as evidenced by FT-IR analyses (Fig. 2a). In fact, this shortening of the helices is mostly due to the presence of co-added solvents (DCM and acetone) as demonstrated by: (i) control catalytic experiments in absence of TPPCl and $NaNTf_2$ (double red arrows, Fig. 3) which provide roughly the same selectivity for run 3 and 5, (ii) the fact that, in toluene:DCM:acetone 15:1:1, the FT-IR, NMR and CD spectra of the co-assemblies in absence or presence of TPPCl and $NaNTf_2$ are similar (Figs. 2 and S7). This substantiates the efficiency of the metathesis salt reaction and infers that full reassembly is hampered by the competitive and polar nature of the solvents employed to dissolve the salts. Interestingly, the selectivity decrease (19%) observed after a single disassembly/reassembly switch (from 52% *e.e.* for run 1 to 43% *e.e.* for run 3) correlates well with the lower intensity (25%) of the ICD signal measured for co-assemblies in presence of the salt mixture and the co-solvents (Fig. 2b). There is thus a good correlation between the average length of the assemblies, the chiral environment of the ligand and the selectivity of the reaction (Table S2). For the present catalytic system, the critical length of the supramolecular helices required to locate most of the copper centres in a chiral environment suitable for asymmetric induction is thus in the range of a ten monomers.

III Conclusion

In conclusion, a multi-configurable catalyst is obtained by reversibly shortening and lengthening the supramolecular helices formed by assembly of BTA monomers. This can undoubtedly be extended to other families of hydrogen-bonded supramolecular polymers and organogels with the aim of tuning their macroscopic properties. Further progress in the design of such functional supramolecular assemblies is required for the implementation of more efficient smart systems in the field of switchable catalysis.

IV Supporting information

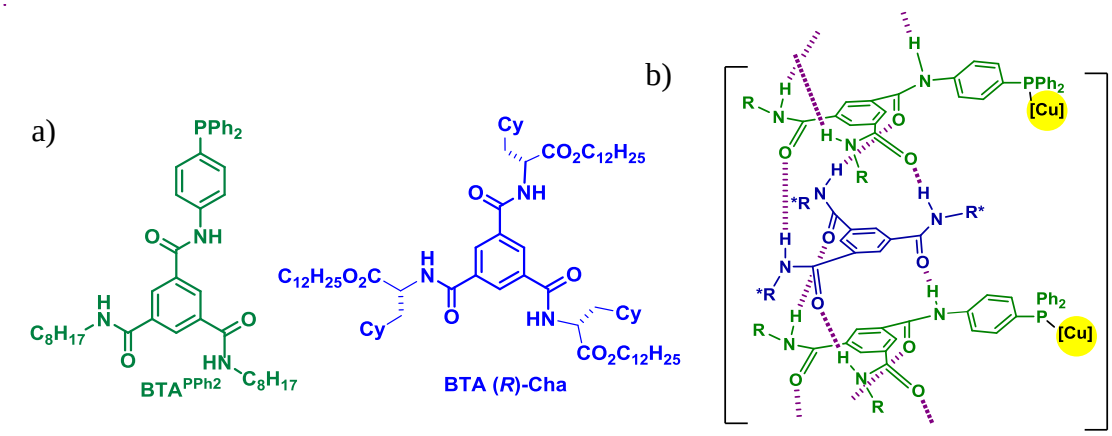

Chart S1 a) Chemical structures of the BTA molecules investigated in this study. b) Representation of the rod-like co-assemblies between **BTA^{PPh2}** and **BTA (*R*)-Cha**. The ratio ligand: co-monomer (≈ 2:1) reflects the composition determined by analytical techniques (see below). It provides predominantly the (*S*) product in the hydrosilylation of the 1-(4-nitrophenyl)ethanone.[29] (The distribution of the two BTAs along the rod is not known as well as the coordination mode and the fraction of coordinated PPh_2 groups in the co-assemblies).

General Procedures.

BTA^{PPh2},[29] and **BTA (*R*)-Cha**,[53] were prepared according to published procedures. $PhSiH_3$ (>97%, Sigma-Aldrich), $Cu(OAc)_2{\cdot}H_2O$ (>99%, Sigma-Aldrich), 1-(4-nitrophenyl)ethanone (NPnone, >98% Alfa Aesar), $TBANTf_2$ (purity≥ 99%, Fluka) and $NaNTf_2$ (purity≥ 98%, Fluorochem) were stored under vacuum prior to use. Dried solvents were obtained from an SPS solvent purification system (IT-Inc).

Fourier-Transform Infrared (FT-IR) analyses: FT-IR measurements were performed on a Nicolet iS10 spectrometer. Spectra were measured in 0.02 cm pathlength CaF_2 cells at 293 K and were corrected for air, solvent and cell absorption.

Deconvolution procedure for quantitative analysis of FT-IR spectra - determination of f Cha in stacks and DP_n (Figs. S2 and S7): The bands corresponding to ester C=O (1717-1753 cm^{-1}) and amide C=O (1627-1680 cm^{-1}) in the FT-IR spectra of different samples (**BTA (*R*)-Cha**, **BTA^{PPh2}**, co-assemblies with and without salts) are deconvoluted simultaneously into two Gaussian peaks and three Gaussian peaks respectively. The procedure yields five bands with the same position and width for each sample but with different intensities: free ester (≈1745 cm^{-1}), bonded ester (≈1725 cm^{-1}), free amide (≈1671 cm^{-1}), bonded amide peak 1 (≈1650 cm^{-1}) and bonded amide peak 2 (≈1635 cm^{-1}). The molar extinction coefficients of the bonded amide peak 2, the free amide peak and the bonded ester peak were obtained from the individual spectra of **BTA^{PPh2}** and **BTA (*R*)-Cha**. Then, the fraction of **BTA (*R*)-Cha** in stacks (f Cha in stacks) and the DP_n values are obtained by means of the following formula:

$$[\text{BTA Cha dimers}] = \frac{\text{area of bonded ester band}}{\varepsilon_{\text{bonded ester}} \times \text{pathlength}}$$

$$[\text{BTA Cha in stacks}] = [\text{BTA Cha}]_0 - [\text{BTA Cha dimers}]$$

$$\textbf{f Cha in stacks} = \frac{[\text{BTA Cha in stacks}]}{[\text{BTA}^{\text{PPh2}}]_0 + [\text{BTA Cha in stacks}]}$$

$$[\text{bonded amide functions}] = \frac{\text{area of bonded amide bands 1 and 2}}{\varepsilon_{\text{bonded amide}} \times \text{pathlength}}$$

$$[\text{free amide functions}] = \frac{\text{area of free amide band}}{\varepsilon_{\text{free amide}} \times \text{pathlength}}$$

$$[\text{stack end}] = [\text{free amide functions}] - [\text{BTA Cha dimers}]$$

$$\textbf{DP}_\textbf{n} = 1 + \frac{[\text{bonded amide functions}]}{[\text{stack end}]}$$

with [**BTA Cha**]$_0$ and [**BTA^{PPh2}**]$_0$ the introduced amount of the respective monomers in the mixture. $\varepsilon_{\text{bonded ester}}$, $\varepsilon_{\text{bonded amide}}$ and $\varepsilon_{\text{free amide}}$ are the molar extinction coefficients of the corresponding functions. Low values for [stack end] (and thus large values for DP_n) cannot be reliably determined by this approach.

Circular dichroism (CD) analyses*:* CD measurements were performed on a Jasco J-1500 spectrometer equipped with a Peltier thermostated cell holder and Xe laser. Data were recorded at 20°C with the following parameters: 20 $nm.min^{-1}$ sweep rate, 0.05 nm data pitch, 2.0 nm bandwidth, and between 400 and 270 nm. Toluene and cell contributions at the same temperature were subtracted from the obtained signals. A dismountable quartz cell of 0.01 mm pathlength was used. For all samples, LD contribution was negligible ($\Delta LD < 0.005$ dOD) and the shape of the CD signal was independent of the orientation of the quartz slide. Molar CD values are reported in $L.mol^{-1}.cm^{-1}$ and are expressed as follows: $\Delta\varepsilon=\theta/(32980\times l\times c)$ where θ is the measured ellipticity (mdeg), l is the optical path length in cm, and c is the concentration in $mol.L^{-1}$.

Small-angle neutron scattering (SANS) analyses: SANS measurements were made at the LLB (Saclay, France) on the PA20 instrument, at three distance-wavelength combinations to cover the 2.4×10^{-3} to $0.46 Å^{-1}$ *q*-range, where the scattering vector q is defined as usual, assuming elastic scattering, as $q=(4\pi/\lambda)\sin(\theta/2)$, where θ is the angle between incident and scattered beam. Data were corrected for the empty cell signal and the solute and solvent incoherent background. A light water standard was used to normalize the scattered intensities to cm^{-1} units. The data was fitted with the DANSE software SasView. The number *n* of molecule in the cross-section can be derived from n_L (the number of molecule per unit length)[55] by assuming an average intermolecular distance of 3.62 Å, which is the usual spacing between aromatic rings in BTA helical assemblies.

Preparation of BTA solutions for CD (Fig. 2b), NMR (Figs. S3 and S8) and FT-IR (Figs. 2a, S7 and S2) analyses of the co-assemblies without Cu: The concentrations are close to those employed in the catalytic experiments. A stock solution (6.0 mL) was prepared by dissolving **BTA^{PPh2}** (16.7 mM) and **BTA (*R*)-Cha** (18.4 mM) in C_7D_8. The vial was sealed with a PTFE-coated cap to avoid contamination from leaching plasticizer, gently heated for ensuring dissolution and placed on a shaking table for 12 h. Four samples were prepared from the same stock solution:

"pristine" co-assemblies: a given amount of this stock solution was directly used for analyses (298 K).

co-assemblies + TPPCl: TPPCl (1.0 equiv. relatively to **BTA^{PPh2}**) dissolved in CD_2Cl_2 (40 µL) was added to an aliquot (600 µL) of this stock solution, the solution was stirred for 1 hour, and a given amount was taken for analyses.

co-assemblies + TPPCl + $NaNTf_2$: TPPCl (1.0 equiv.) dissolved in CD_2Cl_2 (40 µL) and $NaNTf_2$ (1.0 equiv.) dissolved in acetone-d_6 (40 µL) were added to an aliquot (600 µL) of the stock solution, the solution was stirred for 1 hour, and a given amount was taken for analyses.

co-assemblies + DCM + acetone: CD_2Cl_2 (40 µL) and acetone-d_6 (40 µL) were added to an aliquot (600 µL) of the stock solution, the solution was stirred for 1 hour, and a given amount was taken for analyses.

All samples were heated prior to analysis

Preparation of BTA solutions for NMR (Fig. S4a) and FT-IR (Fig. S4b) analyses of the co-assemblies with Cu: The concentrations are close to those employed in the catalytic experiments. Sample "pristine co-assemblies·Cu": A stock solution (3.0 mL) was prepared by dissolving **BTA^{PPh2}** (16.7 mM), $Cu(OAc)_2 \cdot H_2O$ (8.35 mM), and **BTA (*R*)-Cha** (18.4 mM) in THF and stirring for 12 h. The THF was removed under vacuum and the obtained solid was dried for 1 h. C_7D_8 (3.0 mL) was added and the mixture was stirred for 12 h. The sample was heated prior to analysis.

Preparation of BTA solutions for SANS analyses - characterization of the co-assemblies (Fig. S1): Three samples were prepared by dissolving **BTA^{PPh2}** (5.98 g.L-1, 8.6 mM), **BTA (*R*)-Cha** (19.9 g.L-1, 16.9 mM), and a mixture of **BTA^{PPh2}** (3.98 g.L-1, 5.8 mM) and **BTA (*R*)-Cha** (4.39 g.L-1, 3.7 mM) in C7D8.

Preparation of BTA solutions for SANS analyses - addition of salts (Fig. S5): A stock solution A was prepared by dissolving **BTA^{PPh2}** (41.0 mg) and **BTA (*R*)-Cha** (45.0 mg) in 4.088 g of THF. A stock solution B was obtained by dissolving $CuOAc \cdot H_2O$ (3.95 mg) in 2.698 g of stock solution A. Three samples were prepared from stock solution B:

SANS co-assemblies·Cu: 399.8 mg of stock solution B was taken, the solvent was removed under vacuum and the tube was further put under vacuum ($1x10^{-3}$ mbar) for 1 hour. 939.7 mg of C_7D_8 was added and the vial was sealed with PTFE-coated cap and placed on a shaking table for 12 h

SANS co-assemblies·Cu + TPPCl: 1.097 g of stock solution B was added to a vial containing TPPCl (7.10 mg). The mixture was stirred for 1 h, the solvent was removed under vacuum and the tube was further put under vacuum ($1x10^{-3}$ mbar) for 1 hour. 2.600 g of C_7D_8 was added and the vial was sealed with PTFE-coated cap, gently heated to ensure dissolution and placed on a shaking table for 12 h

SANS co-assemblies·Cu + TPPCl + $NaNTf_2$: 1.097 g of stock solution B was added to a vial containing TPPCl (7.03 mg) and $NaNTf_2$ (4.73 mg). The mixture was stirred for 1 h, the solvent was removed under vacuum and the tube was further put under vacuum ($1x10^{-3}$ mbar) for 1 hour. 2.596 g of C_7D_8 was added and the vial was sealed with PTFE-coated cap, gently heated to ensure dissolution and placed on a shaking table for 12 h.

All samples have been heated prior to analysis. The concentrations of the different components for the three samples are indicated in Fig. S5. These samples have also been analysed by FT-IR (Fig. S6).

Chiral GC analyses: 1-(4-nitrophenyl)ethanol (NPnol). The optical purity was determined by GC analysis: Chiral Cyclosil-B column, 30 m × 250 µm x 0.25 µm, inlet pressure = 12.6 psi. Injection temperature = 250°C; detector temperature = 300°C; column temperature = 145°C. Retention time: 17.9 min (1-(4-nitrophenyl)ethanone), 47.6 min ((R)-enantiomer), 49.9 min ((S)-enantiomer).[56]

Catalytic experiments: see detailed procedures in page S-21.

Evaluation of salts and solvents in catalysis (Table S1)

Table S1 Influence of solvent, concentration and salts on the selectivity of the catalytic co-assemblies for the copper-catalysed hydrosilylation of 1-(4-nitrophenyl)ethanone (NPnone)

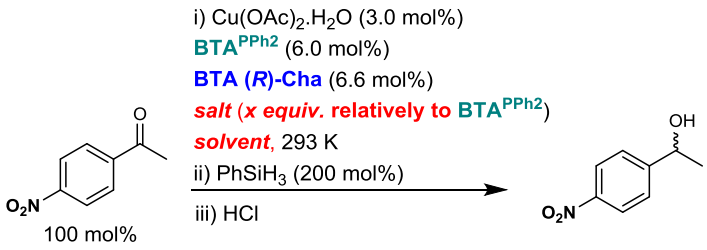

entry	solvent	[NPnone]	salt/equivalent	conversion (%, after 1h)	selectivity (*e.e.*)
1	toluene	0.28 M	-	>99	54±1[29]
2	THF	0.28 M	-	>99	0
3	toluene	0.008 M[a]	-	*nd*	19
4	toluene:DCM 15:1	0.26 M	TPPCl/0.3	>99	44
5	toluene:DCM 15:1	0.26 M	TPPCl/0.5	97	40
6	toluene:DCM 15:1	0.26 M	TPPCl/0.75	91	23
7	toluene:DCM 15:1	0.26 M	TPPCl/0.85	75	8
8	toluene:DCM 15:1	0.26 M	TPPCl/1.0	63	0
9	toluene	0.28 M	NaCl/1.0	>99	53
10	toluene	0.28 M	$TBANTf_2$/1.0[b]	>99	51

Reaction conditions: 1-(4-nitrophenyl)ethanone (NPnone), $Cu(OAc)_2 \cdot H_2O$ (3.0 mol%), **BTA^{PPh2}** (6.0 mol%), **BTA (*R*)-Cha** (6.6 mol%), $PhSiH_3$ (200 mol%), solvent, 293 K, 12 h. Conversion > 90% as determined by GC analyses. The *e.es.* were determined by chiral GC analyses[56] and are given with an error bar of ±1.5% except for entry 1 ±1%.[29] For reactions with TPPCl: TPPCl is introduced in DCM such as the solvent mixture for the catalytic experiment is toluene:DCM 15:1. Nd : not determined. [a] [**BTA^{PPh2}**] = 0.5 mM which is close to the critical concentration for self-assembly.[29][b] $TBANTf_2$ and $TPPNTf_2$ (the latter being the salt generated upon the salt metathesis reaction) are expected to behave similarly.

Characterization of the "pristine" co-assemblies (Figs. 2, S1-S3).

The length of the co-assemblies at a concentration of [**BTA^{PPh2}**] = 5.8 mM and [**BTA (*R*)-Cha**] = 3.7 mM is determined to be 870 Å, *i.e.* DP_n = 125 by SANS (Fig. S1). For the catalytic experiments, the concentrations are *ca.* 4 times higher ([**BTA^{PPh2}**] = 16.7 mM and [**BTA (*R*)-Cha**] = 18.3 mM), so that a value twice higher is expected ($DP_n \approx 250$).[57] FT-IR measurements (Fig. S2) are in agreement with this order of magnitude because the concentration of stack ends is too low to be determined. These analyses also allow to determine a fraction of **BTA (*R*)-Cha** in stacks equals to 0.33. The co-assembly process from monomers (378 K) to stacks (293 K) is probed by NMR (Fig. S3). Finally, CD analysis of the co-assembly is consistent with the formation of homochiral left-handed helices (Fig. 2b).

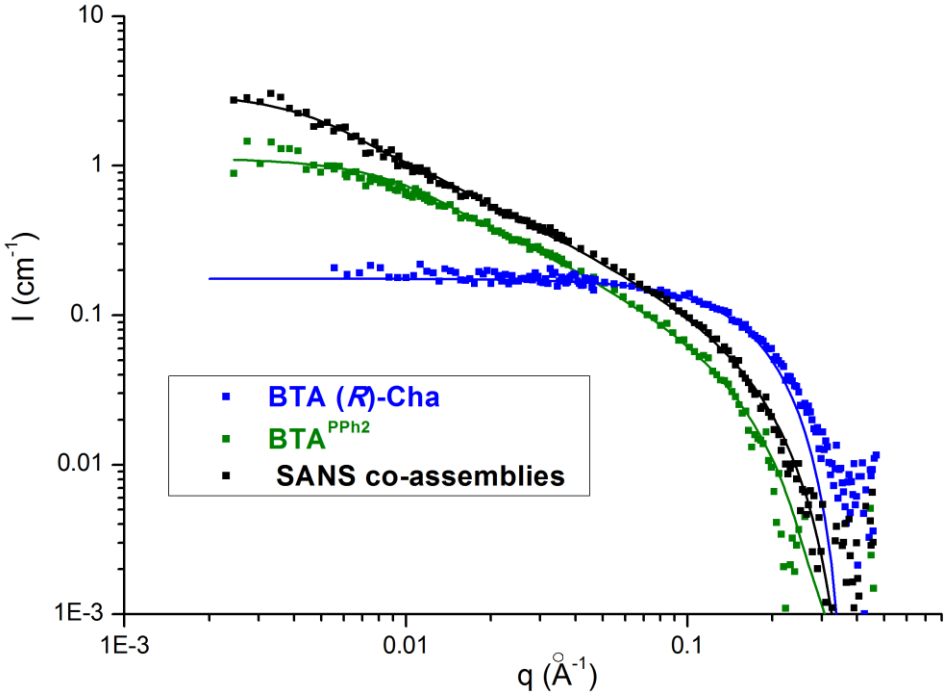

Figure S1 Characterization of the co-assemblies by SANS analyses (293 K, C_7D_8).[a],[b],[c]

[a] Composition and result of the fits (n: number of molecule in the cross-section):

sample	[BTA (*R*)-Cha]	[BTA^{PPh2}]	r (Å)[b]	n	length(Å)/ DP_w[b]	f Cha in stacks[b]
BTA (*R*)-Cha	19.9 g.L^{-1} 16.9 mM	-	**12.0**	-	**dimer**	-
BTA^{PPh2}		5.98 g.L^{-1} 8.6 mM	**11.1**	**0.7**	**420/120**	-
SANS co-assemblies	4.39 g.L^{-1} 3.7 mM	3.98 g.L^{-1} 5.8 mM	**10.4**	**0.6**	**870/250**	**0.33**

[b] SANS data of **BTA (*R*)-Cha** is fitted according to the form factor for spherical objects. The molar mass of the spherical object (M=1993 g/mol) is 1.7 times the molar mass of the monomer which is consistent with **BTA (*R*)-Cha** being a dimer. This dimer was thoroughly characterized in our previous reports.[52-54] SANS data of **BTA^{PPh2}** is fitted according to the form factor for rigid rods of finite length with a circular cross-section and a uniform scattering length density. It gives a radius of 11.1 Å, a number of molecules in the cross-section n=0.7 (which is consistent with isolated stacks of BTAs) and a length of 420 Å ($DP_w \approx 120$). It was previously shown that **BTA (*R*)-Cha** in part co-assembles with **BTA^{PPh2}** and that the remaining **BTA (*R*)-Cha** exists as dimers.[29] Therefore, SANS data of the mixture of **BTA^{PPh2}** and **BTA (*R*)-Cha** is fitted as the sum of the form factors for spherical objects and for rigid rods of finite length. The latter yields a length of 870 Å ($DP_w \approx 250$, $DP_n \approx 125$).[57] The obtained volume fraction of spherical objects yields the amount of **BTA (*R*)-Cha** present as dimers: 77% of **BTA (*R*)-Cha** is incorporated into stacks which means that the fraction of **BTA (*R*)-Cha** in the stacks is 0.33 ($f_{Cha\ in\ stacks}^{SANS} = 0.33$). The radius (10.4 Å) and number of molecules in the cross-section (n=0.6) were extracted from this SANS curve after removing the contribution of dimers. These values are consistent with the co-assembly being isolated stacks of BTA molecules. [c] In our previous publication, the length determined by SANS for **BTA^{PPh2}** and for the mixture of **BTA^{PPh2}** and **BTA (*S*)-Cha** (Fig. S5 in ref [1])[29] was under evaluated as a result of the interactions between objects at the higher concentrations employed in these analyses.

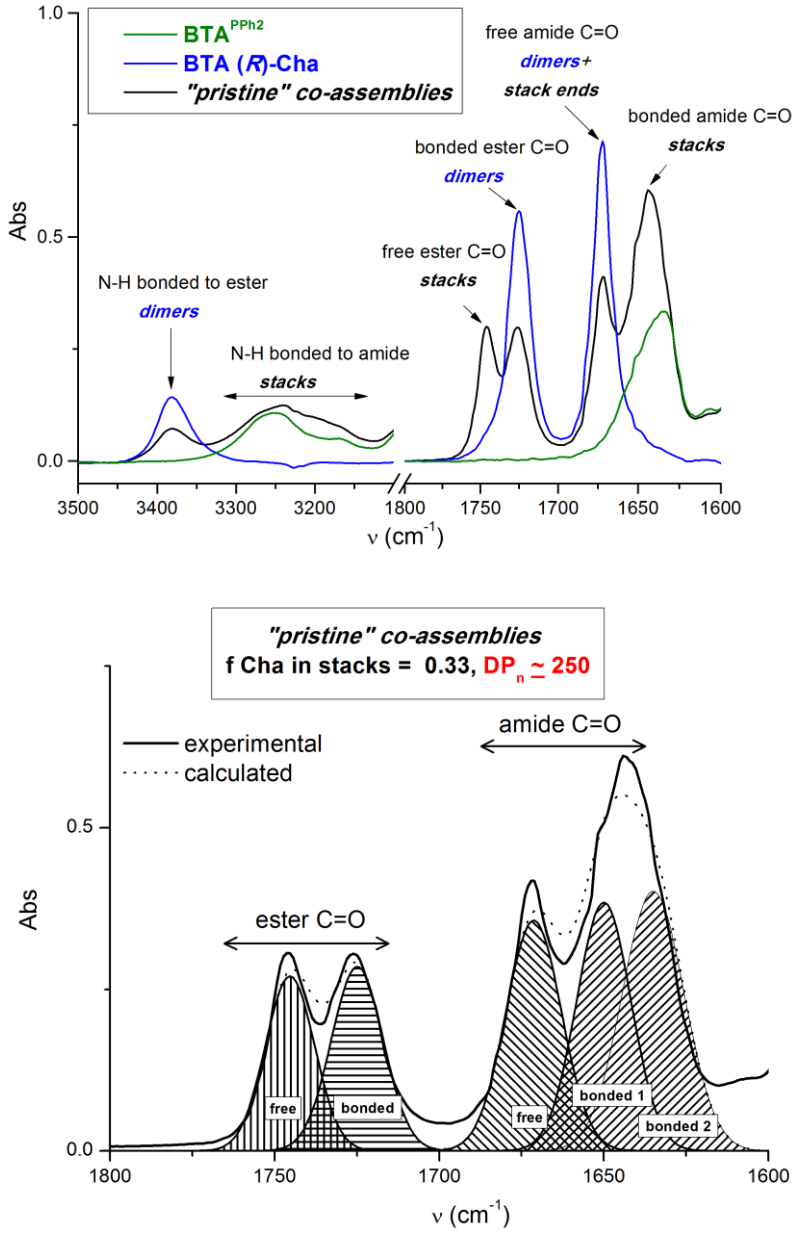

Figure S2 Characterization of the co-assemblies by FT-IR analyses (293 K, C_7D_8). Top: Assignment of the N-H and C=O bands in the homo- and co-assemblies.[52-54] Bottom: Deconvoluted FT-IR spectrum of the co-assemblies (C=O region).[a],[b],[c]

[a] Composition (The concentrations are close to those employed in the catalytic experiments.): **BTA^{PPh2}**: [**BTA^{PPh2}**] = 16.7 mM, **BTA (*R*)-Cha**: [**BTA (*R*)-Cha]** = 18.4 mM, **"pristine" co-assemblies**: [**BTA^{PPh2}**] = 16.7 mM, **[BTA (*R*)-Cha]** = 18.4 mM. [b] Value obtained after deconvolution: f Cha in stacks^{FT-IR} = 0.33. This value is in good agreement with that obtained previously by processing the N-H region of the FT-IR spectrum (f Cha in stacks^{FT-IR} = 0.35).[29] The fact that SANS analyses (Fig.. S1) give the same value under different conditions is fortuitous. [c] The concentration of stack ends is too low to be reliably determined so that the indicated DP_n value is deduced from SANS analysis (Fig. S1) by considering that the concentrations are here *ca.* 4 times higher.[57]

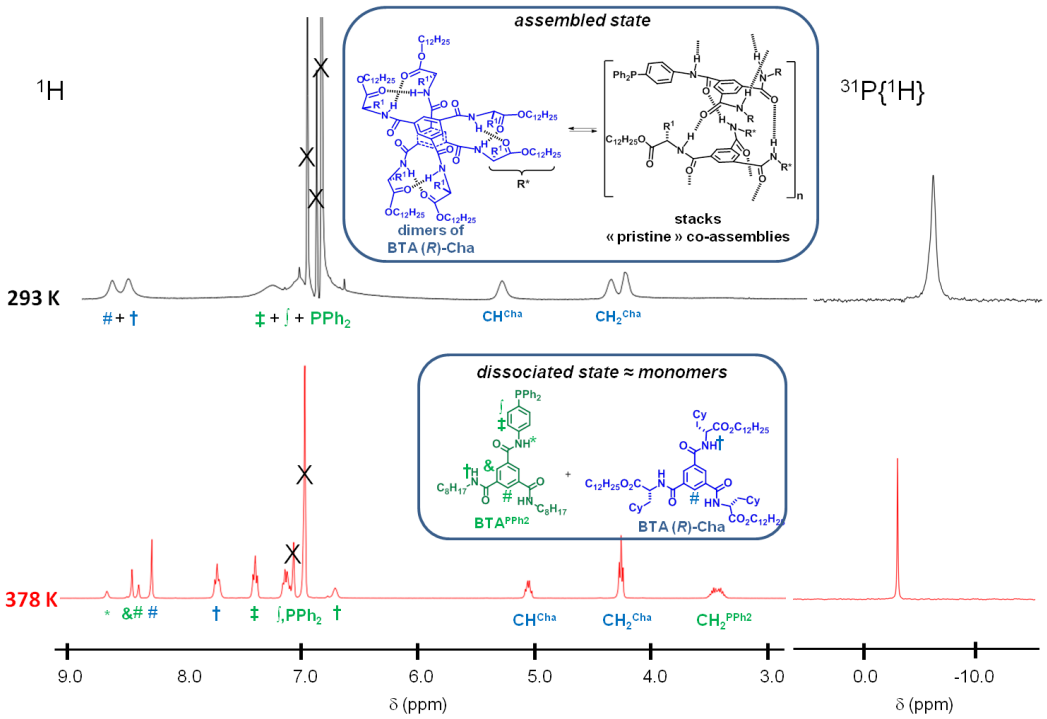

Figure S3 Characterization of the co-assemblies by ^{1}H and $^{31}P\{^{1}H\}$ NMR analyses. Sample "pristine" co-assemblies at 378 K and 293 K (C_7D_8).[a] x = residual protons of C_7D_8.

[a] Interpretation: <u>At 378 K</u>: the fact that the signals are well-defined is consistent with the presence of a dissociated state in which all molecules are monomers (or weakly associated). Assignment of the different protons has been made based on the ^{1}H NMR analyses of the individual molecules (data not shown). <u>At 293 K</u>: the fact that the signals broaden upon lowering the temperature is indicative of the formation of assemblies.[53, 58-59] At this temperature, the observed signals are attributed to **BTA (*R*)-Cha** and to the aryl rings connected to the phosphorus atoms of **BTA^{PPh2}** in the co-assemblies; all the others signals are too broad to be detected. We attribute the detected signals of **BTA (*R*)-Cha** to dimers in equilibrium with the co-assemblies (stacks). The singlet corresponding to the PPh_2 group ($^{31}P\{^{1}H\}$ NMR analyses) also broadens upon formation of the assemblies.

Characterization of the "pristine" co-assemblies coordinated to Cu (Fig. S4).

$^{31}P\{^{1}H\}$ NMR analysis (Fig. S4a) of the **BTA^{PPh2}-BTA (*R*)-Cha** mixture in presence of $Cu(OAc)_2 \cdot H_2O$ clearly shows two singlets: one (broad) corresponding to Cu coordinated to phosphine (δ = -1.5 ppm) and one corresponding to free phosphine (δ = -5.5 ppm). This indicates that, in the co-assemblies, only a fraction of the phosphine ligands are coordinated to Cu. ^{1}H NMR spectra of the **BTA^{PPh2}-BTA (*R*)-Cha** mixture with and without $Cu(OAc)_2 \cdot H_2O$ are similar which shows that the presence of Cu does not disturb much the aggregation. No significant change in the hydrogen-bond network is observed either, upon coordination to Cu (FT-IR, Fig. S4b). SANS analysis reveals that the presence of Cu does not significantly influence the composition and shape of the co-assemblies (see the Table below and Fig. S4c). Co-assemblies with Cu are slightly longer which can be attributed to the fact that the basic character (and thus the hydrogen bond competition) of the PPh_2 group is withdrawn upon coordination. These analyses thus corroborate that the size of the catalytic helices can be roughly estimated by determining the length of the co-assemblies without copper (Figs. S5 to S7).

Comparison of the geometrical features of the co-assemblies with and without Cu as deduced from SANS analyses.[a],[b]

sample	[BTA^{PPh2}]	[BTA(*R*)-Cha]	[$Cu(OAc)_2 \cdot H_2O$]	r (Å)[b]	n	length(Å)/DP_w	f Cha in stacks[b]
SANS co-assemblies	3.98 g.L^{-1} 5.8 mM	4.39 g.L^{-1} 3.7 mM	-	**10.4**	**0.6**	**870/250**	**0.33**
SANS co-assemblies·Cu	3.99 g.L^{-1} 5.77 mM	4.37 g.L^{-1} 3.72 mM	0.58 g.L^{-1} 2.90 mM	**11.4**	**0.6**	**>1000/>280**	**0.34**

[a] For comparing the SANS spectra, see Figure 4c. For the fitting procedure, see captions of Figures S1 and S5. [b] The presence of copper does not modify significantly the structure of the co-assemblies in term of dimensionality and composition. Co-assemblies with Cu are slightly longer which can be attributed to the fact that the basic character of PPh_2 group is withdrawn upon coordination.

a)

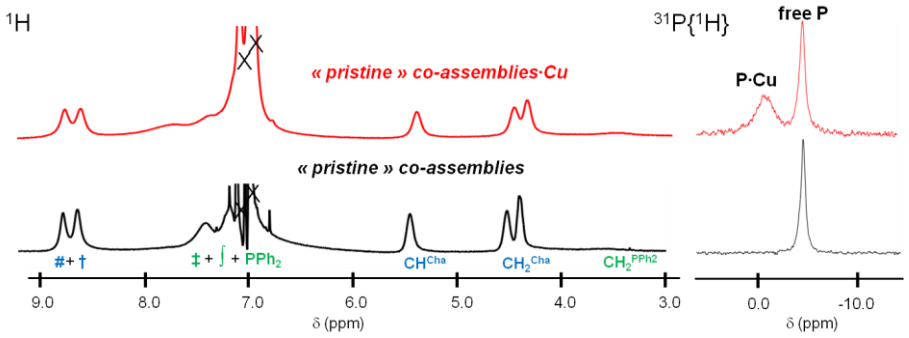

b)

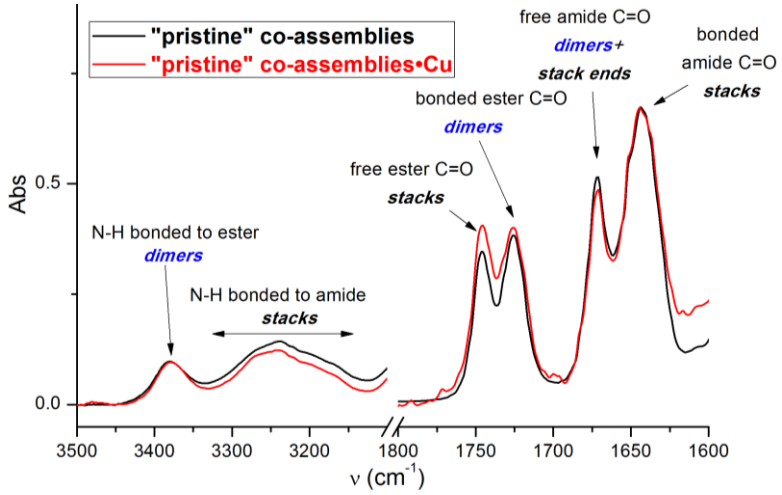

c)

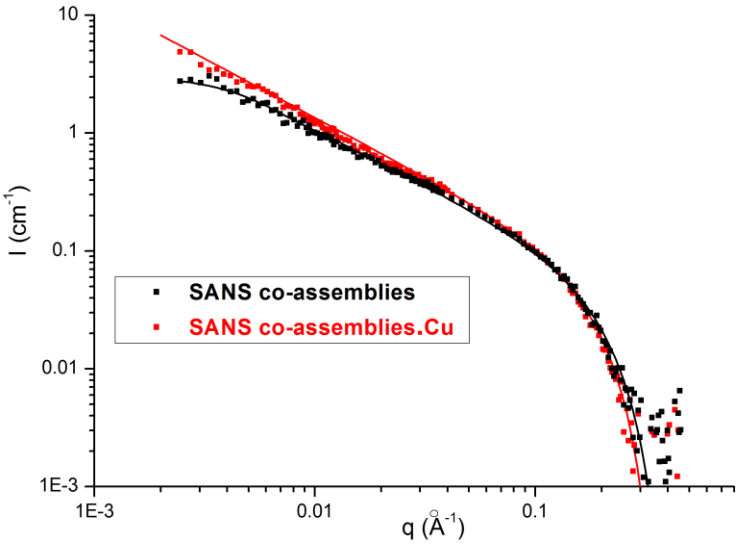

Figure S4 (a) Coordination of copper to the co-assemblies probed by ^{1}H and ^{31}P{^{1}H} NMR. Sample "pristine co-assemblies·Cu" analyzed at 293 K and comparison with sample "pristine co-assemblies" (C_7D_8). (b) FT-IR analysis of sample "pristine co-assemblies·Cu" and comparison with sample "pristine co-assemblies" (C_7D_8, 293 K). (c) SANS analysis of sample "SANS co-assemblies" and comparison with sample "SANS co-assemblies·Cu".

Characterization of the co-assemblies in presence of additives at concentrations *ca.* 4 times lower than those of catalytic experiments (Figs. S5-S6).

The influence of the salts on the nature of the co-assemblies is probed by SANS at concentrations *ca.* 4 times lower than those employed in catalysis in order to avoid interactions between objects (Fig. S5). In that specific conditions, the salts are poorly dissolved (no co-solvents). The co-assemblies are almost fully disassembled (in presence of TPPCl) and partly reassembled (in presence of TPPCl and $NaNTf_2$). The SANS samples are analyzed by FT-IR and the resulting spectra are deconvoluted (Fig. S6). It confirms that FT-IR analyses allow a valid estimation of the DP_n value of the BTA co-assemblies.

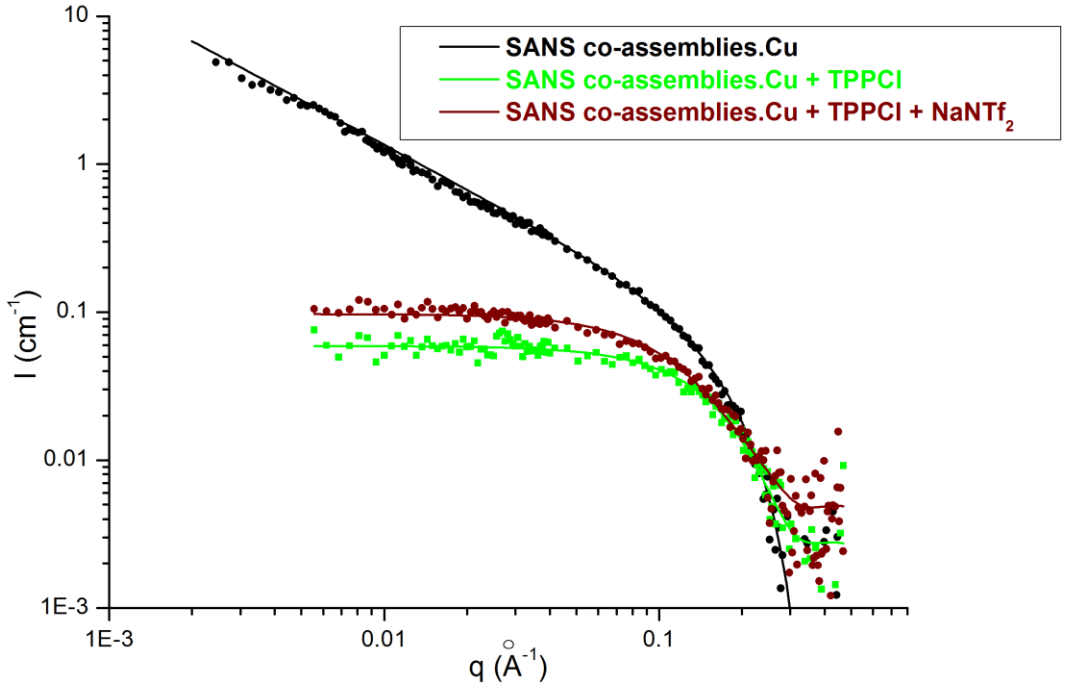

Figure S5 SANS analysis of the samples "SANS co-assemblies·Cu", "SANS co-assemblies·Cu + **TPPCl**" and "SANS co-assemblies·Cu + **TPPCl** + **$NaNTf_2$**" (293 K, C_7D_8).[a],[b],[c],[d]

[a] Composition:

sample	[BTA^{PPh2}]	[BTA(*R*)-Cha]	[$Cu(OAc)_2 \cdot H_2O$]	[TPPCl]	[$NaNTf_2$]	r (Å)[b]	length(Å)/ DP_w[b]	DP_n[d]
SANS co-assemblies·Cu	4.03 g.L^{-1} 5.81 mM	4.42 g.L^{-1} 3.76 mM	0.59 g.L^{-1} 2.94 mM	-	-	**11.4**	**>1000/>280**	
SANS co-assemblies·Cu + TPPCl	3.99 g.L^{-1} 5.77 mM	4.37 g.L^{-1} 3.72 mM	0.58 g.L^{-1} 2.90 mM	2.58 g.L^{-1} 6.88 mM	-	-	**25/7**	**5**
SANS co-assemblies·Cu + TPPCl + $NaNTf_2$	4.00 g.L^{-1} 5.77 mM	4.38 g.L^{-1} 3.72 mM	0.58 g.L^{-1} 2.92 mM	2.55 g.L^{-1} 6.81 mM	1.72 g.L^{-1} 5.66 mM	-	**41/11**	**8**
catalytic system (Table S3, run 3) toluene:DCM:acetone 15:1:1	13.8 mM	15.2 mM	6.9 mM	13.8 mM	13.8 mM			

[b] The curves are fitted according to a form factor for rigid rods of infinite length (sample without salt) or finite length (with salt) with a circular cross-section and a uniform scattering length density. The weight-average degrees of polymerization (DP_w) are calculated by dividing the obtained length by the distance between two BTAs in the stacks (≈ 3.5 Å). It gives a length of 25 Å (DP_w ≈7) and 41 Å (DP_w ≈11) for the sample with TPPCl and the sample with both TPPCl and $NaNTf_2$, respectively.

[c] Interpretation: The DP_w values are in qualitative agreement with a shortening and lengthening of the assemblies but do not reflect the true length of the BTA assemblies during the catalytic reaction given that the conditions for the SANS and catalytic experiments are very different. Also, the poor solubility of *$NaNTf_2$* in the conditions employed in the SANS analysis (pure C_7D_8) may explain the limited size of the objects formed upon reassembly. The DP_w value of the BTA co-assemblies determined by SANS analyses correlates well with those obtained by deconvolution of the FT-IR spectra (Fig. S6).

[d] Determined by deconvolution of the corresponding FT-IR spectra (Fig. S6).

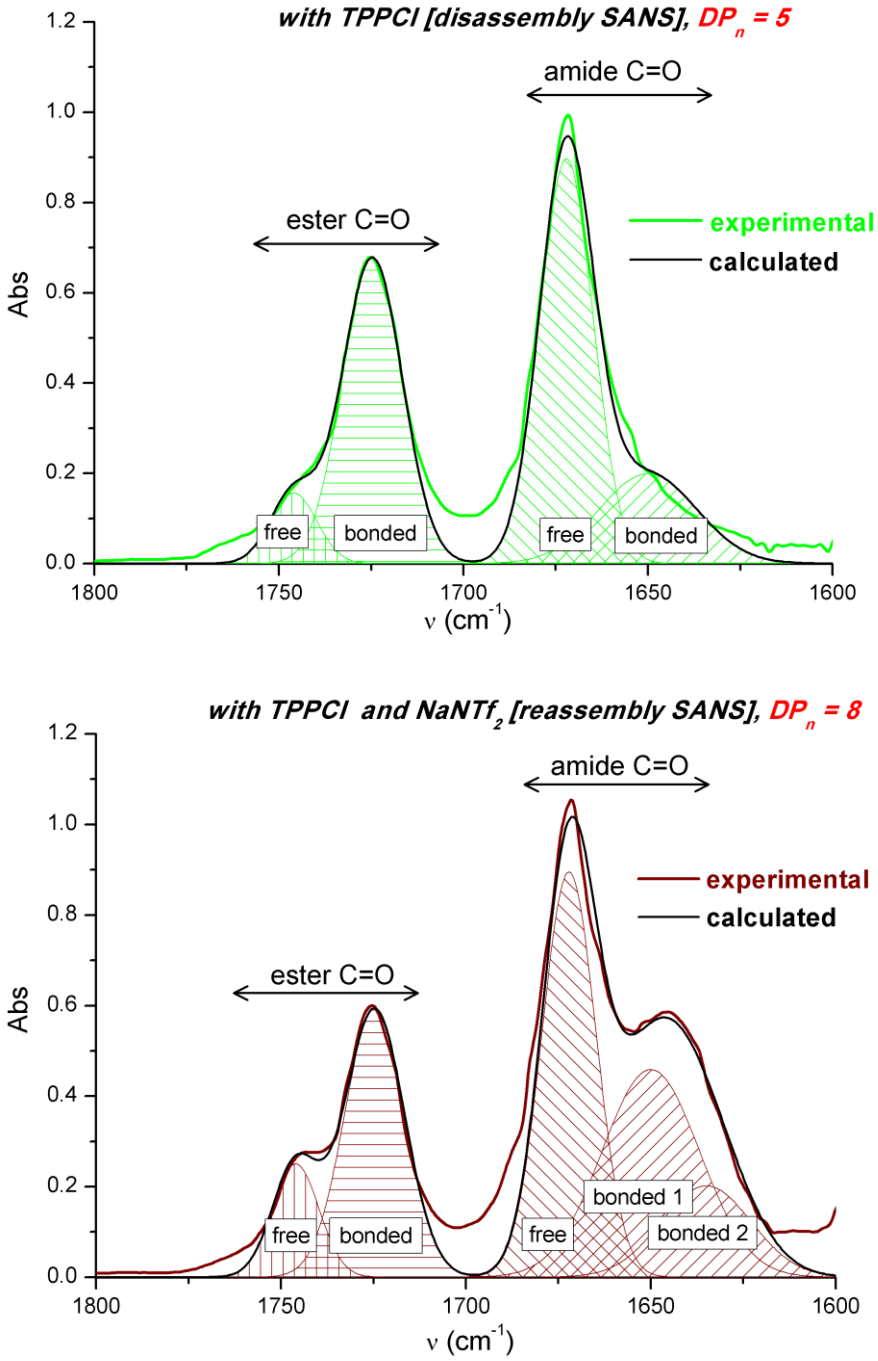

Figure S6 Deconvoluted FT-IR spectra of the solutions analyzed by SANS (Fig. S4). See the precise composition and conditions of the preparation of the samples in Fig. S4.[a],[b]

[a] *Values obtained after deconvolution*: bonded amide peak 1 (ν =1650 cm^{-1}, width=13 cm^{-1}), bonded amide peak 2 (ν = 1635 cm^{-1}, width=12 cm^{-1}, ν =35090 L.mol^{-1}.cm^{-1}), free amide (ν =1672 cm^{-1}, width=7 cm^{-1}, ν =40380 L.mol^{-1}.cm^{-1}), bonded ester (ν =1725 cm^{-1}, width=8 cm^{-1}, ν =38560 L.mol^{-1}.cm^{-1}) and free ester (ν =1746 cm^{-1}, width=6 cm^{-1}). The obtained DP_n values are indicated in red next to the title. [b] The fact that the values obtained from processing of the FT-IR spectra are close to that determined by SANS (Fig. S4) confirm that our deconvolution procedure provides a valid estimation of the DP_n values.

Characterization of the co-assemblies in presence of additives at concentrations close to those of catalytic experiments (Figs. 2, S7-S8).

The influence of the salts on the nature of the co-assemblies is probed by FT-IR (Figs. 2a and S7) and NMR (Fig. S8) at concentrations close to those employed in catalysis. FT-IR analyses indicate that the co-assemblies are disassembled in presence of TPPCl and partly re-assembled in presence of both TPPCl and $NaNTf_2$ (see the changes in the intensities of free amide and bonded amide bands, Fig. 2a). NMR analyses are in agreement with these observations (Fig. S8). Deconvolution of the FT-IR spectra allow the determination of the fraction of **BTA (*R*)-Cha** in stacks and an estimation of the DP_n values, the latter being in agreement with full disassembly and incomplete reassembly processes (Fig. S7). The incomplete reassembly process is due to presence of acetone-d_6 and CD_2Cl_2 as confirmed by similar FT-IR and ^1H NMR spectra and estimated DP_n values for the samples in presence and absence of TPPCl and $NaNTf_2$ analyzed in the same solvent mixture (C_7D_8:CD_2Cl_2:acetone-d_6 15:1).

Composition**: "pristine co-assemblies" ("run 1")**: [**BTA^{PPh2}**] = 16.7 mM, [**BTA (*R*)-Cha] =** 18.4 mM, C_7D_8; "**co-assemblies + TPPCl" ("run 2")**: [**BTA^{PPh2}**] = 15.7 mM, **[BTA (*R*)-Cha] =** 17.3 mM, [**TPPCl**] = 15.7 mM, C_7D_8:CD_2Cl_2 15:1; "**co-assemblies + TPPCl + $NaNTf_2$" ("run 3")**: [**BTA^{PPh2}**] = 14.7 mM, [**BTA (*R*)-Cha] =** 16.2 mM, [**TPPCl**] = 14.7 mM, [**$NaNTf_2$**] = 14.7 mM, C_7D_8:CD_2Cl_2:acetone-d_6 15:1:1; **"co-assemblies + DCM + acetone" ("run 3 without salts")**: [**BTA^{PPh2}**] = 14.7 mM, [**BTA (*R*)-Cha] =** 16.2 mM, C_7D_8:CD_2Cl_2:acetone-d_6 15:1:1.

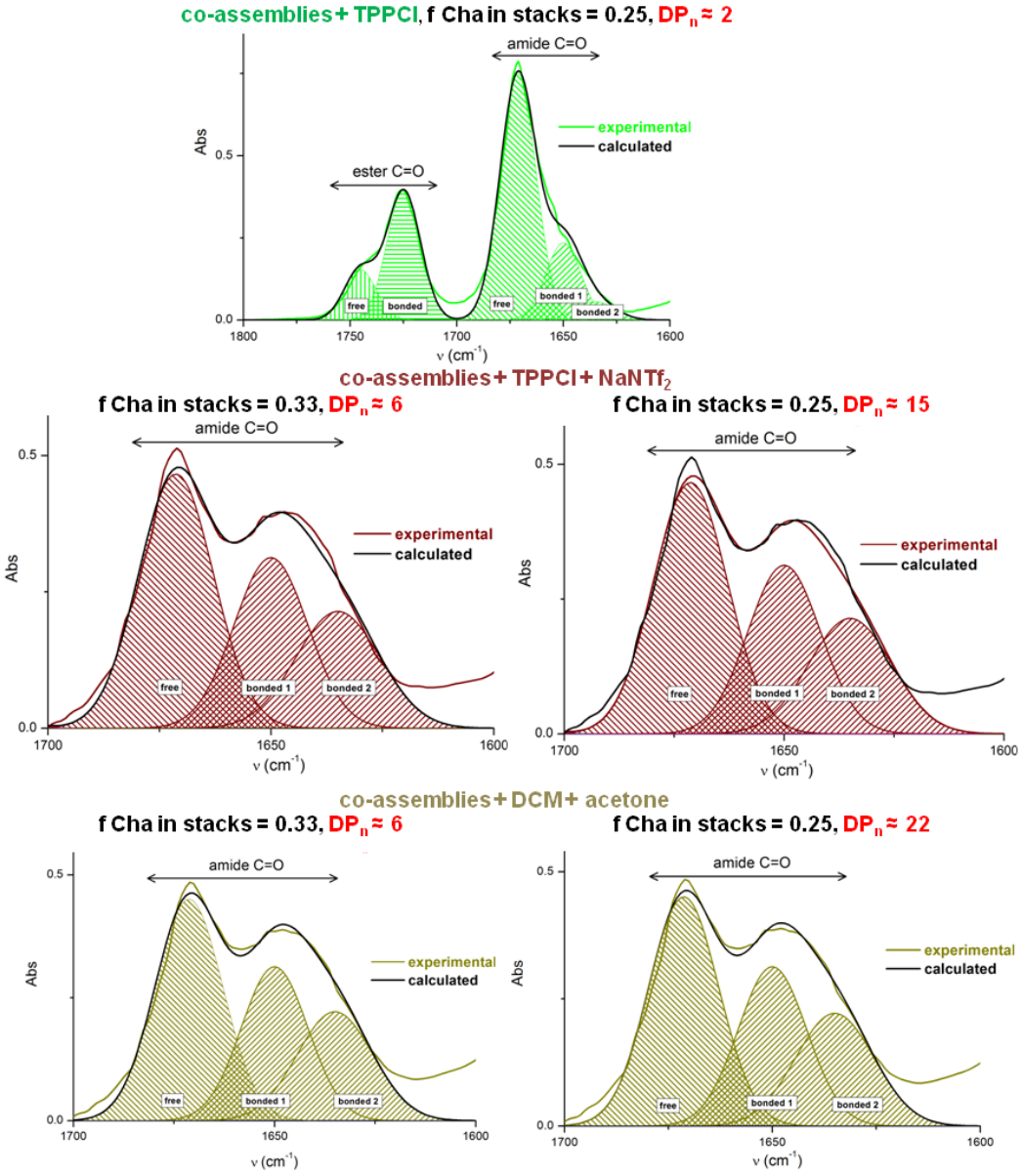

Figure S7 Deconvoluted FT-IR spectrum of the samples "**co-assemblies + TPPCl**", "**co-assemblies + TPPCl + $NaNTf_2$**" and "**co-assemblies + DCM + acetone**" (293 K).[a],[b]

[a] For samples "**co-assemblies + TPPCl + $NaNTf_2$**" and "**co-assemblies + DCM + acetone**", the presence of acetone prevents the deconvolution of the ester C=O bands A range of DP_n values was determined by assuming two extreme values of f Cha in stacks: 0.25, *i.e.* the value obtained upon full disassembly, and 0.33, *i.e.* the value in the pristine co-assemblies. [b] *Values obtained after deconvolution*: bonded amide peak 1 (ν=1650 cm^{-1}, width=8 cm^{-1}), bonded amide peak 2 (ν= 1635 cm^{-1}, width=10 cm^{-1}, ν=31750 $L.mol^{-1}.cm^{-1}$), free amide (ν=1671 cm^{-1}, width=8 cm^{-1}, ν=34180 $L.mol^{-1}.cm^{-1}$), bonded ester (ν=1725 cm^{-1}, width=8 cm^{-1}, ν=28950 $L.mol^{-1}.cm^{-1}$) and free ester (ν=1745 cm^{-1}, width=7 cm^{-1}). These values are in agreement with those obtained by deconvoluting the FT-IR corresponding to the samples analyzed by SANS (Fig. S5).

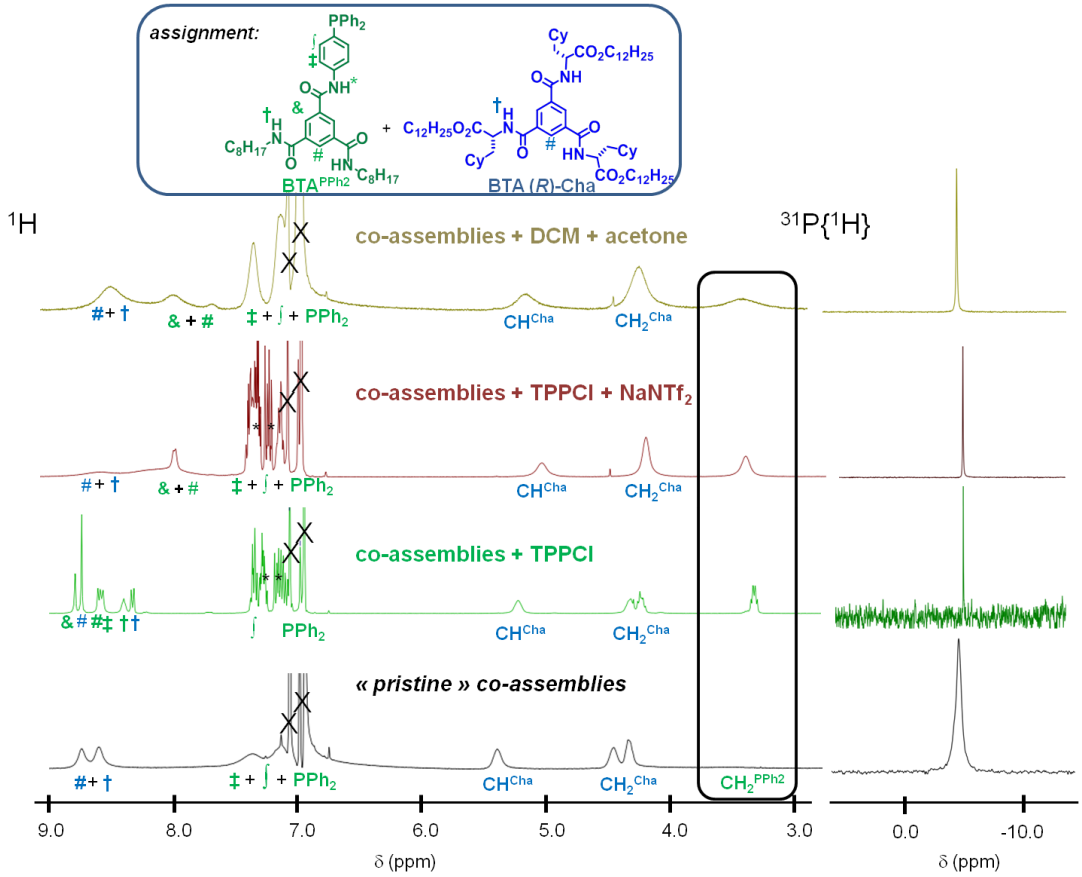

Figure S8 ^{1}H and $^{31}P\{^{1}H\}$ NMR analyses of the samples "**pristine co-assemblies**", "**co-assemblies + TPPCl**", "**co-assemblies + TPPCl + $NaNTf_2$**", and **"co-assemblies + DCM + acetone**" (293 K).[a] x = residual protons of C_7D_8, * = proton signals of **TPPCl**. For the sample "**co-assemblies + TPPCl**" the proton signal labelled as * is downfield shifted to ≈ 11 ppm. The ^{31}P signal of TPPCl (δ ≈ 23 ppm) is not shown.

[a] Interpretation: ^{1}H NMR analyses of the samples "**co-assemblies + TPPCl**", "**co-assemblies + TPPCl + $NaNTf_2$**" and "**co-assemblies + DCM + acetone**" can be interpreted in the same way as that of sample "**pristine co-assemblies**" (see caption [a] in Fig. S3) with the exception that additional signals corresponding to **BTA^{PPh2}** can be detected as a result of the decreased length of the co-assemblies in these samples. In fact, the width of proton signal CH_2^{PPh2} (surrounded in black) and of the phosphorus signal of the PPh_2 group reflects the degree of polymerization which increases in the following order: "**co-assemblies + TPPCl**" < "**co-assemblies + TPPCl + $NaNTf_2$**" ≈ "**co-assemblies + DCM + acetone**" < "**pristine co-assemblies**".

Summary of the structural data and correlation between length and selectivity (Table S2).

Table S2 Structural data and relation between the selectivity and the length for the different samples investigated in this study.

sample	"run"	DP_n[a]	f Cha in stacks[FT-IR[a]]	*e.e.* (%)
"pristine" co-assemblies	run 1	≈ 250[b]	0.33	51
co-assemblies + TPPCl	run 2	≈ 2	0.25	0-6
co-assemblies + TPPCl + $NaNTf_2$	run 3	6-15	0.25-0.33	43
co-assemblies + DCM + acetone	run3 without salts	6-22	0.25-0.33	37

[a] DP_n and f Cha in stacks values were determined by FT-IR analyses unless otherwise stated.

[b] Deduced form SANS analysis (Fig. S1).

Reversible switch of the selectivity (Table S3).

Table S3 Copper-catalysed hydrosilylation of 1-(4-nitrophenyl)ethanone with successive additions of substrate, salt (TPPCl or $NaNTf_2$) and $PhSiH_3$.[a]

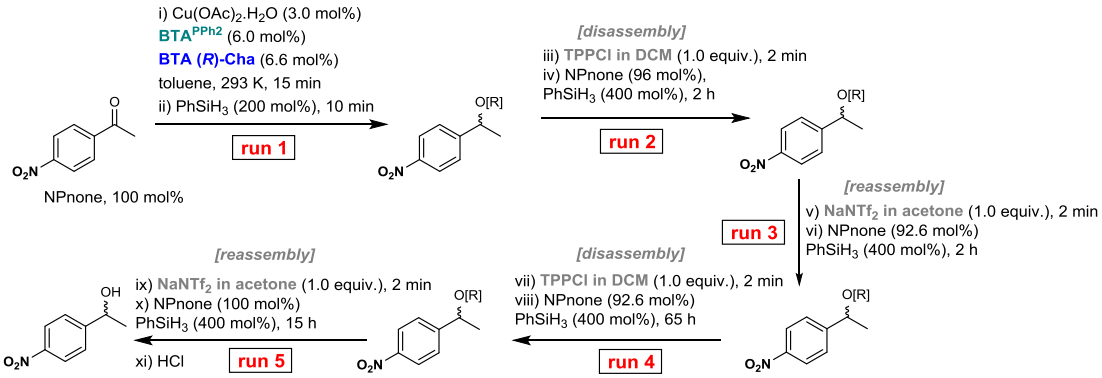

run	substrate (subs^0 n)	cumulated substrate (subs n)[b]	cumulated conversion (cconv n) ±0.5%	cumulated enantioselectivity (c *e.e.* n) ±0.5%	conversion for the run (conv n) ±0.5% [c]	enantioselectivity for the run (*e.e.* n)[d]
1	100	100	99	52	99	52±0.5%
2	96	97	93	31	86	6±1.0%
3	92.6	106.3	96	35	89	43±1.5%
4	92.6	104.1	87	29	53	0±5%
5	100	149.6	95	29	84	29±5%

[a] Reaction conditions: 1-(4-nitrophenyl)ethanone (subs^0 1=100 mol%^{run1}, subs^0 2 = 96 mol%^{run2}, subs^0 3 = 92.6 mol%^{run3}, subs^0 4 = 92.6 mol%^{run4}, subs^0 5 = 100 mol%^{run5}= 481.2 mol% in total), $Cu(OAc)_2{\cdot}H_2O$ (3.0 mol%), **BTA^{PPh2}** (6.0 mol%), **BTA (*R*)-Cha** (6.6 mol%), $PhSiH_3$ (100 mol% for run 1 and then 400 mol% for run 2, run 3, run 4 and run 5 = 1700 mol% in total), TPPCl in 40 µL of DCM (1.0 equiv. relatively to **BTA^{PPh2}** for run 2 and 4), $NaNTf_2$ in acetone (1.0 equiv. relatively to **BTA^{PPh2}** for run 3 and 5), toluene (600 µL), 293 K. Conversion (cconv n) and *e.e.* (c *e.e.* n) for each run were determined by GC analyses of the aliquots (see pages S-20 to S-22). The conversion and enantioselectivity for each run have been calculated as indicated below. [b] subs n = $subs0\ n + [(1 - cconv\ (n-1)) \times \sum_{i=1}^{n-1} subs0\ i]$. The amount of substrate is normalized to 100 for 27 mg of 1-(4-nitrophenyl)ethanone (100 mol%).

[c] $$conv\ n = \frac{cconv\ n \times \sum_{i=1}^{n} subs0\ i - \sum_{i=1}^{n-1} conv\ i \times subs\ i}{subs\ n}$$

[d] $$e.e.\ n = \frac{(c\ e.e.\ n \times \sum_{i=1}^{n}(subs\ i \times conv\ i)) - \sum_{i=1}^{n-1}(e.e.\ i \times subs\ i \times conv\ i)}{conv\ n \times subs\ n}$$

Catalytic experiments.

In all catalytic experiments a *pre-catalytic mixture* composed of the ligand, the enantiopure co-monomer, the copper salt and the substrate was prepared as follows: a tube was loaded with $Cu(OAc)_2 \cdot H_2O$ (1.0 mg, 3.0 mol%) and **BTA^{PPh2}** (6.9 mg, 6.0 mol%) in dry THF (500 µL) and the mixture was stirred for 30 minutes. The solvent was removed under vacuum and the tube was further put under vacuum (1.10^{-3} mbar) for 1 hour. Then 1-(4-nitrophenyl)ethanone (28.0 mg, 0.17 mmol, 100 mol%) was added before flushing the tube with argon for 10 seconds. **BTA (*R*)-Cha** (12.9 mg, 6.6 mol%) in 100 µL of dry toluene was added to the tube as well as 500µL dry toluene. The mixture was stirred for 15 min at room temperature.

Influence of the amount of **TPPCl** on the hydrosilylation of 1-(4-nitrophenyl)ethanone (Fig. 1, Table S1): TPPCl (0.3-1.0 equiv. relatively to **BTA^{PPh2}**) was dissolved in dichloromethane (40 µL), added to the pre-catalytic mixture and the mixture was stirred for 20 seconds. Then, $PhSiH_3$ (42.0 µL, 0.34 mmol, 200 mol%) was added and the reaction mixture was stirred for 12 hours before being hydrolyzed with aqueous HCl and analyzed by chiral GC.

Hydrosilylation of 1-(4-nitrophenyl)ethanone with sequential additions of salt, substrate and $PhSiH_3$ (Fig. 3, Table S3): A tube was loaded with $Cu(OAc)_2 \cdot H_2O$ (1.0 mg, 3.0 mol%) and **BTA^{PPh2}** (6.9 mg, 6.0 mol%) in dry THF (500 µL) and the mixture was stirred for 30 minutes. The solvent was removed under vacuum and the tube was further put under vacuum ($1x10^{-3}$ mbar) for 1 hour. Then 1-(4-nitrophenyl)ethanone (27.0 mg, 0.16 mmol, 100 mol%) was added before flushing the tube with argon for 10 seconds. **BTA (*R*)-Cha** (12.9 mg, 6.6 mol%) in 100 µL of dry toluene was added to the tube as well as 500 µL dry toluene. The mixture was stirred for 15 min at room temperature. $PhSiH_3$ (42.0 µL, 0.34 mmol, 200 mol%) was added and the mixture was stirred for 10 minutes. An aliquot (40 µL) was taken up, hydrolyzed with aqueous HCl and analyzed by chiral GC (*run 1*). TPPCl (3.7 mg, 1.0 equiv. relatively to **BTA^{PPh2}**) in dichloromethane (40 µL) was added and the solution was stirred for 2 minutes before addition of 1-(4-nitrophenyl)ethanone (26.4 mg, 0.16 mmol, 96 mol%) and $PhSiH_3$ (84.0 µL, 0.68 mmol, 400 mol%). The mixture was stirred for 2 h and an aliquot of 40 µL was taken up, hydrolyzed with aqueous HCl and analyzed by chiral GC (*run 2*). $NaNTf_2$ (3.0 mg, 1.0 equiv. relatively to **BTA^{PPh2}**) in acetone (40 µL) was added and the mixture was stirred for 2 minutes before addition of 1-(4-nitrophenyl)ethanone (25.0 mg, 0.15 mmol, 92.6 mol%) and $PhSiH_3$ (84.0 µL, 0.68 mmol, 400 mol%). The mixture was stirred for 2 hours and an aliquot of 40 µL was taken up, hydrolyzed with aqueous HCl and analyzed by chiral GC (*run 3*). TPPCl (3.7 mg, 1.0 equiv. relatively to **BTA^{PPh2}**) in

dichloromethane (40 µL) was added and the solution was stirred for 2 minutes before addition of 1-(4-nitrophenyl)ethanone (25.0 mg, 0.15 mmol, 92.6 mol%) and $PhSiH_3$ (84.0 µL, 0.68 mmol, 400 mol%). The mixture was stirred for 65 hours and an aliquot of 40 µL was taken up, hydrolyzed with aqueous HCl and analyzed by chiral GC (*run 4*). $NaNTf_2$ (3.0 mg, 1.0 equiv. relatively to **BTA^{PPh2}**) in acetone (40 µL) was added and the mixture was stirred for 2 minutes before addition of 1-(4-nitrophenyl)ethanone (27.0 mg, 0.16 mmol, 100 mol%) and $PhSiH_3$ (84.0 µL, 0.68 mmol, 400 mol%). The mixture was stirred for 15 hours, hydrolyzed with aqueous HCl and analyzed by chiral GC (*run 5*).

GC analyses from the aliquots of the different run.

Table S3, run 1:

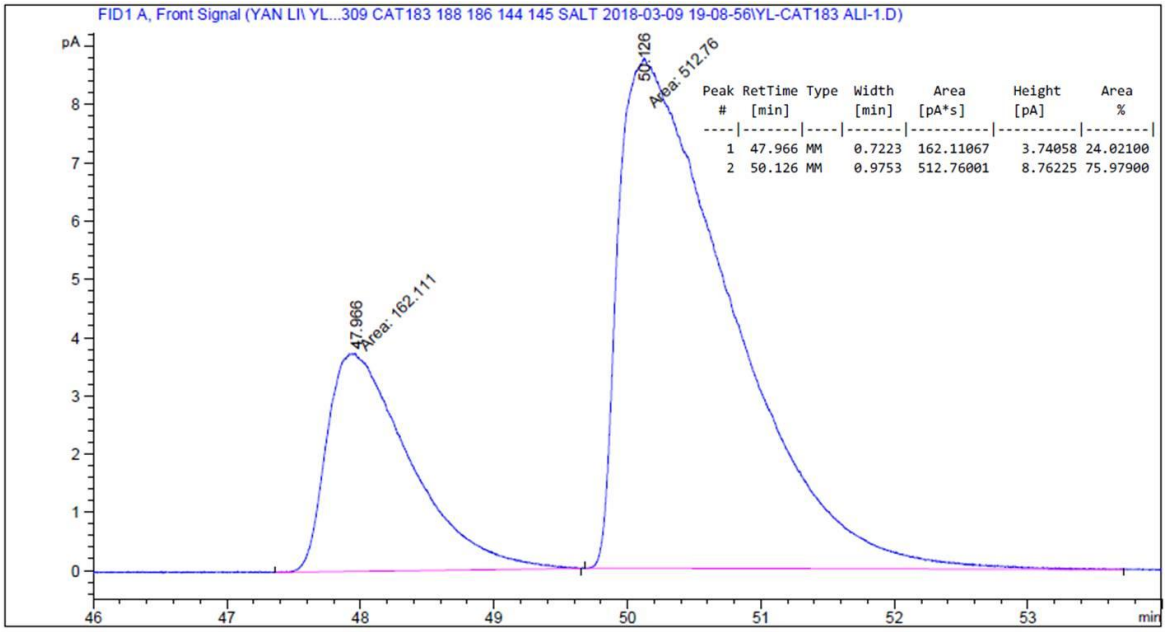

Table S3, run 2:

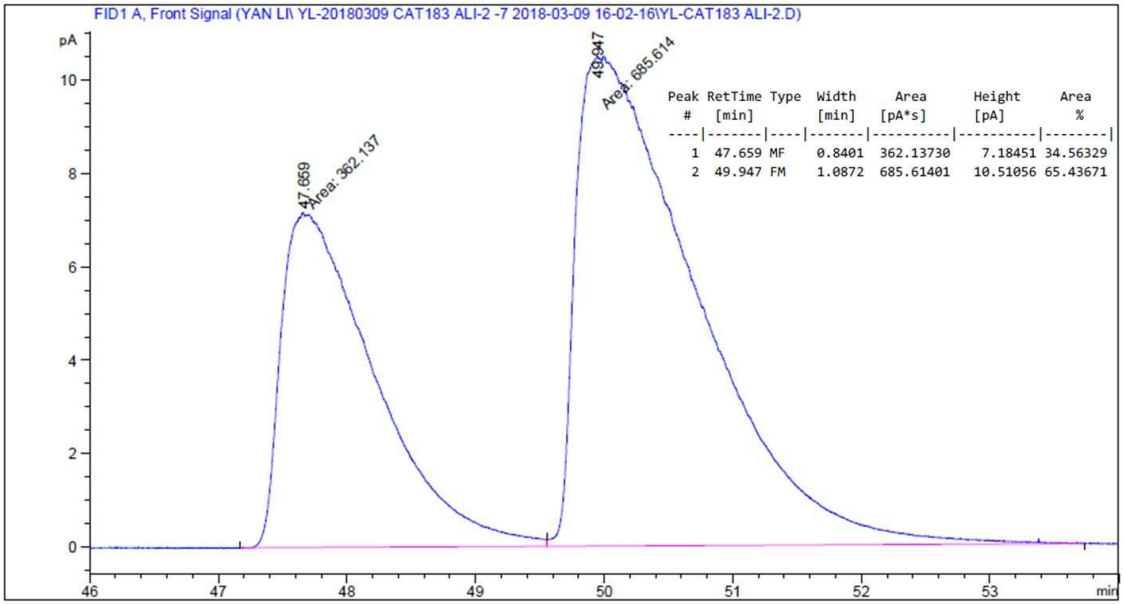

Table S3, run 3:

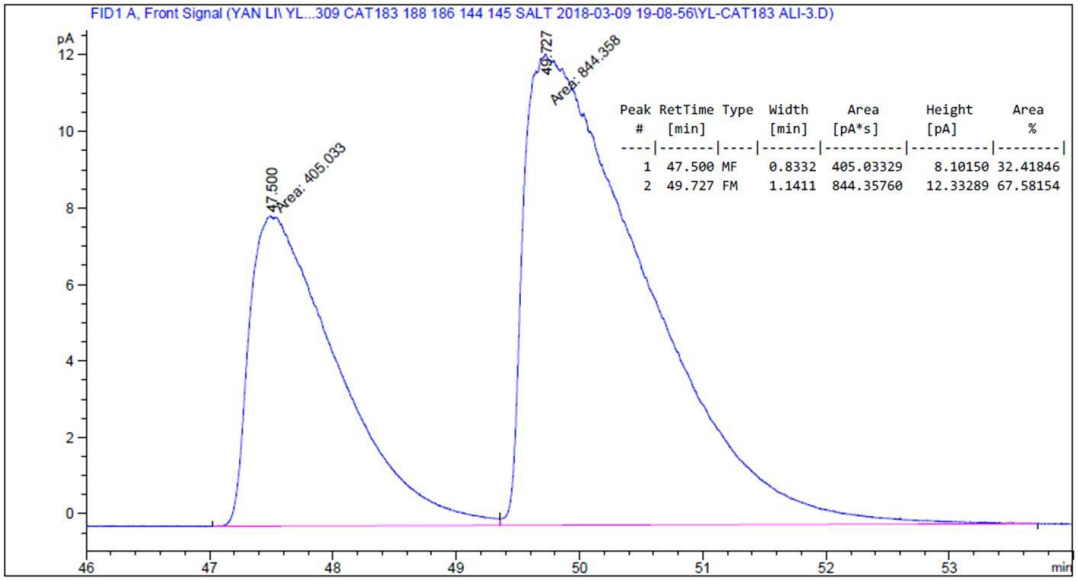

Table S3, run 4:

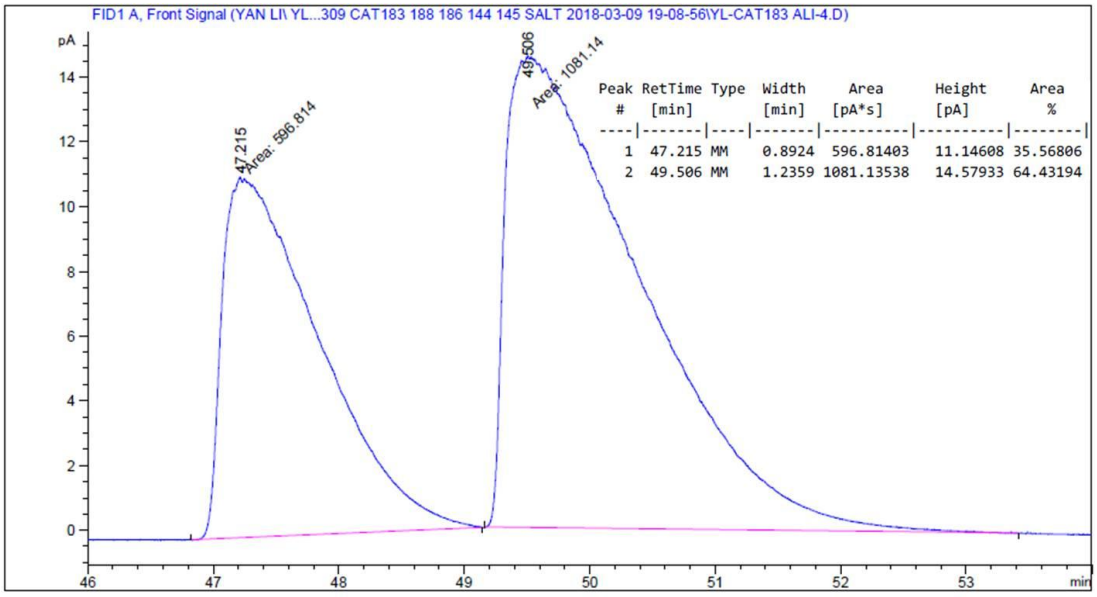

Table S3, run 5:

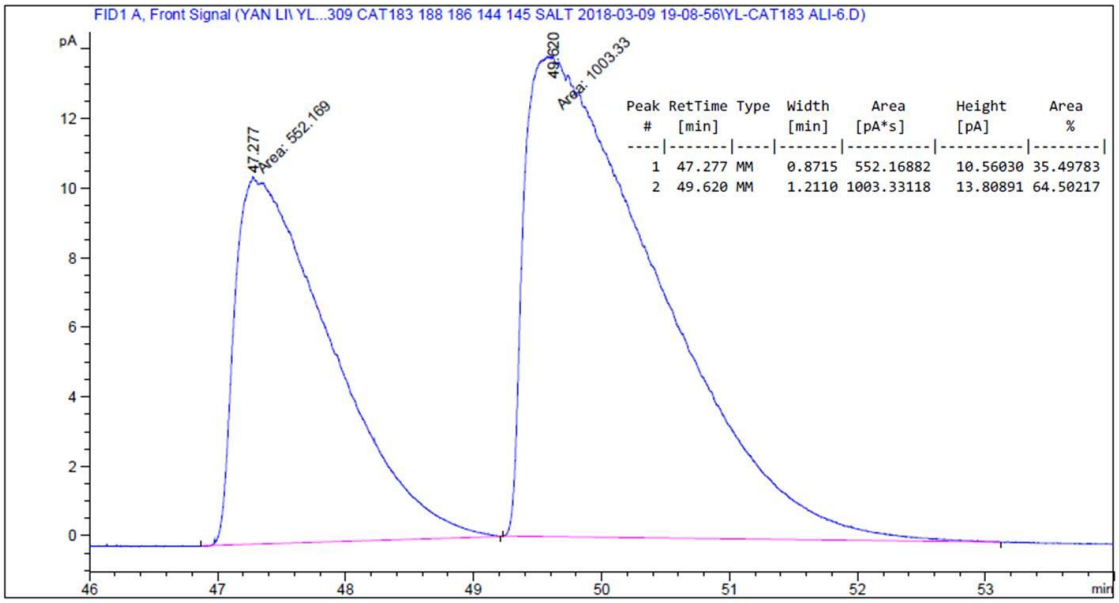

V -Additional material – not included in the publication

We have also probed the influence of various salts of the self-assemblies formed by a BTA of reference, *N*,*N*',*N*''-trioctylbenzene-1,3,5-tricarboxamide (**BTA C8**, Fig. A1). We first probe the hydrogen bond acceptor capability of various anions (Fig. A1). 20.0 mM toluene solutions of **BTA C8** are highly viscous ($\eta_{rel} \approx 11$). The viscosity is strongly reduced in presence of 0.10 equivalent (equiv.) of TPPCl ($\eta_{rel}=2.4$, TPP=tetraphenylphosphonium). $NaNTf_2$ (Tf=trifluoromethanesulfonimide) was selected to trigger the metathesis reaction because of the weak coordination ability and the known chemical stability of the NTf_2 anion. Satisfactorily, addition of 0.10 equiv. of $NaNTf_2$ to a solution of **BTA C8** containing 0.10 equiv. of TPPCl leads to a significant increase of viscosity ($\eta_{rel}=4.7$). The viscosity of **BTA C8** solutions can in fact be modulated by means of sequential additions of TPPCl and $NaNTf_2$ (Fig. A2). Fourier-Transform Infrared (FT-IR) spectroscopy analyses allow determining how the BTA assemblies are affected by these salts at the molecular level. Under the conditions of the viscosity experiments mentioned above (toluene, 20.0 mM), **BTA C8** forms very long helices (Fig. A3, no detected free N-H and C=O bands). However, upon addition of TPPCl (0.10 equiv.), free N-H and C=O functions appear as indicated by absorption bands above 3400 cm^{-1} and 1650 cm^{-1}, respectively. The N-H band is also wider, its intensity is lower and its maximum is slighted shifted to higher wavenumber ($\Delta\nu=+1.5$ cm^{-1}, dark yellow arrow in Fig. A3). This a consequence of the presence of N-H functions bonded to chloride anions. The FT-IR spectrum obtained after adding $NaNTf_2$ to the previous mixture resembles that of pristine **BTA C8** solution even though a residual fraction of free N-H and C=O bands can still be detected. Notably, the maximum of the N-H band has shifted in the opposite direction ($\Delta\nu=-1.0$ cm^{-1}, blue arrow) demonstrating that the number of N-H functions bonded to chloride has drastically decreased. Viscosity measurements and FT-IR analyses clearly show that the length of the BTA assemblies can be modulated by successive additions of TPPCl and $NaNTf_2$ similarly to what was demonstrated above for the precatalytic mixture composed of **BTA^{PPh2}** and **BTA (*R*)-Cha**.

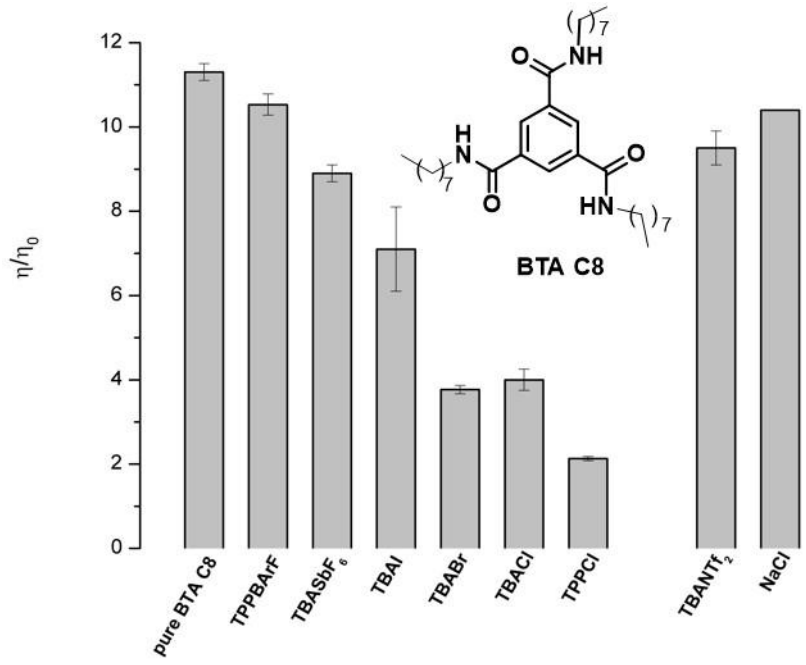

Figure A1 Salt influence on the relative viscosity of **BTA C8** solution (toluene, 20.0 mM, 20°C). Relative viscosity in presence of 0.10 equiv. of salt. (Left) The salts are sorted according to the hydrogen bond accepting capability of the anion.[a] (Right) $TBANTf_2$ and NaCl (insoluble) have been used to probe the competing nature of the salts generated during the metathesis reaction.[b]

[a] The measurements were performed in triplicate. An error bar equals to ± ½ variance was set for the relative viscosity. The higher error bar in the case of TBAI is related to the incomplete dissolution of the salt. BArF= tetrakis[(3,5-trifluoromethyl)phenyl]borate, TPP= tetraphenylphosphonium, TBA= tetrabutylammonium, Tf = trifluoromethanesulfonimide.

[b] $TBANTf_2$ has been used instead of $TPPNTf_2$, but $TPPNTf_2$ is expected to be even less competitor than $TBANTf_2$.

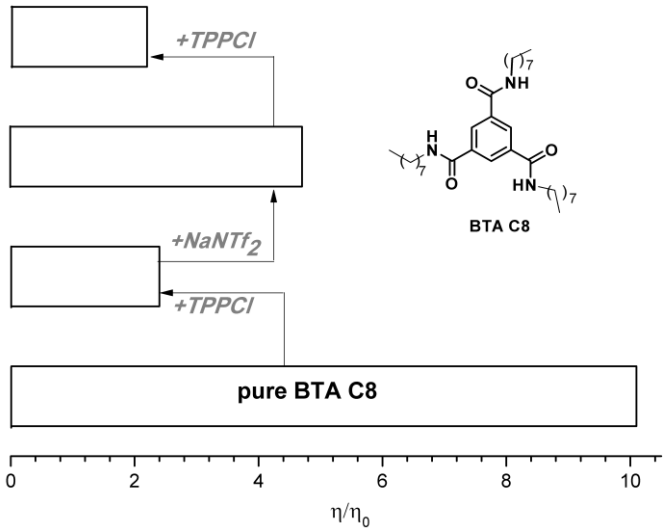

Fig. A2 Relative viscosity of **BTA C8** solution (toluene, 20.0 mM, 20°C) after sequentialadditions of TPPCl (0.10 equiv.), $NaNTf_2$ (0.10 equiv.) and TPPCl (0.10 equiv.).

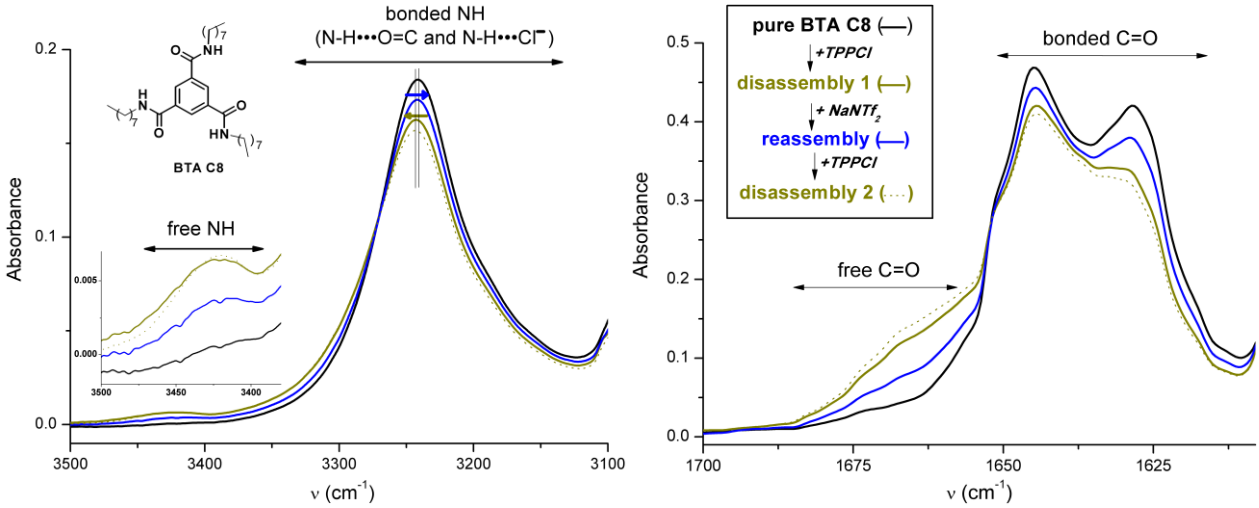

Fig. A3 FT-IR analyses of **BTA C8** solution in toluene (20.0 mM, 20°C) after sequential additions of TPPCl (0.1 equiv.), $NaNTf_2$ (0.1 equiv.) and TPPCl (0.1 equiv.). Zoom on the N-H (Left) and C=O (Right) regions.

VI References

Notes: ‡ To avoid any confusion with the catalytic loading (expressed in mol% of substrate), the amount of TPPCl is expressed in number of equivalent relatively to **BTA^{PPh2}**.

§ $TPPNTf_2$ and NaCl, the salts generated upon the metathesis reaction, are poor hydrogen competitors and poorly soluble, respectively (Table S1).

1. Kumagai, N.; Shibasaki, M., Catalytic chemical transformations with conformationally dynamic catalytic systems. *Catal. Sci. Technol.* **2013,** *3* (1), 41-57.

2. Blanco, V.; Leigh, D. A.; Marcos, V., Artificial switchable catalysts. *Chem. Soc. Rev.* **2015,** *44* (15), 5341-5370.

3. Vlatković, M.; Collins, B. S. L.; Feringa, B. L., Dynamic Responsive Systems for Catalytic Function. *Chem. Eur. J.* **2016,** *22*, 17080-17111.

4. Choudhury, J., Recent developments on artificial switchable catalysis. *Tetrahedron Lett.* **2018,** *59* (6), 487-495.

5. Leibfarth, F. A.; Mattson, K. M.; Fors, B. P.; Collins, H. A.; Hawker, C. J., External Regulation of Controlled Polymerizations. *Angew. Chem. Int. Ed.* **2013,** *52* (1), 199-210.

6. Teator, A. J.; Lastovickova, D. N.; Bielawski, C. W., Switchable Polymerization Catalysts. *Chem. Rev.* **2016,** *116* (4), 1969-1992.

7. Chen, M.; Zhong, M. J.; Johnson, J. A., Light-Controlled Radical Polymerization: Mechanisms, Methods, and Applications. *Chem. Rev.* **2016,** *116* (17), 10167-10211.

8. Eichstaedt, K.; Jaramillo-Garcia, J.; Leigh, D. A.; Marcos, V.; Pisano, S.; Singleton, T. A., Switching between Anion-Binding Catalysis and Aminocatalysis with a Rotaxane Dual-Function Catalyst. *J. Am. Chem. Soc.* **2017,** *139* (27), 9376-9381.

9. Semwal, S.; Choudhury, J., Switch in Catalyst State: Single Bifunctional Bi-state Catalyst for Two Different Reactions. *Angew. Chem. Int. Ed.* **2017,** *56* (20), 5556-5560.

10. Romanazzi, G.; Degennaro, L.; Mastrorilli, P.; Luisi, R., Chiral Switchable Catalysts for Dynamic Control of Enantioselectivity. *ACS Catal.* **2017,** *7*, 4100-4114.

11. Wang, J. B.; Feringa, B. L., Dynamic Control of Chiral Space in a Catalytic Asymmetric Reaction Using a Molecular Motor. *Science* **2011,** *331* (6023), 1429-1432.

12. Vlatković, M.; Bernardi, L.; Otten, E.; Feringa, B. L., Dual stereocontrol over the Henry reaction using a light- and heat-triggered organocatalyst. *Chem. Commun.* **2014,** *50* (58), 7773-7775.

13. Zhao, D. P.; Neubauer, T. M.; Feringa, B. L., Dynamic control of chirality in phosphine ligands for enantioselective catalysis. *Nat. Commun.* **2015,** *6*, 6652.

14. Vlatkovic, M.; Volaric, J.; Collins, B. S. L.; Bernardi, L.; Feringa, B. L., Dynamic control over catalytic function using responsive bisthiourea catalysts. *Org. Biomol. Chem.* **2017,** *15* (39), 8285-8294.

15. Chen, C. T.; Tsai, C. C.; Tsou, P. K.; Huang, G. T.; Yu, C. H., Enantiodivergent Steglich rearrangement of O-carboxylazlactones catalyzed by a chirality switchable helicene containing a 4-aminopyridine unit. *Chem. Sci.* **2017,** *8* (1), 524-529.

16. Storch, G.; Trapp, O., Temperature-Controlled Bidirectional Enantioselectivity in a Dynamic Catalyst for Asymmetric Hydrogenation. *Angew. Chem. Int. Ed.* **2015,** *54* (12), 3580-3586.

17. Mortezaei, S.; Catarineu, N. R.; Canary, J. W., A Redox-Reconfigurable, Ambidextrous Asymmetric Catalyst. *J. Am. Chem. Soc.* **2012,** *134* (19), 8054-8057.

18. Mortezaei, S.; Catarineu, N. R.; Duan, X. Y.; Hu, C. H.; Canary, J. W., Redox-configurable ambidextrous catalysis: structural and mechanistic insight. *Chem. Sci.* **2015,** *6* (10), 5904-5912.

19. Mortezaei, S.; Catarineu, N. R.; Canary, J. W., Dial-in selection of any of four stereochemical outcomes among two substrates by in situ stereo-reconfiguration of a single ambidextrous catalyst. *Tetrahedron Lett.* **2016,** *57* (4), 459-462.

20. Le Bailly, B. A. F.; Byrne, L.; Clayden, J., Refoldable Foldamers: Global Conformational Switching by Deletion or Insertion of a Single Hydrogen Bond. *Angew. Chem. Int. Ed.* **2016,** *55* (6), 2132-2136.

21. Yamamoto, T.; Yamada, T.; Nagata, Y.; Suginome, M., High-Molecular-Weight Polyquinoxaline-Based Helically Chiral Phosphine (PQXphos) as Chirality-Switchable, Reusable, and Highly Enantioselective Monodentate Ligand in Catalytic Asymmetric Hydrosilylation of Styrenes. *J. Am. Chem. Soc.* **2010,** *132* (23), 7899-7901.

22. Nagata, Y.; Nishikawa, T.; Suginome, M., Poly(quinoxaline-2,3-diyl)s Bearing (S)-3-Octyloxymethyl Side Chains as an Efficient Amplifier of Alkane Solvent Effect Leading to Switch of Main-Chain Helical Chirality. *J. Am. Chem. Soc.* **2014,** *136* (45), 15901-15904.

23. Nagata, Y.; Kuroda, T.; Takagi, K.; Suginome, M., Ether solvent-induced chirality inversion of helical poly(quinoxaline-2,3-diyl)s containing L-lactic acid derived side chains. *Chem. Sci.* **2014,** *5* (12), 4953-4956.

24. Akai, Y.; Konnert, L.; Yamamoto, T.; Suginome, M., Asymmetric Suzuki-Miyaura cross-coupling of 1-bromo-2-naphthoates using the helically chiral polymer ligand PQXphos. *Chem. Commun.* **2015,** *51* (33), 7211-7214.

25. Nagata, Y.; Takeda, R.; Suginome, M., Pressure-dependent helix inversion of poly(quinoxaline-2,3-diyl)s containing chiral side chains in non-aqueous solvents. *Chem. Commun.* **2015,** *51* (56), 11182-11185.

26. Ke, Y.-Z.; Nagata, Y.; Yamada, T.; Suginome, M., Majority-Rules-Type Helical Poly(quinoxaline-2,3-diyl)s as Highly Efficient Chirality-Amplification Systems for Asymmetric Catalysis. *Angew. Chem. Int. Ed.* **2015,** *54*, 9333–9337.

27. Nagata, Y.; Nishikawa, T.; Suginome, M., Solvent Effect on the Sergeants-and-Soldiers Effect Leading to Bidirectional Induction of Single-Handed Helical Sense of Poly(quinoxaline-2,3-diyl)s Copolymers in Aromatic Solvents. *ACS Macro Lett.* **2016,** *5* (4), 519-522.

28. Yoshinaga, Y.; Yamamoto, T.; Suginome, M., Chirality-Switchable 2,2 '-Bipyridine Ligands Attached to Helical Poly(quinoxaline-2,3-diyl)s for Copper-Catalyzed Asymmetric Cyclopropanation of Alkenes. *ACS Macro Lett.* **2017,** *6* (7), 705-710.

29. Zimbron, J. M.; Caumes, X.; Li, Y.; Thomas, C. M.; Raynal, M.; Bouteiller, L., Real-Time Control of the Enantioselectivity of a Supramolecular Catalyst Allows Selecting the Configuration of Consecutively Formed Stereogenic Centers. *Angew. Chem. Int. Ed.* **2017,** *56* (45), 14016-14019.

30. Nagata, Y.; Nishikawa, T.; Suginome, M.; Sato, S.; Sugiyama, M.; Porcar, L.; Martel, A.; Inoue, R.; Sato, N., Elucidating the Solvent Effect on the Switch of the Helicity of Poly(quinoxaline-2,3-diyl)s: A Conformational Analysis by Small-Angle Neutron Scattering. *J. Am. Chem. Soc.* **2018,** *140* (8), 2722-2726.

31. Vaquero, M.; Rovira, L.; Vidal-Ferran, A., Supramolecularly fine-regulated enantioselective catalysts. *Chem. Commun.* **2016,** *52* (74), 11038-11051.

32. Zhang, X. C.; Hu, Y. H.; Chen, C. F.; Fang, Q.; Yang, L. Y.; Lu, Y. B.; Xie, L. J.; Wu, J.; Li, S. J.; Fang, W. J., A supramolecularly tunable chiral diphosphine ligand: application to Rh and Ir-catalyzed enantioselective hydrogenation. *Chem. Sci.* **2016,** *7* (7), 4594-4599.

33. Kean, Z. S.; Akbulatov, S.; Tian, Y. C.; Widenhoefer, R. A.; Boulatov, R.; Craig, S. L., Photomechanical Actuation of Ligand Geometry in Enantioselective Catalysis. *Angew. Chem. Int. Ed.* **2014,** *53* (52), 14508-14511.

34. Zhang, Q. Y.; Cui, X. L.; Zhang, L.; Luo, S. Z.; Wang, H.; Wu, Y. J., Redox Tuning of a Direct Asymmetric Aldol Reaction. *Angew. Chem. Int. Ed.* **2015,** *54* (17), 5210-5213.

35. Hong, L.; Sun, W. S.; Yang, D. X.; Li, G. F.; Wang, R., Additive Effects on Asymmetric Catalysis. *Chem. Rev.* **2016,** *116* (6), 4006-4123.

36. Storch, G.; Trapp, O., By-design enantioselective self-amplification based on non-covalent product-catalyst interactions. *Nat. Chem.* **2017,** *9* (2), 179-187.

37. Coates, G. W.; Waymouth, R. M., Oscillating Stereocontrol - a Strategy for the Synthesis of Thermoplastic Elastomeric Polypropylene. *Science* **1995,** *267* (5195), 217-219.

38. Liu, M. H.; Zhang, L.; Wang, T. Y., Supramolecular Chirality in Self-Assembled Systems. *Chem. Rev.* **2015,** *115* (15), 7304-7397.

39. Yashima, E.; Ousaka, N.; Taura, D.; Shimomura, K.; Ikai, T.; Maeda, K., Supramolecular Helical Systems: Helical Assemblies of Small Molecules, Foldamers, and Polymers with Chiral Amplification and Their Functions. *Chem. Rev.* **2016,** *116* (22), 13752-13990.

40. Jiang, J.; Ouyang, G. H.; Zhang, L.; Liu, M. H., Self-Assembled Chiral Nanostructures as Scaffolds for Asymmetric Reactions. *Chem. Eur. J.* **2017,** *23* (40), 9439-9450.

41. Raynal, M.; Portier, F.; van Leeuwen, P. W. N. M.; Bouteiller, L., Tunable Asymmetric Catalysis through Ligand Stacking in Chiral Rigid Rods. *J. Am. Chem. Soc.* **2013,** *135* (47), 17687-17690.

42. Desmarchelier, A.; Caumes, X.; Raynal, M.; Vidal-Ferran, A.; van Leeuwen, P. W. N. M.; Bouteiller, L., Correlation between the Selectivity and the Structure of an Asymmetric Catalyst Built on a Chirally Amplified Supramolecular Helical Scaffold. *J. Am. Chem. Soc.* **2016,** *138*, 4908-4916.

43. Besenius, P., Controlling supramolecular polymerization through multicomponent self-assembly. *J. Polym. Sci. Pol. Chem.* **2017,** *55* (1), 34-78.

44. Pinault, T.; Cannizzo, C.; Andrioletti, B.; Ducouret, G.; Lequeux, F.; Bouteiller, L., Anions as Efficient Chain Stoppers for Hydrogen-Bonded Supramolecular Polymers. *Langmuir* **2009,** *25* (15), 8404-8407.

45. Yoon, H. J.; Kuwabara, J.; Kim, J. H.; Mirkin, C. A., Allosteric Supramolecular Triple-Layer Catalysts. *Science* **2010,** *330* (6000), 66-69.

46. Foli, G.; D'Elia, C. S.; Fochi, M.; Bernardi, L., Reversible modulation of the activity of thiourea catalysts with anions: a simple approach to switchable asymmetric catalysis. *RSC Adv.* **2016,** *6* (71), 66490-66494.

47. Kita, M. R.; Miller, A. J. M., An Ion-Responsive Pincer-Crown Ether Catalyst System for Rapid and Switchable Olefin Isomerization. *Angew. Chem. Int. Ed.* **2017,** *56* (20), 5498-5502.

48. Shen, Q.; Ogata, T.; Hartwig, J. F., Highly reactive, general and long-lived catalysts for palladium-catalyzed amination of heteroaryl and aryl chlorides, bromides, and iodides: Scope and structure-activity relationships. *J. Am. Chem. Soc.* **2008,** *130* (20), 6586-6596.

49. Fors, B. P.; Davis, N. R.; Buchwald, S. L., An Efficient Process for Pd-Catalyzed C-N Cross-Coupling Reactions of Aryl Iodides: Insight Into Controlling Factors. *J. Am. Chem. Soc.* **2009,** *131* (16), 5766-5768.

50. Allenmark, S., Induced Circular Dichroism by Chiral Molecular Interaction. *Chirality* **2003,** *15*, 409-422.

51. Mezailles, N.; Ricard, L.; Gagosz, F., Phosphine gold(I) Bis-(trifluoromethanesulfonyl)imidate complexes as new highly efficient and air-stable catalysts for the cycloisomerization of enynes. *Org. Lett.* **2005,** *7* (19), 4133-4136.

52. Desmarchelier, A.; Raynal, M.; Brocorens, P.; Vanthuyne, N.; Bouteiller, L., Revisiting the assembly of amino ester-based benzene-1,3,5-tricarboxamides: chiral rods in solution. *Chem. Commun.* **2015,** *51* (34), 7397-7400.

53. Desmarchelier, A.; Giordano Alvarenga, B.; Caumes, X.; Dubreucq, L.; Troufflard, C.; Tessier, M.; Vanthuyne, N.; Idé, J.; Maistriaux, T.; Beljonne, D.; Brocorens, P.; Lazzaroni, R.; Raynal, M.; Bouteiller, L., Tuning the nature and stability of self-assemblies formed by ester benzene 1,3,5-tricarboxamides: the crucial role played by the substituents. *Soft Matter* **2016,** *12*, 7824-7838.

54. Caumes, X.; Baldi, A.; Gontard, G.; Brocorens, P.; Lazzaroni, R.; Vanthuyne, N.; Troufflard, C.; Raynal, M.; Bouteiller, L., Tuning the structure of 1,3,5-benzene tricarboxamide self-assemblies through stereochemistry. *Chem. Commun.* **2016,** *52* (91), 13369-13372.

55. Lortie, F.; Boileau, S.; Bouteiller, L.; Chassenieux, C.; Deme, B.; Ducouret, G.; Jalabert, M.; Laupretre, F.; Terech, P., Structural and rheological study of a bis-urea based reversible polymer in an apolar solvent. *Langmuir* **2002,** *18* (19), 7218-7222.

56. Uray, G.; Stampfer, W.; Fabian, W. M. F., Comparison of Chirasil-DEX CB as gas chromatographic and ULMO as liquid chromatographic chiral stationary phase for enantioseparation of aryl- and heteroarylcarbinols. *J. Chromatogr. A* **2003,** *992* (1-2), 151-157.

57. De Greef, T. F. A.; Smulders, M. M. J.; Wolffs, M.; Schenning, A. P. H. J.; Sijbesma, R. P.; Meijer, E. W., Supramolecular Polymerization. *Chem. Rev.* **2009,** *109* (11), 5687-5754.

58. Wegner, M.; Dudenko, D.; Sebastiani, D.; Palmans, A. R. A.; de Greef, T. F. A.; Graf, R.; Spiess, H. W., The impact of the amide connectivity on the assembly and dynamics of benzene-1,3,5-tricarboxamides in the solid state. *Chem. Sci.* **2011,** *2* (10), 2040-2049.

59. van Hameren, R.; van Buul, A. M.; Visser, D.; Heenan, R. K.; King, S. M.; Rowan, A. E.; Nolte, R. J. M.; Pyckhout-Hintzen, W.; Elemans, J. A. A. W.; Feiters, M. C., Solution scattering studies of the hierarchical assembly of porphyrin trimers based on benzene triscarboxamide. *Soft Matter* **2014,** *10* (48), 9688-9694.

Chapter 4 Huge enhancement in the amplification of chirality in dynamic supramolecular helices and catalysts upon incorporation of an achiral monomer

Abstract: Chirality amplification in helical polymers and assemblies refers to the ability of controlling the main chain helicity by a small chiral bias. This feature has motivated the implementation of functional chirally-amplified helices as switchable asymmetric catalysts, chiral sensors and CPL emitters. However, chirality amplification properties remain hard to predict. Previous attempts to optimize the extent of chirality amplification in a given molecular helix focused on subtle tuning the chemical structure of the monomers or the experimental conditions and led to limited improvements. In this chapter, we investigate the chirality amplification properties in dynamic supramolecular helices composed of an achiral benzene-1,3,5-tricarboxamide (BTA) ligand, coordinated to copper, and an enantiopure BTA co-monomer. Amplification effects, probed by varying the amount (sergeants-and-soldiers) or the optical purity (diluted majority-rules) of the enantiopure co-monomer, are modest in this initial system. However, both chirality amplification effects are hugely enhanced upon addition of a second achiral BTA monomer leading to a perfect control of the helicity either by means of a remarkably low amount of sergeants (0.5%) or a small bias from a racemic mixture of enantiopure co-monomers (10% *e.e.*). Such an enhancement in the amplification of chirality is only achieved by mixing the three components, *i.e.* the two achiral and the enantiopure comonomers, highlighting a synergistic effect upon co-assembly of the three monomers. Investigation of the role of the achiral additive by means of several spectroscopic techniques (CD, UV-Vis, FT-IR, SANS) supports its ability to induce a conformational change in the helical co-assemblies leading to no helix reversals *i.e.* conformational defects. Implementation of these helical co-assemblies in the copper-catalysed hydrosilylation of 1-(4-nitrophenyl)ethanone confirms that the effect of the achiral BTA additive is also operative under the conditions of the catalytic experiment. Indeed, 88% of the optimal selectivity is achieved with a catalytic mixture containing 0.5% of enantiopure co-monomers relatively to the ligand which is equal, in our catalytic conditions, to a catalytic loading in chiral species of only 0.06 mol%.

I Introduction

Asymmetric amplification refers to a quite large variety of topics in chemical sciences such as non-linear effects in asymmetric catalysis,[1-2] racemization/deracemization[3] processes and chiral replicators[4-5] that may ultimately constitute a basis to understand the elusive omnipresence of homochirality on Earth. Chirality amplification in helical covalent molecules[6-8] and supramolecular aggregates[9-10] can be considered as another discipline of this domain which deals with controlling the optical purity of these structures, expressed at the macromolecular or supramolecular level, by a small chiral bias. This minute induction is usually too small to be directly measured at the molecular level (with extreme values as low as a few $J.mol^{-1}$ per unit for chiral isotopic substitution)[11-12] but induces a conformational bias that is amplified through the whole nanostructure and may eventually lead to the formation of homochiral structures. The scaffold of dynamic helical covalent and supramolecular polymers is particularly prone to chirality amplification as demonstrated by the diversity of scaffolds in which these phenomena have been expressed.[8] The ultra high sensitivity to a variety of chiral inducers (*e.g.* chiral monomers and inducers, chiral solvents, chiral physical fields) has motivated the implementation of functional helical nanostructures as switchable asymmetric catalysts,[13] chiral stationary phases[14] and as optical devices able to emit[15] or selectively reflect[16] circularly-polarized light.

Green, Selinger and co-workers provided the experimental and theoretical basis of amplification of chirality in covalent poly(isocyanate)s, *i.e.* a class of polymers in which the main chain adopts a stable but dynamic helical conformation in solution.[6] These authors notably reported the possibility of controlling the helical main chain by: (i) introducing a small amount of chiral monomers (sergeants) to copolymers mainly constituted of achiral monomers (soldiers) through the so-called sergeants-and-soldiers (S&S) effect,[17] (ii) mixing enantiopure comonomers in a non-equimolar ratio through the majority-rules (MR) effect[18] and (iii) combining both effects, *i.e.* adding a non-equimolar ratio of enantiopure monomers to terpolymers containing achiral monomers (diluted MR effect).[19-20] For all these cases, the chiral bias imparted by the sergeant or the majority enantiopure monomer is transferred to soldiers (S&S), the minority enantiomer (MR) or both (diluted MR) which remain under its influence in between two helix reversals. Following these pioneering studies, similar effects have been observed for other covalent helical polymers[7] and for supramolecular polymers.[8, 10] The S&S and MR effects are now part of the supramolecular chemist toolbox to probe the induction and amplification of chirality as well as chiral self-sorting in dynamic assemblies. These effects have been well established experimentally and rationalized by means of statistical mechanical[21-24] and numerical[25-28] methods. Meijer and Palmans formulated a number of features that are common to supramolecular systems

displaying chirality amplification such as the strong and cooperative aggregation of the molecules in solution, the involvement of different types of non-covalent interactions in their aggregation process and the formation of a chiral object at the supramolecular scale.[10] However, prediction of the chirality amplification properties of an untested helical system and even optimization of the degree of chirality amplification for a supramolecular helix exhibiting these effects remain poorly addressed challenges.

Extremely high levels of chirality amplification, *i.e.* by means of a minute amount of sergeants (≤ 1%),[29-37] by a mixture of enantiopure monomers only moderately biased from the racemic mixture (≤10% *e.e.*),[37-39] by chiral physical fields[40-46] or through spontaneous mirror-symmetry breaking phenomena[15, 37, 41, 47-50] have been reported for a limited number of helical assemblies in solution or in the gel state. The S&S and MR effects in dynamic one-dimensional polymers constructed by assembly of small disk-like molecules were subject to optimization by changing the nature of the sergeants,[36, 51-52] the nature of the soldiers,[36, 53] or the experimental conditions (concentration,[29, 35] temperature,[51, 54] solvent).[32] However, changing these parameters as well as subtle variations in the nature of the interacting groups[55-60] usually led to mitigated improvement of the chirality amplification properties for a given helical system. *N*,*N*′,*N*″-trialkylbenzene-1,3,5-tricarboxamides (alkyl BTA) and their functional derivatives are ubiquitous synthons in supramolecular chemistry as the result of their robust assembly into dynamic helices stabilized by a threefold hydrogen-bond network and aromatic interactions.[61] S&S and MR effects are good in BTA helices[51, 54, 62-65] but not exceptional and their enhancement would clearly be beneficial for a range of applications. Meijer and co-workers probed the limit of chirality amplification in BTA helical assemblies and their studies reveal that optimization by subtle variation in the structure of the monomer will improve the extent of amplification but solely up to the limits fixed by the number of reversals present in the helix.[51] As this latter parameter is intrinsically related to the strength of the intermolecular interactions stabilizing the BTA assemblies, the authors suggest that further improvement would require changing the chemical structure of the monomers (and thus the nature of the helix). We report herein that, albeit counterintuitive at first sight, the addition of an *achiral* BTA monomer changes the configuration of BTA co-assemblies from poorly helically biased to fully homochiral. The S&S and diluted MR effect are improved by two and one order of magnitude, respectively, which is attributed to the suppression of the helix reversals in presence of the achiral additive. Implementation of the present concept (Scheme 1) to asymmetric catalysts supported by chirally-amplified BTA helices enables optimal enantioselectivity to be reached with as little as 600 ppm of chiral inducer relatively to the substrate.

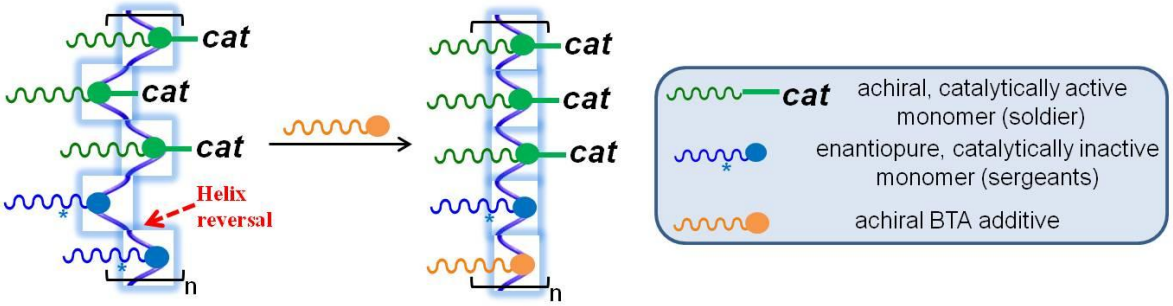

Scheme 1 Schematic representation of the present concept. Catalytic helical co-assemblies consisting of an achiral BTA catalyst and an enantiopure co-monomer (S&S type mixtures) change their configuration from poorly helically biased to homochiral upon addition of an achiral BTA additive. The purple helix represents the non-covalent helical backbone formed upon co-assembly of BTA monomers. The concept also holds true for mixtures between an achiral BTA catalyst and a non-equimolar mixture of enantiopure BTA monomers (diluted MR type mixtures).

II Results and discussion

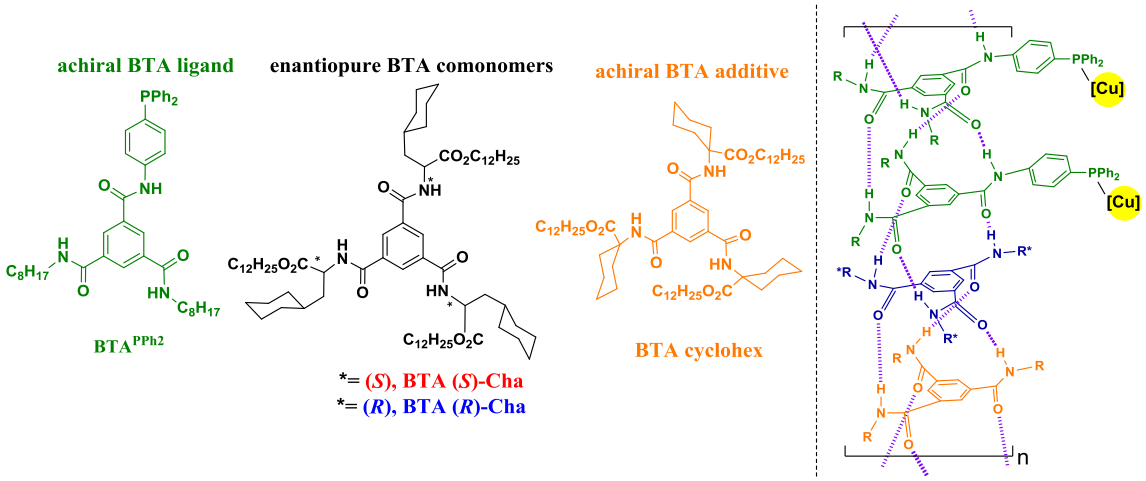

Chart 1 Left: chemical structures of the BTA monomers used in this study. Right: representation of the helical co-assemblies, preferentially left-handed, formed by mixing **BTA^{PPh2}**, [Cu(OAc)$_2$·H$_2$O], **BTA (*R*)-Cha** and **BTA cyclohex**.

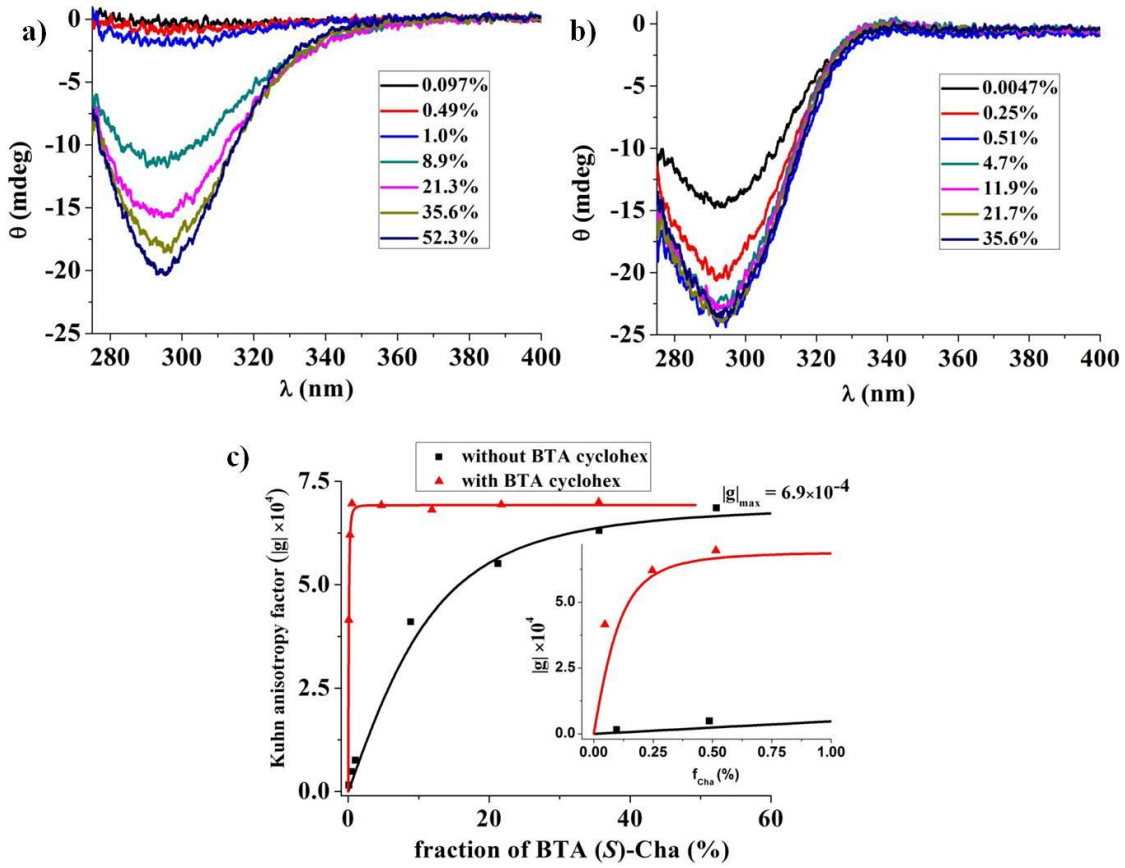

Figure 1 Chirality amplification through the S&S effect as probed by CD spectroscopy. a) CD analyses of the S&S-type mixtures without **BTA cyclohex** ([BTA^{PPh2}]/[$Cu(OAc)_2 \cdot H_2O$]= 4, [BTA^{PPh2}] set constant at 5.80±0.04 mM, 0.0056 mM≤ [**BTA (*S*)-Cha**]≤ 6.35 mM). b) CD analyses of the S&S-type mixtures with **BTA cyclohex** ([BTA^{PPh2}]/[$Cu(OAc)_2 \cdot H_2O$]= 4, [BTA^{PPh2}] and [BTA cyclohex] both set constant at 5.80±0.06 mM, 0.0056 mM≤ [**BTA (*S*)-Cha**]≤ 6.39 mM). c) Kuhn anisotropy factor (g) measured at λ= 295 nm as a function of the fraction of **BTA (*S*)-Cha** in the mixtures. g= θ^{295}/(32980 × Abs^{295}) where θ and Abs are the ellipticity and UV absorbance measured at λ= 295 nm, respectively. f_{Cha}= [BTA Cha]/([BTA Cha]+[BTA^{PPh2}]+[BTA cyclohex]). The data from the S&S and MR experiments have been fitted for the mixtures with and without **BTA cyclohex** (red and black solid lines, respectively) simultaneously following procedures described by Smulders et al.[51] (for S&S) and van Gestel[24] (for diluted MR). The superior maximal ellipticity reached for S&S mixtures with **BTA cyclohex** is related to an increase of the intensity of main UV-Vis absorption band (*vide infra*).

Chirality amplification probed by CD spectroscopy. We previously found that the mixture composed of **BTA^{PPh2}** and of the co-monomer **BTA Cha** (Chart 1) yields very long one-dimensional co-assemblies in solution (DP_n ≈250) with a radius corresponding to a single molecule of BTA in the cross-section.[66] BTA Cha belongs to the family of BTAs derived from amino-esters (ester BTAs)[35, 67-71] which were shown to be efficient chiral inducers for asymmetric reactions performed with helical BTA

catalysts.[66, 72-73] In order to induce a sufficient bias in the handedness of these co-assemblies, an excess of BTA Cha was employed relatively to **BTA^{PPh2}**.[66, 73] We have now investigated the possibility of generating homochiral helices with a lower amount of enantiopure co-monomer. Firstly, mixtures of **BTA^{PPh2}** and **BTA (*S*)-Cha** in toluene are analyzed by CD spectroscopy with the presence of copper coordinated to the BTA ligand in order to be as close as possible of the catalytic conditions we established previously.[74] CD analyses of sergeants-and-soldiers (S&S) type mixtures, in which **BTA^{PPh2}** coordinated to Cu and **BTA (*S*)-Cha** are the soldiers and the sergeants, respectively, are shown in Figure 1a ([BTA^{PPh2}] and [$Cu(OAc)_2 \cdot H_2O$] are set constant at 5.80±0.04 mM and 1.46±0.02 mM, respectively). Mixtures with more than 0.5% of sergeants exhibit a Cotton effect with a maximum at $\lambda \approx$ 295 nm while no CD signal is detected for mixtures containing a lower amount of sergeant. The observed Cotton effect constitutes a direct probe of the extent of chirality induction in the co-assemblies since only the soldier is UV active in this region (induced CD).[66, 73, 75] Accordingly, plotting the Kuhn anisotropy values (g) at λ= 295 nm as a function of the fraction of **BTA (*S*)-Cha** in these mixtures provides the amplitude of the S&S effect operating in this system (Figure 1c). Even though the plot deviates from linearity, no obvious plateau of the g value is reached meaning that a sizable fraction of enantiopure co-monomers ($f_{Cha} \geq$ 52%) is required to get fully biased co-assemblies.

We previously reported that incorporating 1% of a ester BTA was enough to fully bias the handedness of (otherwise racemic) helical assemblies formed by *N*,*N*',*N*''-tris(octyl)benzene-1,3,5-tricarboxamide.[35] We have now hypothesized that the limited amplification of chirality observed in this initial system is related to defects induced by **BTA^{PPh2}** coordinated to Cu, *i.e.* this monomer behaves as a "bad soldier". We thus test the possibility of inducing a conformational change in the co-assemblies upon addition of a second achiral BTA. We selected **BTA cyclohex** (Chart 1) since the cyclohexyl group attached on the amino-ester α-carbon is expected to reduce the conformational freedom of the amide functions and thus rigidifies the hydrogen-bonded network between the complementary monomers in the co-assemblies.[53] A new set of mixtures has been analyzed by CD which differ from the initial ones only by the fact that they now contain two soldiers: **BTA^{PPh2}** coordinated to Cu and **BTA cyclohex** ([BTA^{PPh2}]/[BTA cyclohex]= 1). The influence of **BTA cyclohex** on the amplitude of the S&S effect is dramatic (Figure 1b). The CD spectrum of the mixture with only 0.51% of sergeant is virtually identical to that of the mixtures containing higher fractions of enantiopure co-monomers. The S&S mixture with only 0.25% of **BTA (*S*)-Cha** displays a g value which is equal to 90% of the maximal g value ($|g_{max}| = 6.9 \times 10^{-4}$). A similar g_{max} value is reached for S&S mixtures with and without **BTA cyclohex** corroborating the formation of similar homochiral, preferentially right-handed,[73]

co-assemblies but for drastically different fractions of sergeants, f_{Cha}= 0.05 and 0.52 respectively. The S&S effect is thus enhanced by two orders of magnitude in presence of **BTA cyclohex**.

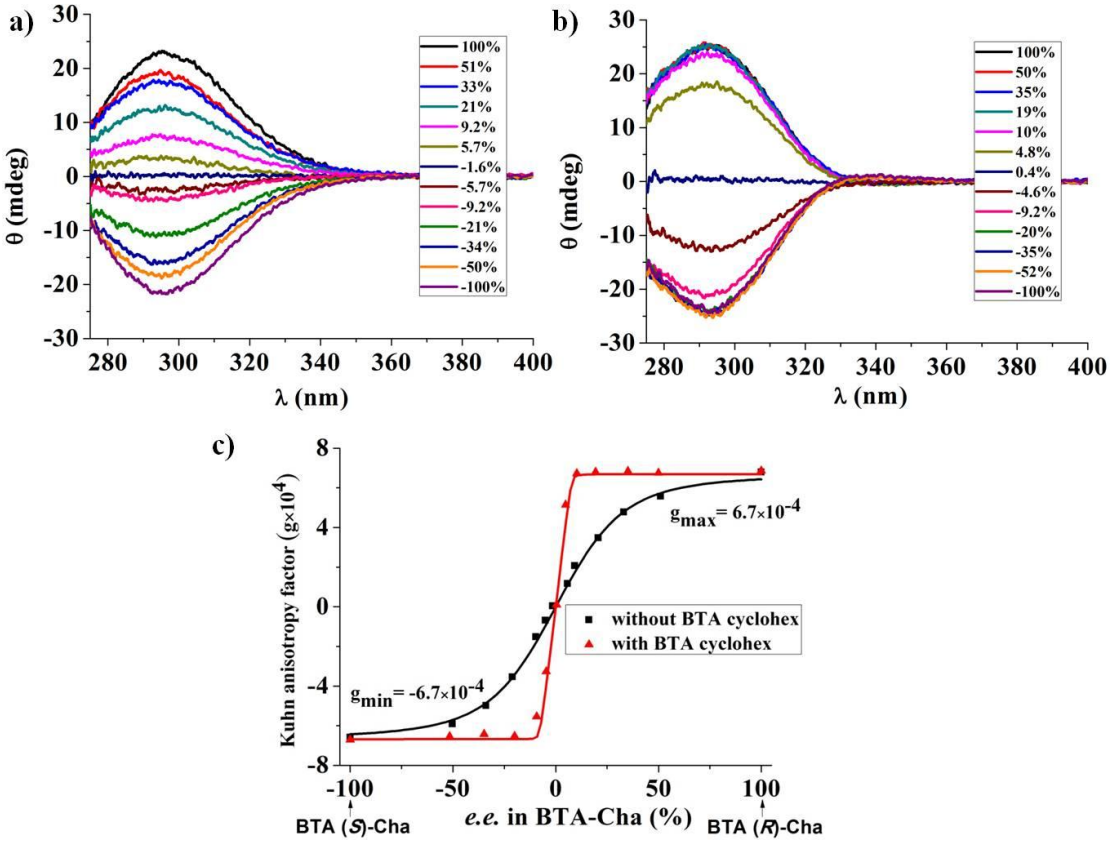

Figure 2 Chirality amplification through the diluted MR effect as probed by CD spectroscopy. a) CD analyses of the diluted majority-rules type mixtures without **BTA cyclohex** ([BTA^{PPh2}]/[$Cu(OAc)_2{\cdot}H_2O$]= 4, [BTA^{PPh2}] set constant at 5.78±0.07 mM, f_{Cha}= 0.53±0.02). b) CD analyses of the diluted majority-rules type mixtures with **BTA cyclohex** ([BTA^{PPh2}]/[$Cu(OAc)_2{\cdot}H_2O$]= 4, [BTA^{PPh2}] and [BTA cyclohex] set constant at 5.80±0.04 mM and 6.40±0.40 mM respectively, f_{Cha}= 0.34±0.02). c) Kuhn anisotropy factor (g) measured at λ= 295 nm as a function of the optical purity in **BTA Cha** in the mixtures. The data from the S&S and MR experiments have been fitted for the mixtures with and without **BTA cyclohex** (red and black solid lines, respectively) simultaneously following procedures described by Smulders et al.[51] (for S&S) and van Gestel[24] (for diluted MR). The superior maximal ellipticity reached for diluted MR mixtures with **BTA cyclohex** is related to an increase of the intensity of main UV-Vis absorption band (*vide infra*).

We have investigated whether a similar effect is operative on co-assemblies obtained by mixing soldiers and non-equimolar amounts of enantiopure sergeants, *i.e.* for amplification of chirality through the diluted majority-rules effect. Mixtures containing **BTA^{PPh2}** coordinated to Cu and **BTA Cha** of

various optical purities (-100% *e.e.*→100% *e.e.*) have been analyzed in absence and presence of **BTA cyclohex** (Figures 2a and 2b, respectively). Without additive, a nonlinear increase of the g value is observed as a function of the optical purity in BTA Cha but no plateau is reached indicating that the amplification of chirality is modest (Figure 2c). Again, the addition of **BTA cyclohex** has a huge effect on the extent of amplification of chirality since homochiral co-assemblies are obtained for scalemic mixtures only slightly biased from the racemic mixture (10% *e.e.*). The diluted MR effect is thus increased by one order of magnitude in presence of **BTA cyclohex.** A modulation in the relative proportion of the enantiomers of only 10% around the racemic composition produces homochiral helices with opposite handedness.

In the previous experiments, the addition **of BTA cyclohex** induces an increase of the total BTA concentration which may be partly responsible for the huge chirality amplification enhancement. To demonstrate the robustness of our data, we have performed similar S&S and diluted MR type experiments except that the total concentration of BTA monomers has been set constant to 5.84±0.2 mM (Figure S1). Even in these conditions, upon the addition of **BTA cyclohex,** a plateau of g values is obtained for mixtures containing 0.5% of sergeants (S&S mixtures) or a 10% *e.e.* scalemic mixture (diluted MR mixtures) inferring a similar enhancement of the amplification of chirality in the helical co-assemblies. It is remarkable that this simple strategy allows to reach extremely high levels of chirality amplification for both the S&S and diluted MR effects with the same sergeant, which outperforms those obtained with helical assemblies of alkyl BTA reported to date.[51, 54, 62-65] Encompassing all monomers forming isolated single helices in solution, such levels of amplification have been reported only sporadically in the literature[29, 32, 35-36, 38, 76] and, to the best our knowledge, never with the same chiral monomer used as both a sergeant and a majority enantiomer.

Assembly behavior of the BTA partners. In order to enravel the role of **BTA cyclohex,** we start by determining whether the presence of the three monomers is necessary to observe high amplification of chirality in our above-mentioned helical BTA systems. We previously reported that **BTA^{PPh2}** monomers aggregate through a cooperative pathway to form hydrogen bonded stacks (Figure 3b), similar to the one described for *N*,*N*',*N*''-tris(methoxyethyl)benzene-1,3,5-tricarboxamide[77] and other BTAs in the literature,[61] at a critical concentration of *ca.* 0.5×10^{-3} M in toluene (see the FT-IR and SANS signatures in Figure 3b and 3c respectively).[73] In the same solvent, **BTA Cha** assembles under the form of dimers only, the structure of which was unambiguously determined[70] and revealed by the presence of hydrogen bonds between amide N-H and ester (instead of amide) carbonyls (see the FT-IR and SANS signatures in Figure 3a and 3c respectively). We have now studied the structure of the self-

assemblies formed by **BTA cyclohex** by means of FT-IR and SANS analyses. The FT-IR spectrum recorded in toluene at 1.0 mM, shows the presence of three broad bands in the N−H region with maxima at ν≈ 3448 cm^{-1}, ν= 3402 cm^{-1} and ν= 3293 cm^{-1} which are attributed to free N−H, N−H bonded to ester C=O,[6-8,24] and N−H (weakly) bonded to amide C=O, respectively (Figure S2a). A similar pattern is observed at 5.8 mM, except that the free NH band has decreased in intensity and the two others have become more intense meaning that a transition occurs between two species (Figure 3a). However, the low intensity of the scattering intensity observed in SANS analyses of **BTA cyclohex** at both 5.4 mM and 9.0 mM indicates that small assemblies are the dominant species in C_7D_8 (Figures 3c and S2b). Subsequently, we have tested the co-assemblies formed by **BTA cyclohex** and **BTA (*S*)-Cha** and found out that the FT-IR spectrum of their 1:1 mixture is virtually identical to that of the individual components (Figure 3a). This means that these monomers self-sort into two their own self-assemblies (self-segregation).

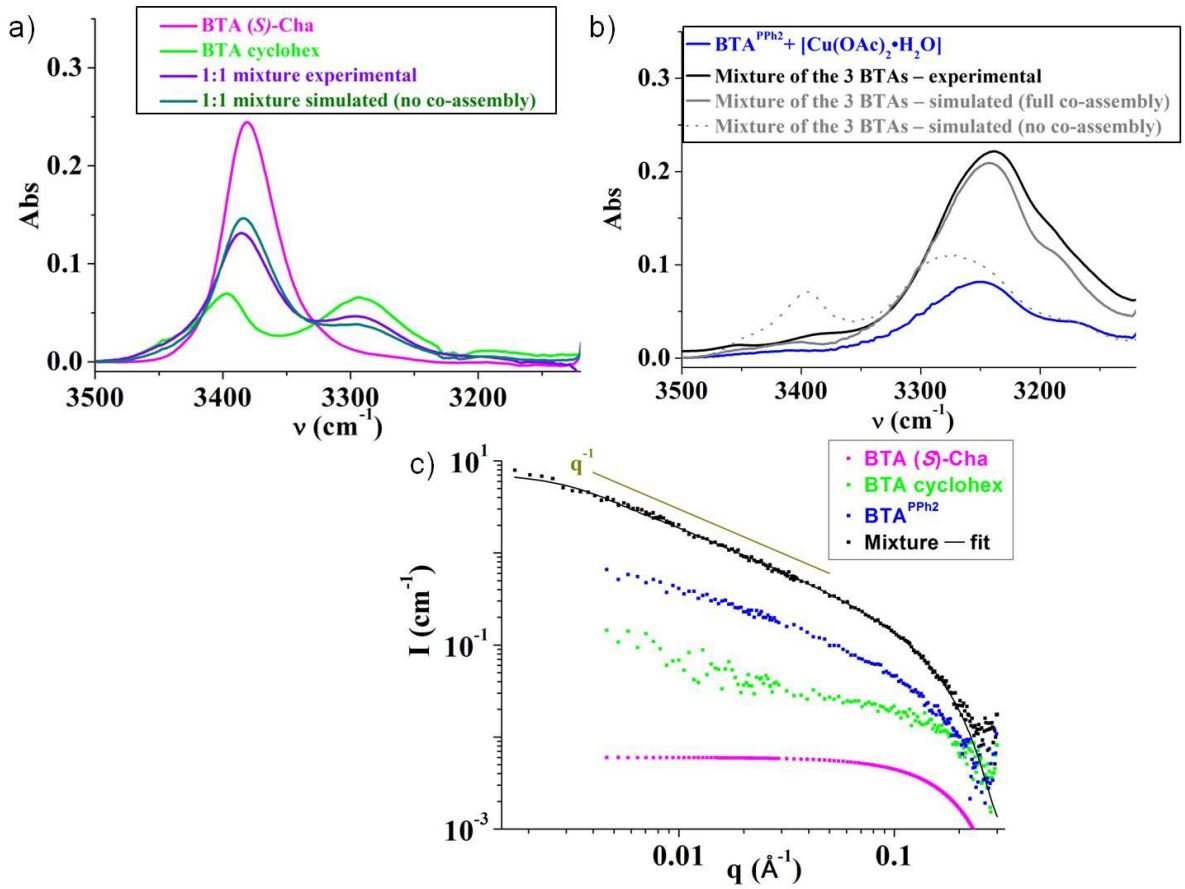

Figure 3 Characterization of the assemblies (293K). a) between **BTA (*S*)-Cha** and **BTA cyclohex**. FT-IR spectra of **BTA (*S*)-Cha** (5.8 mM), **BTA cyclohex** (5.8 mM) and of their 1:1 mixture in toluene. The experimental spectrum for the mixture is shown together with the simulated spectrum for segregated assemblies (no co-assembly). Zoom on the N-H region (for the C=O region see Figure S3a). b) between **BTA^{PPh2}·Cu**, **BTA (*S*)-Cha** and **BTA cyclohex** (f_{Cha}= 0.048). FT-IR spectra of the mixture between **BTA^{PPh2}** (5.8 mM) and [$Cu(OAc)_2$•H_2O] (1.45 mM) and of the mixture between **BTA^{PPh2}** (5.8 mM), [$Cu(OAc)_2$•H_2O] (1.45 mM), **BTA (*S*)-Cha** (0.58 mM) and **BTA cyclohex** (5.8 mM) in toluene. Simulated spectra for no and full co-assembly. Zoom on the N-H region (for the C=O region see Figure S3b). c) between **BTA^{PPh2}·Cu**, **BTA (*S*)-Cha** and **BTA cyclohex** (f_{Cha}= 0.062). SANS analyses of **BTA (*S*)-Cha** (0.68 g.L^{-1}, 0.58 mM), **BTA cyclohex** (9.83 g.L^{-1}, 9.0 mM), **BTA^{PPh2}** (5.98 g.L^{-1}, 8.6 mM) and of the mixture between **BTA^{PPh2}** (3.94 g.L^{-1}, 5.7 mM), [$Cu(OAc)_2$•H_2O] (0.29 g.L^{-1}, 1.45 mM), **BTA (*S*)-Cha** (0.68 g.L^{-1}, 0.58 mM) and **BTA cyclohex** (3.26 g.L^{-1}, 2.99 mM) in C_7D_8. The SANS data of the mixture is fitted by a form factor for rigid rods of finite length, assuming that all BTA monomers are co-assembled within the same stacks.

Conversely, the FT-IR spectrum of the mixture containing the three BTA monomers, *i.e.* **BTA^{PPh2}** coordinated to Cu, **BTA (*S*)-Cha** and **BTA cyclohex** totally differs form the FT-IR spectra of

its individual components since it mainly consists of single band in the N-H region (Figures 3b and S3b). This band with a maximum at ν= 3239 cm^{-1} is the signature of hydrogen-bonded amide functions in well-defined helical BTA stacks. The experimental spectrum is virtually identical to the one simulated in case of full assembly of the 3 BTA partners meaning that, a large fraction (≥ 90%) of **BTA (*S*)-Cha** and **BTA cyclohex** monomers are incorporated into the stacks formed by **BTA^{PPh2}** coordinated to Cu. This is further supported by SANS analysis of a similar mixture which shows a q^{-1} dependence of the scattering intensity at low q values which is indicative of the presence of cylindrical and rigid objects in C_7D_8 (Figure 3c). The SANS data can be fitted by making the assumption of a full incorporation of **BTA (*S*)-Cha** and **BTA cyclohex** into the stacks of **BTA^{PPh2}**. The excellent fit of the SANS data with a form factor for rigid rods of finite length confirms that the stacks are long (length= 120 nm, $DP_n \approx 170$) with a single BTA molecule in the cross-section (r= 12.1Å, n= 0.81) and that, indeed, stacks are the main contributor of the SANS intensity with only a low content (if any) of **BTA (*S*)-Cha** and **BTA cyclohex** self-assemblies. This full set of analyses offers a precise picture of the assembly behavior of the different BTA monomers: the small assemblies formed by **BTA (*S*)-Cha** and **BTA cyclohex** in which there is no or little implication of the amide carbonyls rearrange in the presence of amide-bonded stacks of **BTA^{PPh2}** to generate long helical co-assemblies, while they would self-segregate in its absence. The presence of the three BTA partners thus appears to be crucial to generate rigid helical assemblies whose handedness can be fully biased by the enantiopure co-monomer.

Rationalization of the role of the achiral BTA additive. CD analyses have revealed the ability of **BTA cyclohex** to promote the formation of homochiral helical assemblies when the fraction of sergeant is ≥ 0.5% (or its optical purity is ≥ 10% *e.e.*). We first compare the FT-IR of the mixtures with and without **BTA cyclohex** (Figure S4b). Both spectra are very similar indicating that the helical assemblies display a similar hydrogen bond network. Importantly, in both cases the incorporation of **BTA (*S*)-Cha** into the stacks can be estimated to be superior to 90% which discards a potential bias in the **BTA^{PPh2}/BTA (*S*)-Cha** ratio in the helical co-assemblies as a result of the presence of **BTA cyclohex** (Figure S4a). Also, structural parameters determined above for the assemblies with **BTA cyclohex** (r= 12.1Å, n= 0.81, l= 120 nm) are similar to those determined previously for assemblies without **BTA cyclohex** (r= 11.4 Å, n = 0.6, l> 100 nm) confirming that the achiral BTA additive does not significantly alter the geometry of the supramolecular helices.[66] We thus attribute the synergistic effect observed upon co-assembly of the three partners to a conformational change induced by **BTA cyclohex** upon its incorporation into the co-assemblies formed by **BTA^{PPh2}** and **BTA (*S*)-Cha**.

Closer examination of the FT-IR spectrum with the achiral BTA additive (Figure S4b) reveals the following differences: i) the maximum of the N-H band is shifted from 3248 to 3239 cm^{-1} and ii) the amide I band is narrower. Notable differences are also observed in the CD and UV-Vis (Figures S5a and S5b) spectra of the mixtures with and without of **BTA cyclohex**. The main UV absorption band is narrower and its intensity is significantly increased when **BTA cyclohex** monomers are incorporated into the stacks despite the fact that their self-assemblies barely absorb in that region. A similar change in the intensity and shape of the corresponding Cotton effect is also seen. These observations infer the formation of a stronger and more regular intermolecular hydrogen bond network when **BTA cyclohex** is present in the helical BTA co-assemblies. An additional support towards this hypothesis comes from the quantification of the conformational defects in the supramolecular helices. Amplification of chirality in dynamic supramolecular systems has been consistently modelled by various statistical mechanical[21-24] and numerical[25-28] methods. The statistical model developed by van Gestel and its adaptation by Smulders et al.[51, 54] were successfully applied to quantity chirality amplification in S&S,[21] MR[22] and diluted MR effects.[24] Its robustness was demonstrated for various BTA monomers[12, 51, 54, 59, 64] as well as other types of aggregating disk-like molecules.[36, 56, 59, 78-79] In order to allow a comparison of the present system with those described in the literature, we have fitted the CD data of Figures 1 and 2 simultaneously by following procedures described by Smulders et al.[51] (for S&S) and van Gestel[24] (for diluted MR). It allows to extract two energetic parameters: the helix reversal penalty (HRP) that corresponds to the energy needed to reverse the handedness of the supramolecular helix and the mismatch penalty (MMP) which is the energy paid for incorporating a monomer in a helix of its nonpreferred helicity. The quality of the fits for the CD data allows us to extract a precise set of values for helical co-assemblies with and without **BTA cyclohex** (Table 1) and to compare them with the data published in the literature for other helical systems.

Table 1 Helix reversal penalty (HRP) and mismatch penalty (MMP) (both in kJ.mol^{-1}) determined by simultaneously fitting CD data of Figures 1 and 2 following procedures described by Smulders et al.[51] (for S&S) and van Gestel[24] (for diluted MR). Comparison with the values obtained for selected helical systems in the literature (293 K).

Helical systems		Opt. S&S[(a)]	Opt. diluted MR[(b)]	HRP	MMP
BTA^{PPh2}·Cu + BTA (*S*)-Cha (*this work*)	without **BTA cyclohex**	52%	100% *e.e.*	11.0±2.5	0.4±0.4
	with **BTA cyclohex**	0.5%	10% *e.e.*	**22.1±0.5**	**0.3±0.2**
Alkyl BTA (reference[54])		5%	≥30% *e.e.*	12.6±2.0[(c)]	1.9±0.2[(c)]
Triphenylamine trisamide (reference[36])		0.3%	*Nr*	20.5[(d)]	1.0[(d)]

(a) Minimum amount of sergeants required to get homochiral helices in S&S experiments. (b) Minimal optical purity in sergeant required to get homochiral helices in diluted MR experiments. (c) Obtained by fitting independently S&S and MR experiments yielding a precise value for the HRP and MMP, respectively [conditions: 2×10^{-5} M in MCH]. (d) Obtained by fitting the S&S experiment. nr: not reported [conditions: 3×10^{-5} M in MCH].

Strikingly, the value of HRP doubles in the presence of **BTA cyclohex** (from 11.0 to 22.1 kJ.mol^{-1}) while the MMP value is not impacted. This last point is expected as the MMP is a characteristic of the sergeant. The HRP value determined from the fit is actually an "effective HRP value"[24] which likely reflects the average of the HRP values of each BTA partner in the co-assemblies. Even though an achiral monomer may be anticipated to lower the helicity as it exhibits no preferred helicity,[24] our data show that the HRP value of **BTA cyclohex** is actually very high and this is possibly due to (i) a high conformational rigidity and (ii) the formation of strong intermolecular interactions with the other BTA monomers. In fact, the measured HRP values can be translated into a correlation length between two helix reversals:[21] the presence of the additive increases this value from *ca.* 90 to 9000! Considering the average length of the stacks determined by SANS analysis (see above), it means that the stacks contain, on average, one helix reversal or none in absence or presence of the additive, respectively. Therefore, in the presence of **BTA cyclohex**, the limiting factor to reach full chiral amplification is not the correlation length but the degree of polymerization. The average DP_n value of ≈ 170 determined by SANS analysis can be converted into a limit of one molecule of sergeant controlling the helicity of 169 soldiers, *i.e.* 0.6% (for S&S experiment) and 30 major enantiomers dictating their preference to 29 minor enantiomers and 111 soldiers, *i.e.* 2% *e.e.* (for diluted MR experiment). This simple description is in good agreement with our experimental values of 0.5 % and 10% *e.e.*, respectively and validates the consistency of the analysis. Compared to previously reported BTA

mixtures, the better chirality amplification properties observed in the present system is likely related to its higher HRP value (Table 1).[51, 54] Most supramolecular helical systems with high S&S effects, such as triphenylamine trisamides (Table 1),[36] rely on the introduction of gallamide groups which allows nine stereogenic centres to be present at the periphery of the helices.[29, 80] However, increasing the number of stereogenic centres into the monomer reduces its ability to behave as an efficient majority monomer in diluted MR and MR mixtures.[51, 79] Conversely, the MMP value of the **BTA (*S*)-Cha** is suitable to achieve high level of chirality amplification in both the S&S and diluted MR experiments at the condition that the number of helix reversals in the BTA helical system is decreased, as it is the case in presence of **BTA cyclohex**.

Asymmetric catalysts built on an extremely chirally-amplified helical backbone. Introducing intrinsically achiral catalytic monomers into the preferred-handed helical scaffold of covalent or supramolecular polymers enables the formation of an enantio-enriched product whose configuration is determined solely by the handedness of the helices.[13, 81-83] A new class of switchable asymmetric catalysts has emerged by means of this strategy. Additionally, as a result of the chirality amplification phenomena at work in these helical systems, the amount of chiral monomers or inducers both relatively to the catalytically active species (S&S ratio) and to the substrate (catalytic loading in mol%) can be drastically reduced. Very recently, Shen et al.[84] and Arlegui et al.[85] Independently reported that scalemic products are formed by performing a catalytic reaction with spontaneous mirror symmetry-broken helical assemblies functionalized with catalytic centres. Absolute asymmetric synthesis is at work in these systems, since no chiral species are present, but the degree of enantioinduction is low (*e.e.*≤ 46%) and the configuration of the major enantiomer is left to chance. Chirally-amplified S&S-type helical catalysts which display high levels of enantioselectivity have been reported for BTA[72-73, 86] and poly(quinoxaline-2,3-diyl)[87-90] (PQX) scaffolds. However, the amount of chiral inducers required to get *e.e.*> 80% was of the order of 0.2 mol% for PQX[87] and 0.5 mol% for BTA.[72] Chiral solvents have also been efficiently employed as a sole source of enantioinduction in the case of PQX asymmetric catalysts.[91] We now investigate if our extremely chirally-amplified helical precatalyst constitutes an alternative approach to reduce drastically the catalytic loading in chiral species.

Helical co-assemblies with an excess of **BTA (*S*)-Cha** relatively to **BTA^{PPh2}** provided 1-(4-nitrophenyl)ethanol (NPnol) with 54±2% *e.e.* when applied in the copper-catalysed hydrosilylation of 1-(4-nitrophenyl)ethanone (NPnone) at 293 K (reaction of reference).[66, 73] We now probe whether the generation of homochiral helices in the presence of **BTA cyclohex** as determined by CD spectroscopy

also holds for catalytic mixtures. Except otherwise stated, catalytic experiments are implemented at a concentration in [BTA^{PPh2}] set constant at 16.9 mM, a catalytic loading of 3 mol% in [$Cu(OAc)_2 \cdot H_2O$], with $PhSiH_3$ acting both as an activator of the copper precatalyst and as a reducing agent.[92] For S&S-type catalytic mixtures (16 µM≤ [BTA (*S*)-Cha]≤ 18.4 mM) without **BTA cyclohex**, the optical purity

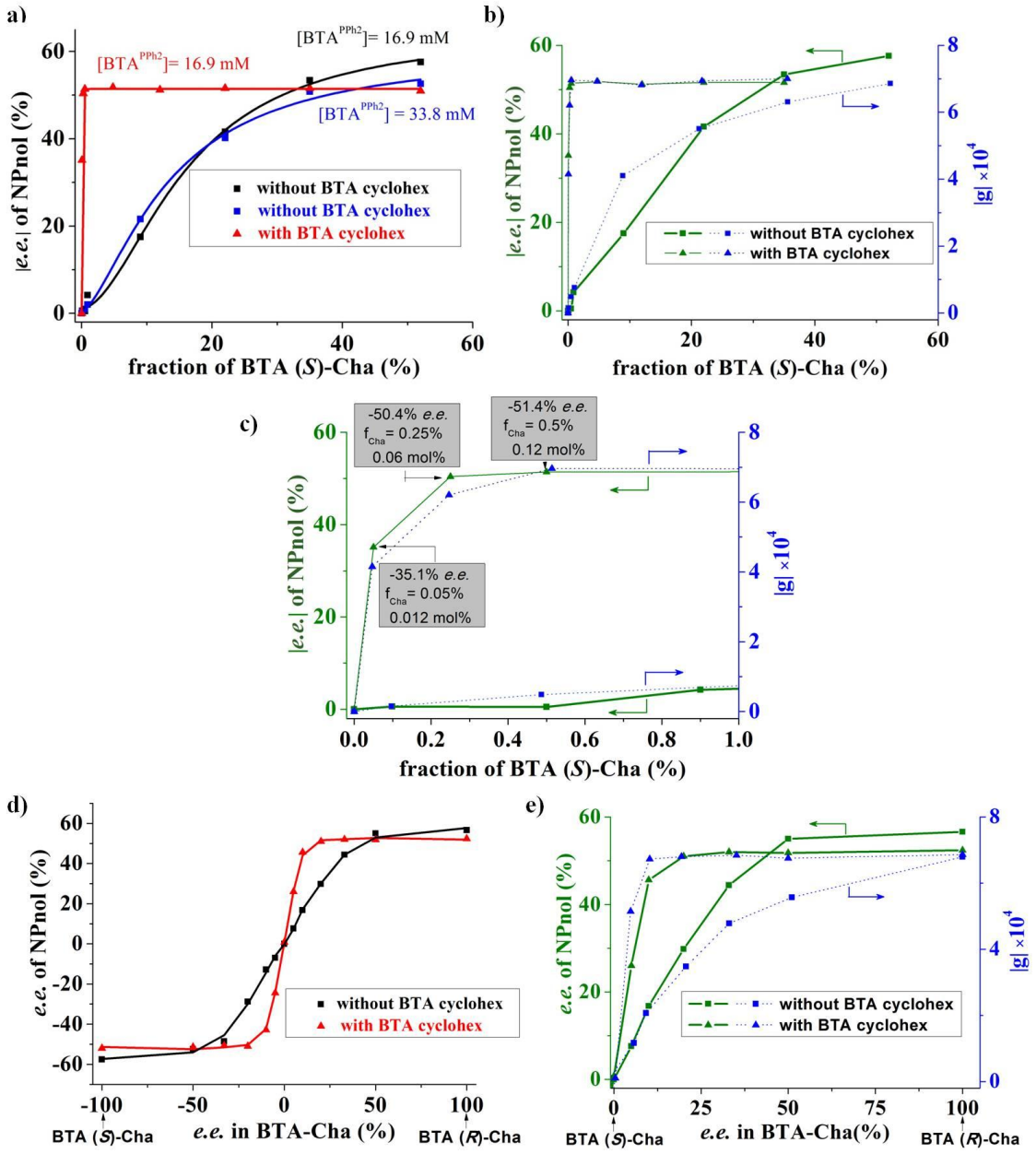

Figure 4 Asymmetric catalysis with S&S- and diluted MR-type helical catalysts (293K). a) Enantioselectivity in NPnol as a function of the fraction of **BTA (*S*)-Cha** in the catalytic mixtures with and without **BTA cyclohex**. Conditions of black and red curves: [BTA^{PPh2}]= 16.4 mM (12 mol%), [$Cu(OAc)_2 \cdot H_2O$]= 4.11 mM (3 mol%), 16 µM (0.012 mol%)≤ [BTA (*S*)-Cha]≤ 18.4 mM (13.4 mol%), [BTA cyclohex]= 16.4 mM (12 mol%, red curve only), [$PhSiH_3$]= 274 mM (200 mol%), [NPnone]= 137 mM (100 mol%). Conditions of blue curve: same as above except that the concentration in BTA^{PPh2}

has been doubled. b) Plot of the enantioselectivity in NPnol and of the Kuhn anisotropy factor as a function the fraction of **BTA (*S*)-Cha** in the catalytic mixtures. c) Zoom on the region corresponding to low f_{Cha} values. The outcome of the catalytic experiments with f_{Cha}= 0.05%, 0.25% and 0.50% is highlighted. d) Enantioselectivity in NPnol as a function of the optical purity in BTA Cha in the catalytic mixtures with and without **BTA cyclohex**. Conditions: [BTA^{PPh2}]= 16.4 mM (12 mol%), [$Cu(OAc)_2 \cdot H_2O$]= 4.11 mM (3 mol%), [BTA Cha] 18.4 mM (13.4 mol%), [BTA cyclohex]= 16.4 mM (12 mol%, red curve only), [$PhSiH_3$]= 274 mM (200 mol%), [NPnone]= 137 mM (100 mol%). e) Plot of the enantioselectivity in NPnol and of the Kuhn anisotropy factor as a function of the optical purity in BTA Cha in the catalytic mixtures. Zoom on the scalemic mixtures biased in **BTA (*R*)-Cha**. Conversion >99% was obtained for all catalytic experiments as determined by GC and ^{1}H NMR analyses. The optical purity was determined by GC analysis, *e.e.* are set as positive and negative when (*S*)-NPnol and (*R*)-NPnol are the majority enantiomers, respectively.

in NPnol increases non linearly with the fraction of **BTA (*S*)-Cha** present in the catalytic mixture, but no plateau is reached ($|e.e._{max}|$ = 57.6%, Figure 4a, black curve). Conversely, in presence of **BTA cyclohex** ([$\mathbf{BTA^{PPh2}}$]/ ([**BTA cyclohex**]= 1), a plateau is reached with a concentration in **BTA (*S*)-Cha** of 160 µM (f_{Cha}= 0.50%, $|e.e._{max}|$ = 51.4±0.3%), and 98% of the plateau value is achieved with only 80 µM of sergeant (f_{Cha}= 0.25%, 50.4% $|e.e.|$, Figure 4a, red curve). This is in good agreement with the minimal fraction of **BTA (*S*)-Cha** required to get homochiral helices as probed by CD spectroscopy. This drastic effect of **BTA cyclohex** on the selectivity is not related to a change in the total BTA concentration since doubling the concentration in $\mathbf{BTA^{PPh2}}$ (without additive) has no significant influence (compare blue and black curves in Figure 4a). In fact, a remarkable correlation is found between the selectivity and the optical purity of the supramolecular helices as shown by the similarity of their curves as a function of f_{Cha} (Figures 4b and 4c). It demonstrates that the enhancement of the enantioselectivity observed at low f_{Cha} values in presence of **BTA cyclohex** is related to its ability to promote the formation of homochiral helices. The only discrepancy arises for mixtures containing a higher fraction of **BTA (*S*)-Cha** since the optimal selectivities with and without additive slightly differ, 51.4±0.3% and 57.6% *e.e.*, respectively, despite the respective helices being homochiral. We assume that this gap is related to a slight difference in the conformation of the PPh_2 moiety and the related copper catalyst that modifies the energetic of the enantiodiscriminating event without affecting the optical purity of the helical main chain. The effect of the achiral BTA additive on the selectivity was also probed for diluted MR-type catalytic mixtures ([**BTA Cha**] set constant at 18.4 mM). Whilst reaching the optimal selectivity requires a significantly optically-enriched mixture of BTA enantiomers in absence of **BTA cyclohex** (*e.e.* in BTA Cha≥ 50% *e.e.*), a plateau is reached with a 20% *e.e.* scalemic

mixture in presence of **BTA cyclohex** ($|e.e._{max}|$ = 51.7±0.7%, Figure 4d). A mixture in BTA Cha slightly biased from the racemic mixture (10% *e.e.*) yields (*S*)-NPnol (+44.0% *e.e.*) and (*R*)-NPnol (-42.4% *e.e.*) when BTA (*R*)-Cha and BTA (*S*)-Cha are the majority enantiomers, respectively. The degree of selectivity provided by the catalyst is directly related to the optical purity of the supramolecular helices probed by CD spectroscopy, with the limitation that, again, homochiral helices with and without **BTA cyclohex** provide slightly different selectivities (51.6% and 57.0% *e.e.* respectively, Figure 4e).

The results obtained with these chirally-amplified helical catalysts deserve further comments. Significant selectivities are found for mixtures containing very low amounts of **BTA (*S*)-Cha** monomers (see highlight in Figure 4c). More specifically, for the mixtures with f_{Cha}= 0.25%, the addition of **BTA cyclohex** switches the state of the helical catalyst from non selective (*e.e.*< 1%) to significantly selective (50.4% *e.e.*). The fraction of **BTA (*S*)-Cha** (relatively to **BTA^{PPh2}**, 0.5%) and its catalytic loading (relatively to NPnone, 0.06 mol% *i.e.* 600 ppm) are fifty times and two times lower, respectively, than those reported for other chirally-amplified helical catalysts in the literature.[72, 87-88] Here, one molecule of **BTA (*S*)-Cha** is able to impose its chiral preference to 50 catalytically active copper centres that will conjointly produce 1667 molecules of NPnol, 75.2% of them being (*R*)-NPnol. Long-range chiral information transfer in these helical catalysts allows chirality inducers to be employed at drastically lower amount than the catalytic sites thus offering a strategy that circumvent the selectivity – activity paradigm, *i.e.* it paves the way towards a new class of active asymmetric catalysts which operate at ppm levels of chiral species.

III Conclusion

In conclusion, we disclose the ability of an achiral BTA monomer to fully bias the helicity of co-assemblies that are otherwise almost racemic in its absence, and which contain as little as 0.5% of sergeants (S&S effect) or a 10% *e.e.* scalemic mixture of enantiopure comonomers (diluted MR effect). This strategy, albeit counterintuitive at first sight, improves both the S&S and the diluted MR effect by two orders and one order of magnitude, respectively, thus reaching levels of chirality amplification that are usually achieved by the best, but distinct for each effect, supramolecular single helices reported to date. Precise investigation of the assembly behavior of the different BTA partners by different analytical techniques reveals that each monomer plays a precise role towards the generation of homochiral co-

assembly: the BTA ligand forms long but racemic and disordered stacks that favor the co-assembly of the other BTA monomers, the enantiopure co-monomer imposes a preferred-helical conformation to the BTA assemblies and the BTA achiral additive reduces the number of defects in the co-assembly. The last point is reflected by the absence of helix reversals in the 120 nm-long co-assemblies embedding *ca.* 170 monomers among which *ca.* one third are the achiral BTA additives. The MMP value seems also suitable for allowing high levels of chirality amplification by both the S&S and diluted MR effects. The helical catalysts generated from these homochiral co-assemblies display significant selectivities (> 50% *e.e.*) despite the limited amount of sergeant (600 ppm relatively to the substrate) or low optical purity of the sergeant (10−20% *e.e.*) present in the catalytic mixture. Further work is directed towards gathering higher chirality amplification in these helical assemblies, *e.g.* by changing the nature of the BTA partners in order to further increase the size of the objects, with the aim of developing a new class of asymmetric catalysts that operate at ultra low amount of chiral inducers but predictably promote the formation of the desired enantiomer.

IV Supplementary Figures.

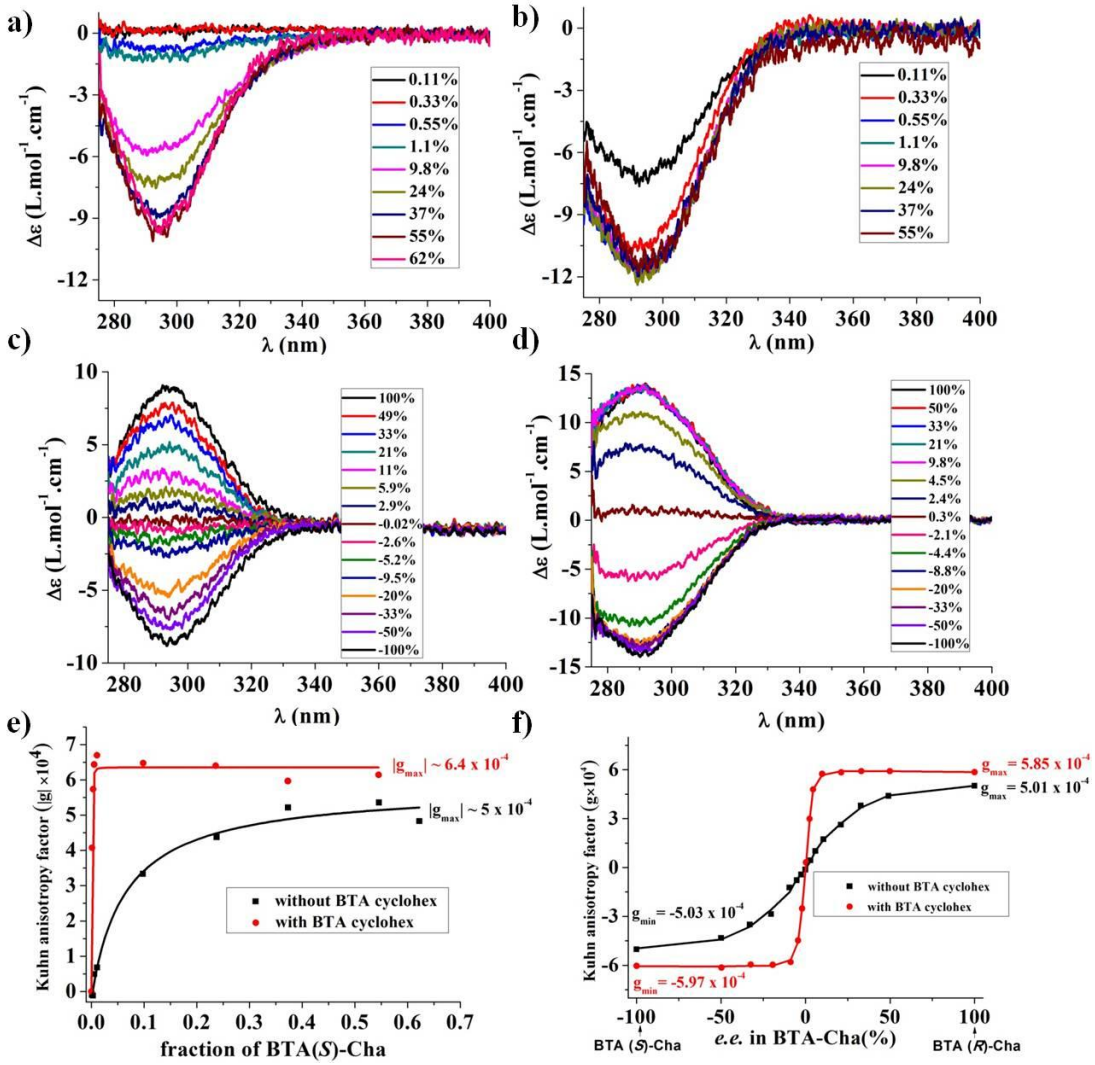

Figure S1 Effect of the achiral BTA additive on S&S and diluted MR effects performed at constant concentration in BTA monomers (5.84±0.2 mM). a) CD analyses of the S&S-type mixtures without **BTA cyclohex** ([BTA^{PPh2}]/[$Cu(OAc)_2{\cdot}H_2O$]= 4, 2.33 mM≤ [BTA^{PPh2}]≤ 5.82 mM, 0.0066 mM≤ [BTA (*S*)-Cha]≤ 3.84 mM). b) CD analyses of the S&S-type mixtures with **BTA cyclohex** ([BTA^{PPh2}]/[$Cu(OAc)_2{\cdot}H_2O$]= 4, [BTA^{PPh2}]/[BTA cyclohex]= 1, 1.36 mM≤ [BTA^{PPh2}]≤ 2.90 mM, 0.0064 mM≤ [BTA (*S*)-Cha]≤ 3.26 mM, 1.36 mM≤ [BTA cyclohex]≤ 2.90 mM). c) CD analyses of the diluted majority-rules type mixtures without **BTA cyclohex** ([BTA^{PPh2}]/[$Cu(OAc)_2{\cdot}H_2O$]= 4, [BTA^{PPh2}] set constant at 2.79±0.03 mM, f_{Cha}= 0.52). d) CD analyses of the diluted majority-rules type mixtures with **BTA cyclohex** ([BTA^{PPh2}]/[$Cu(OAc)_2{\cdot}H_2O$]= 4, [BTA^{PPh2}] and [BTA cyclohex] set constant at 1.39±0.02 mM, f_{Cha}= 0.52). e) Kuhn anisotropy factor (g) measured at λ= 295 nm as a function of the fraction of **BTA (*S*)-Cha** in the mixtures. Lines are guides for the eye. f) Kuhn anisotropy factor (g) measured at λ= 295 nm as a function of the optical purity in **BTA Cha** in the mixtures. Lines are guides for the eye. The CD signal is reported in molar extinction coefficient as Δε= θ/(32982×[BTA^{PPh2}]×l) in which θ is the measured ellipticity in mdeg and l is the path length of the quartz cell in cm.

Interpretation: In presence of **BTA cyclohex**, both S&S and diluted MR effects are enhanced in the same proportion as observed for the experiments performed at constant concentration in [BTA^{PPh2}] (Figures 1 and 2). However, the $|g_{max}|$ values obtained in the S&S experiments without additive and in the diluted MR experiments both with and without additive are lower than the $|g_{max}|$ values reached for the experiments performed at constant concentration in [BTA^{PPh2}]. The fact that a homochiral state is not reached under these conditions probably comes from the lower concentration in [BTA^{PPh2}] since relatively short assemblies of the BTA ligand can be expected close to its critical concentration (measured at ≈ 0.5 mM).[73]

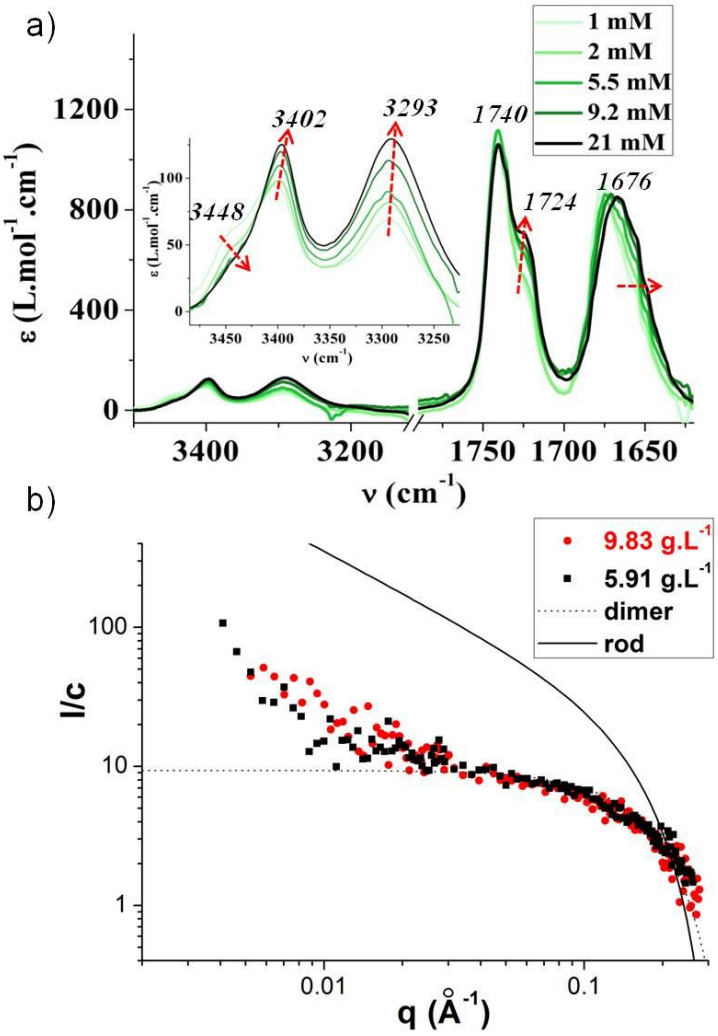

Figure S2 Characterization of the self-assemblies formed by **BTA cyclohex** (293K). a) FT-IR spectra at different concentrations in toluene (Inset: zoom on the N−H region). Tentative assignment of the N−H and C=O bands: free N−H (3448 cm^{-1}), N−H bonded to ester C=O (3402 cm^{-1}),[35, 69-70, 93] N−H weakly bonded to amide C=O (3293 cm^{-1}), free ester C=O (1740 cm^{-1}), bonded ester C=O (1724 cm^{-1}),[35, 69-70, 93] and free/weekly bonded amide C=O (1676 cm^{-1}, the fact that this band is broad means that there is a large distribution of carbonyl functions in the self-assemblies). b) SANS analyses at 5.91 $g.L^{-1}$ (5.42 mM) and 9.83 $g.L^{-1}$ (9.01 mM) in C_7D_8 together with the theoretical curves expected for a dimer (sphere of radius 12Å) or for a rod (infinitely long cylinder of radius 12Å).

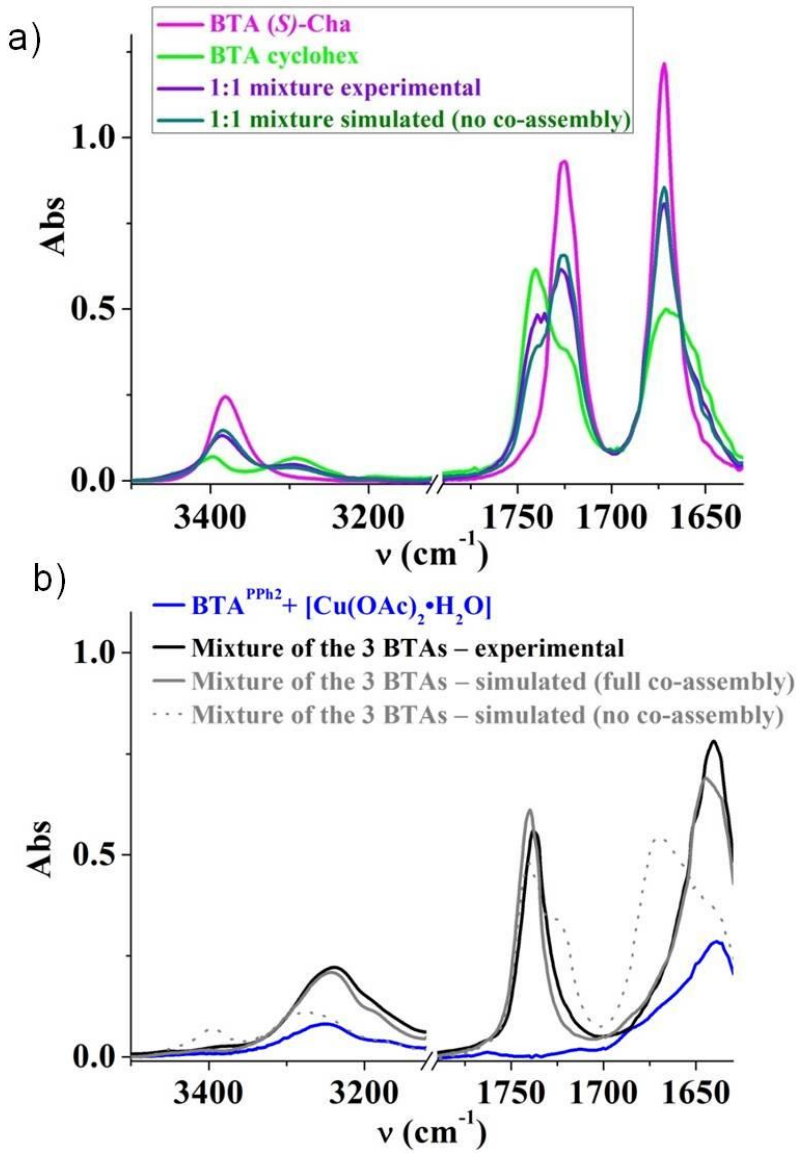

Figure S3 Characterization of the assemblies (293K). a) between **BTA (*S*)-Cha** and **BTA cyclohex**. FT-IR spectra of **BTA (*S*)-Cha** (5.8 mM), **BTA cyclohex** (5.8 mM) and of their 1:1 mixture in toluene. The experimental spectrum for the mixture is shown together with the simulated spectrum for segregated assemblies (no co-assembly, sum of the individual spectra). Zoom on the N-H and the C=O regions. b) between **BTA^{PPh2}·Cu**, **BTA (*S*)-Cha** and **BTA cyclohex** (f_{Cha}= 0.048). FT-IR spectra of the mixture between **BTA^{PPh2}** (5.8 mM) and [$Cu(OAc)_2$•H_2O] (1.45 mM) and of the mixture between **BTA^{PPh2}** (5.8 mM), [$Cu(OAc)_2$•H_2O] (1.45 mM), **BTA (*S*)-Cha** (0.58 mM) and **BTA cyclohex** (5.8 mM) in toluene. Simulated spectra for segregated assemblies and for full co-assembly. The simulated spectrum for full co-assembly was obtained by considering that all **BTA (*S*)-Cha** and **BTA cyclohex** monomers adopt the conformation of **BTA Aib** monomers in the co-assembled helical stacks (*i.e.* that they have the same IR spectrum).[69] The good agreement of this simulation with the experimental spectrum means that most of the BTA monomers stack into the same helical co-assembly (fraction≥ 90% by considering the measurement uncertainty). Zoom on the N-H and the C=O regions.

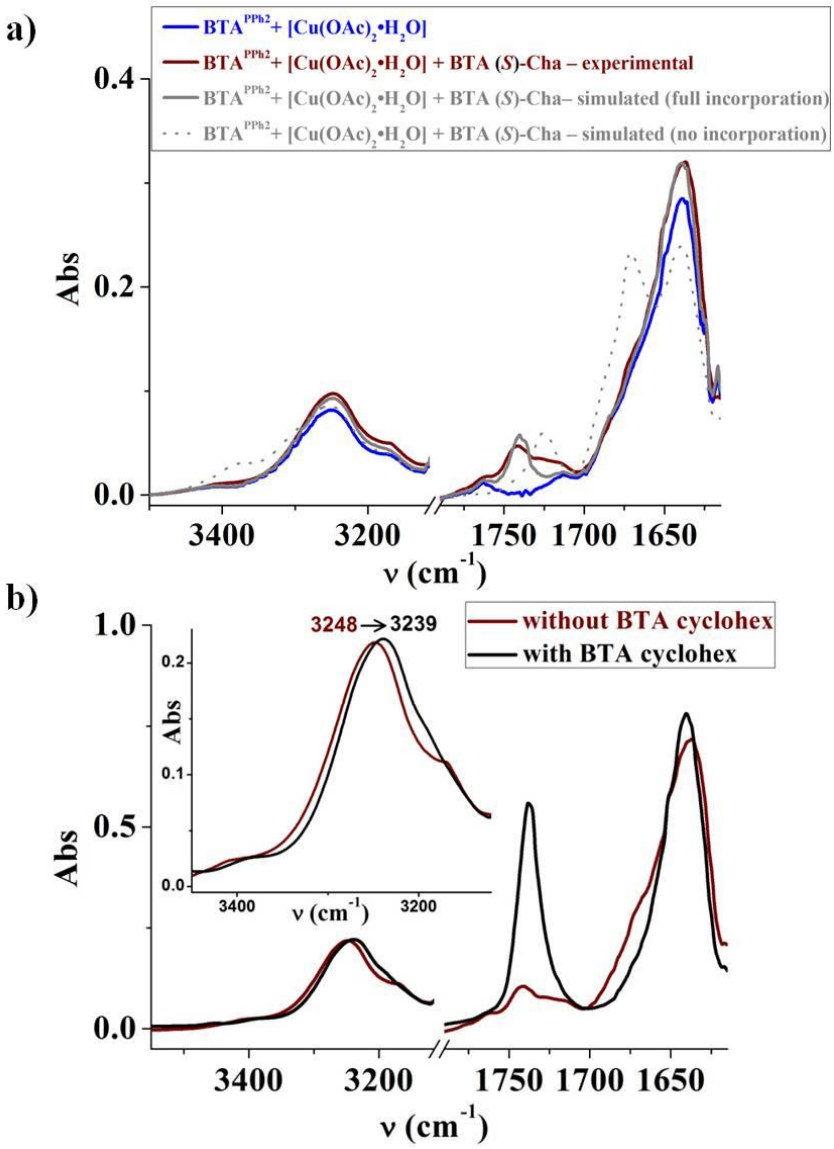

Figure S4 Probing the role of BTA cyclohex in the co-assemblies. a) Characterization of the co-assemblies between **BTA^{PPh2}·Cu** and **BTA (*S*)-Cha** (f_{Cha}= 0.090). FT-IR spectrum of the mixture between **BTA^{PPh2}** (5.8 mM), [$Cu(OAc)_2$•H_2O] (1.45 mM) and **BTA (*S*)-Cha** (0.58 mM) in toluene. Simulated spectra for segregated assemblies and for full co-assembly. The simulated spectrum for full co-assembly was obtained by considering that all **BTA (*S*)-Cha** monomers adopt the conformation of **BTA Aib** monomers in the co-assembled helical stacks (*i.e.* that they have the same IR spectrum).[69] The good agreement of this simulation with the experimental spectrum means that most of the BTA monomers stack into the same helical co-assembly (fraction≥ 90% by considering the measurement uncertainty). Zoom on the N-H and the C=O regions. b) Overlap of the FT-IR spectra of the mixtures with and without **BTA cyclohex** (see composition in the caption of Figures S3b and S4a, respectively). The spectra have been normalized at the same absorbance value for ν= 3247 cm^{-1}. The major difference is the higher intensity of the band at ν= 1738 cm^{-1} which is related to the free ester C=O functions of **BTA cyclohex** in the co-assemblies. Minor differences are: i) the shift of the maximum N-H band from 3248 to 3239 cm^{-1} and ii) the narrowing of the amide I band in presence of **BTA cyclohex**. Both observations support the formation of a stronger and more regular intermolecular hydrogen bond network in the presence of the achiral BTA additive.

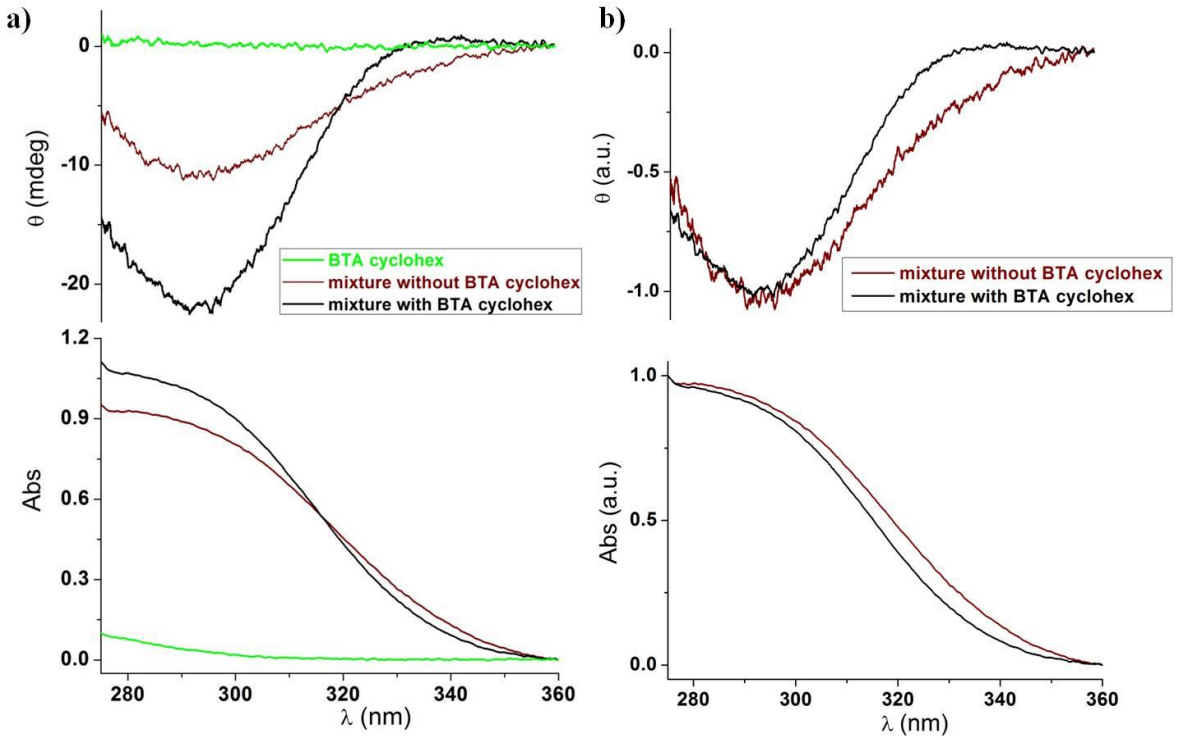

Figure S5 Probing the role of BTA cyclohex in the co-assemblies (2). a) CD (top) and UV-Vis analyses (bottom) of mixtures with and without of **BTA cyclohex** (see composition in the caption of Figures S3b and S4a, respectively) and of **BTA cyclohex**. b) CD (top) and UV-Vis analyses (bottom) of mixtures with and without of **BTA cyclohex** normalized at the maxima of the CD signal or UV-Vis main absorption band.

General procedures

Fourier-Transform Infrared (FT-IR) analyses: FT-IR measurements were performed on a Nicolet iS10 spectrometer. Spectra were measured in 0.1 cm pathlength CaF_2 cells at 293 K and were corrected for air, solvent and cell absorption.

Circular dichroism (CD) analyses*:* CD measurements were performed on a Jasco J-1500 spectrometer equipped with a Peltier thermostated cell holder and Xe laser. Data were recorded at 20°C with the following parameters: 50 $nm.min^{-1}$ sweep rate, 0.05 nm data pitch, 2.0 nm bandwidth, and between 400 and 275 nm. All solutions were pre-heated before measurements. Toluene and cell contributions at the same temperature were subtracted from the obtained signals. Cylindrical spectrosil quartz cells (Starna® 31/Q/0/1 and 31/Q/0.2) of 0.10 and 0.20 mm pathlength were used. For all samples, LD contribution was negligible ($\Delta LD < 0.005$ dOD) and the shape of the CD signal was independent of the orientation of the quartz cells. Molar CD values are reported in $L.mol^{-1}.cm^{-1}$ and are expressed as follows: $\Delta\varepsilon=\theta/(32980\times l\times c)$ where θ is the measured ellipticity (mdeg), l is the optical path length in cm, and c is the **BTA^{PPh2}** concentration in $mol.L^{-1}$.

Small-angle neutron scattering (SANS) analyses: SANS measurements were made at the LLB (Saclay, France) on the PA20 instrument, at three distance-wavelength combinations to cover the 2×10^{-3} to $0.3Å^{-1}$ *q*-range, where the scattering vector q is defined as usual, assuming elastic scattering, as $q=(4\pi/\lambda)\sin(\theta/2)$, where θ is the angle between incident and scattered beam. Data were corrected for the empty cell signal and the solute and solvent incoherent background. A light water standard was used to normalize the scattered intensities to cm^{-1} units. The data was fitted with the DANSE software SasView. The number *n* of molecule in the cross-section can be derived from n_L (the number of molecule per unit length)[94] by assuming an average intermolecular distance of 3.62 Å, which is the usual spacing between aromatic rings in BTA helical assemblies.

Preparation of the solutions for CD analyses (Figure 1 and 2). S&S-type experiments ([BTA^{PPh2}] set constant at 5.8 mM): **v**ials were loaded with $Cu(OAc)_2\cdot H_2O$ (0.28 mg) and **BTA^{PPh2}** (4.0 mg) in dry THF (500 µL) and the mixture was stirred for 30 minutes. The solvent was removed under vacuum and the tube was further put under vacuum (1.10^{-3} mbar) for 1 hour. The desired amount of **BTA (*S*)-Cha** was added to vials, and then 6.2 mg **BTA cyclohex** were added to tubes for the CD measurements with the achiral BTA additive. The total solvent volume is set to 1.0 mL. MR-type experiments ([BTA^{PPh2}] set constant at 5.8 mM): vials were loaded with $Cu(OAc)_2\cdot H_2O$ (0.28 mg) and **BTA^{PPh2}** (4.0 mg) in dry THF (500 µL) and the mixture was stirred for 30 minutes. The solvent was removed under vacuum and

the tube was further put under vacuum (1.10^{-3} mbar) for 1 hour. A mixture of **BTA Cha** monomers with the desired *e.e.* (7.5 mg in total) was added to vials, and then 6.2 mg **BTA cyclohex** were added to tubes for the CD measurements with the achiral BTA additive. The total solvent volume is set to 1.0 mL.

Catalytic experiments

In all catalytic experiments a *pre-catalytic mixture* composed of the ligand, the copper salt and the substrate was prepared as follows: a tube was loaded with $Cu(OAc)_2 \cdot H_2O$ (0.5 mg, 3.0 mol%) and **BTA^{PPh2}** (6.9 mg, 12.0 mol%) in dry THF (500 µL) and the mixture was stirred for 30 minutes. The solvent was removed under vacuum and the tube was further put under vacuum (1.10^{-3} mbar) for 1 hour. Then 1-(4-nitrophenyl)ethanone (14.0 mg, 0.085 mmol, 100 mol%) was added before flushing the tube with argon for 10 seconds.

Then, the desired amount of **BTA (*S*)-Cha** or the mixture of **BTA Cha** monomers with the desired *e.e.* as well as **BTA cyclohex** (10.9 mg, 12.0 mol%) were added to the tube as well as dry toluene. The total solvent volume was set equal to 600 µL. The mixture was stirred for 15 min at room temperature, and then the solution was briefly heated to reflux. After cooling down to room temperature, $PhSiH_3$ (21.0 µL, 0.17 mmol, 200 mol%) was added to the tube and the reaction mixture was stirred for 12 hours before being hydrolyzed with aqueous HCl and analyzed by ^{1}H NMR and chiral GC.

S&S-type type catalytic experiments: A 10.0 mM stock solution of **BTA (*S*)-Cha** was prepared by mixing 11.7 mg of **BTA (*S*)-Cha** and 1.0 mL (867 mg) of toluene. Then 1.0 mM and 0.1 mM stock solutions were prepared by dilution. Then the desired amount of **BTA (*S*)-Cha** monomers was introduced: 86.7 mg of the 0.1 mM stock solution (16 µM), 43.4 mg of the 1.0 mM stock solution (80 µM), 86.7 mg of the 1.0 mM stock solution (160 µM), 86.7 mg of the 10.0 mM stock solution (1.6 mM), 238.4 mg of the 10.0 mM stock solution (4.4 mM), 6.5 mg of solid **BTA (*S*)-Cha** (9.3 mM) and 12.9 mg of solid **BTA (*S*)-Cha** (18.4 mM).

MR-type type catalytic experiments: 110.0 mM stock solutions of **BTA (*S*)-Cha** and **BTA (*R*)-Cha** were prepared by mixing 117.0 mg of the respective monomers and 1.0 mL (867 mg) of toluene. These 110.0 mM stock solutions were mixed together in order to get the solutions with desired *e.e.* Then 86.7 mg of the solution was added to the tube.

Chiral GC analyses: 1-(4-nitrophenyl)ethanol (NPnol). The optical purity was determined by GC analysis: Chiral Cyclosil-B column, 30 m × 250 µm x 0.25 µm, inlet pressure = 12.6 psi. Injection temperature = 250°C; detector temperature = 300°C; column temperature = 145°C. Retention time: 17.9 min (1-(4-nitrophenyl)ethanone), 47.6 min ((*R*)-enantiomer), 49.9 min ((*S*)-enantiomer).[95]

Synthetic procedures

Materials preparation and methods: The synthesis and characterization of **BTA^{PPh2}**,[73] of **BTA (*S*)-Cha**[69] and of **BTA (*R*)-Cha**[69] have been described previously. **BTA (*S*)-Cha** and **BTA (*R*)-Cha** monomers used in this study have been purified by preparative HPLC. 1-Aminocyclohexanecarboxylic acid was purchased from Sigma-Aldrich and used as received. Benzene-1,3,5-tricarbonyl chloride, 1-(4-nitrophenyl)ethanone (>98%), $PhSiH_3$ (>97%) and $Cu(OAc)_2{\cdot}H_2O$ (>99%) were purchased from Alfa Aesar. 1-dodecanol and *p*-TsOH.H_2O were acquired from Sigma Aldrich and were used directly. Unless otherwise noted, chromatography-grade solvents were used as received. Dried solvents were obtained from an SPS solvent purification system (IT-Inc). NMR spectra were recorded on a Bruker Avance 300 spectrometer and calibrated to the residual solvent peak: DMSO-d_6 (^{1}H: 2.50 ppm; ^{13}C: 39.52 ppm); Acetone-d6 (^{1}H: 2.05 ppm; ^{13}C: 29.84 ppm). Peaks are reported with their corresponding multiplicity (s: singlet; d: doublet, t: triplet; q: quartet; p: pentuplet; hept: heptuplet; dt: doublet of triplets; td: triplet of doublets) and integration, and respective *J* coupling constants are given in Hertz. Exact mass measurements (HRMS) were obtained on TQ R30-10 HRMS spectrometer by ESI+ ionization and are reported in m/z for the major signal.

Synthesis of **BTA cyclohex**:

Step 1: Synthesis of dodecyl ester *p*-TsOH salt of 1-aminocyclohexanecarboxylic acid

In a Dean-Stark apparatus-mounted one-neck flask, 1-aminocyclohexanecarboxylic acid (1.0 equiv., 7.0 mmol) is suspended in toluene (0.047 M, 150 mL), and *p*-TsOH.H_2O (1.2 eq., 8.4 mmol) is added at room temperature. Dodecanol (1.1 eq., 7.7 mmol) is then added, and the resulting slurry is stirred at reflux temperature until the mixture turns totally clear. After cooling the reaction mixture to room temperature, the crude reaction mixture is evaporated under reduced pressure to give a thick oil or a solid. This residue is taken up in *ca.* 70 mL of Et_2O, gently heated to 35°C, and let cool in an ice bath. The resulting precipitate is filtered under vacuum and washed with ice cold ether to remove residual reactants. The white solid is then dried under vacuum to yield the pure ammonium tosylate salt (90% yield). ^{1}H NMR (400 MHz, DMSO-d_6) δ (ppm) = 8.37 (s, 3H), 7.47 (d, 2H), 7.12(d, 2H), 4.18 (t, ^{3}J=6.5 Hz, 2H), 2.29 (s, 3H), 2.02-1.15 (m, 30H), 0.87 (t, 3H). ^{13}C{^{1}H} NMR (101 MHz, DMSO-d_6) δ(ppm)= 171.42, 128.49, 125.95, 66.43, 59.14, 31.72, 28.99, 28.34, 24.29, 22.55, 21.24, 20.71, 14.41. HRMS (ESI, *m/z*): Calculated for $C_{19}H_{38}NO_2$, $[M\text{-}OTs]^+$: 312.2897, found: 312.2896.

Step 2: Synthesis of BTAcyclohex:

In a flame-dried round-bottom flask under argon atmosphere, benzene-1,3,5-tricarbonyl chloride (1.0 equiv., 3.0 mmol) is dissolved in dry CH_2Cl_2 (100 mL) at room temperature. The ammonium tosylate salt (3.3 equiv., 9.9 mmol) is then added in one portion, and the resulting mixture is cooled to 0°C with an ice/water bath. Dry Et_3N (6.6 equiv., 19.8 mmol) is then added dropwise, the reaction is let warm to room temperature and stirred for 36h. Brine is then added to the flask, and the crude mixture is extracted thrice with CH_2Cl_2. The combined organic phases are dried over $MgSO_4$, filtered, and the solvent is evaporated under reduced pressure. The product is then purified by column chromatography on silica gel, eluting with DCM/EtOAc 100:0 – 85:15 gradient yielding B**TAcyclohex** as an off-white gum (40% yield). ^{1}H NMR (acetone-d_6): δ (ppm) = 8.39(s, 3H), 7.98 (s, 3H), 4.07(t, ^{3}J=6.5 Hz, 6H), 2.30-2.15 (m, 6H), 2.01-1.91(m, 4H), 1.77-1.10 (m, 80H), 0.87 (t, 9H). ^{13}C{^{1}H} NMR (acetone-d_6): δ (ppm)= 174.48, 166.45, 136.13, 129.80, 65.22, 60.35, 33.28, 32.67, 26.72, 26.23, 23.36, 22.50, 14.38. HRMS (ESI, *m/z*): Calculated for $C_{66}H_{111}N_3O_9Na$, $[M+Na]^+$: 1112.8213, found: 1112.8224. FT-IR (ATR, cm^{-1}): 606 (m), 680 (m), 1139 (s), 1202 (s), 1295 (m), 1370 (w), 1451 (m), 1551 (s), 1632 (s), 1732 (s), 2848 (s), 2923 (s), 3054 (w), 3228 (w).

NMR spectra

Ammonium tosylate salt

^{1}H NMR (DMSO-d_6)

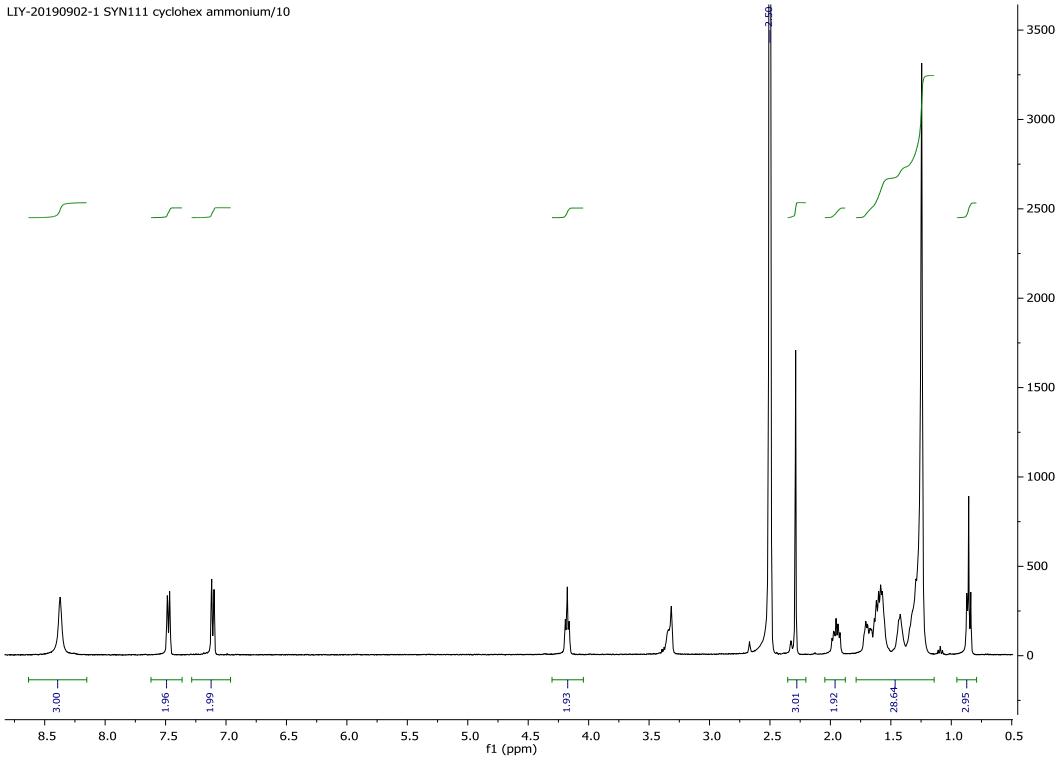

^{13}C{^{1}H} NMR (DMSO-d_6)

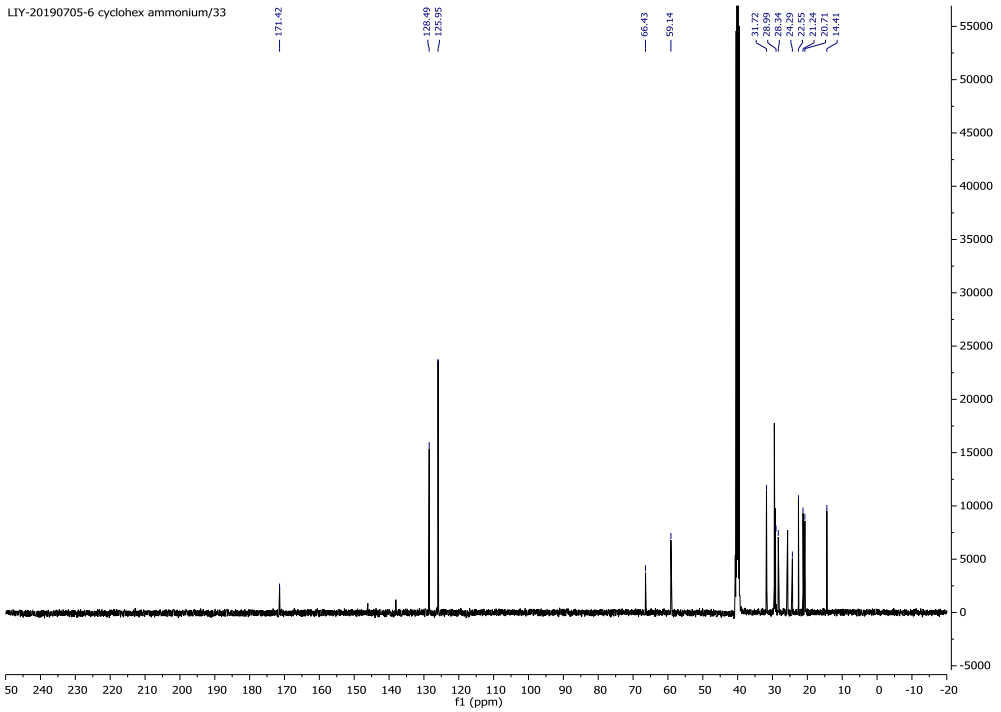

BTA cyclohex

^{1}H NMR (acetone-d_6)

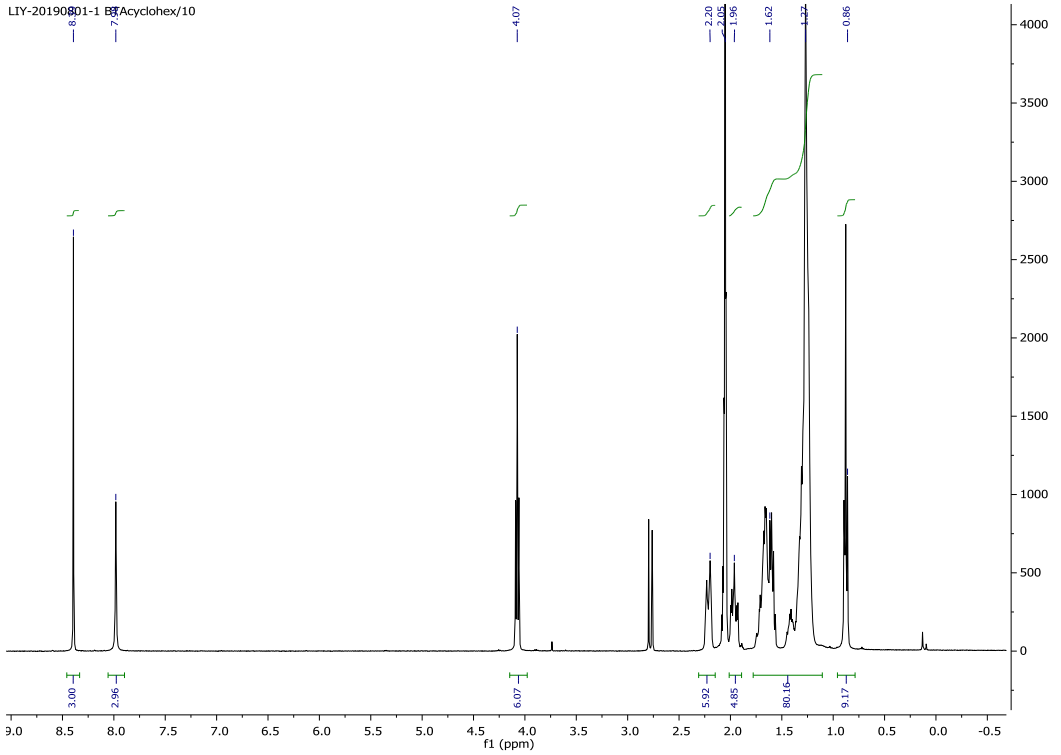

^{13}C{^{1}H} NMR (acetone-d_6)

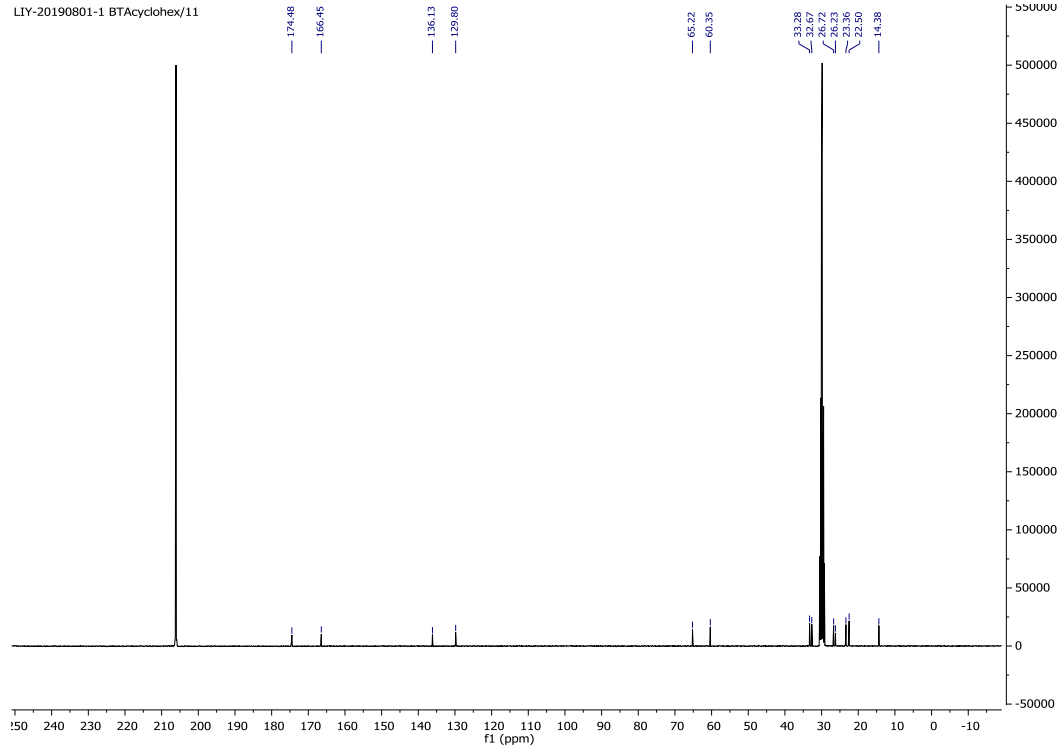

V References

1. Noyori, R.; Kitamura, M., Enantioselective Addition of Organometallic Reagents to Carbonyl-Compounds - Chirality Transfer, Multiplication, and Amplification. *Angew. Chem. Int. Ed. Engl.* **1991,** *30* (1), 49-69.

2. Satyanarayana, T.; Abraham, S.; Kagan, H. B., Nonlinear Effects In Asymmetric Catalysis. *Angew. Chem. Int. Ed.* **2009,** *48* (3), 456-494.

3. Palmans, A. R. A., Deracemisations under kinetic and thermodynamic control. *Mol. Syst. Des. Eng.* **2017,** *2* (1), 34-46.

4. Storch, G.; Trapp, O., By-design enantioselective self-amplification based on non-covalent product-catalyst interactions. *Nat. Chem.* **2017,** *9* (2), 179-187.

5. Soai, K.; Kawasaki, T.; Matsumoto, A., Asymmetric Autocatalysis of Pyrimidyl Alkanol and Its Application to the Study on the Origin of Homochirality. *Acc. Chem. Res.* **2014,** *47* (12), 3643-3654.

6. Green, M. M.; Park, J. W.; Sato, T.; Teramoto, A.; Lifson, S.; Selinger, R. L. B.; Selinger, J. V., The macromolecular route to chiral amplification. *Angew. Chem. Int. Ed.* **1999,** *38* (21), 3139-3154.

7. Yashima, E.; Maeda, K.; Iida, H.; Furusho, Y.; Nagai, K., Helical Polymers: Synthesis, Structures, and Functions. *Chem. Rev.* **2009,** *109* (11), 6102-6211.

8. Yashima, E.; Ousaka, N.; Taura, D.; Shimomura, K.; Ikai, T.; Maeda, K., Supramolecular Helical Systems: Helical Assemblies of Small Molecules, Foldamers, and Polymers with Chiral Amplification and Their Functions. *Chem. Rev.* **2016,** *116* (22), 13752-13990.

9. Prins, L. J.; Timmerman, P.; Reinhoudt, D. N., Amplification of Chirality: The "Sergeants and Soldiers" Principle Applied to Dynamic Hydrogen-Bonded Assemblies. *J. Am. Chem. Soc.* **2001,** *123*, 10153-10163.

10. Palmans, A. R. A.; Meijer, E. W., Amplification of chirality in dynamic supramolecular aggregates. *Angew. Chem. Int. Ed.* **2007,** *46* (47), 8948-8968.

11. Green, M. M.; Peterson, N. C.; Sato, T.; Teramoto, A.; Cook, R.; Lifson, S., A Helical Polymer with a Cooperative Response to Chiral Information. *Science* **1995,** *268* (5219), 1860-1866.

12. Cantekin, S.; Balkenende, D. W. R.; Smulders, M. M. J.; Palmans, A. R. A.; Meijer, E. W., The effect of isotopic substitution on the chirality of a self-assembled helix. *Nat. Chem.* **2011,** *3* (1), 42-46.

13. Li, Y.; Bouteiller, L.; Raynal, M., Catalysts Supported by Homochiral Molecular Helices: A New Concept to Implement Asymmetric Amplification in Catalytic Science. *ChemCatChem* **2019**, 10.1002/cctc.201901246.

14. Shimomura, K.; Ikai, T.; Kanoh, S.; Yashima, E.; Maeda, K., Switchable enantioseparation based on macromolecular memory of a helical polyacetylene in the solid state. *Nat. Chem.* **2014,** *6* (5), 429-434.

15. Shen, Z. C.; Wang, T. Y.; Shi, L.; Tang, Z. Y.; Liu, M. H., Strong circularly polarized luminescence from the supramolecular gels of an achiral gelator: tunable intensity and handedness. *Chem. Sci.* **2015,** *6* (7), 4267-4272.

16. Nagata, Y.; Uno, M.; Suginome, M., Three-Way-Switchable (Right/Left/OFF) Selective Reflection of Circularly Polarized Light on Solid Thin Films of Helical Polymer Blends. *Angew. Chem. Int. Ed.* **2016,** *55* (25), 7126-7130.

17. Green, M. M.; Reidy, M. P.; Johnson, R. J.; Darling, G.; Oleary, D. J.; Willson, G., Macromolecular Stereochemistry - the out-of-Proportion Influence of Optically-Active Co-Monomers on the Conformational Characteristics of Polyisocyanates - the Sergeants and Soldiers Experiment. *J. Am. Chem. Soc.* **1989,** *111* (16), 6452-6454.

18. Green, M. M.; Garetz, B. A.; Munoz, B.; Chang, H. P.; Hoke, S.; Cooks, R. G., Majority Rules in the Copolymerization of Mirror-Image Isomers. *J. Am. Chem. Soc.* **1995,** *117* (14), 4181-4182.

19. Selinger, J. V.; Selinger, R. L. B., Cooperative chiral order in polyisocyanates: New statistical problems. *Macromolecules* **1998,** *31* (8), 2488-2492.

20. Jha, S. K.; Cheon, K. S.; Green, M. M.; Selinger, J. V., Chiral optical properties of a helical polymer synthesized from nearly racemic chiral monomers highly diluted with achiral monomers. *J. Am. Chem. Soc.* **1999,** *121* (8), 1665-1673.

21. van Gestel, J.; van der Schoot, P.; Michels, M. A. J., Amplification of chirality in helical supramolecular polymers. *Macromolecules* **2003,** *36* (17), 6668-6673.

22. van Gestel, J., Amplification of chirality in helical supramolecular polymers: The majority-rules principle. *Macromolecules* **2004,** *37* (10), 3894-3898.

23. van Gestel, J.; van der Schoot, P.; Michels, M. A. J., Amplification of chirality in helical supramolecular polymers beyond the long-chain limit. *J. Chem. Phys.* **2004,** *120* (17), 8253-8261.

24. van Gestel, J., Amplification of Chirality of the Majority-Rules Type in Helical Supramolecular Polymers: The Impact of the Presence of Achiral Monomers. *J. Phys. Chem. B* **2006,** *110*, 4365-4370.

25. Markvoort, A. J.; ten Eikelder, H. M. M.; Hilbers, P. A. J.; de Greef, T. F. A.; Meijer, E. W., Theoretical models of nonlinear effects in two-component cooperative supramolecular copolymerizations. *Nat. Commun.* **2011,** *2*, 509.

26. ten Eikelder, H. M. M.; Markvoort, A. J.; de Greef, T. F. A.; Hilbers, P. A. J., An Equilibrium Model for Chiral Amplification in Supramolecular Polymers. *J. Phys. Chem. B* **2012,** *116* (17), 5291-5301.

27. ten Eikelder, H. M. M.; Adelizzi, B.; Palmans, A. R. A.; Markvoort, A. J., Equilibrium Model for Supramolecular Copolymerizations. *J. Phys. Chem. B* **2019,** *123* (30), 6627-6642.

28. de Windt, L. N. J.; Kulkarni, C.; ten Eikelder, H. M. M.; Markvoort, A. J.; Meijer, E. W.; Palmans, A. R. A., Detailed Approach to Investigate Thermodynamically Controlled Supramolecular Copolymerizations. *Macromolecules* **2019,** *52*, 7430-7438.

29. Brunsfeld, L.; Lohmeijer, B. G. G.; Vekemans, J. A. J. M.; Meijer, E. W., Amplification of chirality in helical supramolecular columns. *J. Incl. Phenom. Macro.* **2001,** *41* (1-4), 61-64.

30. Haino, T.; Tanaka, M.; Fukazawa, Y., Self-assembly of tris(phenylisoxazolyl) benzene and its asymmetric induction of supramolecular chirality. *Chem. Commun.* **2008,** (4), 468-470.

31. Nam, S. R.; Lee, H. Y.; Hong, J. I., Control of macroscopic helicity by using the sergeants-and-soldiers principle in organogels. *Chem. Eur. J.* **2008,** *14* (20), 6040-6043.

32. Ishi-i, T.; Kuwahara, R.; Takata, A.; Jeong, Y.; Sakurai, K.; Mataka, S., An enantiomeric nanoscale architecture obtained from a pseudoenantiomeric aggregate: Covalent fixation of helical chirality formed in self-assembled discotic triazine triamides by chiral amplification. *Chem. Eur. J.* **2006,** *12* (3), 763-776.

33. Tanaka, M.; Ikeda, T.; Mack, J.; Kobayashi, N.; Haino, T., Self-Assembly and Gelation Behavior of Tris(phenylisoxazolyl)benzenes. *J. Org. Chem.* **2011,** *76* (12), 5082-5091.

34. Cao, H.; Yuan, Q. Z.; Zhu, X. F.; Zhao, Y. P.; Liu, M. H., Hierarchical Self-Assembly of Achiral Amino Acid Derivatives into Dendritic Chiral Nanotwists. *Langmuir* **2012,** *28* (43), 15410-15417.

35. Desmarchelier, A.; Raynal, M.; Brocorens, P.; Vanthuyne, N.; Bouteiller, L., Revisiting the assembly of amino ester-based benzene-1,3,5-tricarboxamides: chiral rods in solution. *Chem Commun* **2015,** *51* (34), 7397-7400.

36. Kim, T.; Mori, T.; Aida, T.; Miyajima, D., Dynamic propeller conformation for the unprecedentedly high degree of chiral amplification of supramolecular helices. *Chem. Sci.* **2016,** *7*, 6689-6694.

37. Karunakaran, S. C.; Cafferty, B. J.; Weigert-Munoz, A.; Schuster, G. B.; Hud, N. V., Spontaneous Symmetry Breaking in the Formation of Supramolecular Polymers: Implications for the Origin of Biological Homochirality. *Angew. Chem. Int. Ed.* **2019,** *58* (5), 1453-1457.

38. Isare, B.; Linares, M.; Zargarian, L.; Fermandjian, S.; Miura, M.; Motohashi, S.; Vanthuyne, N.; Lazzaroni, R.; Bouteiller, L., Chirality in Dynamic Supramolecular Nanotubes Induced by a Chiral Solvent. *Chem. Eur. J.* **2010,** *16* (1), 173-177.

39. Cao, H.; Zhu, X. F.; Liu, M. H., Self-Assembly of Racemic Alanine Derivatives: Unexpected Chiral Twist and Enhanced Capacity for the Discrimination of Chiral Species. *Angew. Chem. Int. Ed.* **2013,** *52* (15), 4122-4126.

40. El-Hachemi, Z.; Arteaga, O.; Canillas, A.; Crusats, J.; Escudero, C.; Kuroda, R.; Harada, T.; Rosa, M.; Ribo, J. M., On the mechano-chiral effect of vortical flows on the dichroic spectra of 5-phenyl-10,15,20-tris(4-sulfonatophenyl)porphyrin J-aggregates. *Chem. Eur. J.* **2008,** *14* (21), 6438-6443.

41. Crusats, J.; El-Hachemi, Z.; Ribo, J. M., Hydrodynamic effects on chiral induction. *Chem. Soc. Rev.* **2010,** *39* (2), 569-577.

42. Micali, N.; Engelkamp, H.; van Rhee, P. G.; Christianen, P. C. M.; Scolaro, L. M.; Maan, J. C., Selection of supramolecular chirality by application of rotational and magnetic forces. *Nat. Chem.* **2012,** *4* (3), 201-207.

43. Kim, J.; Lee, J.; Kim, W. Y.; Kim, H.; Lee, S.; Lee, H. C.; Lee, Y. S.; Seo, M.; Kim, S. Y., Induction and control of supramolecular chirality by light in self-assembled helical nanostructures. *Nat. Commun.***2015,** *6*.

44. Sun, J. S.; Li, Y. K.; Yan, F. S.; Liu, C.; Sang, Y. T.; Tian, F.; Feng, Q.; Duan, P. F.; Zhang, L.; Shi, X. H.; Ding, B. Q.; Liu, M. H., Control over the emerging chirality in supramolecular gels and solutions by chiral microvortices in milliseconds. *Nat. Commun.* **2018,** *9*.

45. Sang, Y. T.; Yang, D.; Duan, P. F.; Liu, M. H., Towards homochiral supramolecular entities from achiral molecules by vortex mixing-accompanied self-assembly. *Chem. Sci.* **2019,** *10* (9), 2718-2724.

46. Hu, J. G.; Xie, Y. F.; Zhang, H. L.; He, C. L.; Zhang, Q. J.; Zou, G., Chiral induction, modulation and locking in porphyrin based supramolecular assemblies with circularly polarized light. *Chem. Commun.* **2019,** *55* (34), 4953-4956.

47. Stals, P. J. M.; Korevaar, P. A.; Gillissen, M. A. J.; de Greef, T. F. A.; Fitie, C. F. C.; Sijbesma, R. P.; Palmans, A. R. A.; Meijer, E. W., Symmetry Breaking in the Self-Assembly of Partially Fluorinated Benzene-1,3,5-tricarboxamides. *Angew. Chem. Int. Ed.* **2012,** *51* (45), 11297-11301.

48. Shen, Z. C.; Wang, T. Y.; Liu, M. H., Macroscopic Chirality of Supramolecular Gels Formed from Achiral Tris(ethyl cinnamate) Benzene-1,3,5-tricarboxamides. *Angew. Chem. Int. Ed.* **2014,** *53* (49), 13424-13428.

49. Shen, Z. C.; Jiang, Y. Q.; Wang, T. Y.; Liu, M. H., Symmetry Breaking in the Supramolecular Gels of an Achiral Gelator Exclusively Driven by pi-pi Stacking. *J. Am. Chem. Soc.* **2015,** *137* (51), 16109-16115.

50. Sang, Y. T.; Liu, M. H., Symmetry Breaking in Self-Assembled Nanoassemblies. *Symmetry* **2019,** *11* (8), 950; doi:10.3390/sym11080950.

51. Smulders, M. M. J.; Stals, P. J. M.; Mes, T.; Paffen, T. F. E.; Schenning, A. P. H. J.; Palmans, A. R. A.; Meijer, E. W., Probing the Limits of the Majority-Rules Principle in a Dynamic Supramolecular Polymer. *J. Am. Chem. Soc.* **2010,** *132* (2), 620-626.

52. Garcia, F.; Sanchez, L., Structural Rules for the Chiral Supramolecular Organization of OPE-based Discotics: Induction of Helicity and Amplification of Chirality. *J. Am. Chem. Soc.* **2012,** *134* (1), 734-742.

53. Anderson, T. W.; Sanders, J. K. M.; Dan Pantoş, G., The sergeants-and-soldiers effect: chiral amplification in naphthalenediimide nanotubes. *Org. Biomol. Chem.* **2010,** *8*, 4274-4280.

54. Smulders, M. M. J.; Filot, I. A. W.; Leenders, J. M. A.; van der Schoot, P.; Palmans, A. R. A.; Schenning, A. P. H. J.; Meijer, E. W., Tuning the Extent of Chiral Amplification by Temperature in a Dynamic Supramolecular Polymer. *J. Am. Chem. Soc.* **2010,** *132* (2), 611-619.

55. van Gorp, J. J.; Vekemans, J. A. J. M.; Meijer, E. W., C-3-symmetrical supramolecular architectures: Fibers and organic gels from discotic trisamides and trisureas. *J. Am. Chem. Soc.* **2002,** *124* (49), 14759-14769.

56. Stals, P. J. M.; Everts, J. C.; de Bruijn, R.; Filot, I. A. W.; Smulders, M. M. J.; Martin-Rapun, R.; Pidko, E. A.; de Greef, T. F. A.; Palmans, A. R. A.; Meijer, E. W., Dynamic Supramolecular Polymers Based on Benzene-1,3,5-tricarboxamides: The Influence of Amide Connectivity on Aggregate Stability and Amplification of Chirality. *Chem. Eur. J.* **2010,** *16* (3), 810-821.

57. Mes, T.; Cantekin, S.; Balkenende, D. W. R.; Frissen, M. M. M.; Gillissen, M. A. J.; De Waal, B. F. M.; Voets, I. K.; Meijer, E. W.; Palmans, A. R. A., Thioamides: Versatile Bonds To Induce Directional and Cooperative Hydrogen Bonding in Supramolecular Polymers. *Chem. Eur. J.* **2013,** *19* (26), 8642-8649.

58. Garcia, F.; Korevaar, P. A.; Verlee, A.; Meijer, E. W.; Palmans, A. R. A.; Sanchez, L., The influence of pi-conjugated moieties on the thermodynamics of cooperatively self-assembling tricarboxamides. *Chem. Commun.* **2013,** *49* (77), 8674-8676.

59. Li, Y.; Dubreucq, L.; Alvarenga, B. G.; Raynal, M.; Bouteiller, L., N-Substituted Benzene-1-Urea-3,5-Biscarboxamide (BUBA): Easily Accessible C-2-Symmetric Monomers for the Construction of Reversible and Chirally Amplified Helical Assemblies. *Chem. Eur. J.* **2019,** *25* (45), 10650-10661.

60. Greciano, E. E.; Calbo, J.; Buendia, J.; Cerda, J.; Arago, J.; Orti, E.; Sanchez, L., Decoding the Consequences of Increasing the Size of Self-Assembling Tricarboxamides on Chiral Amplification. *J. Am. Chem. Soc.* **2019,** *141* (18), 7463-7472.

61. Cantekin, S.; de Greef, T. F. A.; Palmans, A. R. A., Benzene-1,3,5-tricarboxamide: a versatile ordering moiety for supramolecular chemistry. *Chem. Soc. Rev.* **2012,** *41* (18), 6125-6137.

62. Brunsveld, L.; Schenning, A. P. H. J.; Broeren, M. A. C.; Janssen, H. M.; Vekemans, J. A. J. M.; Meijer, E. W., Chiral amplification in columns of self-assembled N,N ',N "-tris((S)-3,7-dimethyloctyl)benzene-1,3,5-tricarboxamide in dilute solution. *Chem. Lett.* **2000,** (3), 292-293.

63. Wilson, A. J.; Masuda, M.; Sijbesma, R. P.; Meijer, E. W., Chiral amplification in the transcription of supramolecular helicity into a polymer backbone. *Angew. Chem. Int. Ed.* **2005,** *44* (15), 2275-2279.

64. Wilson, A. J.; van Gestel, J.; Sijbesma, R. P.; Meijer, E. W., Amplification of chirality in benzene tricarboxamide helical supramolecular polymers. *Chem. Commun.* **2006,** (42), 4404-4406.

65. Smulders, M. M. J.; Schenning, A. P. H. J.; Meijer, E. W., Insight into the Mechanisms of Cooperative Self-Assembly: The "Sergeants-and-Soldiers" Principle of Chiral and Achiral C3-Symmetrical Discotic Triamides. *J. Am. Chem. Soc.* **2008,** *130*, 606-611.

66. Li, Y.; Caumes, X.; Raynal, M.; Bouteiller, L., Modulation of catalyst enantioselectivity through reversible assembly of supramolecular helices. *Chem. Commun.* **2019,** *55* (15), 2162-2165.

67. de Loos, M.; van Esch, J. H.; Kellogg, R. M.; Feringa, B. L., C-3-symmetric, amino acid based organogelators and thickeners: a systematic study of structure-property relations. *Tetrahedron* **2007,** *63* (31), 7285-7301.

68. Veld, M. A. J.; Haveman, D.; Palmans, A. R. A.; Meijer, E. W., Sterically demanding benzene-1,3,5-tricarboxamides: tuning the mechanisms of supramolecular polymerization and chiral amplification. *Soft Matter* **2011,** *7* (2), 524-531.

69. Desmarchelier, A.; Alvarenga, B. G.; Caumes, X.; Dubreucq, L.; Troufflard, C.; Tessier, M.; Vanthuyne, N.; Ide, J.; Maistriaux, T.; Beljonne, D.; Brocorens, P.; Lazzaroni, R.; Raynal, M.; Bouteiller, L., Tuning the nature and stability of self-assemblies formed by ester benzene 1,3,5-tricarboxamides: the crucial role played by the substituents. *Soft Matter* **2016,** *12* (37), 7824-7838.

70. Caumes, X.; Baldi, A.; Gontard, G.; Brocorens, P.; Lazzaroni, R.; Vanthuyne, N.; Troufflard, C.; Raynal, M.; Bouteiller, L., Tuning the structure of 1,3,5-benzene tricarboxamide self-assemblies through stereochemistry. *Chem. Commun.* **2016,** *52* (91), 13369-13372.

71. Bejagam, K. K.; Remsing, R. C.; Klein, M. L.; Balasubramanian, S., Understanding the self-assembly of amino ester-based benzene-1,3,5-tricarboxamides using molecular dynamics simulations. *Phys. Chem. Chem. Phys.* **2017,** *19* (1), 258-266.

72. Desmarchelier, A.; Caumes, X.; Raynal, M.; Vidal-Ferran, A.; van Leeuwen, P. W. N. M.; Bouteiller, L., Correlation between the Selectivity and the Structure of an Asymmetric Catalyst Built on a Chirally Amplified Supramolecular Helical Scaffold. *J. Am. Chem. Soc.* **2016,** *138* (14), 4908-4916.

73. Zimbron, J. M.; Caumes, X.; Li, Y.; Thomas, C. M.; Raynal, M.; Bouteiller, L., Real-Time Control of the Enantioselectivity of a Supramolecular Catalyst Allows Selecting the Configuration of Consecutively Formed Stereogenic Centers. *Angew. Chem. Int. Ed.* **2017,** *56* (45), 14016-14019.

74. , CD spectroscopy analyses are performed with [BTA^{PPh2}] ⩽5.8 mM to limit the absorbance of the sample in toluene whilst catalytic experiments are performed with [BTA^{PPh2}] = 16.9 mM

75. Allenmark, S., Induced Circular Dichroism by Chiral Molecular Interaction. *Chirality* **2003,** *15*, 409-422.

76. Kang, J.; Miyajima, D.; Mori, T.; Inoue, Y.; Itoh, Y.; Aida, T., A rational strategy for the realization of chain-growth supramolecular polymerization. *Science* **2015,** *347* (6222), 646-651.

77. Lightfoot, M. P.; Mair, F. S.; Pritchard, R. G.; Warren, J. E., New supramolecular packing motifs: pi-stacked rods encased in triply-helical hydrogen bonded amide strands. *Chem. Commun.* **1999,** (19), 1945-1946.

78. van Gestel, J.; Palmans, A. R. A.; Titulaer, B.; Vekemans, J. A. J. M.; Meijer, E. W., "Majority-rules" operative in chiral columnar stacks of C-3-symmetrical molecules. *J. Am. Chem. Soc.* **2005,** *127* (15), 5490-5494.

79. Helmich, F.; Smulders, M. M. J.; Lee, C. C.; Schenning, A. P. H. J.; Meijer, E. W., Effect of Stereogenic Centers on the Self-Sorting, Depolymerization, and Atropisomerization Kinetics of Porphyrin-Based Aggregates. *J. Am. Chem. Soc.* **2011,** *133* (31), 12238-12246.

80. Palmans, A. R. A.; Vekemans, J. A. J. M.; Havinga, E. E.; Meijer, E. W., Sergeants-and-soldiers principle in chiral columnar stacks of disc-shaped molecules with C-3 symmetry. *Angew. Chem. Int. Ed.* **1997,** *36* (23), 2648-2651.

81. Megens, R. P.; Roelfes, G., Asymmetric Catalysis with Helical Polymers. *Chem. Eur. J.* **2011,** *17* (31), 8514-8523.

82. Suginome, M.; Yamamoto, T.; Nagata, Y.; Yamada, T.; Akai, Y., Catalytic asymmetric synthesis using chirality-switchable helical polymer as a chiral ligand. *Pure Appl. Chem.* **2012,** *84* (8), 1759-1769.

83. Jiang, J.; Ouyang, G. H.; Zhang, L.; Liu, M. H., Self-Assembled Chiral Nanostructures as Scaffolds for Asymmetric Reactions. *Chem. Eur. J.* **2017,** *23* (40), 9439-9450.

84. Shen, Z. C.; Sang, Y. T.; Wang, T. Y.; Jiang, J.; Meng, Y.; Jiang, Y. Q.; Okuro, K.; Aida, T.; Liu, M. H., Asymmetric catalysis mediated by a mirror symmetry-broken helical nanoribbon. *Nat. Commun.* **2019,** *10*, doi/10.1038/s41467-019-11840-3.

85. Arlegui, A.; Soler, B.; Galindo, A.; Arteaga, O.; Canillas, A.; Ribo, J. M.; El-Hachemi, Z.; Crusats, J.; Moyano, A., Spontaneous mirror-symmetry breaking coupled to top-bottom chirality transfer: from porphyrin self-assembly to scalemic Diels–Alder adducts. *Chem. Commun.* **2019,** *55*, 12219-12222.

86. Raynal, M.; Portier, F.; van Leeuwen, P. W. N. M.; Bouteiller, L., Tunable Asymmetric Catalysis through Ligand Stacking in Chiral Rigid Rods. *J. Am. Chem. Soc.* **2013,** *135* (47), 17687-17690.

87. Yamamoto, T.; Suginome, M., Helical Poly(quinoxaline-2,3-diyl)s Bearing Metal-Binding Sites as Polymer-Based Chiral Ligands for Asymmetric Catalysis. *Angew. Chem. Int. Ed.* **2009,** *48* (3), 539-542.

88. Nagata, Y.; Nishikawa, T.; Suginome, M., Exerting Control over the Helical Chirality in the Main Chain of Sergeants-and-Soldiers-Type Poly(quinoxaline-2,3-diyl)s by Changing from Random to Block Copolymerization Protocols. *J. Am. Chem. Soc.* **2015,** *137* (12), 4070–4073.

89. Ke, Y.-Z.; Nagata, Y.; Yamada, T.; Suginome, M., Majority-Rules-Type Helical Poly(quinoxaline-2,3-diyl)s as Highly Efficient Chirality-Amplification Systems for Asymmetric Catalysis. *Angew. Chem. Int. Ed.* **2015,** *54*, 9333–9337.

90. Yamamoto, T.; Murakami, R.; Komatsu, S.; Suginome, M., Chirality-Amplifying, Dynamic Induction of Single-Handed Helix by Chiral Guests to Macromolecular Chiral Catalysts Bearing Boronyl Pendants as Receptor Sites. *J. Am. Chem. Soc.* **2018,** *140*, 3867.

91. Nagata, Y.; Takeda, R.; Suginome, M., Asymmetric Catalysis in Chiral Solvents: Chirality Transfer with Amplification of Homochirality through a Helical Macromolecular Scaffold. *ACS Cent. Sci.* **2019,** *5*, 1235-1240.

92. Jordan, A. J.; Lalic, G.; Sadighi, J. P., Coinage Metal Hydrides: Synthesis, Characterization, and Reactivity. *Chem. Rev.* **2016,** *116*, 8318-8372.

93. Scerba, M. T.; DeBlase, A. F.; Bloom, S.; Dudding, T.; Johnson, M. A.; Lectka, T., Characterization of Highly Unusual NH+-O Hydrogen Bonding to Ester Ether Oxygen Atoms through Spectroscopic and Computational Studies. *J Phys Chem A* **2012,** *116* (14), 3556-3560.

94. Lortie, F.; Boileau, S.; Bouteiller, L.; Chassenieux, C.; Deme, B.; Ducouret, G.; Jalabert, M.; Laupretre, F.; Terech, P., Structural and rheological study of a bis-urea based reversible polymer in an apolar solvent. *Langmuir* **2002,** *18* (19), 7218-7222.

95. Uray, G.; Stampfer, W.; Fabian, W. M. F., Comparison of Chirasil-DEX CB as gas chromatographic and ULMO as liquid chromatographic chiral stationary phase for enantioseparation of aryl- and heteroarylcarbinols. *J Chromatogr A* **2003,** *992* (1-2), 151-157.

Chapter 5 *N*-substituted benzene-1-urea-3,5-biscarboxamide (BUBA): easily accessible C_2-symmetric monomers for the construction of reversible and chirally-amplified helical assemblies

Abstract: Non C_3-symmetric supramolecular helices are gaining interest for the design of hierarchical assemblies, for the compartmentalization or the self-assembly of polymer chains and for application in asymmetric catalysis. We introduce *N*-substituted benzene-1-urea-3,5-biscarboxamide (BUBA) monomers, which consist of one urea and two carbon-connected amide functions linked to an aromatic ring, as an easily-accessible class of C_2-symmetric supramolecular synthons. In apolar solvents, BUBA monomers assemble into long helical assemblies by means of hydrogen-bonding and aromatic interactions, as assessed by several analytical techniques. In order to probe the influence of the urea function, BUBA and related benzene-1,3,5-tricarboxamide (BTA) helical polymers have been compared in terms of their thermodynamics of formation, stability, reversibility and chirality amplification properties. Like BTA, BUBA monomers form long helices reversibly through a highly cooperative mechanism and the helicity of their assemblies is governed by chiral amplification effects. However, precise quantification of their properties reveals that BUBA monomers assemble in a more cooperative manner. Also, chirality amplification operates to a higher extent in BUBA helices as probed by both sergeants-and-soldiers and majority-rules experiments. Compatibility between urea and amide functions also allows the formation of co-assemblies incorporating both BUBA and BTA monomers. Importantly, a small amount of chiral BUBA monomers in these co-assemblies is enough to get single-handed helices which paves the way towards the development of functional supramolecular helices. This work was published as *Chem. Eur. J* .**2019**, *25*, 10650 *(Yan Li, Ludovic Dubreucq, Bruno G. Alvarenga, Matthieu Raynal and Laurent Bouteiller),* and was reported here as published with formatting to match with the rest of the thesis.

I Introduction

Inspired by non-covalent helical biomacromolecules such as DNA, collagen and F-actin, huge efforts have been devoted to the synthesis of artificial helices,[1-2] not only in order to better control their mechanism of formation but also as a result of their exciting properties as asymmetric catalysts,[1-3] as sensors,[4] as templating agents,[5] as lyotropic,[6] or ferroelectric materials,[7-9] as organic luminophores,[10-12] and as spin filters.[13-14] The predictable assembly of small building blocks by means of directional non-covalent interactions constitutes the method of choice for the construction of supramolecular helical assemblies. Notably, aromatic scaffolds connected with hydrogen-bonding groups[15] are known that stack upon each other through a cooperative mechanism and yield long one-dimensional supramolecular polymers in solution.[16-17] Moreover, chirality induction and amplification phenomena are operative in these dynamic systems and are key elements for the preparation of functional assemblies.[18-20]

Benzene-1,3,5-tricarboxamide monomers (BTA, Chart. 1) are ubiquitous supramolecular synthons for the construction of helical stacks.[21] Adjacent monomers are connected by means of three hydrogen-bonds and an aromatic interaction between the BTA rings. The main advantages of the BTA platform are the simplicity of the BTA chemical structure, the predictability and cooperativity of the assembly process and the strong chirality amplification properties governing the formation of the helical assemblies. *N*,*N*',*N*''-substituted C_3-symmetric BTA monomers are easily prepared by direct functionalization of benzene-1,3,5-tricarboxylic acid or its acyl chloride derivative and have found numerous applications in various fields of chemical sciences. When it comes to imparting BTA assemblies with specific properties, the integration of one or two functional groups on the BTA unit is highly desired. C_2-symmetric BTA monomers have notably been used in organic solvents as assembling ligands for performing asymmetric reactions,[22-27] as building blocks for the design of hierarchical structures,[28] and as pendant units to trigger the folding or the self-assembly of polymer chains.[29-33] These desymmetrized BTAs are obtained *via* the incomplete hydrolysis of trimethyl benzene-1,3,5-tricarboxylate,[34] the partial esterification of trimesic acid,[33] or the stoichiometrically-biased addition of alkyl amines to trimesic chloride,[22, 35] all these routes being lengthy and modestly efficient.[36-37] Avoiding such desymmetrization protocols will significantly leverage the synthetic effort towards C_2-symmetric assembling units and their corresponding helical assemblies.

C_2-symmetric starting materials such as 3,5-dinitroaniline,[38-39] 3,5-dinitrobenzoic acid,[40-41] and 5-aminoisophthalic acid[39, 42-46] not only facilitate the preparation of disk-like molecules with two different side chains but also allow to connect urea and amide functions to the same aromatic ring. However, the influence of different recognition units on the assembly properties of these monomers has

been scarcely investigated. Meijer and co-workers reported on unsymmetrical "gallic" disks composed of two urea and one nitrogen-connected amide functions and found that the urea groups promoted the formation of columnar helical aggregates in dilute alkane solutions.[38] However, the supramolecular helices formed by these monomers or by related C_3-symmetric benzene-1,3,5-trisureas[47] are poorly dynamic and display modest chirality amplification properties. Clearly, a balance has to be found between the stronger hydrogen bond-forming capability of urea functions and the dynamics of the assemblies in order to maintain (or outperform) the properties observed in BTA helices. Here, we introduce *N*-substituted benzene-1-urea- 3,5-biscarboxamide (BUBA, Chart 1) monomers, comprising one urea function and two carbon-connected amide groups, as a new family of easily-accessible C2-symmetric supramolecular synthons. The assembly behaviour of BUBA monomers has been probed by several analytical techniques and compared to that of BTA analogues in order to precisely assess the influence of the urea function on the structure and properties of the supramolecular helices. Our study reveals that BUBA monomers form long, stable and reversible helical assemblies in apolar solvents. The presence of the urea function positively influences the extent of cooperativity and the degree of chirality amplification operating in these helical supramolecular systems. The compatibility between the urea and amide functions is further exploited to generate single-handed BUBA/BTA co-assemblies which will foster the development of functional supramolecular helices.

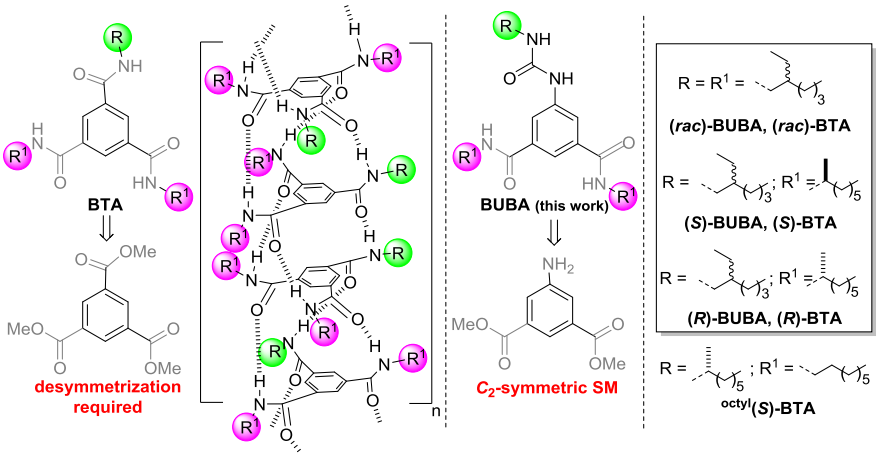

Chart 1 Molecular structures of the monomers investigated throughout this paper. Representation of the supramolecular BTA helices (the R and R^1 groups are assumed to be randomly distributed at the periphery of the helices). **(*rac*)-BUBA** is racemic by synthesis and thus consists of the stereoisomers (S_{urea},*S*,*S*), (S_{urea},*R*,*S*), (S_{urea},*R*,*R*), (R_{urea},*S*,*S*), (R_{urea},*R*,*S*), (R_{urea},*R*,*R*) in a 1:2:1:1:2:1 ratio. **(*rac*)-BTA** is racemic by synthesis and thus consists of the stereoisomers (*S*,*S*,*S*), (*S*, *S*, *R*), (*R*,*R*,*S*), (*R*,*R*,*R*) in a 1:3:3:1 ratio. **(*S*)-BUBA** and **(*S*)-BTA** consist of a 1:1 mixture of the (*S*,*S*,*S*) and (*R*,*S*,*S*) stereoisomers. The assembly properties of **(*S*)-BTA** will be compared to that of its structural analogue **^{octyl}(*S*)-BTA**, reported in the literature.[48-52]

II Results and Discussion

II.1 Synthesis of the monomers

Gram-scale synthesis of BUBA monomers has been achieved in three steps from dimethyl 5-aminoisophthalate, a cheap starting material (SM), through conventional synthetic protocols with overall yields ≥ 50% (see Fig. 1 for **(*S*)-BUBA**). Branched alkyl side chains ((*rac*)-2-ethylhexyl for **(*rac*)-BUBA** and both (*rac*)-2-ethylhexyl and optically pure 1-methylheptyl for **(*S*)-BUBA** and **(*R*)-BUBA**) have been preferred over linear ones to favour the formation of one-dimensional soluble assemblies.[53] After recrystallization in acetonitrile, **(*rac*)-BUBA** is obtained as an amorphous solid and **(*S*)-BUBA** and **(*R*)-BUBA** are crystalline solids. The high purity of the BUBA monomers is confirmed by ^{1}H NMR, ^{13}C NMR and High-Resolution Mass Spectrometry analyses. As a result of the chiral racemic nature of the 2-ethylhexyl side chain, **(*rac*)-BUBA** is a racemic mixture of 6 stereoisomers and **(*S*)-BUBA** consists of a 1:1 mixture of the (*S*,*S*,*S*) and (*R*,*S*,*S*) stereoisomers (see caption of Chart 1).

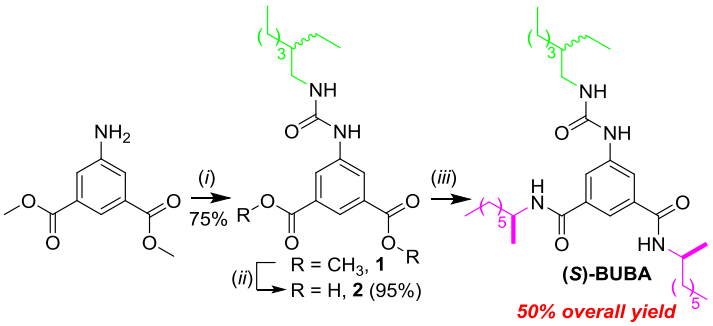

Figure 1 Synthesis of **(*S*)-BUBA**. (*i*) Triphosgene/DIEA/2-ethylhexylamine, (*ii*) LiOH/H_2O and (*iii*) EDC·HCl/DMAP/(*S*)-2-octylamine.

BTA analogues of these BUBA monomers have been prepared with the purpose of precisely probing the influence of the urea function on the structure of the assemblies as well as on their chiroptical and dynamic properties. C_3-symmetric **(*rac*)-BTA** is obtained in a single step according to literature.[54] For C_2-symmetric BTAs, a well-established route has been followed which consists in the partial hydrolysis of trimethyl benzene-1,3,5-tricarboxylate[34] and subsequent amidation − hydrolysis − amidation steps. This four-steps procedure furnishes **(*S*)-BTA** and **(*R*)-BTA** with an overall yield of 10% and 6%, respectively, as a result of the limited efficiency of the desymmetrization step (see Chart S1 for the compared syntheses of **(*S*)-BUBA** and **(*S*)-BTA**). Starting from a C_2-symmetric starting material thus allows BUBA monomers to be obtained in significantly higher yields than their BTA analogues.

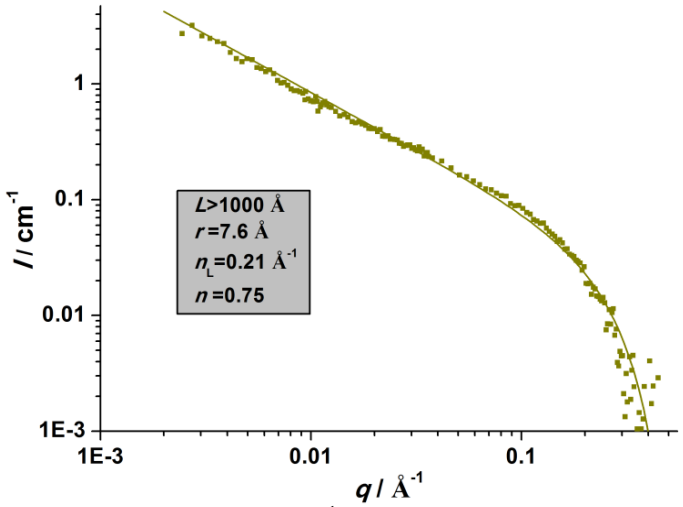

Figure 2 SANS analysis of (*rac*)-BUBA (6.0 g.L^{-1}, 10.8 mM) in C_7D_8 at 293 K. The curve was fitted according to the form factor for rigid rods of infinite length with a circular cross section and a uniform scattering length density (L =length, r =radius, n_L =number of molecule per unit length, n= number of molecule in the cross-section assuming a repeat distance of 3.6Å).[55]

II.2 Structure of the self-assemblies

The structure of **(*rac*)-BUBA** self-assemblies has been probed by means of Small-Angle Neutron Scattering (SANS), Fourier-Transform Infrared (FT-IR), Circular Dichroism (CD) and UV-Vis absorption analyses. The q^{-1} dependence of the scattering intensity at low q values is indicative of the presence of rigid one-dimensional objects (Fig. 2). Fitting of the SANS data shows that these objects are very long (length>1000 Å, DP_w>275) and contain a single molecule of BUBA in the cross-section (r = 7.6 Å,[56] n=0.75).[55] FT-IR analysis of a 5 mM solution of (*rac*)-BUBA in decahydronaphthalene (DHN, Fig. 3b) provides information about the nature of the hydrogen-bond network in BUBA assemblies. Two distinct absorption maxima are detected in the N-H region, at □=3369 cm^{-1} and □=3250 cm^{-1}, which correspond to bonded urea N-H and bonded amide N-H functions, respectively, by analogy with the FT-IR spectra of 4TEHU (Chart S2) and **(*rac*)-BTA** (Fig. 3a). In fact, models for free urea and amide moieties have also been recorded (Fig. S1) which allows for a quantitative analysis of the proportion of free N-H groups in BUBA self-assemblies. The resulting simulated FT-IR spectrum is shown in Fig. 3b (see Fig. S2 for its deconvolution into bands for bonded and free groups). The following points concerning the structure of BUBA self-assemblies are inferred from these analyses: (i) most of the urea (99%) and amide (97%) functions are bonded, (ii) the free urea and amide groups are not located at the chain ends[57] but can be rather considered as "defects" in the hydrogen-bond network since their amount does not decrease when the concentration in BUBA monomers increases (Fig. S1) and, (iii) the bonded urea N-H band in the experimental spectrum is blue-shifted comparatively to that

in the simulated spectrum which indicates that the N-H urea groups in BUBA polymers are less strongly associated than in 4TEHU assemblies.

(*S*)-BUBA and **(*R*)-BUBA** form helical assemblies in DHN as probed by CD analyses (Fig. 4). Four CD signals are observed with maxima at 299 nm ($|\Delta\varepsilon|$=3 L.mol^{-1}.cm^{-1}), 250 nm ($|\Delta\varepsilon|$=16 L.mol^{-1}.cm^{-1}), 224 nm ($|\Delta\varepsilon|$=28 L.mol^{-1}.cm^{-1}) and 207 nm ($|\Delta\varepsilon|$=66 L.mol^{-1}.cm^{-1}) whereas no detectable signals are seen in the molecularly-dissolved state. Interestingly, the Cotton effect at 299 nm is related to an electronic transition ($\pi-\pi^*$ or $n-\pi^*$) of the urea carbonyl group.[58] The marked difference between the CD spectra of **(*S*)-BTA** (Fig. S4) and **(*S*)-BUBA**, the presence of an ECD band exclusively attributed to the urea function and the FT- IR analyses (vide supra) all corroborate the involvement of the urea group in the hydrogen-bonding network of BUBA assemblies. The main UV-Vis absorption band is hypsochromically shifted upon assembly (dotted arrow in Fig. 4 bottom, $\Delta\lambda$=9 nm) which indicates a H-type aggregation mode for BUBA monomers. The CD spectra of **(*S*)-BUBA** and **(*R*)-BUBA** are, as anticipated, mirror images but it remains to be determined whether their handedness is identical to **(*S*)-BTA** and **(*R*)-BTA** respectively since it has been previously found that subtle modification in the structure of the monomer can lead to inversion in the sense of rotation of the respective assemblies.[48, 50-52]

The above-mentioned analyzes provide a precise picture of the structure adopted by BUBA self-assemblies: they are one-dimensional with a single molecule in the cross-section and they form helices with a preferred handedness in which most of amide and urea functions are bonded and the aromatic rings are stacked upon each other. Preliminary modeling studies show that helical assemblies in which the urea (resp. amide) functions are preferentially connected to the urea (resp. amide) functions, as represented in Figures 3b and S3,[56] constitute a possible structural arrangement of the BUBA monomers. Other arrangements are probably possible, but whatever their precise connections, amide and urea groups in BUBA monomers are compatible and both stabilize the helical assemblies through hydrogen bonding.

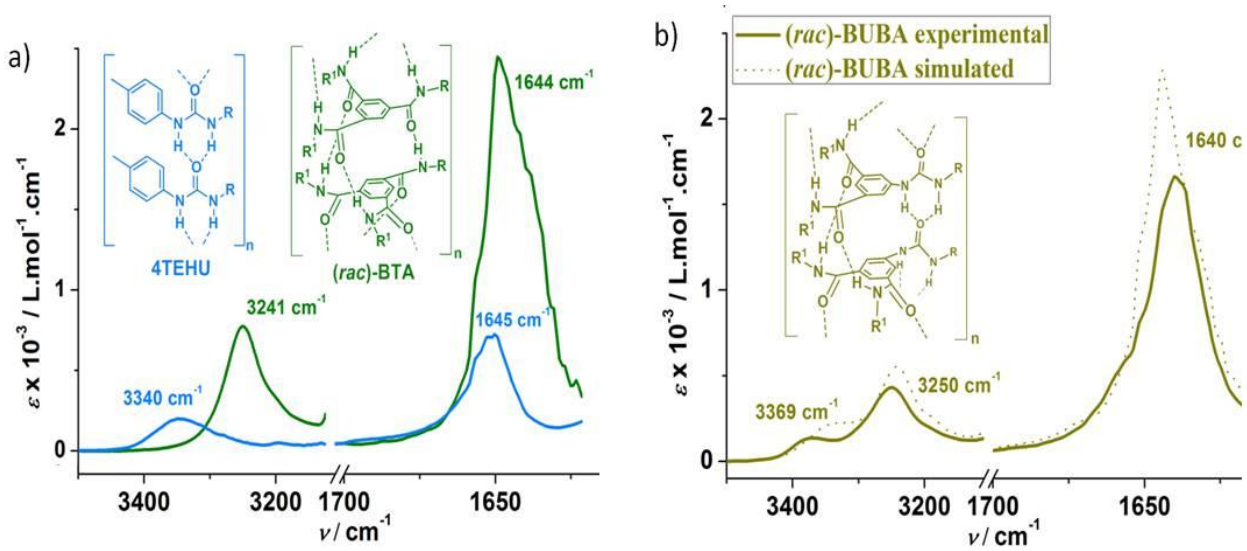

Figure 3 (a) FT-IR analyses of **(*rac*)-BTA** (10 mM, toluene) and 1-(4-tolyl)-3-(2-ethylhexyl)-urea (4TEHU, 25 mM, DHN), symmetric "models" for fully bonded amide and urea functions, respectively. (b) FT-IR analysis of **(*rac*)-BUBA** (5 mM, DHN, 293 K) and simulated spectrum aimed at probing the hydrogen bond network of BUBA assemblies as discussed in the main text and in the SI (Figs. S1 and S2).

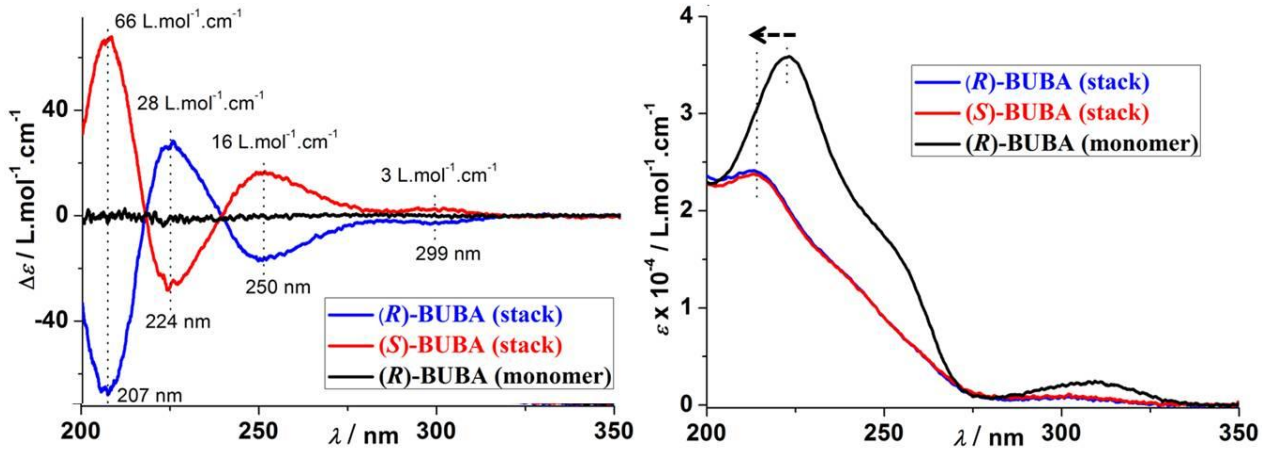

Figure 4 CD (left) and UV-Vis absorption spectra (right) of **(*R*)-BUBA** and **(*S*)-BUBA** in the assembled state (0.2 mM, DHN, 293 K) and of **(*R*)-BUBA** in the dissociated state (0.2 mM, EtOH, 293 K).

II.3 Thermodynamic parameters of self-assembly

In the following parts, the assembly properties of BUBA monomers will be probed by several techniques and compared to those of BTA analogues of Chart 1. Spectroscopic analyses of solutions of these BTAs in toluene (Fig. 3a) and in DHN (Fig. S4) are fingerprint of the presence of very long hydrogen-bonded helices with the structure represented in Chart 1.[48, 50, 59-60] The (*rac*)-2-ethylhexyl

moiety does not prevent the formation of homochiral self-assemblies, left-handed and right-handed for **(*S*)-BTA** and **(*R*)-BTA**, respectively (Fig. S4).

CD analyses of a 0.2 mM solution of **(*R*)-BUBA** in DHN show a gradual decrease of the intensity of the CD signals upon heating (Fig. 5a). The spectra obtained at 293 K and 373 K are diagnostic of the polymer and the monomer, respectively. The self-assembly process can thus be precisely probed by monitoring the CD signal at a given wavelength (Fig. 5b). The CD cooling and heating curves of **(*R*)-BUBA** have been recorded at 0.3 $K.min^{-1}$, a sufficiently slow rate to ensure that the assembly process is under thermodynamic equilibrium.

Firstly, the self-assembly process is fully reversible since the transitions in the cooling and heating cycles have the same amplitude. Secondly, both transitions are nonsigmoidal which implies a cooperative aggregation process of **(*R*)-BUBA** monomers in DHN. The cooperative aggregation mode of BTA monomers in organic solvents has previously been quantified by the nucleation-growth model developed by van der Schoot and co-workers,[61] and the same model has thus been applied to fit the CD cooling and heating curves of **(*R*)-BUBA** (Fig. 5b) and **(*S*)-BTA** (Fig. S5) in DHN. The extracted parameters are the dimensionless equilibrium constant *Ka* (activation of the monomer) and the enthalpy release upon elongation (*he*) at the elongation temperature (*Te*). These values are compiled in Table 1.

We first comment on the thermodynamic data obtained for **(*S*)-BTA**. The average enthalpy of elongation obtained from the CD measurements, $\overline{he} = -57\ kJ.mol^{-1}$, is consistent with the value obtained for a range of structurally-similar BTA monomers, including **^{octyl}(*S*)-BTA** (Chart 1).[48] This value is expected to be concentration/temperature independent and is thus characteristic of the enthalpically-driven assembly of the BTA monomers into the threefold hydrogen-bonded helix. The value of Ka must be interpreted cautiously since it is concentration and temperature dependent.[48, 62] The equilibrium constant determined for **(*S*)-BTA** at 0.2 mM, Ka =10^{-4}, is more than one order of magnitude higher than that reported for **^{octyl}(*S*)-BTA** (Ka <10^{-5}, c =0.05 mM)[50] but is close to the value obtained for achiral BTA (c =0.05 mM).[62] The lower cooperativity of **(*S*)-BTA** compared its analogues is probably due to the presence of three branched side chains connected to the central BTA core and/or the presence of two stereoisomers which (slightly) weakens the strength of the hydrogen-bonding (HB) interactions.[63]

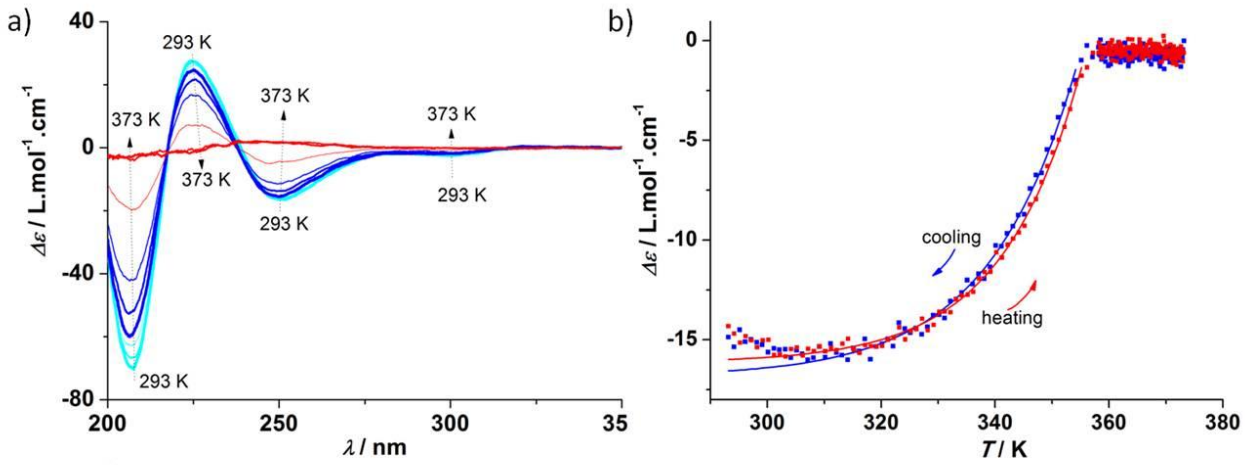

Figure 5 (a) CD spectra of **(*R*)-BUBA** from 293 K to 373 K in the heating cycle (0.2 mM, DHN), one spectrum recorded every 10 K. (b) CD cooling (■) and heating (■) curves of (*R*)-BUBA (0.2 mM, DHN, λ =250 nm), between 293 K and 373 K, cooling and heating rate =0.3 K.min^{-1}. The curves have been fitted with the nucleation-growth model.[61] It requires both the nucleation and elongation regimes to be fitted by two independent equations. For sake of clarity, only the fit of the elongation regime is shown. The decreasing of the CD values at the lower temperatures is attributed to partial precipitation.

Table 1 Thermodynamic parameters for the self assembly of 0.2 mM solutions of **(*R*)-BUBA** and **(*S*)-BTA** in DHN, determined by applying the nucleation-growth model to the CD cooling and heating curves**.**

monomers	data	T_e /K	h_e / kJ.mol^{-1}	K_a
(*R*)-BUBA	CD (cooling)	354.9	−68.2	10^{-5}
	CD (heating)	355.8	−76.1	10^{-5}
(*S*)-BTA	CD (cooling)	374.7	−53.7	10^{-4}
	CD (heating)	373.8	−60.2	10^{-4}

The average thermodynamic parameters obtained by fitting the CD cooling and heating curves of **(*R*)-BUBA** are: $\overline{T_e}$ =355 K, $\overline{h_e}$ =-72 kJ.mol^{-1} and $\overline{K_a}$ =10^{-5}. The higher absolute value of the elongation enthalpy for **(*R*)-BUBA** compared to **(*S*)-BTA** ($|\Delta h_e|$ =15 kJ.mol^{-1}) probably stems from the additional hydrogen bond donor provided by the urea group. Despite the higher strength of its HB network, **(*R*)-BUBA** assemblies are slightly weaker than those of (*S*)-BTA as indicated by the lower T_e value (ΔT_e =-19 K). Therefore, the energetic gain from the enthalpy term is over compensated by an entropic cost,

possibly due to a higher conformational order (more internal order) of the BUBA monomers within their helical self-assemblies.

The determined K_a value clearly reveals that polymerization of **(*R*)-BUBA** monomers proceeds with a good level of cooperativity and thus corroborates the formation of very long assemblies in solution. Although the values of K_a are determined at slightly different temperatures, the significant different values obtained show that BUBA assemblies are more cooperative than BTA. It is also supported by overlaying the CD cooling curves of **(*R*)-BUBA** and **(*S*)-BTA** since the change in CD intensity at T_e is clearly more abrupt in the former case (Fig. S6).

II.4 Chirality amplification properties

Chirality amplification is achieved when the main chain chirality of polymers is controlled by a small amount of chiral monomers (sergeant) combined with achiral ones (soldier) or by a small bias in the optically purity of a mixture of enantiomerically-related monomers.[18, 64] The former phenomenon is referred to as the sergeants-and-soldiers (S&S) effect and the latter as the majority-rules (MR) principle. Cooperative assembly of monomers, notably when governed by hydrogen-bonding interactions, generates supramolecular polymers with strong chirality amplification properties. Previous studies have demonstrated the possibility of preparing homochiral BTA helices with sergeants-and-soldiers mixtures or scalemic mixtures of BTA enantiomers.[49, 59, 62, 65] Chirality amplification in helical supramolecular polymers has been modelled by assuming energy penalties for the inversion of handedness of the stacks (helix reversal penalty, HRP) and for the incorporation of a monomer in a stack of its unpreferred helicity (mismatch penalty, MMP).[66-71] Only a few studies have addressed the correlation between the structure of the monomers and the extent of chirality amplification in the resulting polymer assemblies.[65, 72-75] As both BUBA and BTA monomers associate in a cooperative manner (vide supra), it makes it possible to probe the influence of the urea function on the induction and amplification of chirality in the related hydrogen-bonded helices.

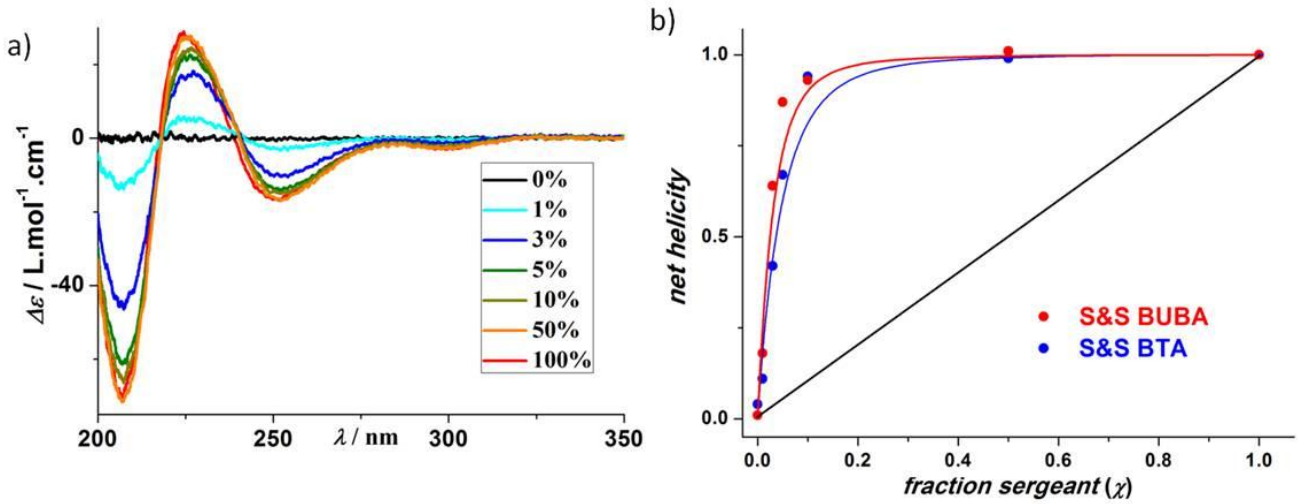

Figure 6 (a) CD spectra of the sergeants-and-soldiers type experiments obtained by mixing solutions of **(*R*)-BUBA** and **(*rac*)-BUBA** at 293 K (c_{tot} =0.2 mM, DHN). (b) Net helicity as a function of the fraction of sergeant obtained from CD mixtures of **(*R*)-BUBA** and **(*rac*)-BUBA** or of **(*S*)-BTA** and **(*rac*)-BTA** at 293 K (c_{tot} =0.2 mM, DHN). The net helicity is obtained by dividing the molar CD value at =207 nm (for BUBA) and at =225 nm (for BTA) of the S&S mixtures by the molar CD value of the pure sergeant. For each type of monomers, the data of the S&S and MR experiments have been fitted (blue and red solid lines) simultaneously following the procedures described by Smulders et al.[65] (for S&S) and by van Gestel[67] (for MR). Please see the excel spreadsheet in the Supporting Material of this paper for all the details of the calculation. The result of the fit is indicated in the caption of Fig. 7. The black solid line represents the fate of net helicity in absence of chirality amplification.

We have first performed typical sergeants-and-soldiers experiments except that in our case the soldier is racemic instead of achiral. CD spectra of mixtures of **(*R*)-BUBA** and **(*rac*)-BUBA** (c_{tot} = 0.2 mM) in DHN differ by their intensity, not by their shape, which suggest that the sergeant and the soldier adopt the same conformation in the helical stacks (Fig. 6a). The same holds true for S&S mixtures between **(*S*)-BTA** and **(*rac*)-BTA** (Fig. S7a). The net helicity, *i.e.* the ratio between left-handed and right-handed fragments in the one-dimensional helical stacks, is plotted as a function of the fraction of sergeants for BUBA and BTA mixtures (Fig. 6b). Both S&S type supramolecular polymers exhibit chirality amplification properties.

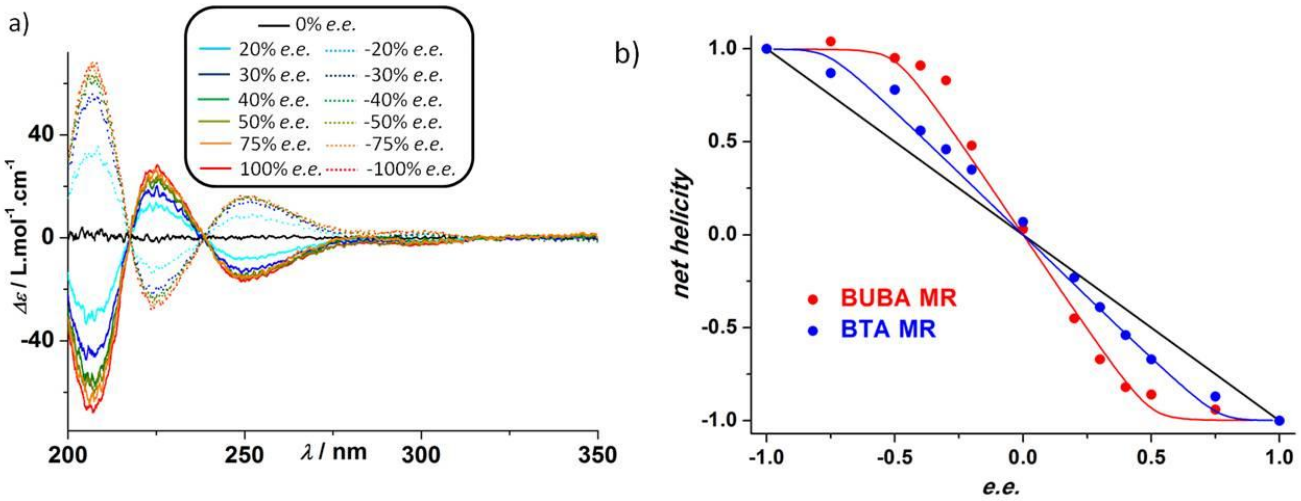

Figure 7 (a) CD spectra of the majority-rules type experiments obtained by mixing solutions of **(*R*)-BUBA** and **(*S*)-BUBA** at 293 K (c_{tot} =0.2 mM, DHN). Positive (negative) *e.e.* values correspond to mixtures enantioenriched in **(*R*)-BUBA** (**(*S*)-BUBA** resp.) monomers. (b) Net helicity as a function of the *e.e.* of the monomer obtained from CD mixtures of **(*R*)-BUBA** and **(*S*)-BUBA** or of **(*R*)-BTA** and **(*S*)-BTA** at 293 K (c_{tot}=0.2 mM, DHN). The net helicity is obtained by dividing the molar CD value at λ =207 nm (for BUBA) and at λ =225 nm (for BTA) of the MR mixtures by the molar CD value of the pure monomer. For each type of monomers, the data of the S&S and MR experiments have been fitted (blue and red solid lines) simultaneously following the procedures described by Smulders et al.[65] (for S&S) and by van Gestel[67] (for MR). Please see the excel spreadsheet in the Supporting Material of this paper for all the details of the calculation. It provides the following values: HRP =10 kJ.mol^{-1}, MMP =2.4 kJ.mol^{-1} for BUBA and HRP =8.2 kJ.mol^{-1}, MMP =4.5 kJ.mol^{-1} for BTA. The black solid line represents the fate of the net helicity in absence of chirality amplification.

For the BTA mixtures, the maximal helicity is attained for the mixture containing *ca.* 10% of sergeants. A similar level of amplification was obtained with **^{octyl}(*S*)-BTA**[65] whereas a BTA with three chiral side chains proved to be more efficient.[59, 62] A net helicity of 0.87 and 0.67 is reached for mixtures containing 5% of BUBA and BTA soldiers, respectively, highlighting a sligthly better induction of chirality by the sergeants in the BUBA helical assemblies.

A 3:2 mixture of **(*R*)-BUBA** and **(*S*)-BUBA** monomers in DHN (c_{tot} = 0.2 mM, 20% *e.e.*) exhibits a CD signal which is *ca.* half as intense as the one of pure **(*R*)-BUBA** (Fig. 7a). This supports the strong non-linearity in the handedness of the BUBA helices as a function of the optical purity of the monomers (Fig. 7b) and is in sharp contrast with the modest amplification of chirality observed for the mixtures of **(*S*)-BTA** and **(*R*)-BTA** (Figs. 7b and S7b).

A more precise determination of the extent of chirality amplification operating in BUBA and BTA helices is gleaned by simultaneously fitting the S&S and MR experiments for each platform following the procedures described by Smulders et al.[65] (for S&S) and by van Gestel[67] (for MR). For the BTA platform, the HRP (8.2 $kJ.mol^{-1}$) and MMP (4.5 $kJ.mol^{-1}$) values deduced from the fits are lower and higher, respectively, to that reported in the literature for **^{octyl}(*S*)-BTA** in methylcyclohexane.[65] This is consistent with the modest degree of chirality amplification exhibited by this set of BTA helices in both S&S and MR experiments. This also connects well with the lower extent of cooperativity observed during their supramolecular polymerization (*vide supra*). We presume that the branched nature of the side chain, the presence of racemic centres in the side chains (instead of achiral or chiral ones) and/or subtle solvent effects explain the mitigated chirality amplification ability of the BTA helices investigated in this study.

The better chirality amplification of the BUBA relatively to the BTA platform is reflected by its higher HRP (10 $kJ.mol^{-1}$) and lower MMP (2.4 $kJ.mol^{-1}$) values. The mutation of a single amide function by a urea one modifies the intermolecular non-covalent network which thereby remarkably affects the energy penalties. We presume that the higher strength of the hydrogen-bond network in BUBA stacks, as deduced from the elongation enthalpy value, is responsible for the increase of the HRP which in turn lower the MMP since the two values are interconnected for a given supramolecular platform.[49]

II.5 Mixing BUBA and BTA stacks

Combining monomers possessing different but compatible units appears as an attractive approach to generate complex architectures or co-assemblies with improved properties.[76] Previous studies related the formation of co-assemblies upon mixing C_3-symmetric monomers such as C=O-centred BTA and nitrogen-centred BTA monomers[72] or C=O-centred BTA and benzene-1,3,5-trisurea monomers,[47] even though in the latter case segregation into single-component stacks quickly occurs after mixing. Since both BUBA and BTA self-assemble through a cooperative pathway (*vide supra*), it is interesting to probe the possibility of lowering the symmetry of BTA helices by incorporation of BUBA monomers.

Mixtures of **(*R*)-BUBA** and **(*rac*)-BTA** monomers in DHN were analyzed by CD spectroscopy (c_{tot} =0.2 mM). Firstly, the formation of copolymers was confirmed by comparing the experimental CD spectra with those simulated for a combination of the homopolymers (see Fig. 8a for the mixture containing 30% of **(*R*)-BUBA)**. The much higher intensity of the experimental CD curve compared to the simulated one indicates that both co-assembly and strong chirality amplification occur. This

conclusion qualitatively holds for fractions of **(*R*)-BUBA** in the mixture below 60% (Fig. S8). The compatibility between the urea and the amide functions thus prevents segregation. Interestingly, virtually identical CD spectra are obtained, shortly after mixing the preassembled homopolymers at 293 K and by slowly cooling a mixture of the monomers from 383 K down to 293 K (Fig. 8a). Thus, different pathways lead to the same co-assemblies and the dynamic nature of BTA and BUBA assemblies allows rapid equilibration of the composition and favours the formation of the copolymers. Further information on the co-assembly process is disclosed by the CD cooling curve of the mixture containing 30% of **(*R*)-BUBA** (Fig. 8b). Co-polymerization occurs cooperatively with a Te value of 366 K, i.e. higher than for **(*R*)-BUBA** homopolymer and close to the one found for **(*S*)-BTA** homopolymer. Importantly, the presence of a single Te value is an additional testimony of a co-assembly rather than a self-sorting process since the latter one would have exhibited two distinct transitions.

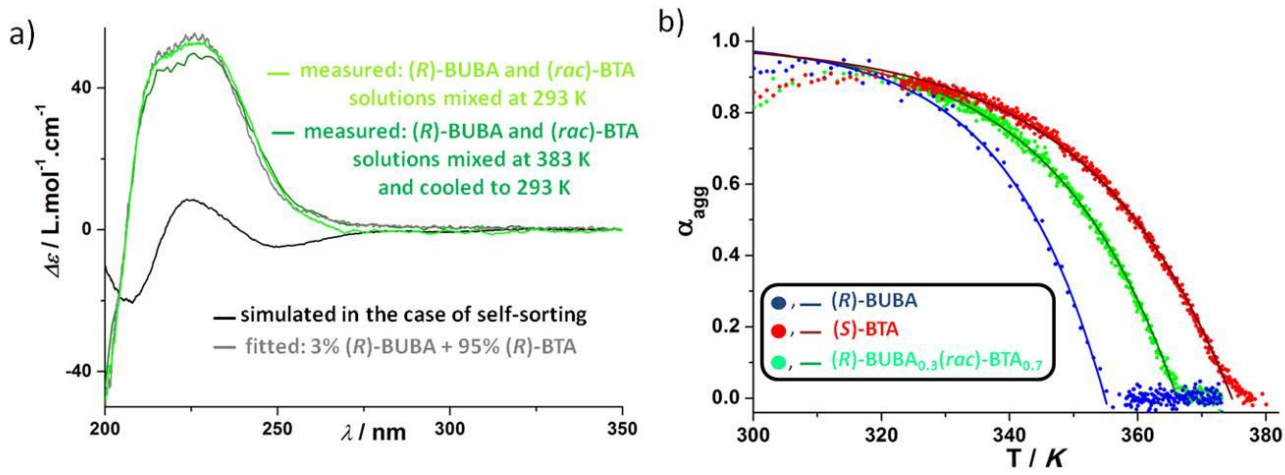

Figure 8 (a) CD spectra for the mixture of **(*R*)-BUBA** and **(*rac*)-BTA** (3:7) prepared by two different methods (c_{tot} =0.2 mM, DHN). The experimental spectra are shown together with the fitted spectrum (see Fig. S8 and the text for more details) and the simulated CD curve for segregated stacks (no co-assembly). (b) CD cooling curve of **(*R*)-BUBA/(*rac*)-BTA** 3/7 mixture (c_{tot} = 0.2 mM, DHN =225 nm), between 293 K and 383 K, cooling and heating rate =0.3 K.min^{-1}. The curves have been fitted with the nucleation-growth model.[61] Result of the fit: T_e =366 K, h_e =−58 kJ.mol^{-1}, K_a =10^{-5}. For the sake of comparison, the CD curves of pure **(*R*)-BUBA** and **(*S*)-BTA** are also shown.

Although BUBA and BTA self-assemblies share structural similarities (*vide supra*), their strikingly different CD spectroscopic signatures infer that they do not adopt identical conformations and this must be taken into consideration when interpreting the CD spectra of their mixtures. A closer look at the experimental CD curves at 293 K (Fig. 9a) reveals that all spectra, except the one containing 95% of **(*R*)-BUBA**, exhibit a CD signal which has a similar shape as the CD signal of **(*R*)-BTA**. From this, it can be deduced qualitatively that the **(*rac*)-BTA** units adopt preferentially the conformation of **(*R*)-BTA** helices in presence of **(*R*)-BUBA**. Fitting the CD curves can provide more quantitative information

about the extent of chirality amplification and the conformation displayed by these helical co-assemblies (Figs. 8a and S8). More precisely, the experimental CD spectrum is simulated by combining the individual spectra of **(*R*)-BUBA** and **(*R*)-BTA** and their content is adjusted to minimize the difference between the simulated and experimental spectra. The good quality of the fits allows to extract the relative contribution of **(*R*)-BUBA** and **(*R*)-BTA** to the overall CD signal displayed by the co-assemblies (Table S1). The fraction of stacks adopting **(*R*)-BUBA**-like (blue dots) or **(*R*)-BTA**-like (red dots) conformations is plotted in Fig. 9b as a function of the introduced fraction of **(*R*)-BUBA** in the mixture, and the concentration of all species present (*i.e.* the speciation plot) is shown in Fig. S9.

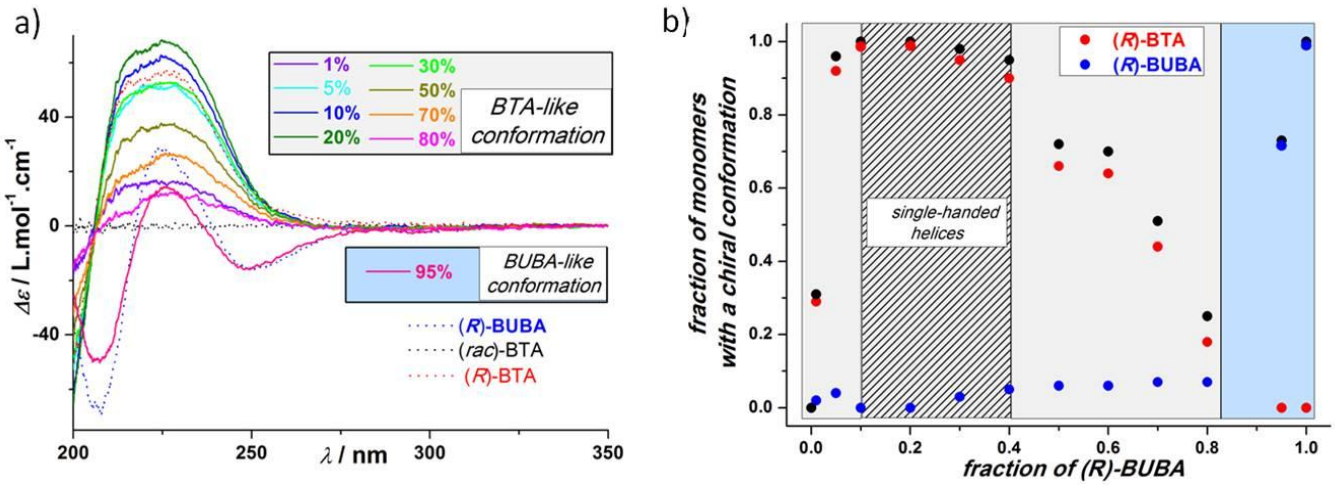

Figure 9 (a) CD spectra of mixtures of **(*R*)-BUBA** (0-100%) and **(*rac*)-BTA** at 293 K (c_{tot} =0.2 mM, DHN). In the caption, the mixtures are sorted according to the conformation preferentially adopted by the co-assemblies as determined by fitting the CD curves (Figs. 8 and S8). (b) Fraction of monomers with a chiral conformation in the co-assemblies as a function of the fraction of **(*R*)-BUBA** in the mixtures. The total fraction of chiral monomers (black dots) corresponds to the sum of monomers with **(*R*)-BTA**-like (red dots) and **(*R*)-BUBA**-like (blue dots) conformations as determined by fitting the experimental CD curves of the different mixtures (Fig. S8 and Table S1). The zones filled in light grey and light blue correspond to co-assemblies which preferentially adopt a BTA-like and BUBA-like conformation, respectively. The hatched area correspond to fully chirally-amplified co-assemblies.

Three characteristic zones emerge from this analysis: (i) for mixtures containing between 5% and 40% of **(*R*)-BUBA** most of the monomers adopt a chiral conformation (*i.e.* full chiral amplification occurs). Moreover, **(*R*)-BUBA** (the sergeant) imposes its helical preference, but (*rac*)-BTA (the soldier, which is present in excess) imposes its conformation. (ii) In the intermediate range (from 50% to 80% **(*R*)-BUBA**) the soldier still imposes its conformation to a significant fraction of the sergeant but it also creates defects that result in a reduced chirality amplification.[77] (iii) In the range above 80% of **(*R*)-BUBA** both the helicity and the conformation are imposed by the sergeant. These results stress out the

strong interaction between the monomers in the helical co-assemblies which is in striking contrast with the weak interactions between structurally-similar hydrogen-bonded monomers recently reported in the literature.[78] This also points towards an alternate or random organization of the monomers within the BUBA/BTA copolymers.

Most importantly, these mixing experiments highlight the efficient incorporation of BUBA monomers into the one-dimensional helical assemblies of BTA. Thanks to chirality-amplification phenomena, 10% of BUBA "sergeants" are enough to generate single-handed co-assemblies with a BTA-like conformation. The compatibility between the urea and amide functions in the mixed aggregates also dictates the monomer interactions and this can probably be further extended to control the monomer sequences in such types of chiral supramolecular co-polymers.[78-83]

III Conclusion

Compatibility between the recognition units dictates the assembly properties of disk-like molecules possessing multiple functional groups. Here, we show that *N*-substituted benzene-1-urea-3,5-biscarboxamide (BUBA) monomers, comprising one urea function and two carbon-centred amide functions connected to the same aromatic ring, form long, reversible and highly chirally-amplified helical assemblies in apolar solvents. This class of monomers provides an easy access to non C_3-symmetric supramolecular helices which are useful for the design of hierarchical assemblies, for the compartmentalization or self-assembly of polymer chains and for application-driven studies in asymmetric catalysis. Single-handed helices are obtained by self-assembly of BUBA monomers possessing chiral sides chains and more importantly by incorporating a small amount of chiral BUBA monomers in a racemic mixture of left- and right-handed benzene-1,3,5-tricarboxamide (BTA) stacks.

By comparing the structure BUBA and BTA monomers, our study also provides the influence of a single mutation on the structure and properties of the resulting supramolecular polymers. Such structure – properties relationships, notably when considering the triad: stability – mechanism of aggregation – chirality amplification, are currently lacking despite their necessity for the design of more efficient supramolecular polymer platforms. Clearly, BUBA and BTA assemblies have more similarities than differences. They both aggregate through hydrogen bonding and aromatic interactions by means of a cooperative mechanism, form long helices in solution, are reversible and their main chain helicity can be amplified. Nevertheless, the stability of BUBA assemblies is slightly lower despite the presence of an additional hydrogen bond interaction provided by the urea groups (as reflected by the higher elongation enthalpy). Conversely, BUBA self-assembly proceeds with a higher level of cooperativity and the main chain chirality of their resulting helices is more strongly amplified. It is worth to note that

previous modification of the BTA structure led to mitigated properties for the resulting assemblies in term of reversibility, stability, cooperativity and chirality amplification.[47, 51-52, 72-73]

Ongoing work in our laboratory is focused on better understanding of the BUBA assemblies at the molecular level and notably the position of the urea groups, the possibility of controlling the monomer sequence in BUBA co-assemblies and the implementation of BUBA assemblies in asymmetric catalysis.

IV Supporting Information

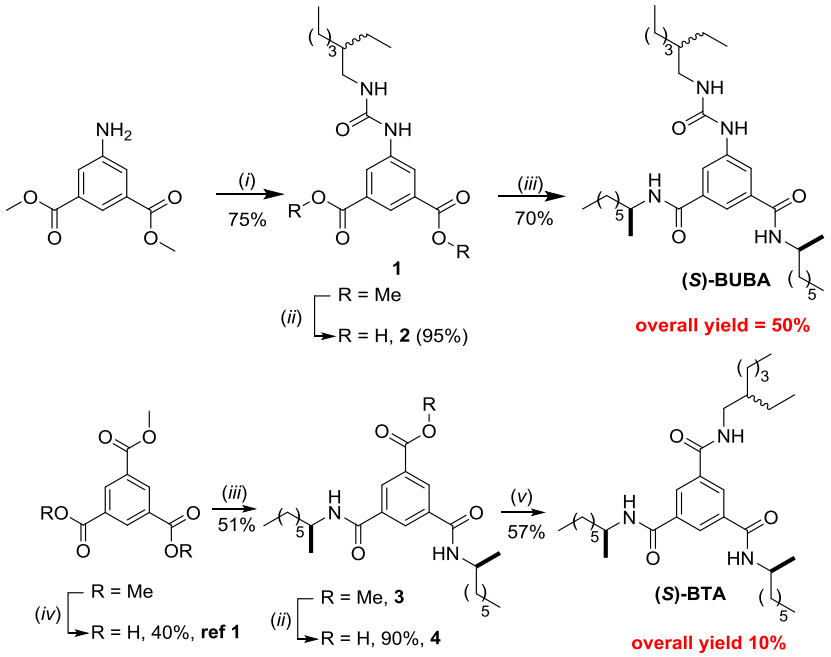

Chart S1 Compared synthesis of **(*S*)-BUBA** and **(*S*)-BTA**. (*i*) Triphosgene/DIEA/2-ethylhexylamine; (*ii*) LiOH/H_2O; (*iii*) EDC·HCl/DMAP/(*S*)-2-octylamine; (*iv*) NaOH;[34] (*v*) EDC·HCl/DMAP/2-ethylhexylamine.

Note: An alternative synthesis of **(*S*)-BTA** can be envisaged by partial esterification of trimesic acid according to the procedure described by Ślęczkowski et al.[33] Assuming the same yields than in Fig. 1 for the hydrolysis and amidation steps, an overall yield of 13% is found for **(*S*)-BTA** prepared *via* this method.

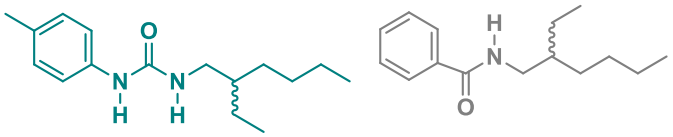

model for bonded and free urea functions

model for free amide functions

Chart S2 Chemical structures of the models used throughout this study. **4TEHU**= 1-(4-tolyl)-3-(2-ethylhexyl)-urea, **EHBA** = *N*-(2-ethylhexyl)benzenecarboxamide.

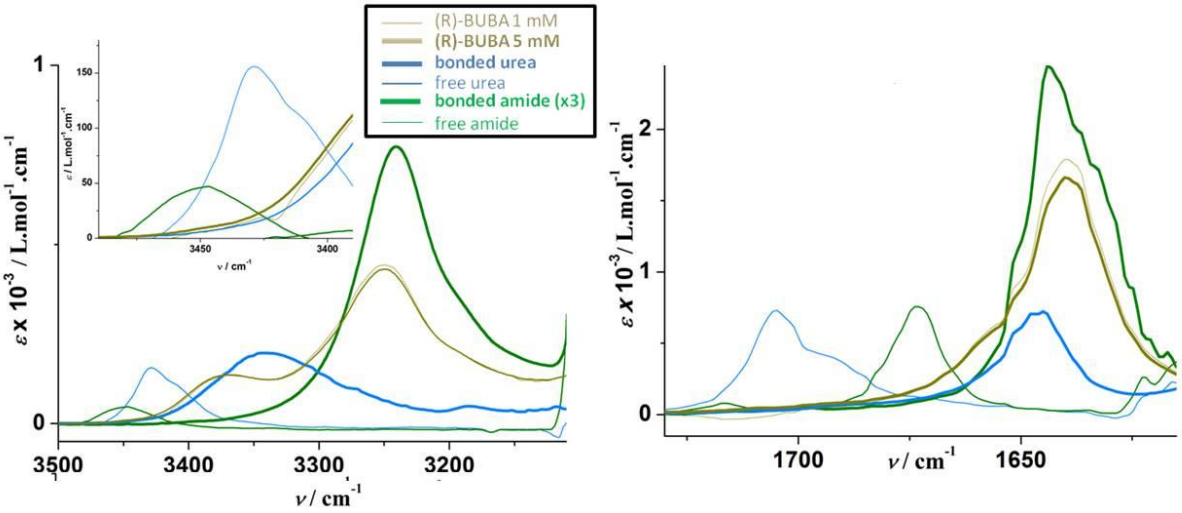

Figure S1 Characterization of BUBA self-assemblies. FT-IR analyses of **(*rac*)-BUBA** (1 and 5 mM, DHN) and of various models (Chart S2): **(*rac*)-BTA** (10 mM, toluene) for bonded amide functions, *N*-(2-ethylhexyl)benzenecarboxamide (**EHBA**, 2 mM, toluene) for free amide functions, 1-(4-tolyl)-3-(2-ethylhexyl)-urea (**4TEHU**, 25 mM, DHN) for bonded urea functions and **4TEHU** (2 mM, toluene) for free urea functions. Zoom on the N-H (left) and amide I C=O (right) absorption bands.

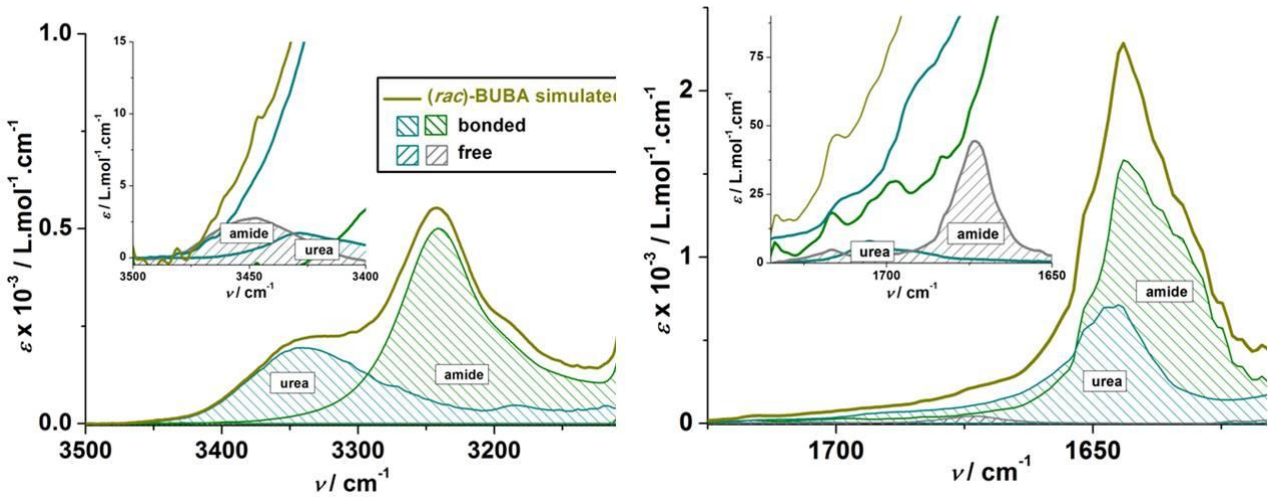

Figure S2 Characterization of BUBA self-assemblies. Simulated FT-IR spectrum of **(*rac*)-BUBA** and its deconvolution into free and bonded amide and free and bonded urea bands. The region corresponding to free amide or urea groups is shown in the insets. Zoom on the N-H (Top) and amide I C=O (Bottom) absorption bands.

Procedure for simulation of the FT-IR spectrum of (rac)-BUBA: The region of the experimental spectrum of **(*rac*)-BUBA** between 3425 cm^{-1} and 3500 cm^{-1} is fitted by combining the spectra of the models described in Fig. S1 and minimizing the difference error with the Solver function of Excel software. The simulated spectrum is calculated according to the relative contributions of urea and amide functions in BUBA. The following result is obtained: simulated spectrum =2×0.03×EHBA + $0.01\times4TEHU^{free}$ + 2/3×0.97×(*rac*)-BTA + $0.99\times4TEHU^{bonded}$. It provides the percentage of free amide (3%) and free urea (1%) functions which means an average of 2% of free N-H bond.

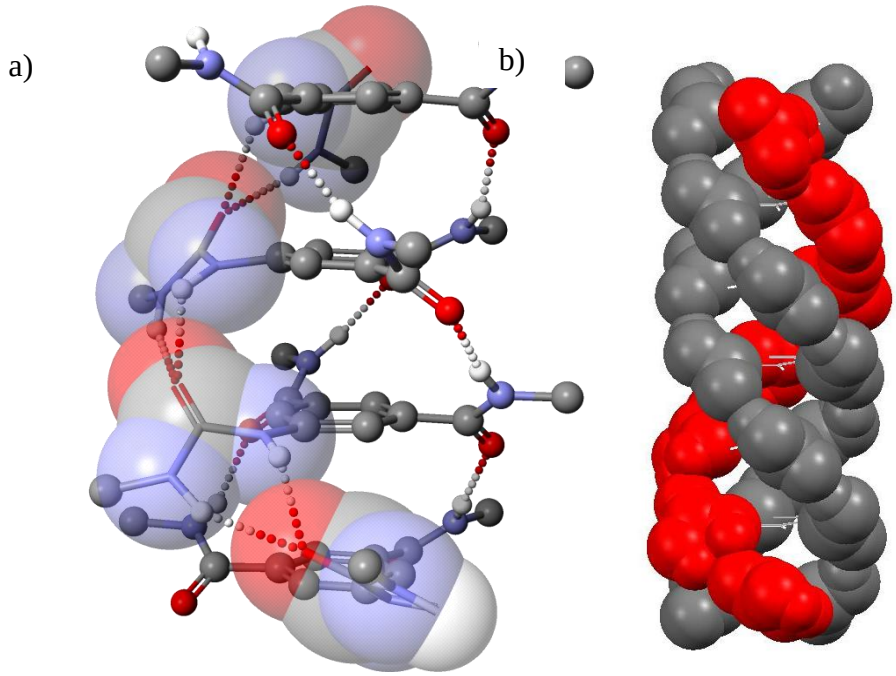

Figure S3 Modeled structure of BUBA self-assemblies in which the urea and amide functions are connected in an orthogonal manner to urea and amide respectively. (a) "Ball-and-stick" representation of a BUBA tetramer in which the urea functions have been represented in the space filling and wireframe styles. (b) Diagram highlighting the threefold hydrogen bonding array corresponding to one helix turn (6 monomers). The urea groups are highlighted in red.

Construction of the threefold hydrogen-bonded helix: The X-ray structure of *N*,*N*',*N*''-tris(2-methoxyethyl)benzene-1,3,5-tricarboxamide[84] was selected as a model for the construction of BUBA stacks. A hexamer was extracted, the side chains were removed, replaced by methyl groups and one helical strand of amide functions was replaced by a helical strand of urea functions. Helical stacks of *N*,*N*',*N*''- tris(methyl)benzene-1-urea-3,5-biscarboxamide were optimized by means of a molecular mechanics method (MM3) using the software Scigress (Fujitsu) keeping fixed the two helical strands of amide functions. An extensive modeling study, following well-known simulation procedures for self-assembling supramolecular systems,[85] is required to probe the precise geometry of the columnar stacks formed by BUBA units.

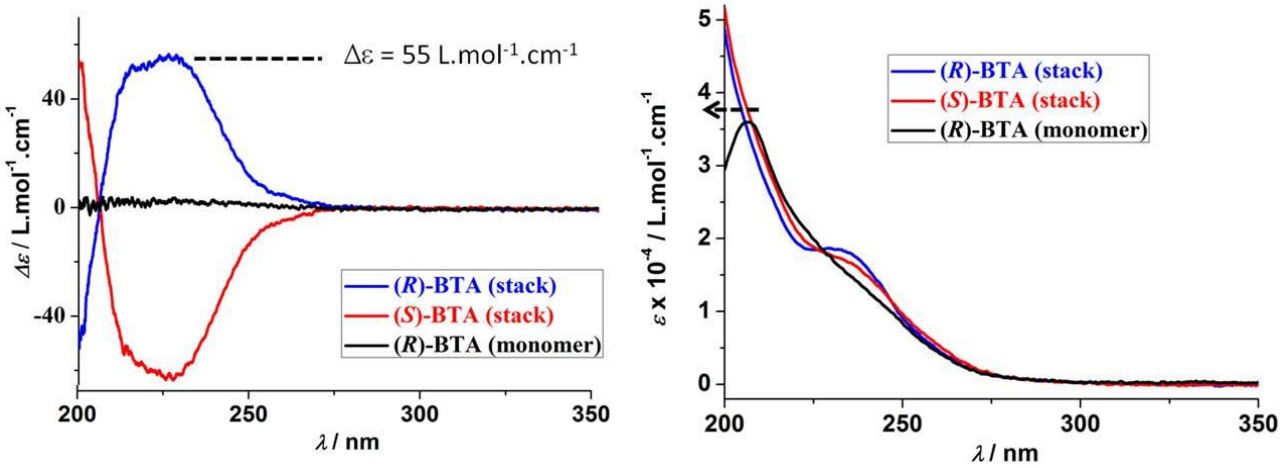

Figure S4 Characterization of BTA self-assemblies. CD (left) and UV-Vis absorption spectra (right) of **(*R*)-BTA** (DHN, stack), **(*S*)-BTA** (DHN, stack) and **(*R*)-BTA** (ethanol, monomer) at 0.2 mM.

Interpretation: Spectroscopic analyses of solutions of the selected BTAs in toluene (Fig. 3a) and DHN (Fig. S4) are fingerprint of the presence of very long hydrogen-bonded helices with the structure represented in Chart 1.[48, 50, 59-60] The absorption maxima observed by Fourier-Transform Infrared (FT-IR) analysis of **(*rac*)-BTA** (Fig. 3a), located at ν =3241 cm^{-1} and ν =1644 cm^{-1}, are diagnostic of bonded amide functions in BTA helical assemblies. The hypsochromic shift, observed in the UV-Vis absorption spectrum, when going from monomer to assemblies of **(*S*)-BTA** and **(*R*)-BTA** is consistent with the formation of H-type aggregates. The Circular Dichroism (CD) spectrum of **(*S*)-BTA** in DHN exhibits a broad band with one maximum at ≈ 225 nm in the n−π* transition region (type I spectrum according to Nakano et al.).[50] The sign and shape of this CD signal is similar to that previously found for a BTA monomer substituted with two linear octyl chains and a single (1*S*)-methylheptyl group ($^{\mathbf{octyl}}$**(*S*)-BTA**, Chart 1).[48-52] This shows that the (*rac*)-2-ethylhexyl group in **(*S*)-BTA** does not change the handedness of the helices and does not significantly alter the conformation of the assemblies. Also, despite **(*S*)-BTA** and **(*R*)-BTA** being a 1:1 mixture of two stereoisomers, the maximal intensity of their CD signals (|Δε|=55 $L.mol^{-1}.cm^{-1}$) is identical, or even higher than those previously reported for enantiopure BTA monomers, even those appended with three (*S*)-3,7-dimethyloctyl groups.[48, 59-60, 62] Accordingly, the (*rac*)-2-ethylhexyl moiety does not prevent the formation of homochiral self-assemblies, left-handed and right-handed for **(*S*)-BTA** and **(*R*)-BTA**, respectively.[59]

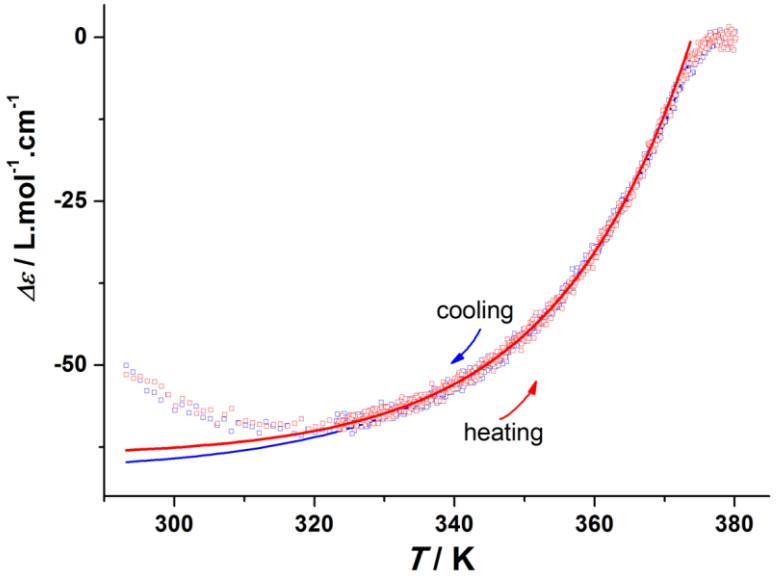

Figure S5 Stability of BTA self-assemblies. (a) CD cooling (blue) and heating (red) curves of **(*S*)-BTA** (0.2 mM, DHN, λ =225 nm), between 293 K and 390 K, cooling and heating rate =0.3 K.min^{-1}. The curves have been fitted with the nucleation-growth model.[61] For sake of clarity, only the fit of the elongation regime is shown. The decreasing of the CD values at the lower temperatures is attributed to partial precipitation occurring under these conditions. The thermodynamic parameters extracted from the fits are compiled in Table 1.

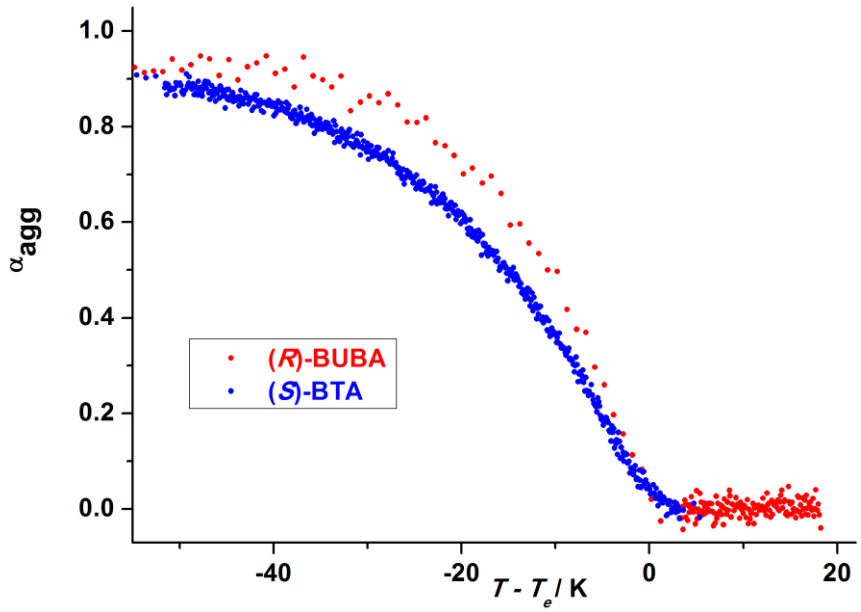

Figure S6 Comparison of the extent of cooperativity in **(*R*)-BUBA** and **(*S*)-BTA** self-assembly process. Plot of the degree of association (as deduced from CD cooling curves) as a function of $T-T_e$.

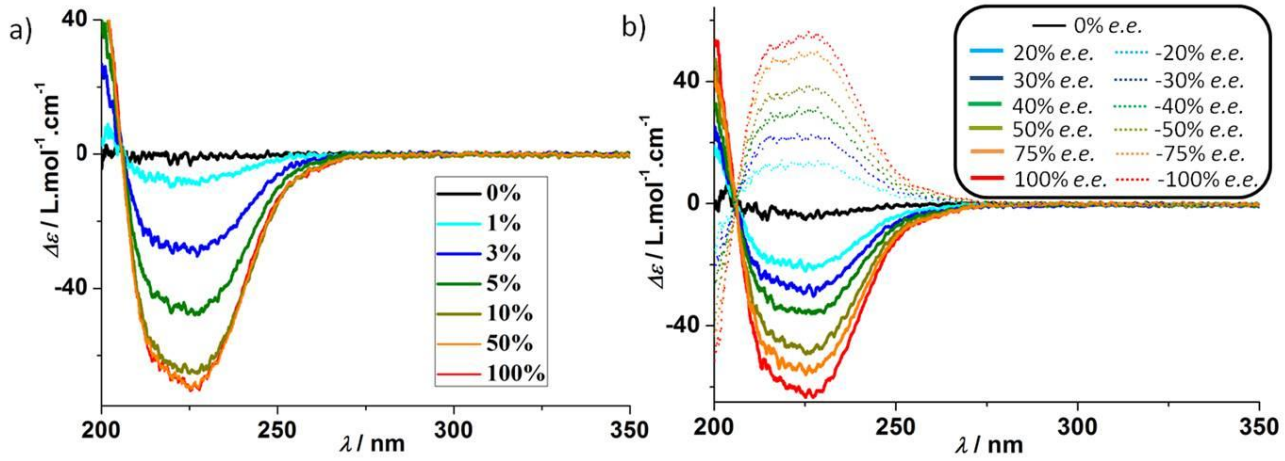

Figure S7 Chirality amplification properties of BTA assemblies. (a) CD spectra of the sergeants-and-soldiers type experiments obtained by mixing solutions of **(*S*)-BTA** and **(*rac*)-BTA** at 293 K (c_{tot} =0.2 mM, DHN). (b) CD spectra of the majority-rules type experiments obtained by mixing solutions of **(*R*)-BTA** and **(*S*)-BTA** at 293 K (c_{tot}=0.2 mM, DHN). Positive (negative) *e.e.* values correspond to mixtures enantioenriched in **(*S*)-BTA** (**(*R*)-BTA** resp.) monomers. Net helicity plotted as a function of the fraction of sergeant and net helicity as a function of the *e.e.* of the BTA monomers are shown in Figs. 6 and 7, respectively.

Note: For each type of monomers, the data of the S&S and MR experiments have been fitted simultaneously following the procedures described by Smulders et al.[65] (for S&S) and by van Gestel[67] (for MR). It provides a single set of energetic parameters (MMP and HRP). Please see the excel spreadsheet in the Supporting Material of this paper for all the details of the calculation.

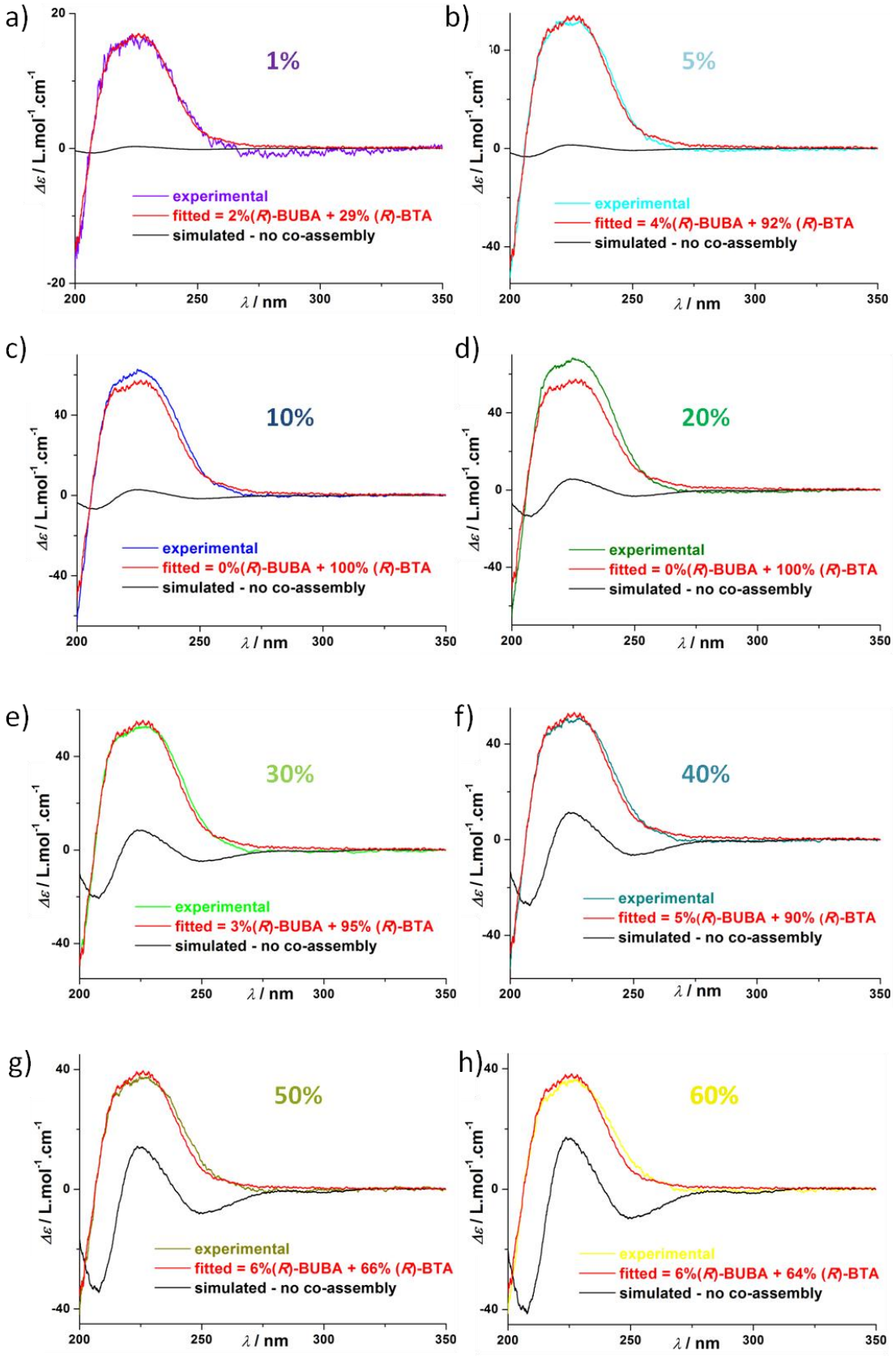
a)
1%
experimental
fitted = 2%(R)-BUBA + 29% (R)-BTA
simulated - no co-assembly
b)
5%
experimental
fitted = 4%(R)-BUBA + 92% (R)-BTA
simulated - no co-assembly
c)
10%
experimental
fitted = 0%(R)-BUBA + 100% (R)-BTA
simulated - no co-assembly
d)
20%
experimental
fitted = 0%(R)-BUBA + 100% (R)-BTA
simulated - no co-assembly
e)
30%
experimental
fitted = 3%(R)-BUBA + 95% (R)-BTA
simulated - no co-assembly
f)
40%
experimental
fitted = 5%(R)-BUBA + 90% (R)-BTA
simulated - no co-assembly
g)
50%
experimental
fitted = 6%(R)-BUBA + 66% (R)-BTA
simulated - no co-assembly
h)
60%
experimental
fitted = 6%(R)-BUBA + 64% (R)-BTA
simulated - no co-assembly
Δε / L.mol-1.cm-1
λ / nm

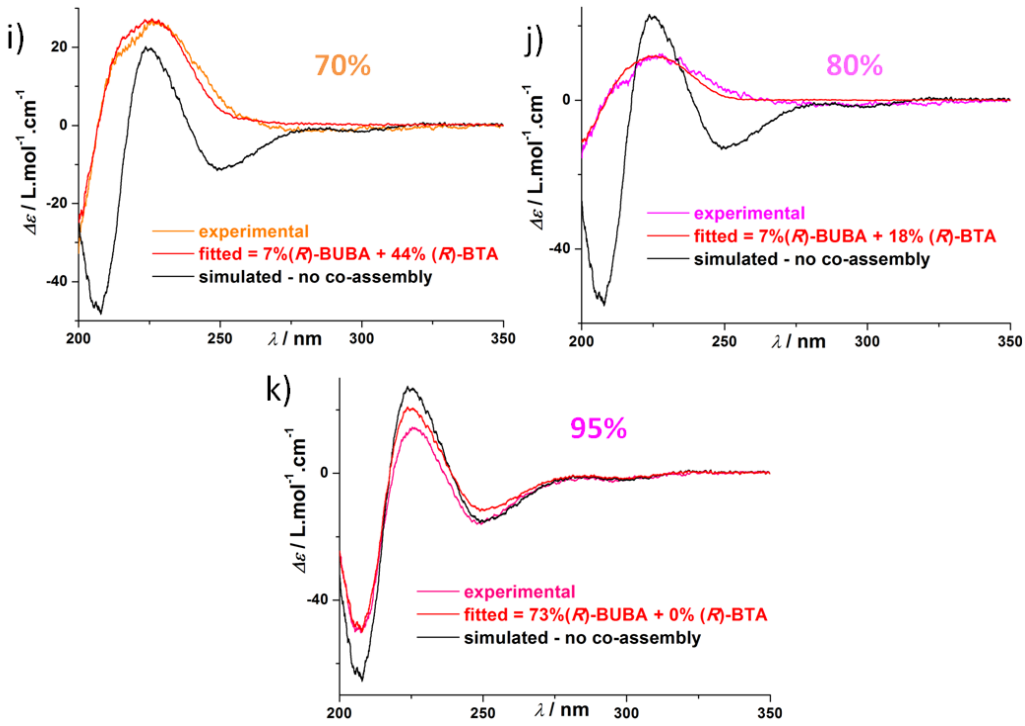

Figure S8 BUBA/BTA co-assemblies. CD spectra obtained by mixing solutions of **(*R*)-BUBA** and **(*rac*)-BTA** at 293 K (c_{tot} =0.2 mM, DHN) with the following fractions of **(*R*)-BUBA**: 1% (a), 5% (b), 10% (c), 20% (d), 30% (e), 40% (f), 50% (g), 60% (h), 70% (i), 80% (j) and 95% (k). For each mixture, the experimental spectrum is shown together with the fitted CD curve and the simulated CD spectrum for segregated stacks (no co-assembly, obtained by considering that only the introduced amount **(*R*)-BUBA** contributes to the CD signal of the mixture).

Fitting procedure: The error difference between the experimental CD curve and the curve obtained by a linear combination of the individual CD plots of **(*R*)-BUBA** and **(*R*)-BTA** is minimized with the FFO function of Origin software such as:

experimental CD curve = *a* × CD curve of **(*R*)-BUBA** + *b* × CD curve of **(*R*)-BTA**

in which *a* and *b* are the fitted parameters. They are indicated in the caption for each mixture. They provide the relative contribution of **(*R*)-BUBA** (for *a*) and **(*R*)-BTA** (for *b*) to the overall CD signal displayed by the co-assemblies. The extent of chirality amplification in the co-assemblies is equal to the sum of the monomers adopting a chiral conformation, *i.e.*:

fraction of monomers with a chiral conformation = a + b

The conformational preference within the co-assemblies is assessed as follows:

conformational preference = b / (a + b)

For 0.5<*conformational preference*<1, the co-assemblies mainly adopt a BTA-like conformation whereas for 0<*conformational preference* <0.5 the co-assemblies mainly adopt a BUBA-like conformation.

All the data extracted from the fits are compiled in Table S1.

Table S1 Molar fractions of the monomers adopting **(*R*)-BUBA** and **(*R*)-BTA**-like conformations in **(*R*)-BUBA/(*rac*)-BTA** mixtures. .

fraction of **(*R*)-BUBA** in the mixture	fraction of monomers with **(*R*)-BUBA** conformation (*a*)	fraction of monomers with **(*R*)-BTA** conformation (*b*)	*a + b*	*b / (a+b)*
0.01	0.02	0.29	0.31	0.94
0.05	0.04	0.92	0.96	0.96
0.1	0	1	1	1
0.2	0	1	1	1
0.3	0.03	0.95	0.98	0.97
0.4	0.05	0.9	0.95	0.95
0.5	0.06	0.66	0.72	0.92
0.6	0.06	0.64	0.70	0.92
0.7	0.07	0.44	0.51	0.86
0.8	0.07	0.18	0.25	0.72
0.95	0.73	0	0.73	0

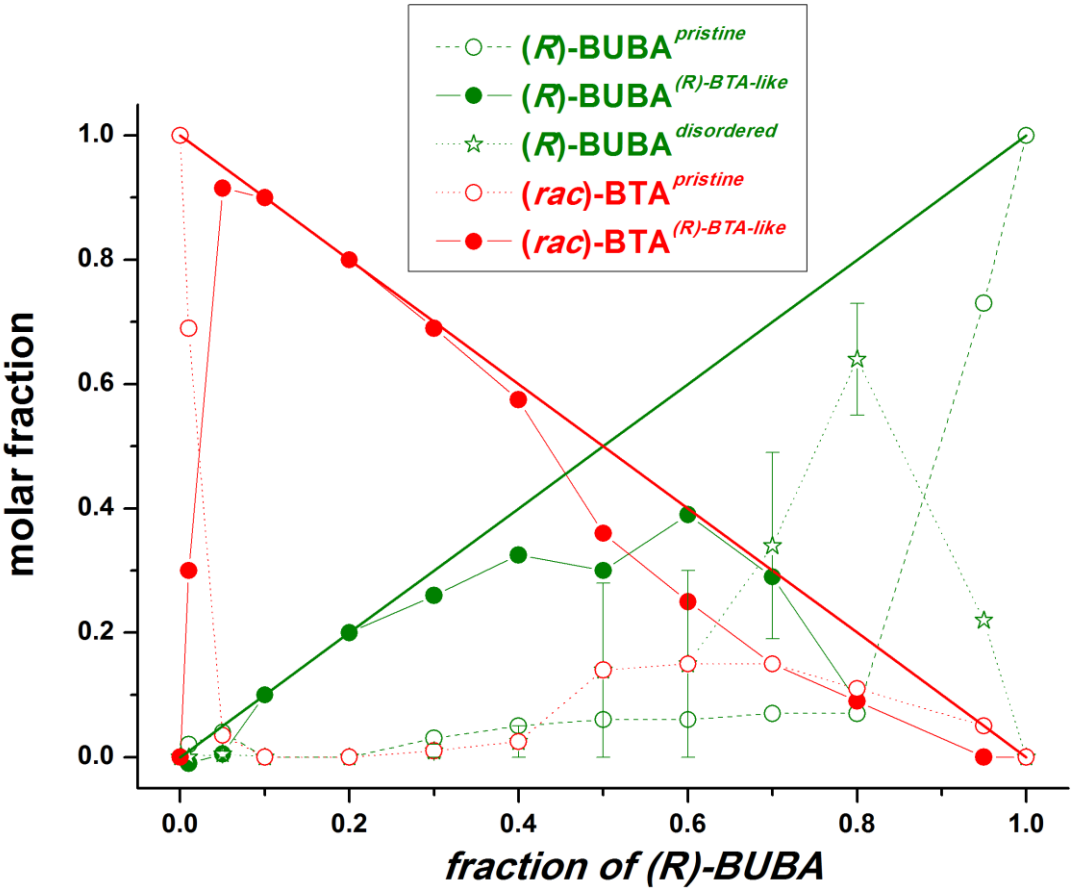

Figure S9 BUBA/BTA co-assemblies. Speciation plot deduced from the fits in Fig. S8. The straight lines represent the total **(*R*)-BUBA** (green) and **(*rac*)-BTA** (red) content.

Speciation: We attempt to account for the values *a* and *b* determined above, by assuming the presence of 5 species:

(*R*)-BUBA$^{\text{pristine}}$ represents the molar fraction of stacked **(*R*)-BUBA** molecules with a conformation similar to pure **(*R*)-BUBA** stacks. Their contribution to the CD signal is supposed to be identical to pure **(*R*)-BUBA** stacks.

(*R*)-BUBA$^{(R)\text{-BTA-like}}$ represents the molar fraction of stacked **(*R*)-BUBA** molecules with a conformation similar to pure **(*R*)-BTA** stacks. Their contribution to the CD signal is supposed to be identical to pure **(*R*)-BTA** stacks.

(*R*)-BUBA$^{\text{disordered}}$ represents the molar fraction of stacked **(*R*)-BUBA** molecules with an irregular conformation. Their contribution to the CD signal is supposed to be negligible.

(*rac*)-BTA$^{\text{pristine}}$ represents the molar fraction of stacked **(*rac*)-BTA** molecules with a conformation similar to pure **(*rac*)-BTA** stacks. Their contribution to the CD signal is supposed to be negligible.

(*rac*)-BTA$^{(R)\text{-BTA-like}}$ represents the molar fraction of stacked **(*rac*)-BTA** molecules with a conformation similar to pure **(*R*)-BTA** stacks. Their contribution to the CD signal is supposed to be identical to **(*R*)-BTA** stacks.

With these assumptions, a and b are determined by the molar fractions of the CD active species:

a = **(*R*)-BUBA**pristine

and

b = **(*R*)-BUBA(*R*)-BTA**-like + **(rac)-BTA(*R*)-BTA**-like

Moreover, mass balance imposes that:

BUBA = **(*R*)-BUBA**pristine + **(*R*)-BUBA(*R*)-BTA**-like + **(*R*)-BUBA**disordered

and

BTA = **(rac)-BTA**pristine + **(rac)-BTA(*R*)-BTA**-like

where BUBA and BTA are the total molar fractions of the two monomers.

These equations can be rearranged as follows:

(*R*)-BUBApristine = a

(*R*)-BUBA(*R*)-BTA-like = BUBA - a - **(*R*)-BUBA**disordered

(rac)-BTApristine = 1 - a - b - **(*R*)-BUBA**disordered

(rac)-BTA(*R*)-BTA-like = a + b - BUBA + **(*R*)-BUBA**disordered

It is not possible to determine unambiguously **(*R*)-BUBA**disordered since we have 5 unknown concentrations and only 4 equations. However, if we express that all molar fractions must be positive, we obtain the following constraints:

(*R*)-BUBAdisordered < BUBA - a

(*R*)-BUBAdisordered < 1 - a - b

(*R*)-BUBAdisordered > BUBA - a - b

For each composition, we assign to **(*R*)-BUBA**disordered the middle of this possible range, with the corresponding uncertainty:

(*R*)-BUBAdisordered = (BUBA - a - b + min{BUBA - a; 1 - a - b})/2

The obtained molar fractions are compiled in Table S.2 and plotted on Fig. S9.

Interpretation: When **(*R*)-BUBA** is the minor component of the mixture (*i.e.* 0.01 < **BUBA** < 0.5) we find that **(*R*)-BUBA**$^{\textbf{disordered}}$, **(*R*)-BUBA**$^{\textbf{pristine}}$ and **(*rac*)-BTA**$^{\textbf{pristine}}$ all have negligible values. There are only two main species: **(*R*)-BUBA**$^{\textbf{(}\textit{R}\textbf{)-BTA-like}}$ and **(*rac*)-BTA**$^{\textbf{(}\textit{R}\textbf{)-BTA-like}}$. In other words, the co-assembly of the two monomers leads to full chirality amplification where **(*R*)-BUBA** (the sergeant) imposes its helical preference, but **(*rac*)-BTA** (the soldier, which is present in excess) imposes its conformation.

When **(*R*)-BUBA** is the major component of the mixture (*i.e.* 0.5 < **BUBA** < 1) the situation is more complex. In particular, it is not possible to obtain consistent values without a significant proportion of **(*R*)-BUBA**$^{\textbf{disordered}}$. This is probably due to the fact that the proportion of soldier (**(*rac*)-BTA**) is insufficient to impose its conformation. Moreover, the sergeant (**(*R*)-BUBA**) is not able to impose its conformation either, because even with **BUBA** = 0.95, the CD signal shows that not all sergeants contribute to the BUBA signature (a = 0.73). Therefore the presence of **(*rac*)-BTA** in stacks rich in **(*R*)-BUBA** create defects that reduce the CD activity of the sergeant in the stacks.

Table S2 Molar fractions of the different species in **(*R*)-BUBA**/**(*rac*)-BTA** mixtures.

fraction of **(*R*)-BUBA** in the mixture	**(*R*)-BUBA** monomers with **(*R*)-BUBA** conformation	**(*R*)-BUBA** monomers with **(*R*)-BTA** conformation	**(*R*)-BUBA** monomers with disordered conformation	**(*rac*)-BTA** monomers with **(*rac*)-BTA** conformation	**(*rac*)-BTA** monomers with **(*R*)-BTA** conformation
Abb.	**(*R*)-BUBA^{pristine}**	**(*R*)-BUBA$^{(R)\text{-}BTA\text{-}like}$**	**(*R*)-BUBA^{disordered}**	**(*rac*)-BTA^{pristine}**	**(*rac*)-BTA$^{(R)\text{-}BTA\text{-}like}$**
0	0	0	0	1	0
0.01	0.02	-0.01	0	0.69	0.3
0.05	0.04	0.005	0.005	0.035	0.915
0.1	0	0.1	0	0	0.9
0.2	0	0.2	0	0	0.8
0.3	0.03	0.26	0.01	0.01	0.69
0.4	0.05	0.325	0.025	0.025	0.575
0.5	0.06	0.3	0.14	0.14	0.36
0.6	0.06	0.39	0.15	0.15	0.25
0.7	0.07	0.29	0.34	0.15	0.15
0.8	0.07	0.09	0.64	0.11	0.09
0.95	0.73	0	0.22	0.05	0
1	1	0	0	0	0

Experimental Section

Materials: *N*,*N*',*N*''-tris(2-ethylhexyl)benzene-1,3,5-tricarboxamide (**(*rac*)-BTA**),[54] 1-(4-Tolyl)-3-(2-EthylHexyl)-Urea (**4TEHU**),[53] *N*-(2-EthylHexyl)BenzenecarboxAmide (**EHBA**),[86] and 5-methoxycarbonyl-benzene-1,3-dicarboxylic acid[34] were prepared by following or adapting published procedures. *N*-(3-dimethylaminopropyl)-*N'*-ethylcarbodiimide hydrochloride (EDC·HCl) was purchased from Fluorochem. 4-(Dimethylamino)pyridine (DMAP), *N*,*N*-diisopropylethylamine (DIEA), dimethyl 5-aminoisophthalate, (*S*)-2-octylamine, (*R*)-2-octylamine, 2-ethylhexylamine, LiOH and triphosgene were purchased from Sigma-Aldrich. All the chemicals were used as received. C_7D_8 was bought from Eurisotop and used without further purification. Decahydronaphthalene (DHN), mixture of *cis* and *trans* isomers (purity≥99%), was bought from Sigma-Aldrich and used without further purification. Dried toluene and dichloromethane (DCM) were obtained from a Solvent Purification System (SPS).

Methods: NMR spectra were recorded on a Bruker Avance 400 spectrometer and calibrated to the residual solvent peak: dmso-d_6 (^{1}H: 2.50 ppm; ^{13}C: 39.52 ppm). Peaks are reported with their corresponding multiplicity (s: singlet; br s: broad singlet, d: doublet, t: triplet; sept.: septuplet, m: multiplet) coupling constants and integration.

Exact mass measurements (HRMS) were obtained on TQ R30-10 HRMS spectrometer by ESI$^+$ ionization and are reported in *m/z* for the major signal.

Fourier-Transform Infrared (FT-IR) measurements were performed on a Nicolet iS10 spectrometer. Spectra for toluene or DHN solutions were measured in 0.02 cm pathlength CaF_2 cells at 293 K and were corrected for air, solvent and cell absorption. Spectra for solids were recorded by reflection on a Ge probe (ATR-FTIR) and the main peaks were reported (m: medium, s: strong, w: wide).

Circular dichroism (CD) measurements were performed on a Jasco J-1500 spectrometer equipped with a Peltier thermostated cell holder and Xe laser. Data were recorded with the following parameters: 50 nm.min^{-1} sweep rate, 0.05 nm data pitch, 2.0 nm bandwidth, and between 350 and 200 nm. A 1 mm quartz cell was used. DHN and cell contributions at the same temperature were subtracted from the obtained signals. For all samples, LD contribution was negligible (ΔLD < 0.005 dOD) and the shape of the CD signal was independent of the orientation of the quartz cell. Molar CD values are reported in L.mol^{-1}.cm^{-1} and are expressed as follows: $\Delta\varepsilon=\theta/(32980\times l\times c)$ where θ is the measured ellipticity (mdeg), l is the optical pathlength in cm, and c is the concentration in mol.L^{-1}. For VT-CD experiments, the temperature was controlled with a Peltier thermostated cell holder, one spectrum was recorded every 10 K between 293 K and 373 K and the heating and cooling rates were set to 1K.min^{-1}. The ellipticity was also recorded at 225 nm (for BTA monomers) and 250 nm (for BUBA monomers) and the heating and cooling rates were set to 1K.min^{-1}.

UV-Vis absorption spectra were extracted from CD analyses on each of the above samples and obtained after correction of the absorption of air, solvent, and cell contribution at the same temperature.

Small-angle neutron scattering (SANS) measurements were made at the LLB (Saclay, France) on the PA20 instrument, at three distance-wavelength combinations to cover the 2.4×10^{-3} to 0.46 Å q^{-1} range, where the scattering vector q is defined as usual, assuming elastic scattering, as $q=(4\pi/\lambda)\sin(\theta/2)$, where θ is the angle between incident and scattered beam. Data were corrected for the empty cell signal and the solute and solvent incoherent background. A light water standard was used to normalize the scattered intensities to cm^{-1} units. The data was fitted with the DANSE software SasView. The number n of molecule in the cross-section can be derived from n_L (the number of molecule per unit length) by assuming an average intermolecular distance of 3.62 Å, which is the usual spacing between aromatic rings in BTA helical assemblies.

Preparation of the solutions of BUBA and BTA homopolymers: Desired amounts of monomer and solvent were introduced in a vial sealed with a PTFE-coated cap to avoid contamination from leaching plasticizer, and briefly heated up to solvent boiling point to ensure dissolution. After cooling down to room temperature, the solutions were quickly analyzed. Preparation of S&S, MR and

BUBA/BTA mixtures: Stock solutions of the pure monomers were mixed in the desired amount, briefly heated up to solvent boiling point, cooled down to room temperature and quickly analyzed.

Synthesis of BUBA precursors. Synthesis of 3,5-dimethyl-1-(2-ethylhexyl urea) benzoate, (**1**): In an oven-dried Schlenk flask, a solution of dimethyl 5-aminoisophthalate (1.0 g, 4.78 mmol, 1.0 equiv.) and DIEA (678 mg, 5.26 mmol 1.1 equiv.) in DCM (40 mL) was added with a syringe pump (10 mL/h) to a solution of triphosgene (0.47 g, 1.57 mmol, 0.33 equiv.) in DCM (10 mL). The solution was stirred 5 additional minutes and 2-ethylhexylamine (678 mg, 5.26 mmol 1.1 equiv.) and DIEA (678 mg, 5.26 mmol, 1.1 equiv.) were added to the solution. The reaction mixture was stirred overnight. The volatiles were evaporated under vacuum and the crude product was taken up in AcOEt and washed successively with an aqueous solution of HCl (2 M), an aqueous solution of NaOH (1 M) and brine. The organic phase was dried over $MgSO_4$ and evaporated under vacuum to yield **1** as a colourless solid which was used for the next step without further purification (1.31 g, 75% yield). ^{1}H NMR (dmso-d_6): δ (ppm) = 8.94 (s, 1H), 8.25 (m, 2H), 8.00 (m, 1H), 6.17 (t, 1H, ^3J=5.8 Hz), 3.87 (s, 6H), 3.05 (m, 2H), 1.55-1.05 (m, 9H), 0.96-0.77 (m, 6H). ^{13}C{^{1}H} NMR (dmso-d_6): δ (ppm) = 165.5, 155.0, 141.6, 130.5, 121.9, 121.8, 52.4, 30.4, 28.4, 23.6, 22.5, 13.9, 10.7. FT-IR (ATR, cm^{-1}): 643 (m), 756 (m), 990 (w), 1122 (m), 1244 (s), 1348 (m), 1442 (m), 1555 (s), 1640 (s), 1724 (s), 2937 (w), 3303 (w). HRMS (ESI, *m/z*): Calculated for $C_{19}H_{28}N_2O_5Na$, [M+ Na]$^+$: 387.1890, found: 387.1890.

Synthesis of {1-(2-ethylhexyl urea)}-3,5-benzoic diacid, (**2**): Compound **1** (1.0 g, 2.58 mmol, 1.0 equiv.) was dissolved in methanol (100 mL). LiOH (197 mg, 8.26 mmol, 3.2 equiv.) and H_2O (1.0 g) were added and the mixture was heated to 55 ℃ overnight. Then, 100 mL of water and 100 mL of an aqueous solution of HCl (1 M) were added successively. A white powder precipitated which was isolated by filtration, washed with H_2O, and dried over P_2O_5 under vacuum to give **2** as a colourless solid (0.88 g, 95% yield). ^{1}H NMR (dmso-d_6): δ (ppm) =13.09 (s, 2H), 8.83 (s, 1H), 8.20 (m, 2H), 8.00 (m, 1H), 6.17 (t, 1H, ^3J=5.8 Hz), 3.05 (m, 2H), 1.55-1.05 (m, 9H), 0.96-0.77 (m, 6H). ^{13}C{^{1}H} NMR (dmso-d_6): δ (ppm) = 166.7, 155.1, 141.3, 131.6, 122.4, 122.0, 41.7, 30,5, 28.5, 23.7, 22.6, 14.0, 10.8. FT-IR (ATR, cm^{-1}): 638 (m),758 (m), 990 (m), 1122 (m), 1231 (s), 1348 (m), 1437 (m), 1555 (s), 1640 (s) , 1730 (s), 2927 (w), 3296 (w). HRMS (ESI, *m/z*): Calculated for $C_{17}H_{24}N_2O_5Na$, [M+ Na]$^+$:359.1577, found :359.1576.

General procedure for the synthesis of BUBA monomers: Compound **2** (1.0 equiv.) was dissolved in THF, and DMAP (3.4 equiv.), the desired amine (3.0 equiv.), and EDC·HCl (3.4 equiv.) were added successively. The solution was refluxed for 2 days. Then, THF was removed, the crude solid was dissolved in CH_2Cl_2 and the solution was washed with an aqueous solution of HCl (1 M), an aqueous solution of $NaHCO_3$ (1 M) and with brine successively. The organic phase was dried over

$MgSO_4$ filtered, and purified by flash column chromatography (SiO_2, CH_2Cl_2/AcOEt). The obtained solids were recrystallized from MeCN yielding pure BUBA monomers as colourless solids.

***(S)*-BUBA** (with (*S*)-2-octylamine, crystalline solid, 1.0 g, 70% yield): ^{1}H NMR (dmso-d_6): δ (ppm) =8.62 (s, 1H), 8.15 (d, ^3J=8.2 Hz, 2H), 7.87 (br s, 2H), 7.69 (br s, 1H), 6.13 (t, ^3J=5.5 Hz, 1H), 3.98 (sept., ^3J=6.5 Hz, 2H), 3.14-2.97 (m, 2H), 1.67-1.18 (m, 29H), 1.12 (d, ^3J = 6.5 Hz, 6H), 1.02-0.83 (m, 12H). ^{13}C{^{1}H} NMR (dmso-d_6): δ (ppm) = 165.7, 155.1, 140.4, 135.9, 118.7, 118.4, 44.9, 41.6, 35.9, 31.2, 30.4, 28.6, 28.4, 25.8, 23.7, 22.5, 22.0, 20.7, 13.9, 10.8. FT-IR (ATR, cm^{-1}): 699 (m), 1225 (m), 1263 (m), 1451 (m),1545 (s), 1620 (m), 2927 (m), 3271 (m), 3345 (s). HRMS (ESI, *m/z*): Calculated for $C_{33}H_{58}N_4O_3Na$, [M+ Na]$^+$: 581.4401, found: 581.4403.

***(R)*-BUBA** (with (*R*)-2-octylamine, crystalline solid, 1.5 g, 78% yield): Spectroscopic data are identical to **(*S*)-BUBA**. HRMS (ESI, *m/z*): Calculated for $C_{33}H_{58}N_4O_3Na$, [M+ Na]$^+$: 581.4401, found: 581.4400.

***(rac)*-BUBA** (with 2-ethylhexylamine, amorphous solid, 2.0 g, 71% yield): ^{1}H NMR (dmso-d_6): δ (ppm) =8.61 (s, 1H), 8.33 (t, ^3J=5.3 Hz, 2H), 7.90 (br s, 2H), 7.72 (br s, 1H), 6.15 (t, ^3J=5.4 Hz, 1H), 3.18 (t, ^3J=5.9 Hz, 4H), 3.11-2.98 (m, 2H), 1.62-1.47 (m, 2H), 1.45-1.14 (m, 25H), 0.95-0.79 (m, 18H). ^{13}C{^{1}H} NMR (dmso-d_6): δ (ppm) = 165.9, 155.1, 140.5, 135.8, 118.4, 118.3, 42.4, 41.6, 30.5, 30.4, 28.4, 28.3, 23.7, 22.5, 13.9, 10.5. FT-IR (ATR, cm^{-1}): 689 (m), 1228 (m), 1271 (m), 1452 (m), 1535 (s), 1638 (m), 2924 (m), 3302 (m). HRMS (ESI, *m/z*): Calculated for $C_{33}H_{58}N_4O_3Na$, [M+ Na]$^+$: 581.4401, found: 581.4402.

Synthesis of BTA precursors.

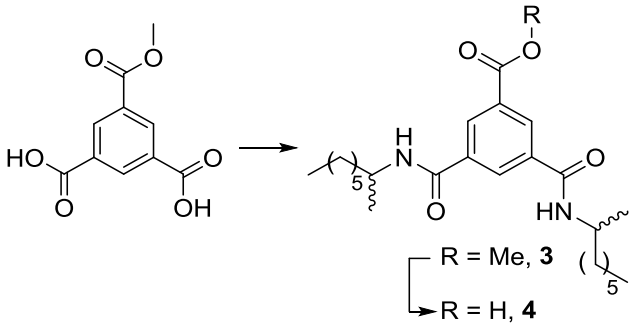

Synthesis of methyl 3,5-bis-(1*S*)-(1-methyl-heptylcarbonyl)-1-methyl-benzoate (**3*S***): 5-methoxycarbonyl-benzene-1,3-dicarboxylic acid[34] (2.48 g, 11.0 mmol, 1.0 equiv.) was dissolved in THF (100 mL), then DMAP (4.60 g, 37.6 mmol, 3.4 equiv.), (*S*)-2-octylamine (4.29 g, 33.2 mmol, 3 equiv.) and EDC·HCl (7.21 g, 37.6 mmol, 3.4 equiv.) were added successively. The solution was reflux for 2 days. Then, THF was evaporated, the crude solid was dissolved in CH_2Cl_2, washed with an aqueous solution of HCl (1M), an aqueous solution of $NaHCO_3$ (10%) and with brine successively. The organic

phase was dried over $MgSO_4$, filtered and purified by flash column chromatography (SiO_2, CH_2Cl_2/AcOEt=92/8) yielding **3*S*** as a colourless solid. (1.9 g, 51% yield). ^{1}H NMR (dmso-d_6): δ (ppm) =8.70-8.22 (m, 5H), 4.14-3.96 (m, 2H), 3.92 (s, 3H), 1.70-103 (m, 26H), 0.95-0.67 (m, 6H). ^{13}C{^{1}H} NMR (dmso-d_6): δ (ppm) =166.5, 164.2, 135.6, 130.8, 129.9, 129.7, 52.4, 45.0, 31.2, 28.5, 25.8, 22.0, 20.6, 13.8. FT-IR (ATR, cm^{-1}): 708 (s), 1265 (s), 1632 (s), 1731 (s), 2855 (w), 2925 (m), 3242 (m). HRMS (ESI, *m/z*): Calculated for $C_{26}H_{42}N_2O_4Na$, [M+ Na]$^+$:469.3037, found : 469.3036.

Compound **3*R*** (1.4 g, 37% yield) was obtained following the same procedure with (*R*)-2-octylamine and spectroscopic data are identical to **3*S***.

Synthesis of 3,5-bis-(1*S*)-(1-methyl-heptylcarbonyl)-1-benzoic acid (**4*S***): compound **3*S*** (1.9 g, 5.6 mmol, 1 equiv.) was dissolved in methanol (150 mL). LiOH (216 mg, 9 mmol, 1.6 equiv.) and H_2O (3 mL) were added and the mixture was heated to 55°C overnight. Then, 500 mL of water was added and the solution was acidified until pH≈1. A white powder precipitated which was isolated by filtration, washed with H_2O and dried over P_2O_5 under vacuum yielding **4*S*** as a colourless solid (1.6 g, 90% yield). ^{1}H NMR (dmso-d_6): δ (ppm) =8.89-7.86 (m, 5H), 4.32-3.85 (m, 2H), 1.70-1.03 (m, 26H), 0.95-0.67 (m, 6H). ^{13}C{^{1}H} NMR (dmso-d_6): δ (ppm) =166.5, 164.2, 135.7, 130.8, 129.9, 129.7, 45.0, 39.5, 35.8, 31.2, 28.5, 25.8, 22.0, 20.6, 13.8. FT-IR (ATR, cm^{-1}): 669 (s), 689 (s), 989 (s), 1021 (s), 1256 (s), 1443 (w), 1538 (s), 1640 (s), 1703 (w), 2853 (w), 2926 (m), 2960 (w), 3283 (m). HRMS (ESI, *m/z*): Calculated for $C_{25}H_{40}N_2O_4Na$, [M+ Na]$^+$: 455.2880, found: 455.2879.

Compound **4*R*** (1.5 g, 84% yield) was obtained following the same procedure with ***3R*** and spectroscopic data are identical to **4*S***.

General procedure for the synthesis of BTA monomers: Compound **4** (1.0 equiv.) was dissolved in THF and DMAP (1.7 equiv.), 2-ethylhexylamine (1.5 equiv.), and EDC·HCl (1.7 equiv.) were added successively. The solution was refluxed for 2 days. Then, THF was removed, the crude solid was dissolved in CH_2Cl_2 and the solution was washed with water. The organic phase was dried over $MgSO_4$, filtered and purified by flash column chromatography (SiO_2, CH_2Cl_2/AcOEt). The obtained solids were recrystallized from MeCN yielding pure BTA monomers as colourless amorphous solids.

(S)*-BTA** (with **4*S, 1.0 g, 57% yield): ^{1}H NMR (dmso-d_6): δ (ppm) =8.58 (t, ^3J=5.5 Hz, 1H), 8.40 (d, ^3J=8.3 Hz, 2H), 8.33 (s, 3H), 4.02 (sept., ^3J=7.0 Hz, 2H), 3.21 (t, ^3J = 6.3 Hz, 2H), 1.65-1.41 (m, 4H), 1.39-1.20 (m, 25H), 1.15 (d, ^3J =6.6 Hz, 6H), 0.95-0.78 (m, 12H). ^{13}C{^{1}H} NMR (dmso-d_6): δ (ppm) =165.7, 165.0, 135.3, 135.1, 128.4, 128.3, 45.1, 42.5, 35.9, 31.2, 30.4, 28.6, 28.3, 25.8, 23.7,

22.5, 22.0, 20.7, 13.9, 13.8, 10.6. FT-IR (ATR, cm^{-1}): 667 (s), 691 (s), 987 (s), 1024 (s), 1254 (s), 1537 (s), 1639 (s), 1706 (m), 2854 (w), 2932 (m), 3287 (m). HRMS (ESI, *m/z*): Calculated for $C_{33}H_{57}N_3O_3Na$, $[M+ Na]^+$: 566.4292, found : 566.4291.

(R)*-BTA**: (with ***4R, 1.5 g, 50% yield): HRMS (ESI, *m/z*): Calculated $C_{33}H_{57}N_3O_3Na$, $[M+ Na]^+$: 566.4292, found: 566.4292.

(*R*)-BUBA

^1H NMR (dmso-d_6)

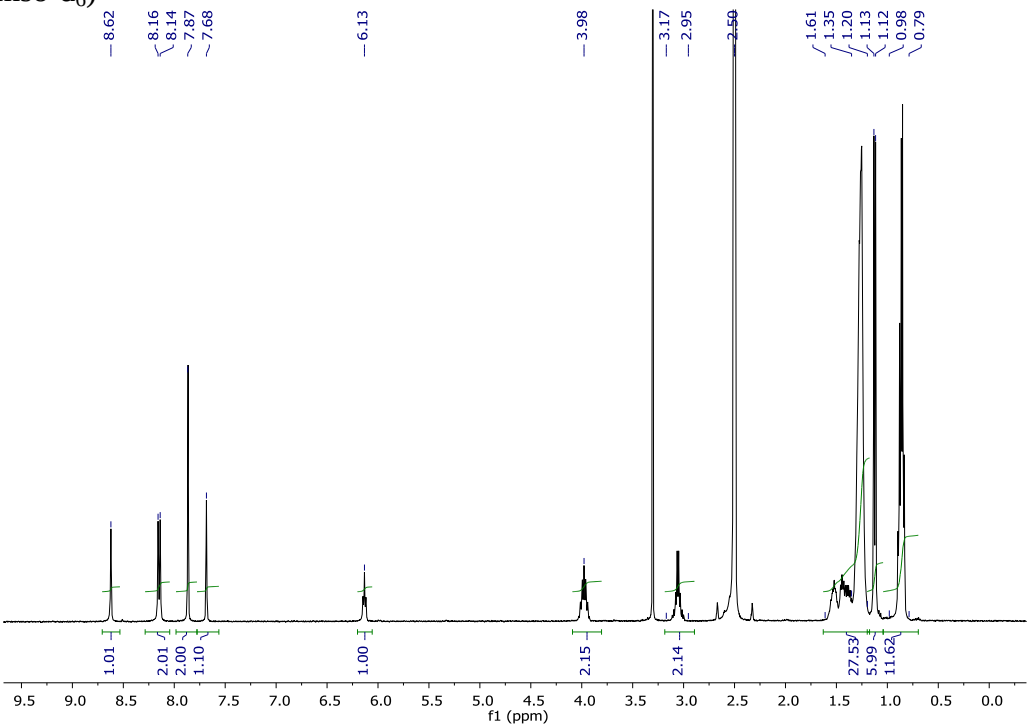

$^{13}C\{^1H\}$ NMR (dmso-d_6) (JMOD)

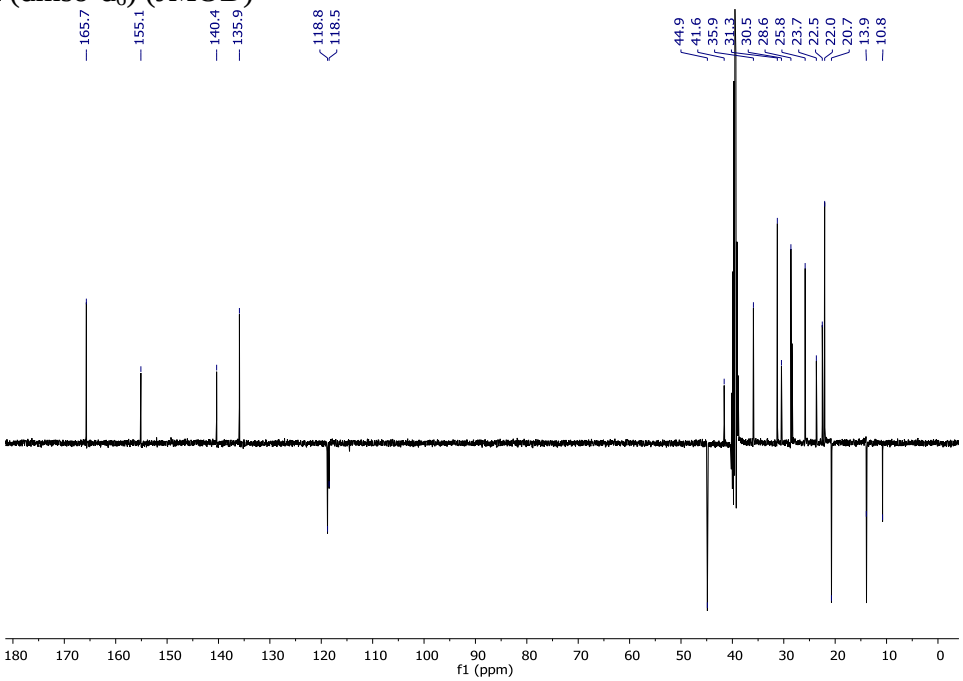

(*S*)-BUBA

^{1}H NMR (dmso-d_6)

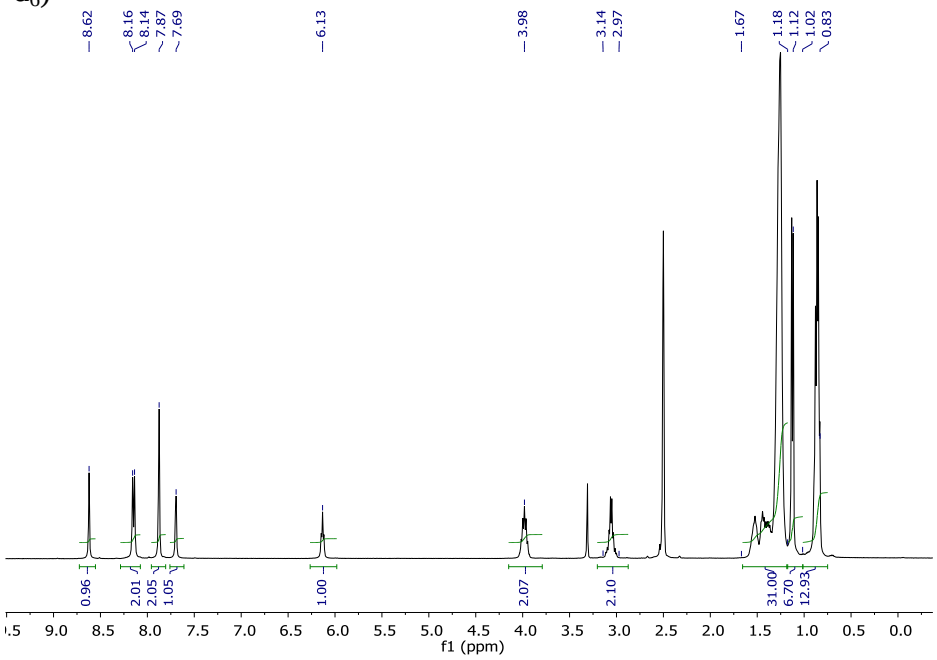

^{13}C{^{1}H} NMR (dmso-d_6) (JMOD)

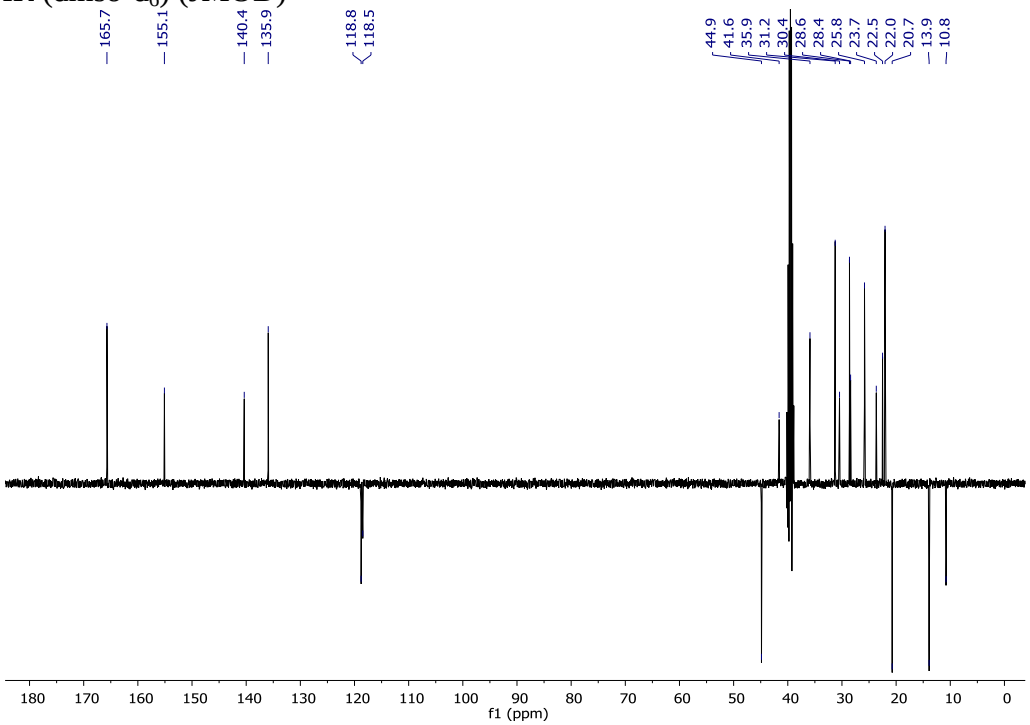

(*rac*)-BUBA

^{1}H NMR (dmso-d_6)

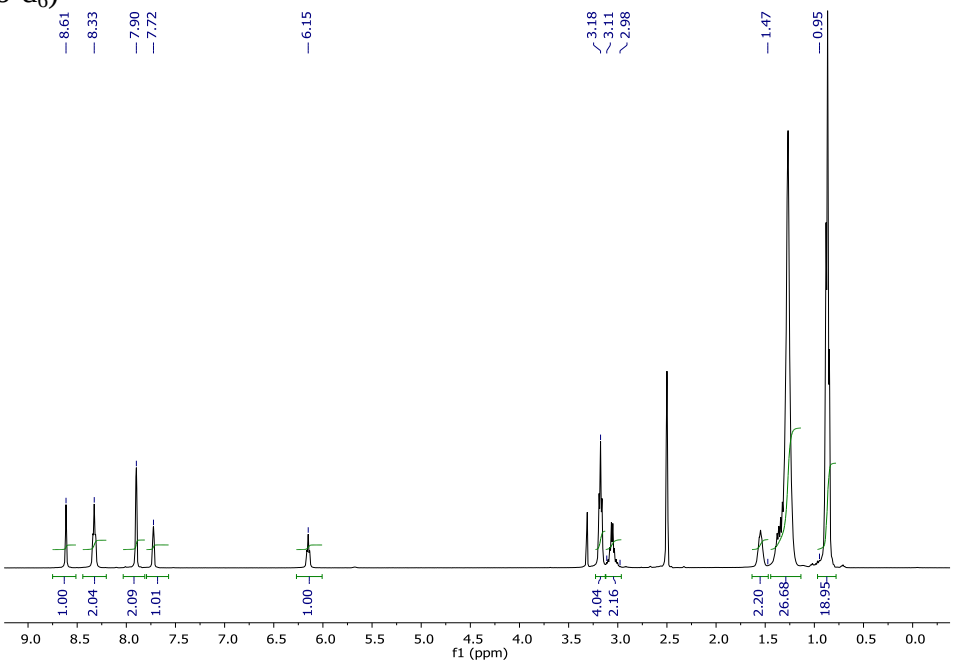

^{13}C{^{1}H} NMR (dmso-d_6) (JMOD)

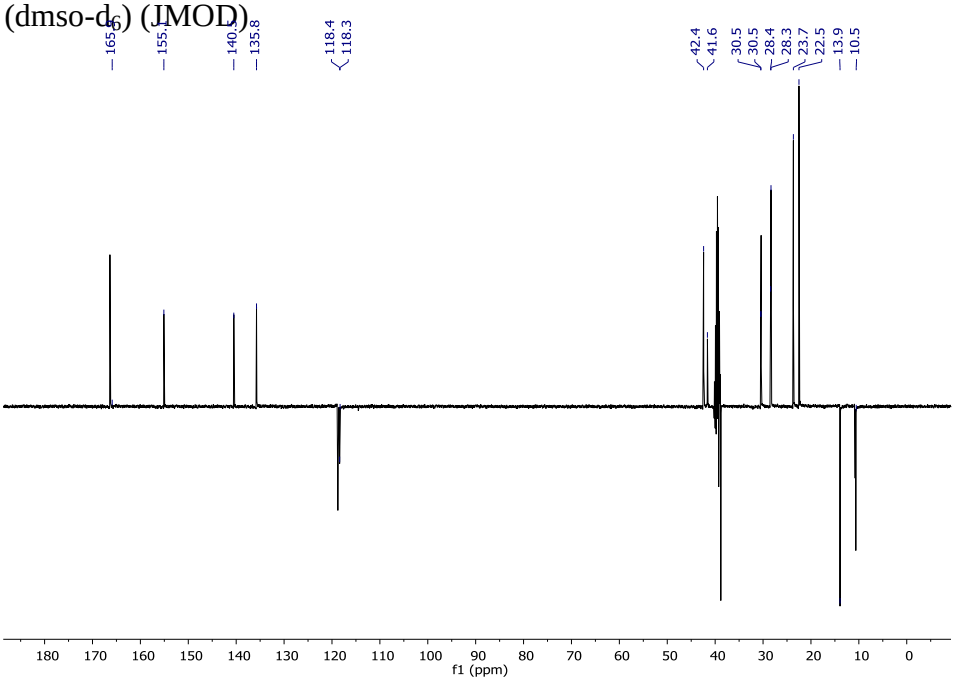

(*R*)-BTA

^{1}H NMR (dmso-d$_6$)

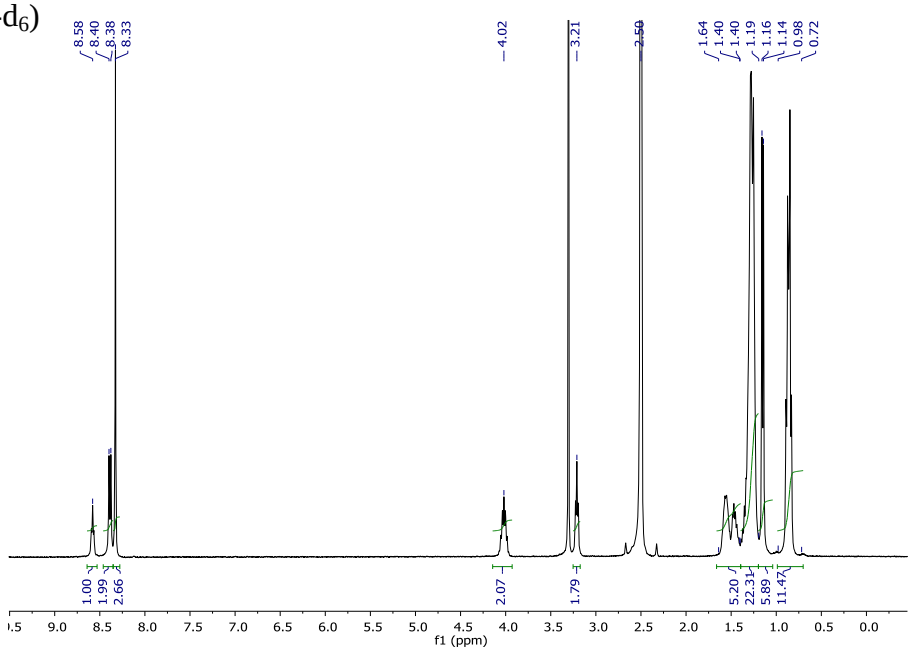

^{13}C{^{1}H} NMR (dmso-d$_6$) (JMOD)

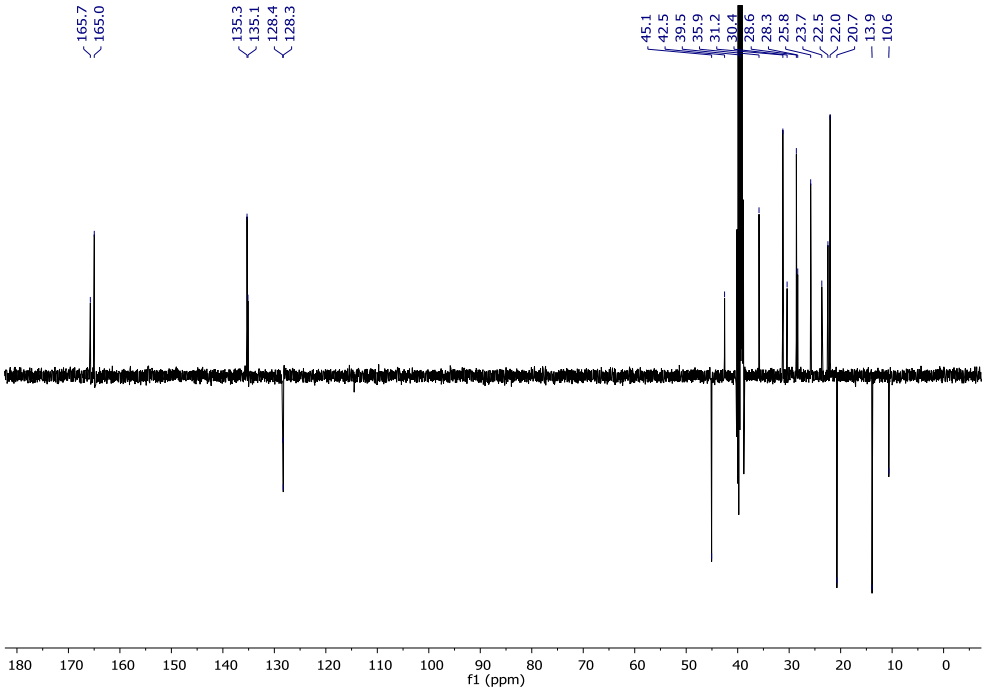

(*S*)-BTA

^{1}H NMR (dmso-d_6)

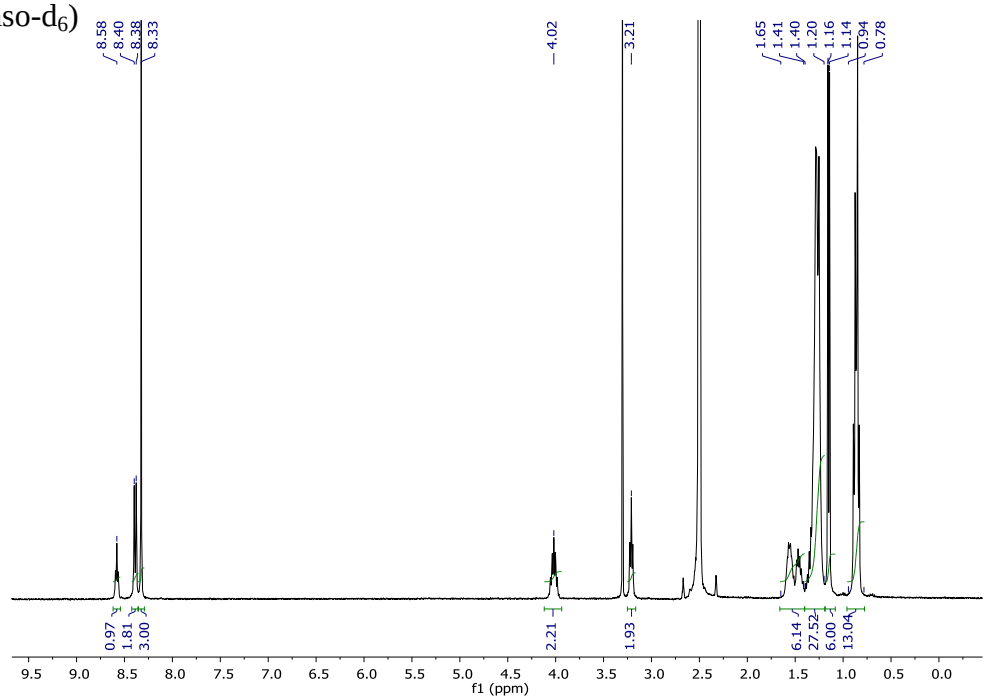

^{13}C{^{1}H} NMR (dmso-d_6) (JMOD)

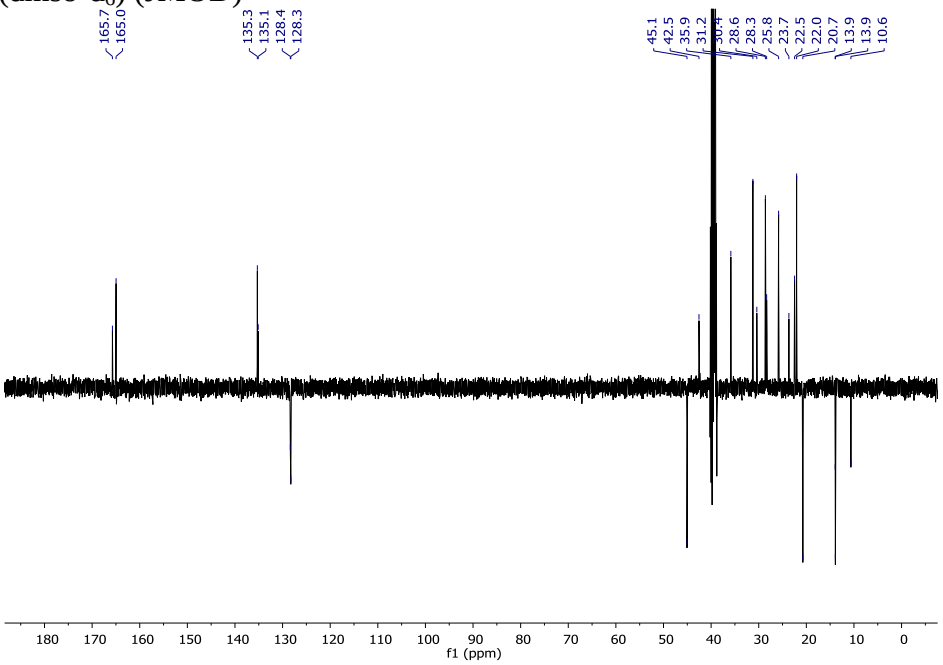

V References

1. Liu, M.; Zhang, L.; Wang, T., Supramolecular Chirality in Self-Assembled Systems. *Chem. Rev.* **2015,** *115* (15), 7304-7397.

2. Yashima, E.; Ousaka, N.; Taura, D.; Shimomura, K.; Ikai, T.; Maeda, K., Supramolecular Helical Systems: Helical Assemblies of Small Molecules, Foldamers, and Polymers with Chiral Amplification and Their Functions. *Chem. Rev.* **2016,** *116* (22), 13752-13990.

3. Boersma, A. J.; Megens, R. P.; Feringa, B. L.; Roelfes, G., DNA-based asymmetric catalysis. *Chem. Soc. Rev.* **2010,** *39* (6), 2083-2092.

4. Kodama, K.; Kobayashi, Y.; Saigo, K., Two-component supramolecular helical architectures: Creation of tunable dissymmetric cavities for the inclusion and chiral recognition of the third components. *Chem. Eur. J.* **2007,** *13* (7), 2144-2152.

5. Jung, S. H.; Jeon, J.; Kim, H.; Jaworski, J.; Jung, J. H., Chiral Arrangement of Achiral Au Nanoparticles by Supramolecular Assembly of Helical Nanofiber Templates. *J. Am. Chem. Soc.* **2014,** *136* (17), 6446-6452.

6. Leyendecker, M.; Meyer, N. C.; Thiele, C. M., Development of New Supramolecular Lyotropic Liquid Crystals and Their Application as Alignment Media for Organic Compounds. *Angew. Chem. Int . Ed.* **2017,** *56* (38), 11471-11474.

7. Fitié, C. F. C.; Roelofs, W. S. C.; Kemerink, M.; Sijbesma, R. P., Remnant Polarization in Thin Films from a Columnar Liquid Crystal. *J. Am. Chem. Soc.* **2010,** *132* (20), 6892-6893.

8. Fitié, C. F. C.; Roelofs, W. S. C.; Magusin, P. C. M. M.; Wübbenhorst, M.; Kemerink, M.; Sijbesma, R. P., Polar Switching in Trialkylbenzene-1,3,5-tricarboxamides. *J. Phys. Chem. B* **2012,** *116* (13), 3928-3937.

9. Urbanaviciute, I.; Meng, X.; Cornelissen, T. D.; Gorbunov, A. V.; Bhattacharjee, S.; Sijbesma, R. P.; Kemerink, M., Tuning the Ferroelectric Properties of Trialkylbenzene-1,3,5-tricarboxamide (BTA). *Adv. Electron. Mater.* **2017,** *3* (7), 1600530.

10. Shen, Z. C.; Wang, T. Y.; Shi, L.; Tang, Z. Y.; Liu, M. H., Strong circularly polarized luminescence from the supramolecular gels of an achiral gelator: tunable intensity and handedness. *Chem. Sci.* **2015,** *6* (7), 4267-4272.

11. Wu, H.; Zhou, Y.; Yin, L.; Hang, C.; Li, X.; Ågren, H.; Yi, T.; Zhang, Q.; Zhu, L., Helical Self-Assembly-Induced Singlet–Triplet Emissive Switching in a Mechanically Sensitive System. *J. Am. Chem. Soc.* **2017,** *139* (2), 785-791.

12. Sandeep, A.; Praveen, V. K.; Kartha, K. K.; Karunakaran, V.; Ajayaghosh, A., Supercoiled fibres of self-sorted donor-acceptor stacks: a turn-off/turn-on platform for sensing volatile aromatic compounds. *Chem. Sci.* **2016,** *7* (7), 4460-4467.

13. Mtangi, W.; Tassinari, F.; Vankayala, K.; Vargas Jentzsch, A.; Adelizzi, B.; Palmans, A. R. A.; Fontanesi, C.; Meijer, E. W.; Naaman, R., Control of Electrons' Spin Eliminates Hydrogen Peroxide Formation During Water Splitting. *J. Am. Chem. Soc.* **2017,** *139* (7), 2794-2798.

14. Zwang, T. J.; Hurlimann, S.; Hill, M. G.; Barton, J. K., Helix-Dependent Spin Filtering through the DNA Duplex. *J. Am. Chem. Soc.* **2016,** *138* (48), 15551-15554.

15. Dorca, Y.; Matern, J.; Fernández, G.; Sanchez, L., C3-symmetrical π-Scaffolds: Useful Building Blocks to Construct Helical Supramolecular Polymers. *Isr. J. Chem.* **2019**, DOI: 10.1002/ijch.201900017.

16. De Greef, T. F. A.; Smulders, M. M. J.; Wolffs, M.; Schenning, A. P. H. J.; Sijbesma, R. P.; Meijer, E. W., Supramolecular Polymerization. *Chem. Rev.* **2009,** *109* (11), 5687-5754.

17. Yang, L. L.; Tan, X. X.; Wang, Z. Q.; Zhang, X., Supramolecular Polymers: Historical Development, Preparation, Characterization, and Functions. *Chem. Rev.* **2015,** *115* (15), 7196-7239.

18. Palmans, A. R. A.; Meijer, E. W., Amplification of chirality in dynamic supramolecular aggregates. *Angew. Chem. Int . Ed.* **2007,** *46* (47), 8948-8968.

19. Ishiwari, F.; Shoji, Y.; Fukushima, T., Supramolecular scaffolds enabling the controlled assembly of functional molecular units. *Chem. Sci.* **2018,** *9* (8), 2028-2041.

20. Dorca, Y.; Greciano, E. E.; Valera, J. S.; Gómez, R.; Sánchez, L., Hierarchy of Asymmetry in Chiral Supramolecular Polymers: Toward Functional, Helical Supramolecular Structures. *Chem. Eur. J.* **2019**, DOI: 10.1002/chem.201805577.

21. Cantekin, S.; de Greef, T. F. A.; Palmans, A. R. A., Benzene-1,3,5-tricarboxamide: a versatile ordering moiety for supramolecular chemistry. *Chem. Soc. Rev.* **2012,** *41* (18), 6125-6137.

22. Raynal, M.; Portier, F.; van Leeuwen, P. W. N. M.; Bouteiller, L., Tunable Asymmetric Catalysis through Ligand Stacking in Chiral Rigid Rods. *J. Am. Chem. Soc.* **2013,** *135* (47), 17687-17690.

23. Huerta , E.; van Genabeek , B.; Lamers, B. A. G.; Koenigs, M. M. E.; Meijer, E. W.; Palmans, A. R. A., Triggering Activity of Catalytic Rod-Like Supramolecular Polymers. *Chem. Eur. J.* **2015,** *21* (9), 3682-3690.

24. Neumann, L. N.; Baker, M. B.; Leenders, C. M. A.; Voets, I. K.; Lafleur, R. P. M.; Palmans, A. R. A.; Meijer, E. W., Supramolecular polymers for organocatalysis in water. *Org. Biomol. Chem.* **2015,** *13* (28), 7711-7719.

25. Desmarchelier, A.; Caumes, X.; Raynal, M.; Vidal-Ferran, A.; van Leeuwen, P. W. N. M.; Bouteiller, L., Correlation between the Selectivity and the Structure of an Asymmetric Catalyst Built on a Chirally Amplified Supramolecular Helical Scaffold. *J. Am. Chem. Soc.* **2016,** *138* (14), 4908-4916.

26. Zimbron, J. M.; Caumes, X.; Li, Y.; Thomas, C. M.; Raynal, M.; Bouteiller, L., Real-Time Control of the Enantioselectivity of a Supramolecular Catalyst Allows Selecting the Configuration of Consecutively Formed Stereogenic Centers. *Angew. Chem. Int . Ed.* **2017,** *56* (45), 14016-14019.

27. Yan, L.; Caumes, X.; Raynal, M.; Bouteiller, L., Modulation of catalyst enantioselectivity through reversible assembly of supramolecular helices. *Chem. Commun.* **2019,** *55*, 2162-2165.

28. Stals, P. J. M.; Korevaar, P. A.; Gillissen, M. A. J.; de Greef, T. F. A.; Fitié, C. F. C.; Sijbesma, R. P.; Palmans, A. R. A.; Meijer, E. W., Symmetry Breaking in the Self-Assembly of Partially Fluorinated Benzene-1,3,5-tricarboxamides. *Angew. Chem. Int . Ed.* **2012,** *51* (45), 11297-11301.

29. Mes, T.; van der Weegen, R.; Palmans, A. R. A.; Meijer, E. W., Single-Chain Polymeric Nanoparticles by Stepwise Folding. *Angew. Chem. Int . Ed.* **2011,** *50* (22), 5085-5089.

30. Hosono, N.; Gillissen, M. A. J.; Li, Y. C.; Sheiko, S. S.; Palmans, A. R. A.; Meijer, E. W., Orthogonal Self-Assembly in Folding Block Copolymers. *J. Am. Chem. Soc.* **2013,** *135* (1), 501-510.

31. Altintas, O.; Artar, M.; ter Huurne, G.; Voets, I. K.; Palmans, A. R. A.; Barner-Kowollik, C.; Meijer, E. W., Design and Synthesis of Triblock Copolymers for Creating Complex Secondary Structures by Orthogonal Self-Assembly. *Macromolecules* **2015,** *48* (24), 8921-8932.

32. Ogura, Y.; Artar, M.; Palmans, A. R. A.; Sawamoto, M.; Meijer, E. W.; Terashima, T., Self-Assembly of Hydrogen-Bonding Gradient Copolymers: Sequence Control via Tandem Living Radical Polymerization with Transesterification. *Macromolecules* **2017,** *50* (8), 3215-3223.

33. Ślęczkowski, M. L.; Meijer, E. W.; Palmans, A. R. A., Cooperative Folding of Linear Poly(dimethyl siloxane)s via Supramolecular Interactions. *Macromol. Rapid. Commun.* **2017,** *38* (24).

34. Roosma, J.; Mes, T.; Leclère, P.; Palmans, A. R. A.; Meijer, E. W., Supramolecular Materials from Benzene-1,3,5-tricarboxamide-Based Nanorods. *J. Am. Chem. Soc.* **2008,** *130* (4), 1120-1121.

35. García-Iglesias, M.; de Waal, B. F. M.; de Feijter, I.; Palmans, A. R. A.; Meijer, E. W., Nanopatterned Superlattices in Self-Assembled C-2-Symmetric Oligodimethylsiloxane-Based Benzene-1,3,5-Tricarboxamides. *Chem. Eur. J.* **2015,** *21* (1), 377-385.

36. Zhang, W.; Horoszewski, D.; Decatur, J.; Nuckolls, C., A folded, secondary structure in step-growth oligomers from covalently linked, crowded aromatics. *J. Am. Chem. Soc.* **2003,** *125* (16), 4870-4873.

37. García, F.; Sánchez, L., Structural Rules for the Chiral Supramolecular Organization of OPE-based Discotics: Induction of Helicity and Amplification of Chirality. *J. Am. Chem. Soc.* **2012,** *134* (1), 734-742.

38. Van Gorp, J. J.; Vekemans, J. A. J. M.; Meijer, E. W., Supramolecular Architectures of C 3 - Symmetrical and Asymmetrical Discotics. *Mol. Cryst. Liq. Cryst.* **2003,** *397* (1), 191-205.

39. San-José, N.; Gómez-Valdemoro, A.; García, F. C.; Serna, F.; García, J. M., Aromatic polyamides with pendant urea moieties. *J. Polym. Sci. A* **2007,** *45* (17), 4026-4036.

40. Bayer 1975.

41. Bera, S.; Maity, S. K.; Haldar, D., Photoelectrochemical properties of CdSe quantum dots doped disk-like tripeptide capsule. *CrystEngComm* **2014,** *16* (22), 4834-4841.

42. Mohan, P.; Singh, R.; Baba, M., Anti-Hiv-1 and Hiv-2 Activity of Naphthalenedisulfonic Acid-Derivatives - Inhibition of Cytopathogenesis, Giant-Cell Formation, and Reverse-Transcriptase Activity. *Biochem. Pharmacol.* **1991,** *41* (4), 642-646.

43. Kassack, M. U.; Braun, K.; Ganso, M.; Ullmann, H.; Nickel, P.; Boing, B.; Muller, G.; Lambrecht, G., Structure-activity relationships of analogues of NF449 confirm NF449 as the most potent and selective known P2X1 receptor antagonist. *Eur. J. Med. Chem.* **2004,** *39* (4), 345-57.

44. McCain, D. F.; Wu, L.; Nickel, P.; Kassack, M. U.; Kreimeyer, A.; Gagliardi, A.; Collins, D. C.; Zhang, Z. Y., Suramin derivatives as inhibitors and activators of protein-tyrosine phosphatases. *J. Biol. Chem.* **2004,** *279* (15), 14713-14725.

45. San-José, N.; Gómez-Valdemoro, A.; Ibeas, S.; García, F. C.; Serna, F.; García, J. M., Colorimetric anion sensing by polyamide models containing urea-binding sites. *Supramol. Chem.* **2010,** *22* (6), 325-338.

46. Wilbur, D. S.; Park, S. I.; Chyan, M. K.; Wan, F.; Hamlin, D. K.; Shenoi, J.; Lin, Y.; Wilbur, S. M.; Buchegger, F.; Pantelias, A.; Pagel, J. M.; Press, O. W., Design and synthesis of bis-biotin-containing reagents for applications utilizing monoclonal antibody-based pretargeting systems with streptavidin mutants. *Bioconjug. Chem.* **2010,** *21* (7), 1225-38.

47. van Gorp, J. J.; Vekemans, J. A. J. M.; Meijer, E. W., C3-Symmetrical Supramolecular Architectures: Fibers and Organic Gels from Discotic Trisamides and Trisureas. *J. Am. Chem. Soc.* **2002,** *124* (49), 14759-14769.

48. Stals, P. J. M.; Smulders, M. M. J.; Martín-Rapún, R.; Palmans, A. R. A.; Meijer, E. W., Asymmetrically Substituted Benzene-1,3,5-tricarboxamides: Self-Assembly and Odd–Even Effects in the Solid State and in Dilute Solution. *Chem. Eur. J.* **2009,** *15* (9), 2071-2080.

49. Smulders, M. M. J.; Filot, I. A. W.; Leenders, J. M. A.; van der Schoot, P.; Palmans, A. R. A.; Schenning, A. P. H. J.; Meijer, E. W., Tuning the Extent of Chiral Amplification by Temperature in a Dynamic Supramolecular Polymer. *J. Am. Chem. Soc.* **2010,** *132* (2), 611-619.

50. Nakano, Y.; Hirose, T.; Stals, P. J. M.; Meijer, E. W.; Palmans, A. R. A., Conformational analysis of supramolecular polymerization processes of disc-like molecules. *Chem. Sci.* **2012,** *3* (1), 148-155.

51. Desmarchelier, A.; Raynal, M.; Brocorens, P.; Vanthuyne, N.; Bouteiller, L., Revisiting the assembly of amino ester-based benzene-1,3,5-tricarboxamides: chiral rods in solution. *Chem. Commun.* **2015,** *51* (34), 7397-7400.

52. Desmarchelier, A.; Alvarenga, B. G.; Caumes, X.; Dubreucq, L.; Troufflard, C.; Tessier, M.; Vanthuyne, N.; Idé, J.; Maistriaux, T.; Beljonne, D.; Brocorens, P.; Lazzaroni, R.; Raynal, M.; Bouteiller, L., Tuning the nature and stability of self-assemblies formed by ester benzene 1,3,5-tricarboxamides: the crucial role played by the substituents. *Soft Matter* **2016,** *12* (37), 7824-7838.

53. Simic, V.; Bouteiller, L.; Jalabert, M., Highly cooperative formation of bis-urea based supramolecular polymers. *J. Am. Chem. Soc.* **2003,** *125* (43), 13148-13154.

54. Timme, A.; Kress, R.; Albuquerque, R. Q.; Schmidt, H. W., Phase Behavior and Mesophase Structures of 1,3,5 - Benzene - and 1,3,5 - Cyclohexanetricarboxamides: Towards an Understanding of the Losing Order at the Transition into the Isotropic Phase. *Chem. Eur. J.* **2012,** *18* (27), 8329-8339.

55. Lortie, F.; Boileau, S.; Bouteiller, L.; Chassenieux, C.; Deme, B.; Ducouret, G.; Jalabert, M.; Laupretre, F.; Terech, P., Structural and rheological study of a bis-urea based reversible polymer in an apolar solvent. *Langmuir* **2002,** *18* (19), 7218-7222.

56. Pinault, T.; Cannizzo, C.; Andrioletti, B.; Ducouret, G.; Lequeux, F.; Bouteiller, L., Anions as Efficient Chain Stoppers for Hydrogen-Bonded Supramolecular Polymers. *Langmuir* **2009,** *25* (15), 8404-8407.

57. Pedragosa-Moreau, S.; Archelas, A.; Furstoss, R., *J. Org. Chem.* **1993,** *58*, 5533-5536.

58. Zhou, Y. P.; Zhang, M.; Li, Y. H.; Guan, Q. R.; Wang, F.; Lin, Z. J.; Lam, C. K.; Feng, X. L.; Chao, H. Y., Mononuclear Gold(I) Acetylide Complexes with Urea Group: Synthesis, Characterization, Photophysics, and Anion Sensing Properties. *Inorg. Chem.* **2012,** *51* (9), 5099-5109.

59. Brunsveld, L.; Schenning, A. P. H. J.; Broeren, M. A. C.; Janssen, H. M.; Vekemans, J. A. J. M.; Meijer, E. W., Chirality Amplification in Columns of Self-Assembled N,N',N''-Tris((S)-3,7-dimethyloctyl)benzene-1,3,5-tricarboxamide in Dilute Solutions. *Chem. Lett.* **2000**, 292-293.

60. Smulders, M. M. J.; Buffeteau, T.; Cavagnat, D.; Wolffs, M.; Schenning, A. P. H. J.; Meijer, E. W., C-3-symmetrical self-assembled structures investigated by vibrational circular dichroism. *Chirality* **2008,** *20* (9), 1016-1022.

61. Jonkheijm, P.; van der Schoot, P.; Schenning, A. P. H. J.; Meijer, E. W., Probing the solvent-assisted nucleation pathway in chemical self-assembly. *Science* **2006,** *313* (5783), 80-83.

62. Smulders, M. M. J.; Schenning, A. P. H. J.; Meijer, E. W., Insight into the Mechanisms of Cooperative Self-Assembly: The "Sergeants-and-Soldiers" Principle of Chiral and Achiral C3-Symmetrical Discotic Triamides. *J. Am. Chem. Soc.* **2008,** *130* (2), 606-611.

63. Kulkarni, C.; Meijer, E. W.; Palmans, A. R. A., Cooperativity Scale: A Structure-Mechanism Correlation in the Self-Assembly of Benzene-1,3,5-tricarboxamides. *Acc. Chem. Res.* **2017,** *50* (8), 1928-1936.

64. Green, M. M.; Park, J. W.; Sato, T.; Teramoto, A.; Lifson, S.; Selinger, R. L. B.; Selinger, J. V., The macromolecular route to chiral amplification. *Angew. Chem. Int. Ed.* **1999,** *38* (21), 3139-3154.

65. Smulders, M. M. J.; Stals, P. J. M.; Mes, T.; Paffen, T. F. E.; Schenning, A. P. H. J.; Palmans, A. R. A.; Meijer, E. W., Probing the Limits of the Majority-Rules Principle in a Dynamic Supramolecular Polymer. *J. Am. Chem. Soc.* **2010,** *132* (2), 620-626.

66. van Gestel, J.; van der Schoot, P.; Michels, M. A. J., Amplification of chirality in helical supramolecular polymers. *Macromolecules* **2003,** *36* (17), 6668-6673.

67. van Gestel, J., Amplification of chirality in helical supramolecular polymers: The majority-rules principle. *Macromolecules* **2004,** *37* (10), 3894-3898.

68. van Gestel, J.; van der Schoot, P.; Michels, M. A. J., Amplification of chirality in helical supramolecular polymers beyond the long-chain limit. *J. Chem. Phys.* **2004,** *120* (17), 8253-8261.

69. Markvoort, A. J.; ten Eikelder, H. M. M.; Hilbers, P. A. J.; de Greef, T. F. A.; Meijer, E. W., Theoretical models of nonlinear effects in two-component cooperative supramolecular copolymerizations. *Nat. Commun.* **2011,** *2*.

70. ten Eikelder, H. M. M.; Markvoort, A. J.; de Greef, T. F. A.; Hilbers, P. A. J., An Equilibrium Model for Chiral Amplification in Supramolecular Polymers. *J. Phys. Chem. B* **2012,** *116* (17), 5291-5301.

71. Jouvelet, B.; Isare, B.; Bouteiller, L.; van der Schoot, P., Direct Probing of the Free-Energy Penalty for Helix Reversals and Chiral Mismatches in Chiral Supramolecular Polymers. *Langmuir* **2014,** *30*, 4570-4575.

72. Stals, P. J. M.; Everts, J. C.; de Bruijn, R.; Filot, I. A. W.; Smulders, M. M. J.; Martín-Rapún, R.; Pidko, E. A.; de Greef, T. F. A.; Palmans, A. R. A.; Meijer, E. W., Dynamic Supramolecular Polymers Based on Benzene-1,3,5-tricarboxamides: The Influence of Amide Connectivity on Aggregate Stability and Amplification of Chirality. *Chem. Eur. J.* **2010,** *16* (3), 810-821.

73. Mes, T.; Cantekin, S.; Balkenende, D. W. R.; Frissen, M. M. M.; Gillissen, M. A. J.; De Waal, B. F. M.; Voets, I. K.; Meijer, E. W.; Palmans, A. R. A., Thioamides: Versatile Bonds To Induce Directional and Cooperative Hydrogen Bonding in Supramolecular Polymers. *Chem. Eur. J.* **2013,** *19*, 8642-8649.

74. Kim, T.; Mori, T.; Aida, T.; Miyajima, D., Dynamic propeller conformation for the unprecedentedly high degree of chiral amplification of supramolecular helices. *Chem. Sci.* **2016,** *7*, 6689-6694.

75. Greciano, E. E.; Calbo, J.; Buendía, J.; Cerdá, J.; Aragó, J.; Ortí, E.; Sánchez, L., Decoding the Consequences of Increasing the Size of Self- Assembling Tricarboxamides on Chiral Amplification. *J. Am. Chem. Soc.* **2019**, DOI: 10.1021/jacs.9b02045.

76. Zhou, Y. F.; Xu, M.; Yi, T.; Xiao, S. Z.; Zhou, Z. G.; Li, F. Y.; Huang, C. H., Morphology-tunable and photoresponsive properties in a self-assembled two-component gel system. *Langmuir* **2007,** *23* (1), 202-208.

77. Webber, M. J.; Appel, E. A.; Meijer, E. W.; Langer, R., Supramolecular biomaterials. *Nat. Mater*. **2015,** *15*, 13.

78. Adelizzi, B.; Aloi, A.; Markvoort, A. J.; Ten Eikelder, H. M. M.; Voets, I. K.; Palmans, A. R. A.; Meijer, E. W., Supramolecular Block Copolymers under Thermodynamic Control. *J. Am. Chem. Soc.* **2018,** *140* (23), 7168-7175.

79. Kang, J.; Miyajima, D.; Mori, T.; Inoue, Y.; Itoh, Y.; Aida, T., A rational strategy for the realization of chain-growth supramolecular polymerization. *Science* **2015,** *347* (6222), 646-651.

80. Narayan, B.; Bejagam, K. K.; Balasubramanian, S.; George, S. J., Autoresolution of Segregated and Mixed p-n Stacks by Stereoselective Supramolecular Polymerization in Solution. *Angew. Chem. Int . Ed.* **2015,** *54* (44), 13053-13057.

81. Zhang, W.; Jin, W. S.; Fukushima, T.; Mori, T.; Aida, T., Helix Sense-Selective Supramolecular Polymerization Seeded by a One-Handed Helical Polymeric Assembly. *J. Am. Chem. Soc.* **2015,** *137* (43), 13792-13795.

82. Ma, X. J.; Zhang, Y. B.; Zhang, Y. F.; Liu, Y.; Che, Y. K.; Zhao, J. C., Fabrication of Chiral-Selective Nanotubular Heterojunctions through Living Supramolecular Polymerization. *Angew. Chem. Int . Ed.* **2016,** *55* (33), 9539-9543.

83. Pal, D. S.; Kar, H.; Ghosh, S., Controllable supramolecular polymerization via a chain-growth mechanism. *Chem. Commun.* **2018,** *54* (8), 928-931.

84. Lightfoot, M. P.; Mair, F. S.; Pritchard, R. G.; Warren, J. E., New supramolecular packing motifs: pi-stacked rods encased in triply-helical hydrogen bonded amide strands. *Chem. Commun.* **1999,** (19), 1945-1946.

85. Frederix, P. W. J. M.; Patmanidis, I.; Marrink, S. J., Molecular simulations of self-assembling bio-inspired supramolecular systems and their connection to experiments. *Chem. Soc. Rev.* **2018,** *47* (10), 3470-3489.

86. Edinger, C.; Waldvogel, S. R., Electrochemical Deoxygenation of Aromatic Amides and Sulfoxides. *Eur. J. Org. Chem.* **2014,** (24), 5144-5148.

General conclusion

The objectives of this thesis were to develop the switchable ability and increase the extent of amplification of chirality in helical benzene-1,3,5-tricarboxamide (BTA) co-assemblies composed of a BTA ligand and enantiopure BTA co-monomers. In the major part of this manuscript **BTA^{PPh2}** and **BTA Cha** served as the BTA ligand and enantiopure BTA co-monomer, respectively. Coordination of the ligand to copper and activation with phenylsilane generate helical catalysts which provide 1-(4-nitrophenyl)ethanol (NPnol) from 1-(4-nitrophenyl)ethanone. The optimal selectivity and the configuration of NPnol are related to the optical purity of the helical main chain and the handedness of the helical co-assemblies, respectively. Prior to this work, no example of organometallic catalyst was reported for which the enantioselectivity can be switched during the course of the reaction in a truly reversible manner thus allowing both enantiomers to be obtained with similar selectivity from the same catalyst. Also, despite several examples of supramolecular systems displaying high levels of amplification of chirality through the S&S (with ≤ 1% of sergeant) and (diluted) MR effects (with ≤ 10% *e.e.* scalemic mixture), no implementation of such systems in asymmetric catalysis has been reported. (Figure 1)

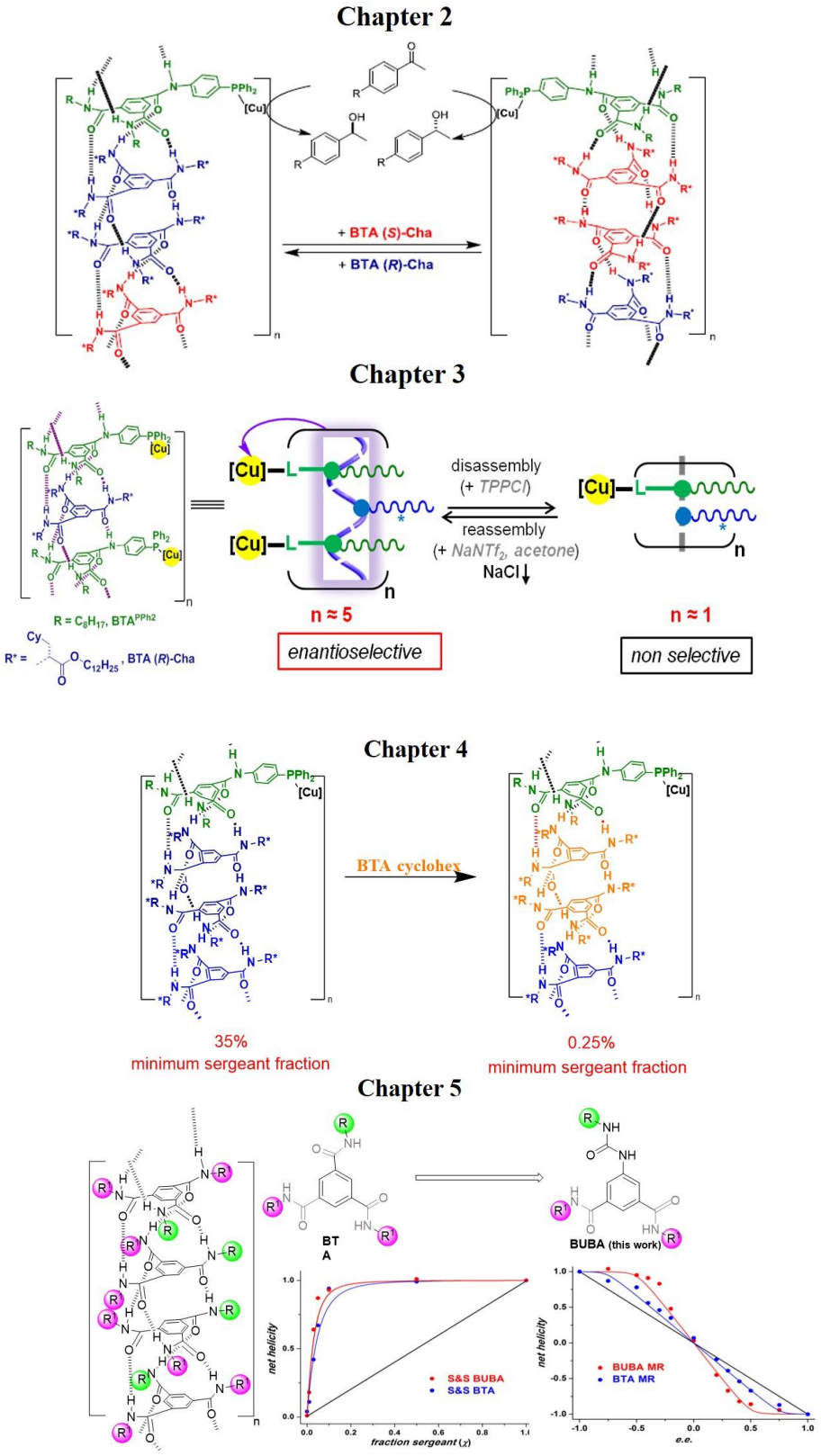

Figure 1 Schematic representation of the main results achieved in each chapter

In chapter 2, the diluted MR effect was exploited to switch the handedness of the co-assemblies, and thus the selectivity of the catalytic reaction in real time. In this system, 33% *e.e.* scalemic mixtures form homochiral assemblies which in turn provide NPnol with 88% of the optimal selectivity at room temperature. By combining CD spectroscopy and catalytic experiments, we demonstrated that the chirality amplification effect observed in the catalytic experiments stems from the chirally-amplified nature of the helical scaffold of the catalyst. Thanks to the diluted MR effect, the enantiomeric state of the supramolecular copper catalyst can be switched *in situ* in *ca.* five seconds by changing the nature of the major enantiopure comonomer in the co-assemblies. As a result of the complete and fast stereochemical switch of this helical catalyst, any combination of the enantiomers was obtained during the conversion of a 1:1 mixture of 1-(4-nitrophenyl)ethanone and 1-(4-biphenylyl)-ethanone.

In chapter 3, we showed that the length of BTA assemblies could be modulated *in a reversible manner* by firstly adding TPPCl (tetraphenylphosphonium chloride) and then removing it by means of a salt metathesis reaction with $NaNTf_2$ (Tf=triflimide)leading to the precipitation of NaCl. The nature of the co-assemblies formed between **BTA^{PPh2}** and **BTA (*R*)-Cha** in toluene and their reversible assembly in the absence or presence of TPPCl and $NaNTf_2$ have been precisely characterized by means of Fourier-Transform Infrared (FT-IR), Nuclear Magnetic Resonance (NMR), Small Angle Neutron Scattering (SANS) and Circular Dichroism (CD) analyses. It is interesting to note that TPPCl allows programmable modulation of the degree of enantioinduction (signal output) in between fully racemic and optimal enantiomeric preference (53% *e.e.*) by simply changing the concentration of TPPCl (signal input). Moreover, the reversible assembly of the supramolecular helices allows to switch reversibly the enantiomeric state of the supported ccopper centres between enantioselective (52% *e.e.*) and non selective (6% *e.e.*). A slowdown of of the reaction rate is observed for the catalytic system in presence of TPPCl, however, the decreased rate for the non-selective state of the supramolecular catalyst is not detrimental since good conversions can be achieved by increasing the amount of silane and the reaction time. Also, the decreased selectivity observed after reassembly is due to the presence of the co-added solvents (DCM, acetone), that are required to dissolve the salts, not to an incomplete metathesis reaction. Finally, a good correlation has been established between the average length of the assemblies, the chiral environment of the ligand and the selectivity of the reaction. For the present catalytic system, the critical length of the supramolecular helices required to locate most of

the copper centres in a chiral environment suitable for asymmetric induction is thus in the range of a ten monomers.

In chapter 4, we have demonstrated a huge enhancement of the extent of amplification of chirality in helical co-assemblies composed of **BTA^{PPh2}·Cu** and **BTA Cha** upon incorporation of an achiral BTA additive (**BTA cyclohex**). The S&S and diluted MR effects are increased by two orders and one order of magnitude, respectively, in the prensece of **BTA cyclohex**. More precisely, only 0.25% of enantiopure **BTA Cha** is sufficient to generate homochiral co-assemblies (as probed by CD analyses), which in turn provides NPnol with 88% of the optimal selectivity (50% *e.e.*) when applied in the asymmetric hydrosilylation of 1-(4-nitrophenyl)ethanone at room temperature. Using a mixture of enantiopure **BTA Cha** monomers which is only slightly biased from the racemic mixture (10% *e.e.*) also provides homochiral assemblies and a selective catalyst (44% *e.e.*). Such an enhancement in the amplification of chirality is only achieved by mixing the three components, *i.e.* the two achiral monomers and the enantiopure comonomer, highlighting a synergistic effect upon co-assembly of the three BTA partners. Investigation of the role of the achiral additive by means of several spectroscopic techniques (CD, UV-Vis, FT-IR, SANS) supports its ability to induce a conformational change in the helical co-assemblies leading to no or fewer helix reversals *i.e.* configurational defects.

In chapter 5, we showed that *N*-substituted benzene-1-urea-3,5-biscarboxamide (BUBA) monomers, comprising one urea function and two carbon-centred amide functions connected to the same aromatic ring, form long, reversible and highly chirally-amplified helical assemblies in apolar solvents. This class of monomers provides an easy access to non C_3-symmetric supramolecular helices which might be useful for the design of hierarchical assemblies, for the compartmentalization or self-assembly of polymer chains and for application-driven studies in asymmetric catalysis. Single-handed helices are obtained by self-assembly of BUBA monomers possessing chiral sides chains and more importantly by incorporating a small amount of chiral BUBA monomers in a racemic mixture of left- and right-handed benzene-1,3,5-tricarboxamide (BTA) stacks. Compared to BTA helices, the stability of BUBA assemblies is slightly lower despite the presence of an additional hydrogen bond interaction provided by the urea groups (as reflected by the higher elongation enthalpy). Conversely, BUBA self-assembly proceeds with a higher level of cooperativity. Moreover,

chirality amplification operates to a higher extent in BUBA helices as probed by both sergeants-and-soldiers and majority-rules experiments.

In the future, one possible outlook is to implement switchable ability of BTA-based supramolecular polymer helices in consecutive reactions or polymerization reactions. It has been reported that the stereochemistry of polyolefins strongly influences their mechanical properties. So it appears quite interesting to test whether these switchable helices can be implemented for the preparation of atactic isotactic multi stereoblock copolymers, such as polylactide. Another possibility is the optimization of the chemical structures of the BTA ligand, the comonomer and the achiral BTA additive in order to improve the enantioselectivity at room temperature. Supporting a high performing BTA ligand with an efficient stimulus-responsive and highly chirally-amplified BTA platform might provide high enantioselectivities under mild conditions. In addition, whilst only organometallic helical catalysts have been reported to date, it would be interesting to develop metal-free helical organocatalyst. For example, certain functional groups (such as the urea moiety) could be induced on the side chains to provide enantioselectivity for the helical stacks. Finally as we have demonstrated that short helices are sufficient to offer high selectivity, it seems enviageable to utilize the free NH groups for hydrogen-bond catalysis, since these groups are more acidic when incorporated in the BTA hydrogen-bonded network than in the monomers.

Résumé

L'induction de la chiralité, l'amplification de la chiralité et la réversibilité sont des caractéristiques clés des hélices dynamiques, et la mise en œuvre de ces propriétés dans le domaine de la catalyse asymétrique suscite un grand intérêt. Une énantiosélectivité élevée a notamment été obtenue pour les catalyseurs situés à la périphérie du squelette hélicoïdal de polymères covalents de type-PQX (poly(quinoxaline-2,3-diyl) et de polymères supramoléculaires de type BTA (benzene-1,3,5-trisamide). L'ampleur de l'énantioinduction et la configuration du produit de la réaction catalytique sont liés à la pureté optique et au sens de rotation, respectivement, de ces catalyseurs hélicoïdaux. Ceci ouvre la voie à diverses applications potentielles uniques pour cette catégorie de catalyseurs. Le contrôle de la configuration d'un catalyseur unique durant la réaction est un défi, en particulier pour les réactions catalysées par des métaux, car la présence du centre métallique peut nuire à l'efficacité et à la dynamique du commutateur chiroptique. L'inversion de l'énantiosélectivité d'un seul catalyseur au cours d'une réaction présente des perspectives prometteuses d'utilisation d'un tel catalyseur pour sélectionner le diastéréoisomère désiré dans une réaction en cascade stéréosélective ou pour contrôler la tacticité des copolymères stéréoblocs. Basé sur notre précédent concept de catalyseurs supportés sur des hélices supramoléculaires de type BTA, **le premier objectif de cette thèse** est de décrire une stratégie qui permet de contrôler en temps réel l'énantiosélectivité d'une réaction catalytique. Deux stratégies ont été utilisées pour contrôler la sélectivité des hélices formées en mélangeant des ligands BTA achiraux et des comonomères énantiopurs. La première stratégie repose sur la possibilité de commuter la sélectivité du ligand hélicoïdal BTA amplifié chirallement en changeant la nature du comonomère énantiopur majoritaire dans les co-assemblages grâce à l'effet de règles de majorité dilué (chapitre 2, figure 1a). Pour la deuxième stratégie, il est attendu que la sélectivité fournie par les co-assemblages hélicoïdaux de BTA puisse être modulée en modifiant la longueur moyenne des hélices supramoléculaires. En conséquence, une combinaison de sels précisément sélectionnée a été ajoutée aux mélanges catalytiques afin de dissocier et de restaurer les co-assemblages et moduler ainsi la nature des sites catalytiques entre des états catalytiques non sélectifs et sélectifs de façon réversible (chapitre 3, figure 1b).

Les effets «sergents et soldats» (S&S) et de «règle de la majorité» (RM) peuvent être utilisés pour contrôler la pureté optique des hélices dynamiques avec une faible quantité de monomères énantiopurs ou avec un mélange non optiquement pur de monomères énantiopurs,

respectivement. Des effets d'amplification de chiralité extrêmement élevés qui permettent d'obtenir des hélices optiquement pures avec moins de 1% de sergent ou avec un mélange scalémique avec 10% d'*e.e.* existent mais sont rares. De plus, les catalyseurs hélicoïdaux reportés jusqu'à présent présentaient une sélectivité > à 80 % *e.e.* seulement lorsque leur teneur en sergents était supérieure à 10 % ou lorsque la pureté optique de l'énantiomère était supérieure ou égale à 20 % *e.e*. L'amélioration des propriétés d'amplification de chiralité de ces catalyseurs hélicoïdaux est particulièrement souhaitable pour diminuer la quantité d'inducteur chiral dans le mélange catalytique (c'est-à-dire sensiblement en dessous du chargement catalytique) et permettre leur commutation stéréochimique avec un faible taux de comonomères enantiopurs. Notre deuxième objectif est donc d'améliorer les propriétés d'amplification de chiralité de nos hélices BTA catalytiques. Premièrement, nos travaux ont révélé que les effets de S&S et de RM dilués dictant l'hélicité des co-assemblages BTA précatalytiques sont exaltés par l'ajout d'un monomère BTA achiral. Cette amélioration des propriétés d'amplification de la chiralité par l'ajout de cet additif achiral est également valable pour les mélanges catalytiques de BTA, ce qui permet d'obtenir une sélectivité optimale avec à peine 0,2% de sergents et un mélange scalémique à 10% *e.e.* d'énantiomères BTAs (Chapitre 4, Figure 1c). Enfin, nous avons étudié les propriétés d'auto-assemblage des monomères *N*-substitués de benzène-1-urée-3,5-biscarboxamide (BUBA), analogues symétriques en C_2 des monomères BTA dans lesquels une fonction amide a été remplacée par une fonction urée. Nous nous sommes particulièrement intéressés à étudier l'influence de la substitution d'un seul groupe sur les propriétés d'amplification de chiralité des assemblages résultants (Chapitre 5, Figure 1d).

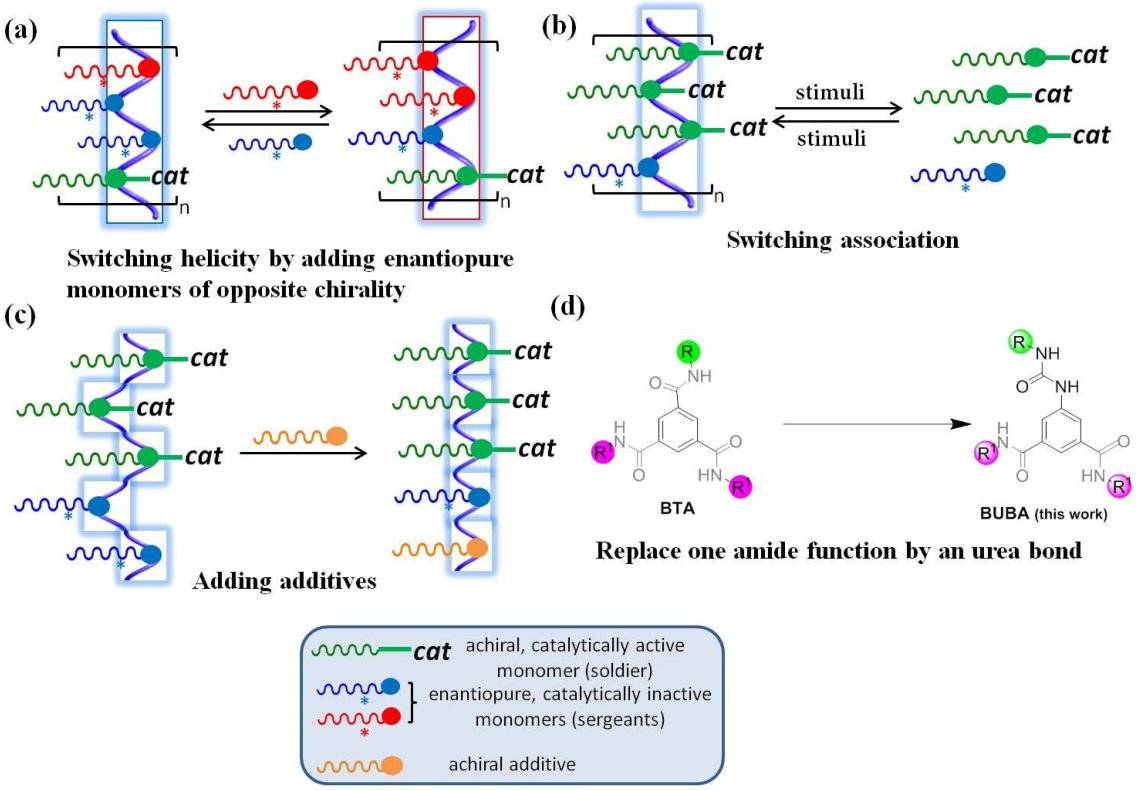

Figure 1 Représentation schématique des différents concepts développés dans les chapitres de ce manuscrit. a) catalyseur dont la sélectivité est commutable (chapitre 2) ; b) catalyseur dont la sélectivité est modulable (chapitre 3); c) catalyseur hélicoïdal extrêmement amplifié chiralement (chapitre 4) ; d) relations structure-propriété des assemblages formés par une nouvelle classe de monomères de symétrie C_2 (chapitre 5).

Dans le chapitre 2, l'effet de RM dilué a été exploité pour commuter le sens de rotationdes co-assemblages, et donc la sélectivité de la réaction catalytique en temps réel. Dans ce système, des mélange scalémiques à 33 % d' *e.e.* forment des assemblages homochiraux qui, à leur tour, fournissent le NPnol vec 88 % de la sélectivité optimale à température ambiante. En combinant la spectroscopie CD et les expériences catalytiques, nous avons démontré que l'effet d'amplification de chiralité observé dans les expériences catalytiques provenait bien de la nature amplifiée chiralement de la matrice hélicoïdale du catalyseur. Grâce à l'effet RM dilué, l'état énantiomérique du catalyseur supramoléculaire au cuivre peut être inversé in situ en cinq secondes environ en modifiant la nature du comonomère énantiopur présent en majorité dans les co-assemblages. Grâce à l'inversion stéréochimique complète et rapide de ce catalyseur hélicoïdal, toute les combinaisons possibles des énantiomères ont été obtenus lors de la conversion d'un mélange 1:1 de 1-(4-nitrophényl)éthanone et de 1-(4-biphénylyl)-éthanone Au chapitre 3, nous avons montré que la longueur des ensembles BTA pouvait être modulée de manière réversible en ajoutant un anion puis en l'enlevantpar une réaction métathèse du sel menant à sa co-précipitation avec un cation. La nature des co-assemblages formés entre **BTA^{PPh2}** et **BTA (*R*)-Cha** dans le toluène et leur assemblage réversible en présence des sels ont été précisément caractérisés au moyen d'analyses par infrarouge à transfert de Fourier (FT-IR), résonance magnétique nucléaire (RMN), diffusion neutronique à petit angle (SANS) et dichroïse circulaire (CD).

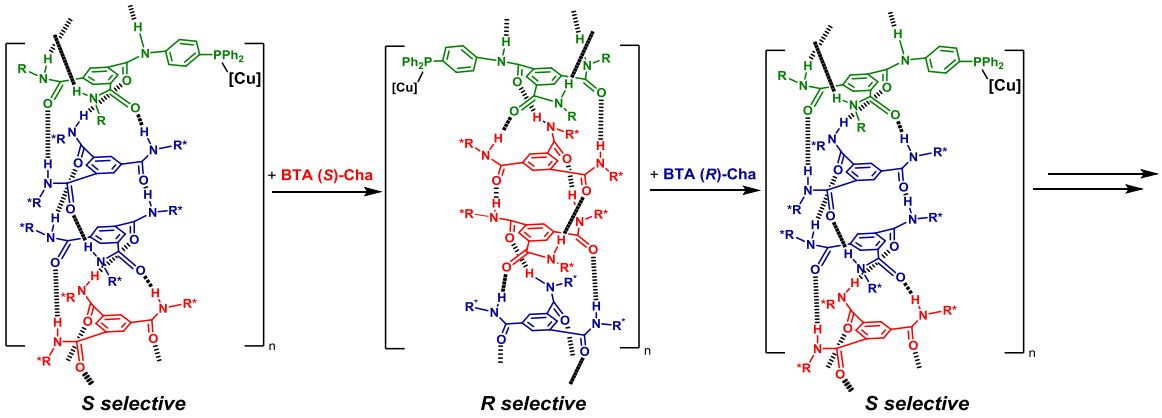

Figure 2 Contrôle en temps réel de l'énantiosélectivité d'un catalyseur supramoléculaire métallique. Les résultats de la réaction catalytique et la structure des assemblages BTA ont été corrélés selon diverses analyses spectroscopiques et de diffusion.

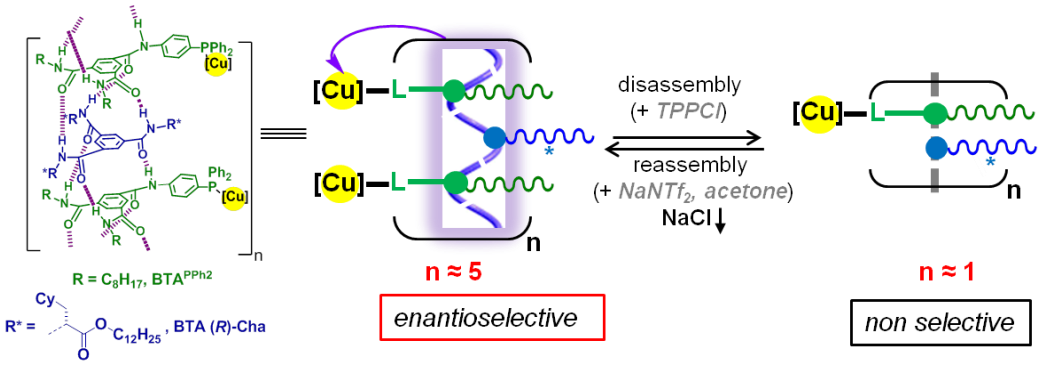

Figure 3 Représentation schématique du concept actuel. Les hélices supramoléculaires formées par co-assemblage entre un ligand BTA achiral (**BTA^{PPh2}**) coordonné à Cu et un comonomère BTA énantiopure (**BTA (*R*)-Cha**), sont raccourcies et allongées de manière réversible par une combinaison appropriée de sels. Cette représentation schématique des co-assemblages est étayée par des données analytiques, mais le mode de coordination du Cu et la fraction des groupes PPh2 coordonnés dans les co-assemblages ne sont pas connus.

Dans le chapitre 4, nous avons démontré que l''amplification de la chiralité dans les co-assemblages hélicoïdaux de **BTA^{PPh2}·Cu** et **BTA Cha** est grandement amélioré lors de l'incorporation d'un additif BTA achiral. En ajoutant des monomères **BTA cyclohex**, seulement 0,25 % de BTA Cha enantiopurs est suffisant pour générer des co-assemblages homochiraux (tels que testés par des analyses CD), ce qui donne au NPnol 88 % de la sélectivité optimale (50 % *e.e.*) lorsqu'appliqué dans l'hydrosilylation asymétrique de 1-(4-nitrophényle)éthanone à température ambiante. L'utilisation d'un mélange de monomères énantiopurs de BTA Cha qui n'est que légèrement biaisé par rapport au mélange racémique (10% *e.e.*) fournit également des assemblages homochiraux et un catalyseur sélectif (44% *e.e.*). Une telle amélioration de l'amplification de la chiralité n'est obtenue qu'en mélangeant les trois composants, c'est-à-dire les deux monomères achiraux et le comonomère énantiopure, mettant en évidence un effet synergique sur le co-assemblage des trois monomères. L'étude du rôle de l'additif achiral au moyen de plusieurs techniques spectroscopiques (CD, UV-Vis, FT-IR, SANS) soutient sa capacité à induire un changement de conformation dans les coassemblages hélicoïdaux n'entraînant pas ou peu d'inversions d'hélice, c'est-à-dire des défauts de configuration. (Figure 4)

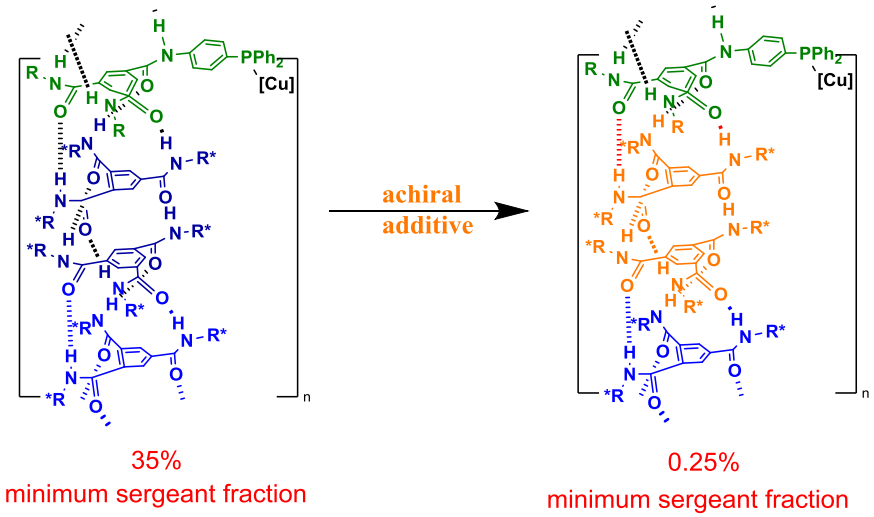

Figure 4 Représentation schématique du concept. Les propriétés d'amplification de la chiralité ont été considérablement améliorées par l'ajout d'additifs achiraux aux hélices formées par le ligand BTA achiral (**BTA^{PPh2}**) coordonné au Cu et un comonomère BTA énantiopure (**BTA-(*R*)-Cha**).

Au chapitre 5, nous présentons, les monomères N-substitués de benzène-1-urée-3,5-biscarboxamide (BUBA), qui consistent en une urée et deux fonctions amide liées au carbone et liées à un cycle aromatique, une nouvelle classe de monomères facilement accessibles de symmétrie C_2. Dans les solvants apolaires, les monomères BUBA s'assemblent en longs assemblages hélicoïdaux au moyen de liaisons hydrogène et d'interactions aromatiques, évaluées par plusieurs techniques analytiques. Afin de sonder l'influence de la fonction urée, on a comparé les assemblage à base de BUBA et les polymères hélicoïdaux de benzène-1,3,5-tricarboxamide (BTA) en termes de thermodynamique de formation, de stabilité, de réversibilité et d'amplification chirale. Comme le BTA, les monomères BUBA forment de longues hélices de manière réversible grâce à un mécanisme hautement coopératif et l'hélicité de leurs assemblages est régie par des effets d'amplification chirale. Cependant, une quantification précise de leurs propriétés révèle que les monomères BUBA s'assemblent d'une manière plus coopérative. De plus, l'amplification de la chiralité fonctionne dans une plus grande mesure dans les assemblages à base de monomères BUBA, comme l'ont montré les expériences de type sergents et les soldats et de règles de la majorité. La compatibilité entre les fonctions urée et amide permet également la formation de co-assemblages incorporant à la fois des monomères BUBA et BTA. Il est important de noter qu'une petite quantité de monomères chiraux BUBA dans ces co-assemblages est suffisante pour obtenir des hélices homochirale ce qui qui ouvre la voie au développement d'hélices supramoléculaires fonctionnelles. (Figure 5)

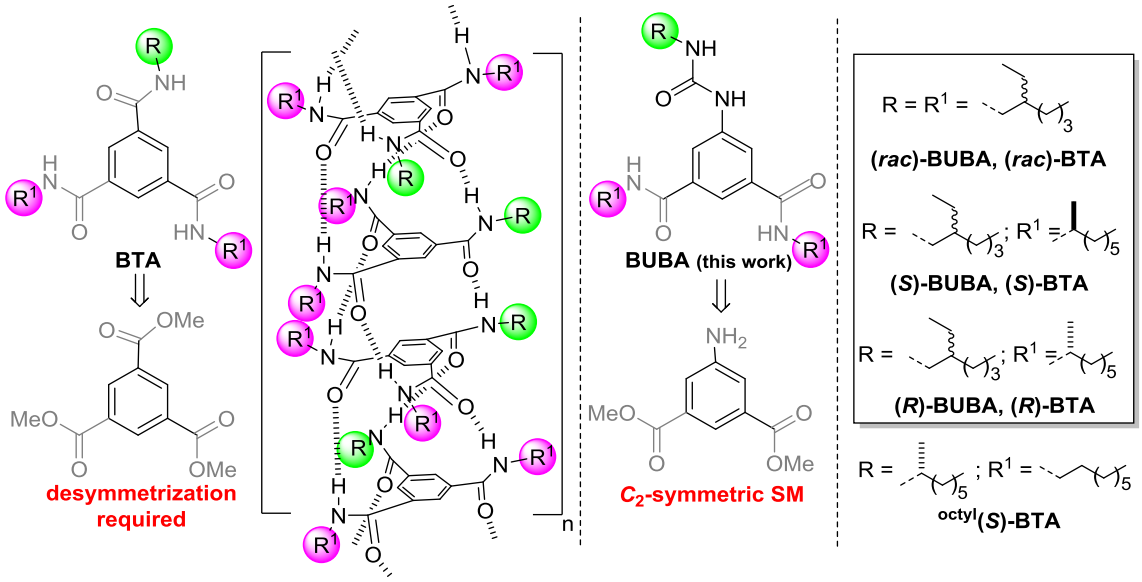

Figure 5 Structures moléculaires des monomères. Représentation des hélices supramoléculaires BTA (les groupes R et R1 sont supposés être répartis aléatoirement à la périphérie des hélices). (rac)-BUBA est racémique par synthèse et se compose donc des stéréoisomères (S_{urea},S,S), (S_{urea},R,S), (S_{urea},R,S), (S_{urea},R,R), (R_{urea},S,S), (R_{urea},R,S), (R_{urea},R,S), (R_{urea},R,R) dans un ratio 1:2:1:1:1:2:1. (rac)-BTA est racémique par synthèse et se compose donc des stéréoisomères (S,S,S,S), (S, S, S, R), (R,R,S), (R,R,S), (R,R,R,R) dans un rapport 1:3:3:3:1. (S)-BUBA et (S)-BTA consistent en un mélange 1:1 des stéréoisomères (S,S,S) et (R,S,S,S). Les propriétés d'assemblage de (S)-BTA seront comparées à celles de son analogue structural octyl(S)-BTA.

Pour conclure, des hélices de polymères supramoléculaires à base de BTA ont été utilisées pour l'hydrosilylation de la 1-(4-nitrophényl)éthanone catalysée au cuivre. Les hélices catalytiques sont composées de **BTA**$^{\mathbf{PPh_2}}$(le ligand) et de comonomères BTA chiraux. Nous avons développé la capacité commutable et les propriétés d'amplification chirale des catalyseurs hélicoïdaux BTA. Tout d'abord, nous avons réussi à inverser réversiblement en temps réel l'hélicité des assemblageshélicoïdales catalytiques en changeant la nature du comonomère majeur énantiopure dans les co-assemblages grâce à l'effet de règle de majorité diluée, qui permet l'inversion de l'énantiosélectivité au cours de la réaction catalytique. Deuxièmement, les co-assemblages peuvent être dissociés et restaurés par l'ajout de sels appropriés, commutant l'état du catalyseur entre non sélectif et sélectif d'une manière réversible. Troisièmement, l'effet d'amplification de la chiralité (effet SS et MR dilué) est grandement amélioré par l'ajout d'un monomère BTA achiral. De plus, l'amélioration des propriétés d'amplification de la chiralité par l'ajout de cet additif achiral est également valable pour les mélanges catalytiques de BTA, ce qui permet d'obtenir une sélectivité optimale avec à peine 0,25% de sergents et avec un mélange scalémique à 10% *e.e.* d'énantiomères BTAs. Enfin, nous avons étudié les propriétés d'auto-assemblage des monomères N-substitués de benzène-1-urée-3,5-biscarboxamide (BUBA), analogues de symétrie C_2 des monomères BTA dans lesquels une fonction amide a été remplacée par une fonction urée. Les propriétés d'amplification de chiralité des assemblages résultants ont été améliorées grâce à la substitution d'un seul groupe.

Title: Switchable and chirally-amplified helices formed by hydrogen-bonded supramolecular polymers for asymmetric catalysis

Abstract: Benzene 1,3,5-tricarboxamide (BTA) supramolecular helical polymerswere utilized as a dynamic and chirally-amplified scaffold for copper catalysts implemented in the asymmetric hydrosilylation of 1-(4-nitrophenyl)ethanone. The catalytic helices are composed of a phosphine-functionalized BTA ligand and of enantiopure BTA comonomers. We have developed the switchable ability and improved the chirality amplification properties of this new class of BTA helical catalysts. Firstly, we successfully switched the handedness of the helices in real time by changing the nature of the major enantiopure comonomer in the co-assemblies. Then it allows controlling the configuration of the stereogenic centres formed during the consecutive transformation of a single substrate or a mixture of subtrates. Secondly, the helical co-assemblies are disrupted and restored by adding suitable salts, which switch the catalytic outcome between non-selective and selective states *in a reversible manner*. Thirdly, the extent of amplification of chirality in the helical co-assemblies as probed by the sergeants-and-soldiers effect and majority-rule effect are hugely exalted upon incorporation of a*n achiral BTA additive*. Moreover the improvement of the chirality amplification properties by addition of this achiral additive also holds for catalytic BTA mixtures which thus allow 80% of the optimal selectivity to be obtained with as low as 0.25% of enantiopure BTA and a 10% *e.e.* scalemic mixture of BTA enantiomers. Finally, we investigate the self-assembly properties of N-substituted benzene-1-urea-3,5-biscarboxamide (BUBA) monomers, C_2-symmetric analogues of BTA monomers in which one amide function has been replaced by an urea function. The chirality amplification properties and extent of cooperativity are slightly higher for BUBA monomers, respectively to BTA monomers. In total, we developed the switchable ability and increase the extent of amplification of chirality of BTA-based helices. It will be interesting to implement the thereof chirally-amplified scaffold in stereoselective cascade reactions or polymerization reactions.

Keywords : supramolecular polymers, hydrogen-bonding interactions, benzene-1,3,5-tricarboxamide (BTA), switchable catalyst, chirality amplification, asymmetric catalysis

Titre : Nouvelle classe de catalyseurs asymétriques commutables basés sur des polymères supramoléculaires dynamiques et amplifiés chirallement.

Résumé: Des polymères supramoléculaires hélicoïdaux à base de monomères de type benzène-1,3,5-trisamide (BTA) ont été étudiés comme supports dynamiques et amplifiés chirallement de catalyseurs de cuivre utilisés dans la réaction d'hydrosilylation asymétrique de la 4-nitro-acétophénone. Les hélices catalytiques sont composées d'un monomère BTA fonctionnalisé avec un groupement PPh_2 servant de ligand et de co-monomères BTA énantiopurs. Nous avons développé le caractère commutable et les propriétés d'amplification de chiralité de cette nouvelle classe de catalyseurs hélicoïdaux. Tout d'abord, le sens de rotation des hélices a été inversée en temps réel en changeant la nature de l'énantiomère BTA majoritaire dans le co-assemblage. Cela a permis de contrôler la configuration du carbone asymétrique formé durant la transformation séquentielle de plusieurs équivalents d'un même substrat ou d'un mélange de deux substrats. Deuxièmement, les assemblages hélicoïdaux ont été dissociés et restaurés par l'ajout d'une combinaison de sels soigneusement sélectionnés ce qui permet de moduler la nature des sites catalytiques entre des états non sélectifs et sélectifs de façon réversible. Troisièmement, la magnitude de l'amplification de chiralité gouvernant la pureté optique des co-assemblages hélicoïdaux est grandement améliorée par l'incorporation d'un monomère BTA achiral et ce phénomène est aussi observé pour les hélices catalytiques. Cela permet d'obtenir le produit de la réaction catalytique avec une sélectivité égale à 80% la sélectivité optimale avec des co-assemblages contenant seulement 0.25% de BTA énantiopurs ou contenant un mélange scalémique d'énantiomères BTA (10% *e.e.*). Enfin, nous avons étudié les propriétés d'auto-assemblage des monomères N-substitués de benzène-1-urée-3,5-biscarboxamide (BUBA), analogues C2-symétriques des monomères BTAs dans lesquels une fonction amide a été remplacée par une fonction urée. Les propriétés d'amplification de chiralité gouvernant la formation des assemblages hélicoïdaux des monomères BUBAs sont légèrement supérieures à celles gouvernant la formation des assemblages à base de monomères BTAs. Au total, nous avons développé le caractère commutable et augmenté l'ampleur de l'amplification de la chiralité des hélices à base de monomères BTAs. Il sera intéressant de mettre en oeuvre ces assemblages hélicoïdaux dans des réactions cascades stéréosélectives ou des réactions de polymérisation.

Mots-clefs: polymères supramoléculaires, liaisons hydrogène, benzene-1,3,5-trisamide (BTA), catalyseur commutable, amplification de chiralité, catalyse asymétrique